Influence of salinity on the coupled ocean-atmosphere dynamics of the tropical Atlantic Ocean

Manon Gevaudan

Université Fédérale
Toulouse Midi-Pyrénées

THÈSE

En vue de l'obtention du

DOCTORAT DE L'UNIVERSITÉ DE TOULOUSE

Délivré par : *l'Université Toulouse 3 Paul Sabatier (UT3 Paul Sabatier)*

Présentée et soutenue le *17/12/2021* **par :**

Manon GÉVAUDAN

Influence de la salinité sur la dynamique couplée océan-atmosphère de l'océan Atlantique tropical

---

JURY

Gregory Foltz	Senior scientist (NOAA, Miami)	Rapporteur
Gilles Reverdin	Directeur de recherche (LOCEAN, Paris)	Rapporteur
Sabrina Speich	Professeure des universités (LMD, Paris)	Examinatrice
Gaëlle De Coëtlogon	Maîtresse de conférences (LATMOS, Paris)	Examinatrice
Hervé Giordani	Directeur de recherche (CNRM, Toulouse)	Examinateur
Sébastien Masson	Physicien adjoint (LOCEAN, Paris)	Examinateur
Julien Jouanno	Directeur de recherche (LEGOS, Toulouse)	Directeur de thèse
Fabien Durand	Chargé de recherche (LEGOS, Toulouse)	Co-directeur de thèse

---

École doctorale et spécialité :
SDU2E : Océan, Atmosphère, Climat
Unité de Recherche :
LEGOS (UMR 5566)
Directeur(s) de Thèse :
Julien JOUANNO et *Fabien DURAND*
Rapporteurs :
Gregory FOLTZ et *Gilles REVERDIN*

Abstract

The tropical Atlantic Ocean has a highly contrasted surface salinity, with low surface salinity in the western and central parts of the basin. This low salinity is due to an important freshwater supply from large rivers such as the Amazon, Orinoco and Congo, and from heavy precipitation in the intertropical convergence zone. This results in a strong salinity stratification that may influence the vertical mixing, and thus the sea surface temperature (SST) and air-sea fluxes. The aim of this thesis is to investigate the influence of salinity – and especially the strong salinity stratification – on the tropical Atlantic Ocean climate. To do so, a 1/4° coupled ocean–atmosphere model of the region is developed, using NEMO as the ocean component, WRF as the atmospheric component and OASIS as the coupler. The use of a coupled ocean-atmosphere model allows to take into account all the air-sea interactions and feedback processes, which have been shown to impact the regional climate and are at the heart of this study. A series of sensitivity experiments is then conducted with this model, in order to assess the impact of increasingly detailed processes. First, the impact of the total salinity stratification on SST and air-sea fluxes is assessed by removing it from the model. Then, the Amazon and Orinoco rivers, major contributors to salinity stratification in the tropical Atlantic, are removed from the model. Interannual variability of river discharge is then studied to quantify the impact of Amazon extreme floods. Finally, the experiment without salinity stratification is conducted in a future climate, where several of the key variables identified in the present climate are very distinct from their present state, allowing a deeper understanding of the processes at stake. From these sensitivity tests, a consistent mechanism emerges in the northwestern tropical Atlantic in summer. The presence of salinity stratification decreases the cooling by vertical mixing, which leads to an increase in SST. This warming is then damped by a negative feedback from the atmosphere: the oceanic response is mitigated by a decrease in net heat flux. This decrease in net heat flux is primarily due to an increase in latent heat loss, but also to a reduction in shortwave radiation reaching the ocean surface, related to an increase in deep convection and associated cloud cover and precipitation. The final change in SST is determined by the balance between the warming due to the vertical mixing and the cooling due to the atmospheric feedback, both depending on the sensitivity test. However, the resulting SST change is always relatively small (0.5°C maximum). In winter, the impacts of salinity stratification are much weaker, most probably because of a deeper mixed layer at this time. SST changes are finally observed in the cold tongue region, related to changes in the thermocline depth. Subsurface temperature changes are present throughout the year, but the seasonality of upwelling occurrence dictates the timing of SST changes. In this thesis, the impact of salinity stratification on the mean tropical Atlantic climate is studied, but the model developed here could be adapted to study the impact of salinity stratification on the cyclones. Indeed, the Amazon plume is crossed by numerous tropical cyclones, and the impact of its associated salinity stratification remains controversial.

Résumé

L'océan Atlantique tropical présente une salinité de surface très contrastée, avec notamment une faible salinité de surface dans l'ouest et le centre du bassin. Cette faible salinité est due à d'importants apports d'eau douce provenant de fortes précipitations dans la zone de convergence intertropicale et de grands fleuves tels que l'Amazone, l'Orénoque et le Congo. Il en résulte une forte stratification en sel qui peut influencer le mélange vertical, et donc la température de surface de la mer et les flux air-mer. L'objectif de cette thèse est d'étudier l'influence de la salinité – et en particulier de la forte stratification en sel – sur le climat de l'océan Atlantique tropical. Pour ce faire, un modèle couplé océan-atmosphère au 1/4° de la région est développé, utilisant NEMO comme composante océanique, WRF comme composante atmosphérique et OASIS comme coupleur. L'utilisation d'un modèle couplé océan-atmosphère permet de prendre en compte toutes les interactions air-mer et les processus de rétroaction, dont l'impact sur le climat régional a déjà été mis en évidence et qui sont au cœur de cette étude. Une série de tests de sensibilité a ensuite été menée avec ce modèle, afin d'évaluer l'impact de processus de plus en plus fins. Tout d'abord, l'impact de la stratification en sel totale sur la température de surface de la mer et sur les flux air-mer est évalué en la retirant du modèle. Ensuite, les fleuves Amazone et Orénoque, contributeurs majeurs à la stratification en sel dans l'Atlantique tropical, sont retirés du modèle. La variabilité interannuelle du débit des fleuves est ensuite étudiée pour quantifier l'impact des crues extrêmes de l'Amazone. Enfin, l'expérience sans stratification en sel est menée dans un climat futur, où plusieurs des variables clés identifiées dans le climat actuel sont très distinctes de leur état actuel, permettant une compréhension plus profonde des processus en jeu. De ces tests de sensibilité se dégage un mécanisme dans l'Atlantique tropical nord-ouest en été, similaire quelle que soit la force de la stratification en sel. La présence de la stratification en sel diminue le refroidissement par mélange vertical, ce qui entraîne une augmentation de la température de surface de la mer. Ce réchauffement est ensuite modéré par une rétroaction négative de l'atmosphère : la réponse océanique est atténuée par le biais d'une diminution du flux thermique, qui est principalement due à une augmentation de la perte de chaleur latente, mais aussi à une réduction du rayonnement solaire atteignant la surface de l'océan, en lien avec une augmentation de la convection profonde et de la couverture nuageuse et des précipitations associées. Le changement de température final est déterminé par l'équilibre entre le réchauffement dû au mélange vertical et le refroidissement dû à la rétroaction atmosphérique, les deux dépendant du type de test de sensibilité. Cependant, le changement de température de surface de la mer résultant est toujours relativement faible (0,5°C au maximum). En hiver, les impacts de la stratification en sel sont beaucoup plus faibles, probablement en raison d'une couche mélangée plus profonde en cette saison. Des changements de température de surface de la mer sont finalement observés dans la région de la langue d'eau froide, liés à des modifications de la profondeur de la thermocline. Des variations de température en subsurface sont présentes tout au long de l'année, mais la saisonnalité de l'apparition de l'upwelling détermine le moment où les changements de température apparaissent à la surface. Dans cette thèse, l'impact de la stratification en sel sur le climat moyen de l'Atlantique tropical est étudié, mais

le modèle développé ici pourrait être adapté pour étudier l'impact de la stratification en sel sur les cyclones. En effet, le panache de l'Amazone est traversé par de nombreux cyclones tropicaux, et l'impact de la stratification en sel qui lui est associée reste controversé.

Remerciements

Cette thèse n'aurait jamais vu le jour sans le soutien de nombreuses personnes, à qui je souhaite exprimer toute ma gratitude. J'espère n'en oublier aucune (je m'en excuse sinon...).

Contrairement à de nombreux doctorants, cette thèse n'est pas l'aboutissement d'un rêve ou l'accomplissement d'une vocation, mais plutôt la conséquence d'une série de hasards. L'un de ces hasards a fait qu'il y a 5 ans, fraîchement sortie de mon école d'ingénieur, j'aie postulé pour un VIA au Pérou avec l'IRD, en océanographie. Le hasard a ensuite voulu que 2 chercheurs du LOCEAN, François Colas et Vincent Echevin, aient accepté ma candidature malgré mon manque flagrant de compétences en la matière. Je voudrais donc commencer par vous remercier chaleureusement tous les deux de m'avoir laissé une chance, et ce faisant de m'avoir ouvert la voie vers la recherche, de m'avoir initiée à l'océanographie et de m'avoir donné goût à la modélisation. L'idée d'une thèse n'aurait jamais germée dans mon esprit sans vous !

Je voudrais ensuite remercier du fond du cœur Julien et Fabien, mes deux encadrants de thèse qui m'ont accompagnée (et supportée !) tout au long de ces trois années. Merci tout d'abord d'avoir imaginé ce sujet de thèse pluridisciplinaire et ambitieux, à l'interface entre l'océan et l'atmosphère, entre la science et la technique. Merci de m'avoir accompagnée dans mon appropriation du sujet et des connaissances théoriques nécessaires, et de m'avoir ensuite fait confiance et laissé le champ libre pour étudier ce que je voulais. Merci pour vos grandes compétences scientifiques, qui se sont soldées par de passionnantes conversations, mais merci surtout pour vos qualité humaines, votre patience et votre gentillesse. Merci Julien d'avoir eu ta porte toujours grande ouverte, prêt à répondre à mes dizaines de questions. Merci Fabien d'avoir su te montrer si disponible, même à l'autre bout du monde, et de m'avoir guidée et cadrée notamment dans la fin de thèse, pas toujours facile à gérer.

Je voudrais également remercier Sébastien Masson et Hervé Giordani d'avoir apporté un œil neuf et des idées nouvelles lors des comités de thèse. Merci aussi aux rapporteurs de cette thèse, Gilles Reverdin et Gregory Foltz pour la lecture attentive et les remarques constructives sur le manuscrit, ainsi qu'à Sabrina Speich et Gaëlle de Coëtlogon pour avoir accepté d'évaluer ce travail de thèse. Merci à tous pour les échanges fructueux lors de la soutenance.

Ces heures passées au LEGOS auraient été bien fades sans votre présence à tous !
Merci donc à tous les doctorants et CDD avec qui j'ai partagé tant de bons moments, et tant de pauses thé. Merci à Romain, Marion et Lise pour les heures de potins (bon ok ça s'applique à pleins de gens, mais surtout à vous !). Merci à Adé d'avoir partagé toutes tes excellentes lectures avec moi, de m'avoir aidé à lancer la chorale et de m'avoir mis pleins de super chansons dans la tête ! Merci à Audrey et Lisa pour toutes les conversations, scientifiques ou non. Merci à Simon et Pierre pour votre excellent boulot de respo doctorants. Merci à tous les choristes du LEGOS (et affiliés) : Adé, Pierre, Audrey, Lise, Lisa, Simon, Gabriela, Julia, Morgane, Benjamin, Juliette, Arne, Antonin, et les petits nouveaux : Elisa, Adrien (et Simon II un jour peut-être ?). Bravo à vous de vous être lancés ! Merci à Alice, Audrey H, Cori,

Aude, toutes ces "vieilles" qui m'ont si bien accueillies quand je suis arrivée. Merci à Marco d'avoir partagé mon bureau pendant 2 ans et de m'avoir aidé à entretenir mon espagnol ! Merci enfin à tous les autres doctorants et CDD que j'ai croisé de près ou de loin pendant ces trois années : Nolwenn, Micaël, Michel, Marion B, Margot, Hahn, Mahmoud, Quentin, Wassim, Tung, Thai, Victorien, et j'en oublie sûrement...

Merci à Brigitte, Agathe, Martine et Nadine, puis Catherine et Sandra, à l'équipe info, Geoffray puis Caroline, ainsi qu'à toute l'équipe de direction passée et présente, Alexandre, Frédéric, Bertrand, de nous aider au quotidien et de faire tourner cette machinerie énorme qu'est le LEGOS. Merci aussi à toute l'école doctorale, et particulièrement Geneviève Soucail, Tanya Robinson et Adrien Bru pour tout le temps consacré et l'aide apportée pour les procédures et le suivi de nos thèses.

Une thèse, c'est aussi des moments de détente pour se ressourcer. Pour ça, un grand merci à la team St-Mich' (Margaux, Julien, Claire, Yann) et à la team LEGOS (Romain, Pierre, Lisa, Adé, Audrey, Lise) pour toutes les soirées jeux, les randos, les aprèms escalade et les dégustations de fromage qui ont su égayer nos week-ends. Un merci tout particulier à Margaux pour les séances de "footing"-papotage et à Romain pour tous ces bons moments à Billière, et pour nous avoir lancé des défis jeux toujours plus grands (Pandemic expert, puis légendaire, puis Robinson !). Merci enfin à Marion pour les week-ends à Autrans et Lafigère, et d'être toujours là malgré toutes ces années à me supporter !

Si j'avais voulu respecter un ordre chronologique, il aurait bien sûr fallu que je commmence par vous : merci à mes parents et à ma sœur de m'avoir soutenue, écoutée et confortée dans mes choix, à chaque étape de ma vie, et d'avoir été là jusqu'au bout (vous avez même fait l'effort de venir supporter des heures de soutenance en anglais !). Je sais tout ce que je vous dois, et je ne serais pas arrivée là sans vous. Merci aussi à toute ma famille et ma belle-famille pour leur bonne humeur constante et leur présence dans les moments durs.

Enfin Flo, merci pour ton soutien, merci pour ton amour, merci pour tout. Sans toi je ne suis rien.

Contents

Acronyms

English acronyms

AMM	*Atlantic Meridional Mode*
AMJ	*April-May-June*
ASO	*August-September-October*
BL	*Barrier Layer*
BLT	*Barrier Layer Thickness*
CMIP	*Coupled Model Intercomparison Project*
CT	*Cold Tongue*
DJF	*December-January-February*
ENSO	*El Niño Southern Oscillation*
EUC	*Equatorial Undercurrent*
GCM	*General Circulation Model*
GHG	*Greenhouse Gases*
HF	*Highest Floods*
ITCZ	*Intertropical Convergence Zone*
IPCC	*Intergovernmental Panel on Climate Change*
JAS	*July-August-September*
JJA	*June-July-August*
LF	*Lowest Floods*
MMEM	*Multi-Model Ensemble Mean*
ML	*Mixed Layer*
MLD	*Mixed Layer Depth*
NEMO	*Nucleus for European Modeling of the Ocean*
NBC	*North Brazil Current*
NBUC	*North Brazil Undercurrent*

NEC *North Equatorial Current*

NECC *North Equatorial Countercurrent*

NWTA *Northwestern Tropical Atlantic*

NH *Northern Hemisphere*

PGW *Pseudo-Global Warming*

SEC *South Equatorial Current*

SH *Southern Hemisphere*

SSS *Sea Surface Salinity*

SST *Sea Surface Temperature*

STD *Standard Deviation*

SSTA *Sea Surface Temperature Anomaly*

TC *Tropical Cyclone*

WRF *Weather Research and Forecasting*

Acronymes français

GIEC *Groupe d'experts Intergouvernemental sur l'Évolution du Climat*

SSM *Salinité de Surface de la Mer*

TSM *Température de Surface de la Mer*

ZCIT *Zone de Convergence Intertropicale*

General introduction

Salinity is one of the key physical variables of the ocean. It originates from continental erosion and hydrothermal vents. It affects the ocean circulation through its contribution to seawater density, and is one of the main drivers of the meridional overturning circulation (also known as thermohaline circulation). At the ocean surface, salinity is modulated by evaporation, precipitation, river runoff and the melting or formation of ice, which makes it a good tracer of the global water cycle (e.g. Durack, 2015). Salinity usually ranges from 31 to 38 PSU, but it can reach higher values in strong evaporative areas such as the Mediterranean sea, or lower values in river plumes for instance. Its regional variations depend on the process that predominates locally. At the high latitudes of the Atlantic Ocean, sea ice formation and high evaporation increase locally the salinity and densifies the surface waters. This causes the cold salty surface waters to sink, forming deep waters and initiating the cold branch of the thermohaline circulation (e.g. Warren, 1983; Killworth, 1983). In the subtropical areas, evaporation prevails and results in a high sea surface salinity (SSS). Finally, in the tropics, precipitation is high and reduces the SSS, leading to the development of a strong salinity stratification.

Salinity stratification can locally affect sea surface temperature (SST) through its control on the depth of the mixed layer (ML). The ML is the ocean surface layer and has homogenized properties (temperature, salinity, and thus density). It is warmer and often less salty than the subsurface. The ML is separated from the deep ocean by a vertical density gradient, the pycnocline, which is generally controlled by the temperature gradient, the thermocline. In areas of strong salinity stratification, however, the depth of the pycnocline - and thus the depth of the ML - can also be partly controlled by salinity. Strong salinity stratification can then induce a ML thinning and cause a change in its heat content. However, these changes are complex and sometimes opposite. With a 1D model of the ML, Miller (1976) showed that strong salinity stratification inhibits the entrainment of cold water by vertical mixing at the base of the ML: when stratification is stronger, the ML is less reactive to wind anomalies for instance, and it does not deepen as much. This reduced entrainment leads to positive SST anomalies. But in case of surface heat loss events, in winter or during the night for instance, a thinner ML results in an increased cooling of the ML.

In regions where salinity stratification is particularly strong, barrier layers (BLs) sometimes develop. These are intermediate layers that can appear between the ML and the deep ocean. In areas of strong salinity stratification, the pycnocline can sometimes be entirely controlled by salinity, and the thermocline can become deeper than the pycnocline. The barrier layer is then defined as the layer between the base of the ML and the top of the thermocline (Godfrey and Lindstrom, 1989; Lukas and Lindstrom, 1991). The presence of a BL implies that the mixing at the base of the ML does not cool the ML, since the temperature of the water in the BL is the same as in the ML: the result is an insulation of the warm ML from the cooler subsurface (Sprintall and Tomczak, 1992). BLs were originally observed in the tropical Pacific Ocean (e.g. Lukas and Lindstrom, 1991), but are also present in the tropical Atlantic.

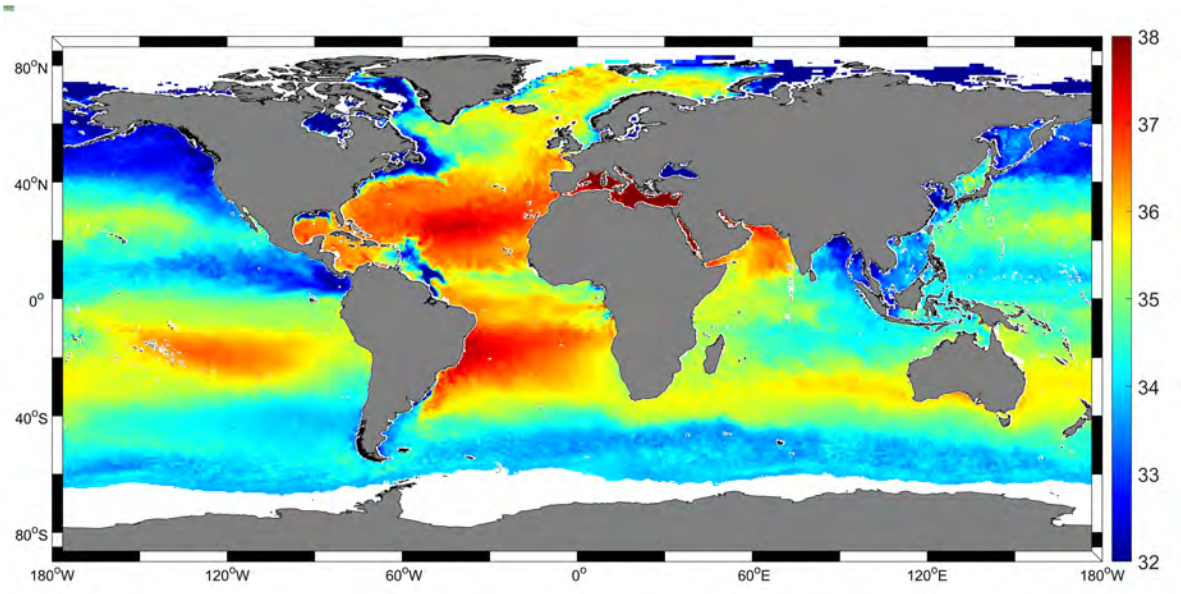

Figure 0.1: Sea surface salinity [PSU] from ESA-CCI, average between 2010 and 2018.
Salinité de surface de la mer [PSU] provenant de ESA-CCI, moyenne entre 2010 et 2018.

They were first observed in the western tropical Atlantic (Pailler et al., 1999; de Boyer Montégut et al., 2007a; Mignot et al., 2009) and more recently in the northeastern Gulf of Guinea (Dossa et al., 2019).

The tropical Atlantic Ocean exhibits a very contrasted surface salinity distribution (Figure 0.1). High SSS areas are located in the subtropical gyres, linked with strong evaporation and low precipitation in these zones. Low SSS areas are due to large amounts of freshwater, supplied by four of the world's largest rivers in terms of discharge (Amazon, Congo, Orinoco and Niger), and high precipitation associated with the Intertropical Convergence Zone (ITCZ). This freshwater supply induces a strong salinity stratification in the Amazon-Orinoco and the Congo river plumes, as well as in the ITCZ (e.g. Pailler et al., 1999; Maes and O'Kane, 2014).

In the western tropical Atlantic, BL and salinity stratification impact on the SST and the air-sea heat fluxes has been extensively studied, but the past conclusions diverge. Observational studies suggest a strong impact of BL and salinity stratification on the SST of 1 to 2°C (Pailler et al., 1999; Ffield, 2007; Foltz and McPhaden, 2009; Fournier et al., 2017), whereas modeling studies show weak impact on the SST (Carton, 1991; Masson and Delecluse, 2001; Breugem et al., 2008; Balaguru et al., 2012a). This controversy also underlies the issue of cyclones intensification in the western tropical Atlantic, with some studies concluding that BL play a significant role in this intensification (Balaguru et al., 2012b; Grodsky et al., 2012; Reul et al., 2014; Androulidakis et al., 2016), and other studies showing the opposite (Newinger and Toumi, 2015; Hernandez et al., 2016).

The purpose of this thesis is to evaluate the impact of salinity on the tropical Atlantic Ocean SST, air sea-fluxes, and more generally on the regional ocean and climate. To do so,

we develop a coupled model configuration of the region, and we perform a series of sensitivity tests with it.

The previous modeling studies evaluating the impact of BL and salinity stratification on the SST, the air-sea heat fluxes and the cyclones were mostly conducted using forced ocean models. This prevents to take into account the ocean-atmosphere feedback processes, which are very important in this region. Indeed, in the tropical Atlantic, air-sea interactions drive the regional climate and its modes of variability, which affect continental rainfall over Africa and South America (Caniaux et al., 2011; Giannini et al., 2004; Meynadier et al., 2016; Lübbecke et al., 2018; Crespo et al., 2019), tropical cyclone formation (Vimont and Kossin, 2007; Wang et al., 2008), and biological productivity (Christian and Murtugudde, 2003; Radenac et al., 2020). It is therefore of great importance to use models that include these feedback processes. To this end, we develop a coupled ocean-atmosphere configuration of the tropical Atlantic Ocean at a 1/4° resolution. We use the ocean model NEMO coupled with the atmospheric model WRF. The parameterization and validation of the configuration are presented in Chapter 2.

Chapter 3 addresses the controversy described previously by revisiting the question of the impact of salinity stratification and BL on the tropical Atlantic climate. To do so, we perform and analyze two simulations in which the salinity stratification is either included or removed from the ocean model (Vialard and Delecluse, 1998).

The next step is to evaluate more specifically the effect of river discharge, and in particular the Amazon and Orinoco discharge. This is motivated by the fact that a large part of the salinity stratification of the tropical Atlantic is due to river runoff. Moreover, numerous studies have investigated this issue (Masson and Delecluse, 2001; Ffield, 2007; Huang and Mehta, 2010; Coles et al., 2013; Newinger and Toumi, 2015; Hernandez et al., 2016; Fournier et al., 2017; Jahfer et al., 2020), and a controversy similar as before appears, with observational and modeling studies having distinct conclusions. These studies were mainly conducted either with observations or with forced models, and the use of a coupled model can provide new insights on the subject. In Chapter 4, we analyze a simulation where Amazon and Orinoco rivers are removed to study the effect on SSS and SST.

These last three decades, the hydrological cycle of the Amazon basin has intensified and extreme floods and droughts are more and more frequent (Espinoza et al., 2009a; Gloor et al., 2013, 2015; Marengo and Espinoza, 2016; Barichivich et al., 2018). The impact of this runoff interannual variability has been little studied, and once again, the conclusions of the different studies diverge. In Chapter 5, we perform another set of sensitivity experiments, where we use alternatively monthly interannual runoff and a monthly runoff climatology. This allows us to quantify the impact of interannual variability of river runoff compared to the rest of the variability.

Finally, we investigate the modulation of the relationship between salinity stratification and SST in a future climate. Indeed, several variables and processes relevant for the impact of salinity stratification on SST will change in the future (e.g. mixed layer depth, ocean stratification, intensification of the water cycle). In Chapter 6, we modify the ocean and

atmospheric forcings in order to model a climate corresponding to a business-as-usual scenario at the end of the 21st century (2086-2100). We then carry out a sensitivity test with and without salinity stratification, and compare it with the results in the present climate discussed in Chapter 3.

The western tropical Atlantic Ocean is regularly crossed by strong tropical cyclones, striking highly populated areas such as the Antilles and the United States. The intense salinity stratification of the area – induced by the Amazon and Orinoco rivers and by precipitation in the ITCZ – could intensify them, and yet we still do not understand the impact of this salinity structure on the regional climate. A better knowledge of the role of salinity stratification in air-sea interactions is therefore essential, and is a first step toward a better understanding of its impact on cyclones. More generally, salinity has long been considered a key variable in the climate of the tropical Atlantic Ocean, although its exact role remains unclear. This thesis therefore aims at a better understanding of the influence of salinity on the regional climate.

Introduction générale

La salinité est l'une des variables physiques clés de l'océan. Elle provient de l'érosion continentale et de sources hydrothermales. Elle affecte la circulation océanique par sa contribution à la densité de l'eau de mer, et est l'un des principaux moteurs de la circulation méridienne de retournement (également connue sous le nom de circulation thermohaline). À la surface de l'océan, la salinité est modulée par l'évaporation, les précipitations, le ruissellement et la fonte ou la formation de glace, ce qui en fait un bon traceur du cycle de l'eau (Durack, 2015). La salinité est généralement comprise entre 31 et 38 PSU, mais elle peut atteindre des valeurs plus élevées dans des zones de forte évaporation comme la mer Méditerranée, ou des valeurs plus faibles dans certains panaches fluviaux par exemple. Ses variations régionales dépendent du processus qui prédomine localement. Aux hautes latitudes de l'océan Atlantique, la formation de glace et une forte évaporation augmentent localement la salinité, ce qui densifie les eaux de surface. Les eaux de surface froides et salées plongent alors, participant à la formation des eaux profondes et initiant la branche froide de la circulation thermohaline (e.g. Warren, 1983; Killworth, 1983). Dans les zones subtropicales, l'évaporation prédomine et résulte en une forte salinité de surface de la mer (SSM). Finalement, dans les tropiques, les précipitations sont fortes et réduisent la SSM, entrainant le développement d'une forte stratification en sel.

La stratification en sel peut affecter la température de surface de la mer (TSM) en modifiant la profondeur de la couche mélangée. La couche mélangée est la couche de surface de l'océan, et présente des propriétés homogènes (température, salinité, et donc densité). Elle est plus chaude et souvent moins salée que l'océan profond, lui-même froid et salé. La couche mélangée est séparée de l'océan profond par un gradient vertical de densité, la pycnocline, qui est généralement contrôlé par le gradient de température, la thermocline. Dans des zones de fortes stratification en sel cependant, la profondeur de la pycnocline - et donc la profondeur de la couche mélangée - peut être aussi en partie contrôlée par la salinité. La forte stratification en sel peut alors amincir la couche mélangée et modifier son contenu thermique. Ces changements sont toutefois complexes, et parfois contradictoires. À l'aide d'un modèle 1D de la couche mélangée, Miller (1976) a montré qu'une forte stratification en sel peut empêcher l'entraînement d'eau froide dû au mélange vertical à la base de la couche mélangée : quand la stratification est plus forte, la couche mélangée est moins réactive aux anomalies de vent par exemple, et elle ne s'approfondit pas autant. Cette réduction de l'entraînement conduit à une augmentation de la TSM. Mais dans le cas où l'océan perd de la chaleur en surface, en hiver ou pendant la nuit par exemple, une couche mélangée plus mince entraîne un refroidissement accru de celle-ci, et donc une diminution de la TSM.

Dans les régions où la stratification en sel est particulièrement forte, des couches barrières peuvent parfois se développer. Il s'agit de couches intermédiaires qui peuvent apparaître entre la couche mélangée et l'océan profond. Dans des zones de fortes stratification en sel, il peut arriver que la profondeur de la pycnocline soit entièrement contrôlée par la salinité, et que la thermocline devienne plus profonde que la pycnocline. La couche barrière est

alors définie comme la couche située entre la base de la couche mélangée et le sommet de la thermocline (Godfrey and Lindstrom, 1989; Lukas and Lindstrom, 1991). La présence d'une couche barrière implique que le mélange à la base de la couche mélangée ne refroidit pas celle-ci, car la température de l'eau dans la couche barrière est la même que dans la couche mélangée : il en résulte une isolation de la couche mélangée chaude par rapport à la subsurface froide (Sprintall and Tomczak, 1992). Les couches barrières ont d'abord été détectées dans l'océan Pacifique (e.g. Lukas and Lindstrom, 1991), mais sont également présentes dans l'océan Atlantique tropical. Elles ont d'abord été observées dans l'ouest de l'océan Atlantique tropical (Pailler et al., 1999; de Boyer Montégut et al., 2007a; Mignot et al., 2009) et plus récemment dans le nord-est du golfe de Guinée (Dossa et al., 2019).

L'océan Atlantique tropical présente une distribution de salinité de surface très contrastée (Figure 0.1). Des zones de fortes SSM sont localisées dans les gyres subtropicaux, dues à une forte évaporation et de faibles précipitations. Des zones de faibles SSM sont dues à l'apport de grandes quantités d'eau douce, fournies par quatre des plus grands fleuves du monde en terme de débit (l'Amazone, le Congo, l'Orénoque et le Niger) et par de fortes précipitations associées à la Zone de Convergence Intertropicale (ZCIT). Cet apport d'eau douce induit une forte stratification en sel dans le panache de l'Amazone et de l'Orénoque, dans le panache du Congo, ainsi que dans la ZCIT (e.g. Pailler et al., 1999; Maes and O'Kane, 2014).

Dans l'ouest de l'océan Atlantique tropical, l'impact des couches barrières et de la stratification en sel sur la TSM et sur les flux de chaleur air-mer a été largement étudié, mais les conclusions divergent. Les études observationnelles suggèrent un fort impact des couches barrières et de la stratification en sel sur la TSM d'un à deux degrés (Pailler et al., 1999; Ffield, 2007; Foltz and McPhaden, 2009; Fournier et al., 2017), tandis que les études de modélisation montrent au contraire un faible impact sur la TSM (Carton, 1991; Masson and Delecluse, 2001; Breugem et al., 2008; Huang and Mehta, 2010; Balaguru et al., 2012a; Jahfer et al., 2020). Cette controverse sous-tend également la question de l'intensification des cyclones dans l'ouest de l'Atlantique tropical, certaines études concluant que les couches barrières jouent un rôle important dans cette intensification (Balaguru et al., 2012b; Grodsky et al., 2012; Reul et al., 2014; Androulidakis et al., 2016), alors que d'autres études montrent le contraire (Newinger and Toumi, 2015; Hernandez et al., 2016).

Le but de cette thèse est d'évaluer l'impact de la salinité sur la TSM et les flux de chaleur air-mer de l'océan Atlantique tropical, et plus généralement sur les variables océaniques et le climat régional. Pour ce faire, nous avons développé une configuration couplée de la région, et effectué une série de tests de sensibilité avec celle-ci.

Les précédentes études de modélisation évaluant l'impact de la stratification de la BL et de la salinité sur la SST, les flux de chaleur air-mer et les cyclones ont été réalisées principalement à l'aide de modèles océaniques forcés. Ceci empêche de prendre en compte les processus de rétroaction océan-atmosphère, qui sont pourtant très importants dans cette région. En effet, les interactions océan-atmosphère influencent le climat de l'Atlantique tropical et ses modes de variabilité, affectant les précipitations continentales en Afrique et en Amérique du Sud, (Caniaux et al., 2011; Giannini et al., 2004; Meynadier et al., 2016; Lübbecke et al., 2018; Crespo et al., 2019), la formation des cyclones tropicaux (Vimont and Kossin, 2007;

Wang et al., 2008), et la productivité biologique (Christian and Murtugudde, 2003; Radenac et al., 2020). Il est donc nécessaire d'utiliser des modèles incluant ces processus de rétroaction. Pour ce faire, nous avons développé une configuration couplée océan-atmosphère de l'océan Atlantique tropical à une résolution de 1/4°. Nous avons utilisé le modèle océanique NEMO que nous avons couplé avec le modèle atmosphérique WRF. La paramétrisation et la validation de la configuration sont présentées dans le Chapitre 2.

Le Chapitre 3 aborde la controverse décrite précédemment en réexaminant la question de l'impact de la stratification en sel et de la couche barrière sur le climat de l'Atlantique tropical. Pour ce faire, nous effectuons et analysons deux simulations dans lesquelles la stratification en sel est soit incluse, soit retirée du modèle océanique (Vialard and Delecluse, 1998).

L'étape suivante consiste à évaluer plus spécifiquement l'effet du débit des fleuves, et en particulier du débit de l'Amazone et de l'Orénoque. Une première motivation vient du fait qu'une grande partie de la stratification en sel de l'Atlantique tropical est due à l'apport d'eau douce des fleuves. De plus, de nombreuses études se sont penchées sur cette question (Masson and Delecluse, 2001; Ffield, 2007; Huang and Mehta, 2010; Coles et al., 2013; Newinger and Toumi, 2015; Hernandez et al., 2016; Fournier et al., 2017; Jahfer et al., 2020), et une controverse similaire à la précédente apparaît : les études utilisant des observations et les études de modélisation ont des conclusions différentes. Enfin, ces études ont là encore été principalement menées avec des observations ou des modèles forcés, et l'utilisation d'un modèle couplé peut apporter de nouvelles perspectives sur le sujet. Dans le Chapitre 4, nous effectuons donc une simulation où l'Amazone et l'Orénoque sont enlevés, afin d'analyser l'effet sur la SSM et la TSM.

Ces trois dernières décennies, le cycle hydrologique du bassin amazonien s'est intensifié et les inondations et sécheresses extrêmes sont de plus en plus fréquentes (Espinoza et al., 2009a; Gloor et al., 2013; Marengo and Espinoza, 2016; Barichivich et al., 2018). L'impact de cette variabilité interannuelle du débit a été peu étudié, et une fois encore les conclusions des différentes études divergent. Dans le Chapitre 5, nous réalisons deux autres tests de sensibilité, où nous utilisons le débit interannuel mensuel pour l'un, et une climatologie de débit mensuel pour l'autre. Cela permet de quantifier l'impact de la variabilité interannuelle du débit par rapport au reste de la variabilité.

Enfin, nous étudions l'impact de la stratification en sel dans un climat futur. En effet, plusieurs variables et processus importants concernant l'impact de la stratification en sel sur la TSM vont changer dans le futur (e.g. profondeur de la couche mélangée, stratification de l'océan, intensification du cycle de l'eau). Dans le Chapitre 6, nous modifions les forçages océaniques et atmosphériques afin de modéliser un climat correspondant à un scénario "business-as-usual" à la fin du 21ème siècle (2086-2100). Nous reproduisons ensuite le test de sensibilité avec et sans stratification en sel, et nous comparons avec les résultats dans le climat présent discutés dans le Chapitre 3.

De violents cyclones tropicaux traversent régulièrement l'ouest de l'océan Atlantique tropical et frappent des zones très peuplées comme les Antilles ou les États-Unis. La stratification en sel intense dans cette zone – induite par les fleuves Amazone et Orénoque et par les précip-

itations dans la ZCIT – pourrait les intensifier, et pour autant nous ne comprenons toujours pas l'impact de cette stratification en sel sur le climat régional. Une meilleure connaissance du rôle de la stratification en sel dans les interactions air-mer est donc essentielle, et constitue un premier pas vers une meilleure compréhension de son impact sur les cyclones. Plus généralement, la salinité a longtemps été considérée comme une variable clé du climat de l'océan Atlantique tropical, bien que son rôle exact reste incertain. Cette thèse vise donc à améliorer notre compréhension de l'influence de la salinité sur le climat régional.

Chapter 1

Background

Contents

1.1 SSS variability of the tropical Atlantic Ocean

The tropical Atlantic Ocean presents warm waters at its surface - over 26-28°C - allowing the development of deep convection (e.g. Sabin et al., 2013; Evans and Webster, 2014) and inducing heavy precipitation in the ITCZ. This precipitation is distributed over the ocean, locally decreasing the SSS, and over the continents, resulting in strong runoff. This runoff in turn decreases the SSS at the location of river plumes. The tropical Atlantic is also a region presenting strong evaporation rates, especially in the subtropical gyres, resulting in SSS increase. SSS variability of the tropical Atlantic Ocean is thus mainly driven by changes in precipitation, evaporation and runoff, but also in currents, winds and tides (e.g. Masson and Delecluse, 2001; Nikiema et al., 2007; Molleri et al., 2010; Coles et al., 2013; Foltz et al., 2015; Ruault et al., 2020). In the following, we will describe the main processes responsible for the SSS variability in the various regions of the tropical Atlantic Ocean.

1.1.1 Precipitation associated with the intertropical convergence zone

The ITCZ is located in the tropics, and is the region of convergence of the trade winds. It is characterized by a belt of clouds around the Earth (Figure 1.1). It corresponds to the ascending branch of the Hadley cell, which is the mechanism of heat redistribution from the Equator to the subtropical regions. The convergence of the moist trade winds combined with warm SST in the tropics lead to the rise of air masses. As they ascend, these air masses

Figure 1.1: Intertropical Convergence Zone in the tropical Atlantic Ocean. Satellite image from NASA Worldview, modified by Christoph Kersten/GEOMAR.

cool and condensate, forming deep convective clouds and leading to intense precipitation. The location of the ITCZ varies from one ocean basin to the other. In the tropical Atlantic Ocean, the ITCZ is localized north of the geographical Equator, varying from 1°N in March to 9°N in August (Fonseca et al., 2004; Schneider et al., 2014).

ITCZ variability is associated with variability in precipitation. Precipitation brings freshwater at the surface of the tropical Atlantic, locally decreasing salinity. This is particularly important in the central tropical Atlantic, in the ITCZ, and is the main process driving the SSS seasonal and interannual variability in this region (Grodsky et al., 2006; Foltz and McPhaden, 2008; Coles et al., 2013; Da-Allada et al., 2013; Foltz et al., 2015; Awo et al., 2018). Moreover, precipitation strongly affects the SSS in the Gulf of Guinea, which is also under the influence of the ITCZ (Coles et al., 2013; Da-Allada et al., 2013, 2014). Nevertheless, Hu et al. (2004) showed that precipitation alone cannot explain the low SSS pattern in the northwestern tropical Atlantic, while Ferry and Reverdin (2004) showed that precipitation does not have a strong impact on SSS interannual variability in the region. Another freshwater source is needed to explain the SSS variability there: river runoff.

1.1.2 River runoff

The tropical Atlantic Ocean is the recipient of four of the largest rivers in the world: the Amazon, the Congo, the Orinoco and the Niger. Together, they account for almost 25% of the global river discharge (Dai and Trenberth, 2002). The Amazon is by far the largest of them, and has therefore the largest impact on SSS. Its plume of low SSS extends over several thousands of kilometers and merges with the Orinoco plume (e.g. Hu et al., 2004; Molleri et al., 2010; Coles et al., 2013). The Congo river is the second largest river, but has been little studied. Its plume extends over a few hundred kilometers, and its impact on SSS is relatively local (Denamiel et al., 2013; Hopkins et al., 2013; Berger et al., 2014).

Several modeling studies assessed the impact of the Amazon and/or Orinoco on the SSS by removing the river discharge in their models (Masson and Delecluse, 2001; Coles et al., 2013; Newinger and Toumi, 2015; Hernandez et al., 2016; Giffard et al., 2019; Varona et al., 2019). They all found a strong impact on SSS, with a decrease in SSS of -2 to -4 PSU on annual average in the Amazon-Orinoco plume (Masson and Delecluse, 2001; Coles et al., 2013; Giffard et al., 2019). Maximum changes are observed in spring and summer northwestward of the Amazon mouth, and year-round near the Amazon and the Orinoco mouths (Newinger and Toumi, 2015; Varona et al., 2019). Using observations, Zeng et al. (2008) found a strong correlation between the plume area and the Amazon discharge, while Molleri et al. (2010) showed that river discharge was the main driver of the plume area seasonal variability. Moreover, Masson and Delecluse (2001) observed that the amplitude of SSS seasonal cycle in the western tropical Atlantic is controlled by the Amazon discharge. However, the impact of river runoff on the SSS interannual variability remains a matter of debate, some studies showing that the Amazon interannual variability impacts the SSS interannual variability (Hellweger and Gordon, 2002; Salisbury et al., 2011; Gouveia et al., 2019a; Jury, 2019), while others suggest the contrary (Grodsky et al., 2014, 2015; Fournier et al., 2017).

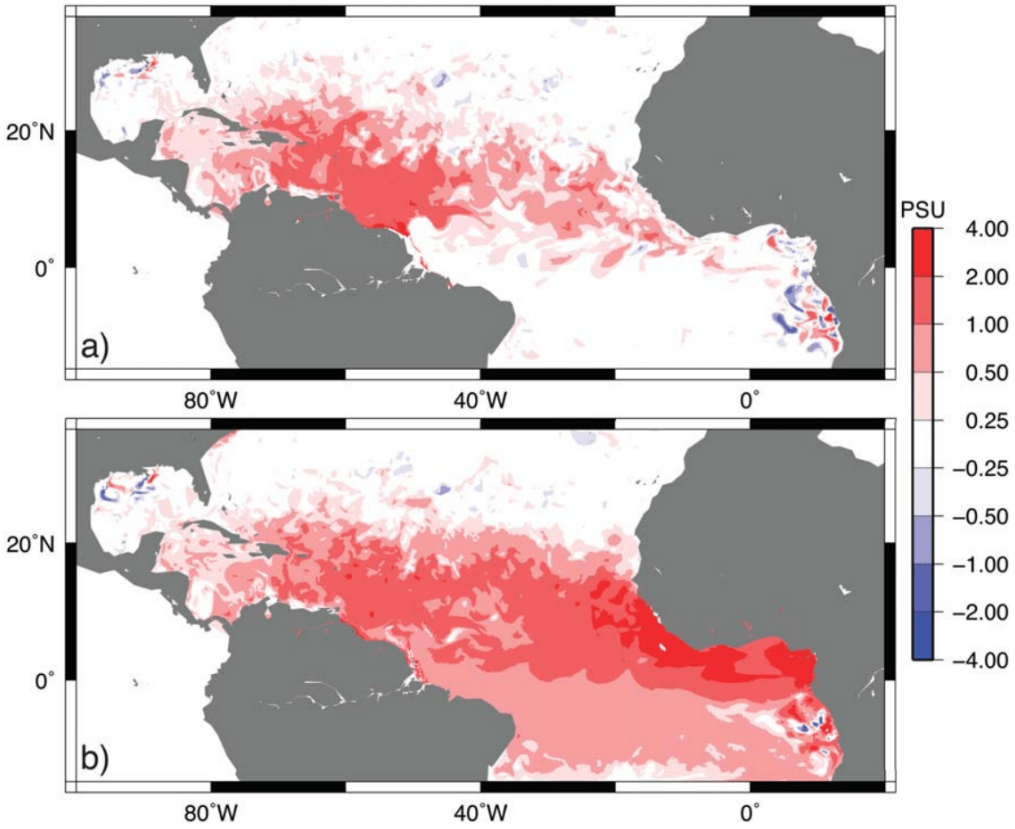

Figure 1.2: Surface salinity anomaly in January after 4 model years (1983) for a) NoRiver-Control experiments and b) NoPrecip-Control experiments. NoRiver is the Control simulation without Amazon and Tocantins rivers. NoPrecip is the Control simulation without precipitation from the Equator to 10°N. Reproduced from Coles et al. (2013).

Coles et al. (2013) compared the impact of precipitation and Amazon runoff on SSS in the whole tropical Atlantic (Figure 1.2). They observed a significant effect of Amazon in the northwestern tropical Atlantic (-1 to -2 PSU) and in the central tropical Atlantic (-0.5 to -1 PSU). The effect of precipitation, however, is broader and stronger: it impacts the whole tropical Atlantic from 10°S to 20°N, with anomalies ranging from -2 to -4 PSU in the Gulf of Guinea, and -1 to -2 PSU in the central tropical Atlantic. The northwestern tropical Atlantic is the only region where Amazon discharge contribution to SSS is equal to or greater than that of precipitation. Coles et al. (2013) also underlined the importance of the currents in SSS variability, and we will now describe them.

1.1.3 Currents system

The tropical Atlantic Ocean circulation (Figure 1.3) is mainly zonal and wind-driven (Fieux, 2010). At the surface, the North Equatorial Current (NEC) and the South Equatorial Current (SEC) are forced by the trade winds and flow westward. They are both composed of several

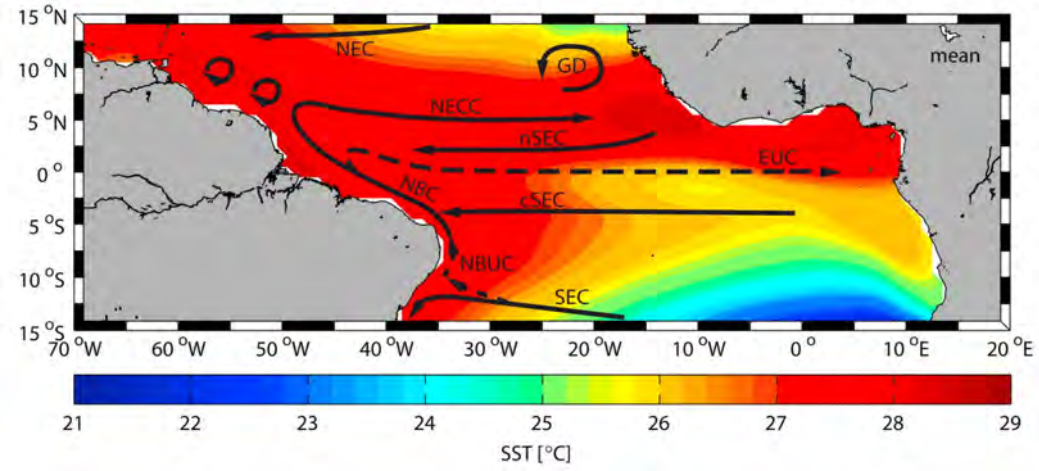

Figure 1.3: Schematic of surface (solid) and thermocline (dashed) tropical Atlantic currents, including the North Equatorial Countercurrent (NECC), North Equatorial Current (NEC), South Equatorial Current (SEC) along with its northern and central branches (nSEC, cSEC), North Brazil Current and Undercurrent (NBC, NBUC), Equatorial Undercurrent (EUC), as well as the cyclonic circulation around the Guinea Dome (GD), superimposed on the mean SST for the period October 1992 to December 2009. Reproduced from Hormann et al. (2012).

branches. The southern branch of the SEC feeds the North Brazil Undercurrent (NBUC), while its central branch feeds the North Brazil Current (NBC). The NBC flows northward along the South-American coast. In winter and spring, it is weak and continues along the coast towards the Lesser Antilles, feeding the Guiana Current. In summer, it starts retroflecting eastward into the North-Equatorial Counter-Current (NECC), releasing eddies into the Guiana Current as it meanders: the NBC rings (Johns et al., 1998; Bourles et al., 1999; Ffield, 2005). The NECC also varies seasonally. It is strong in summer and fall, when the ITCZ is at its northernmost position. It is very weak, almost disappearing in winter and spring, when the ITCZ is at its southernmost position (Fonseca et al., 2004). Finally, the Equatorial Undercurrent (EUC) is an eastward current located at the Equator and fed by the NBUC. It is deeper in the west than in the east as it follows the thermocline slope, almost reaching the surface in the east of the basin. The EUC is characterized by a salty core. These salty waters originate from the subtropical gyre of the southern hemisphere, brought by the SEC then by the NBUC into the EUC (Fieux, 2010).

It is interesting to note that in the tropical Atlantic Ocean, the whole surface currents system is asymmetrical with respect to the equator: the northernmost branch of the SEC is located around 3°N, and the southernmost branch of the NEC is located around 10°N. This is due to the asymmetry of the ITCZ in the tropical Atlantic, which is linked with a northward shift of the trade winds.

Currents are the main process driving the SSS seasonal variability in the northwestern tropical Atlantic, as they control the river plume dispersion (e.g. Masson and Delecluse, 2001; Foltz and McPhaden, 2008; Molleri et al., 2010; Da-Allada et al., 2013; Foltz et al., 2015; Fournier et al., 2017). Indeed, Masson and Delecluse (2001) found that the SSS seasonal cycle

phase was identical with monthly and constant Amazon runoff: regardless of the discharge, the SSS minimum always occur three months after the Amazon flood. Using monthly Amazon runoff only improves the amplitude of the seasonal cycle. They concluded that the currents play an important role in the seasonality of the spreading of the plume waters. Nikiema et al. (2007) also observed that in a model including only Amazon discharge and Coriolis force, the plume has a different trajectory: it does not go northwestward but spreads offshoreward, perpendicular to the coast. The mean northwestward pathway of the plume is not due to wind because it is unchanged regardless of the wind strength and direction (Lentz, 1995; Nikiema et al., 2007), suggesting again a strong effect of the currents.

SSS variability in the northwestern tropical Atlantic is mostly associated with the seasonality of two currents, the NBC and the NECC, which advect the Amazon and Orinoco plumes. In winter, the NBC is weak so the Amazon and Orinoco waters remain near the river mouth. In spring, the NBC strengthens and starts advecting the freshwater from the Amazon and Orinoco plume northwestward, along the North Brazilian coast and into the Guiana current. In summer and fall, the NBC retroflection sets up, deflecting the Amazon waters eastward into the NECC (Müller-Karger et al., 1988; Ferry and Reverdin, 2004; Hu et al., 2004; Coles et al., 2013). Therefore, the NECC also plays an important role in SSS variability of some parts of the central tropical Atlantic by advecting the low salinity plume waters there (Foltz et al., 2004). The EUC has also been shown to participate in SSS variability in the eastern tropical Atlantic, by bringing salty water in subsurface. This then impacts the surface salinity through vertical mixing and upwelling (Da-Allada et al., 2017). Finally, the SEC deflects the Congo plume westward during spring, strongly influencing the SSS of the easternmost part of the tropical Atlantic basin during this season (Denamiel et al., 2013; Hopkins et al., 2013; Berger et al., 2014).

1.1.4 Winds

Winds can impact SSS in three main ways: they drive some surface horizontal currents, they induce evaporation at the air-sea interface, and they induce vertical turbulence in the mixing layer. In the northwestern tropical Atlantic, changes in the trade winds modulate the northward extension of the Amazon plume. For instance in boreal winter, when the trade winds come from the northeast, the Amazon plume is constrained near the coast. However, modulations of wind direction can sometimes occur in this season, favoring temporarily northwestward transport and inducing short-lived freshwater plumes (Reverdin et al., 2021). In summer, a seasonal shift in wind direction from northeasterly to southeasterly increases the northwestward advection and allows a more important cross-shore extension of the plume, decreasing the residence time of the low SSS waters near the Amazon mouth (Nikiema et al., 2007; Molleri et al., 2010; Coles et al., 2013). This wind change is linked with the ITCZ position (Fonseca et al., 2004; Coles et al., 2013). Winds only modulate the plume extension: the mean northwestward advection of the plume is governed by the currents (Lentz, 1995; Masson and Delecluse, 2001; Nikiema et al., 2007; Coles et al., 2013). However, the winds interannual variability in the region drives the interannual variability of the plume extension, and therefore of the SSS (Fournier et al., 2017). This is also the case in the Gulf of Guinea,

where the winds have a weak impact on the seasonal cycle of SSS but a strong impact on SSS interannual variability (Da-Allada et al., 2014). At the Congo mouth, winds play a more important role: seasonal changes in the direction and area of the Congo plume are determined by the seasonal cycle of wind and wind-driven currents (Hopkins et al., 2013; Denamiel et al., 2013). Moreover, a doubling of the wind speed near the Congo mouth causes a decrease of the plume extent, due to an increase of vertical mixing that dilutes faster the freshwater (White and Toumi, 2014).

Wind also impacts the evaporation through changes in latent heat flux (e.g. Kumar et al., 2017). Evaporation then affects the SSS: it removes freshwater from the ocean surface, increasing the salinity locally. This process is particularly important in the subtropical gyres (e.g. Camara et al., 2015), leading to a maximum in salinity there. Foltz and McPhaden (2008) showed that the seasonal variation of the ITCZ modifies the evaporation. In winter and spring, when the ITCZ is at its southernmost position, the trade winds are the strongest between 10°N and 20°N, inducing strong evaporation there. In summer, the ITCZ shifts northward, and so do the trade winds and the core of evaporation maximum. Moreover, Grodsky et al. (2006) attributes the salinization of the tropical Atlantic between 1960 and 1985 to wind changes: a strengthening of the trade winds during this period probably led to enhanced evaporation, as well as an increase in upwelling of EUC salty waters.

Finally, wind is one of the main processes inducing mixing at the ocean surface. Vertical mixing has been shown to impact SSS seasonal and interannual variability in areas of low SSS primarily, such as the ITCZ and the river plumes (Da-Allada et al., 2014; Camara et al., 2015; Foltz et al., 2015; Awo et al., 2018). In these areas, vertical mixing is one of the main terms of the salinity budget, attenuating the strong surface freshening from river runoff and precipitation by bringing saltier water at the surface. In the evaporative regions, mixing has a weaker impact, and can either induce a salinization of the surface as in the northern hemisphere, or a freshening of the surface as in the southern hemisphere, depending on the sign of the salinity gradient (Camara et al., 2015). Finally, the equatorial upwelling is also a region where mixing plays an important role (Camara et al., 2015; Da-Allada et al., 2017; Awo et al., 2018). Mixing indeed induces a strong salinization at the surface in spring, the season when the SEC is maximum, due to an increase in vertical shear between the SEC at the surface and the EUC in subsurface (Camara et al., 2015; Da-Allada et al., 2017).

1.2 Ocean-atmosphere coupling mechanisms in the tropical Atlantic Ocean

The coupling between the ocean and the atmosphere involves several feedback loops that determine the mean state and coupled modes of variability over a wide range of time scales. In this section, we will review the main air-sea coupling mechanisms and the dominant modes of variability in the region. This will help us understand how the salinity could participate to the regional climate and its variability – the focus of the next section.

1.2.1 Bjerknes feedback and Atlantic Niño

The Bjerknes feedback is a positive feedback mostly known for driving the El Niño Southern Oscillation (ENSO) in the Pacific Ocean (Bjerknes, 1969). It is linked with the Walker circulation, discovered in the Pacific but present over all the oceans. Therefore, a mode of variability similar to ENSO, although weaker, occurs in the Atlantic Ocean: the Atlantic Equatorial Mode, or Atlantic Niño for the warm events and Atlantic Niña for the cold events (Zebiak, 1993; Keenlyside and Latif, 2007; Lübbecke and McPhaden, 2017).

Figure 1.4 (McPhaden et al., 2010) presents the Walker circulation and the Bjerknes feedback in the tropical Pacific, but the mechanism is similar in the tropical Atlantic. Under normal conditions (Figure 1.4a), the easterly trade winds push the warm surface waters to the west, deepening the thermocline there and creating a "Warm Pool". The accumulation of mass in the west leads to higher sea level than in the east, and is associated with a shoaling of the thermocline in the east that generates the EUC through pressure adjustments. The shallow thermocline, combined with Ekman divergence and wind-induced equatorial waves explains the presence of an equatorial upwelling (also called Cold Tongue, or CT) in the eastern part of the basin (e.g. Weingartner and Weisberg, 1991; Wang et al., 2017). In the Warm Pool, the SST is higher than the convection threshold (26 to 28°C, Sabin et al., 2013; Evans and Webster, 2014), which allows the development of deep convection and strong precipitation. This is the ascending branch of the Walker cell. The air will then recirculate eastward and subside above the CT because of the cooler SST there, creating the descending branch of the Walker cell. Due to the zonal SST gradient, the trade winds blow westward and connect the two branches, closing the Walker circulation.

An El Niño event (Figure 1.4b for the Pacific, also valid for the Atlantic) is characterized by a relaxation of the trade winds leading to an anomalous eastward extension of the Warm Pool. The trade winds relaxation is associated with a downwelling equatorial Kelvin wave,

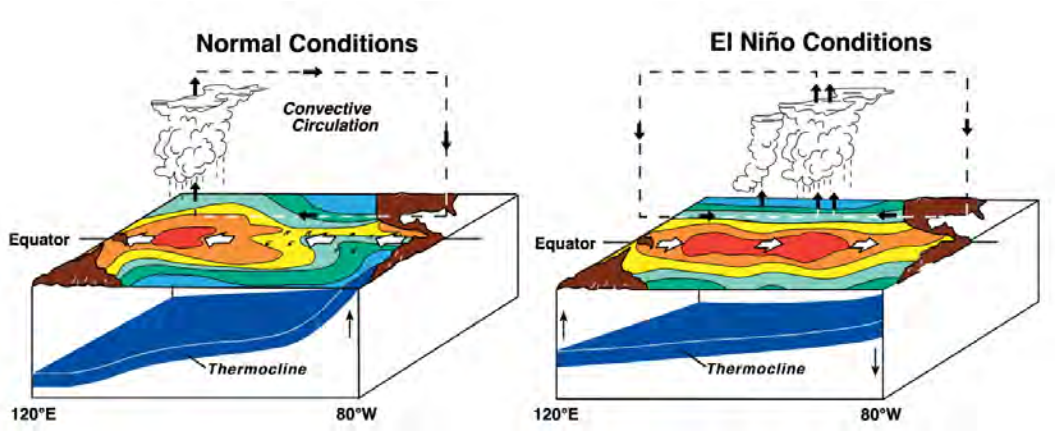

Figure 1.4: Schematic showing a) normal conditions and b) warm ENSO events (El Niño) in the tropical Pacific. It shows the Walker circulation and illustrates the Bjerknes feedback, also at stake in the tropical Atlantic. Reproduced from McPhaden et al. (2010).

which leads to a flattening of the thermocline and a weakening of the CT (Wyrtki, 1975). The zonal SST gradient decreases, causing a further relaxation of the trade winds and closing the positive feedback loop. Conversely, during La Niña events, the trade wind strengthens, increasing the slope of the thermocline. The SST gradient increases as well, leading to a further strengthening of the trade winds. These events occur in boreal summer, and are associated with changes in precipitation. In the Pacific, ENSO impacts the precipitation over South America, with El Niño events being generally associated with lower precipitation and river discharge in most of the Amazon basin while La Niña events are associated with higher precipitation and river discharge in the basin (e.g. Ropelewski and Halpert, 1987; Ronchail et al., 2005; Espinoza et al., 2009b; Towner et al., 2020). In the Atlantic, an increase of precipitation over northeast Brazil and West Africa (Angola and Guinea) as well as droughts in Sahel have been reported during Atlantic Niños, possibly due to a weaker ITCZ shift (Ruiz-Barradas et al., 2000; Polo et al., 2008; Losada et al., 2010; Rodríguez-Fonseca et al., 2015).

1.2.2 Wind-evaporation-SST feedback and Atlantic Meridional Mode

Another important feedback is the Wind-evaporation-SST (WES) feedback. It is associated with an anomalous cross-equatorial SST gradient, for instance positive SST anomalies (SSTAs) in the northern hemisphere (NH) and negative SSTAs in the southern hemisphere (SH). This anomalous northward SST gradient modifies the temperature of the atmospheric boundary layer and forces an anomalous southward sea level pressure gradient, which in turn induces anomalous southerly cross-equatorial winds (Lindzen and Nigam, 1987). Due to the Coriolis force, these winds are deflected to the right (i.e. to the east) in the NH and to the left (i.e. to the west) in the SH. Moreover, the trade winds are northeasterly in the NH, and southeasterly in the SH. Therefore, the anomalous southerly cross-equatorial winds cause a decrease of the trade winds in the NH, leading to a decrease of the evaporation and a further increase in SST (less evaporation means indeed less heat loss by latent heat flux for the ocean). Conversely, the trade winds increase in the SH, leading to an increase of the evaporation and a further decrease in SST. The cross-equatorial SST gradient is thus amplified, which closes the positive feedback loop.

The WES feedback was presented by Xie and Philander (1994) as a mechanism explaining the northward asymmetry of the ITCZ in the Atlantic and Pacific oceans. It is now considered to be the major mechanism driving the Atlantic Meridional Mode (AMM) (e.g. Carton et al., 1996; Chang et al., 1997; Xie, 1999; Mahajan et al., 2010). The AMM is one of the main modes of variability of the tropical Atlantic Ocean. It initiates in winter with changes in trade winds strength, and fully develops in boreal spring (Figure 1.5, from Rugg et al., 2016). Indeed, boreal spring is the season when the ITCZ is the closest to the Equator and therefore the season when the WES feedback is the most effective (Xie and Carton, 2004; Hu and Huang, 2006). Associated with AMM is a change in the ITCZ location: for a positive phase of the AMM for instance (i.e. positive SSTAs in the NH), the increase in southerly winds induces a northward shift of the ITCZ (Hastenrath and Greischar, 1993; Ruiz-Barradas et al., 2000; Chiang and Vimont, 2004). This has strong consequences on the continental rainfall over

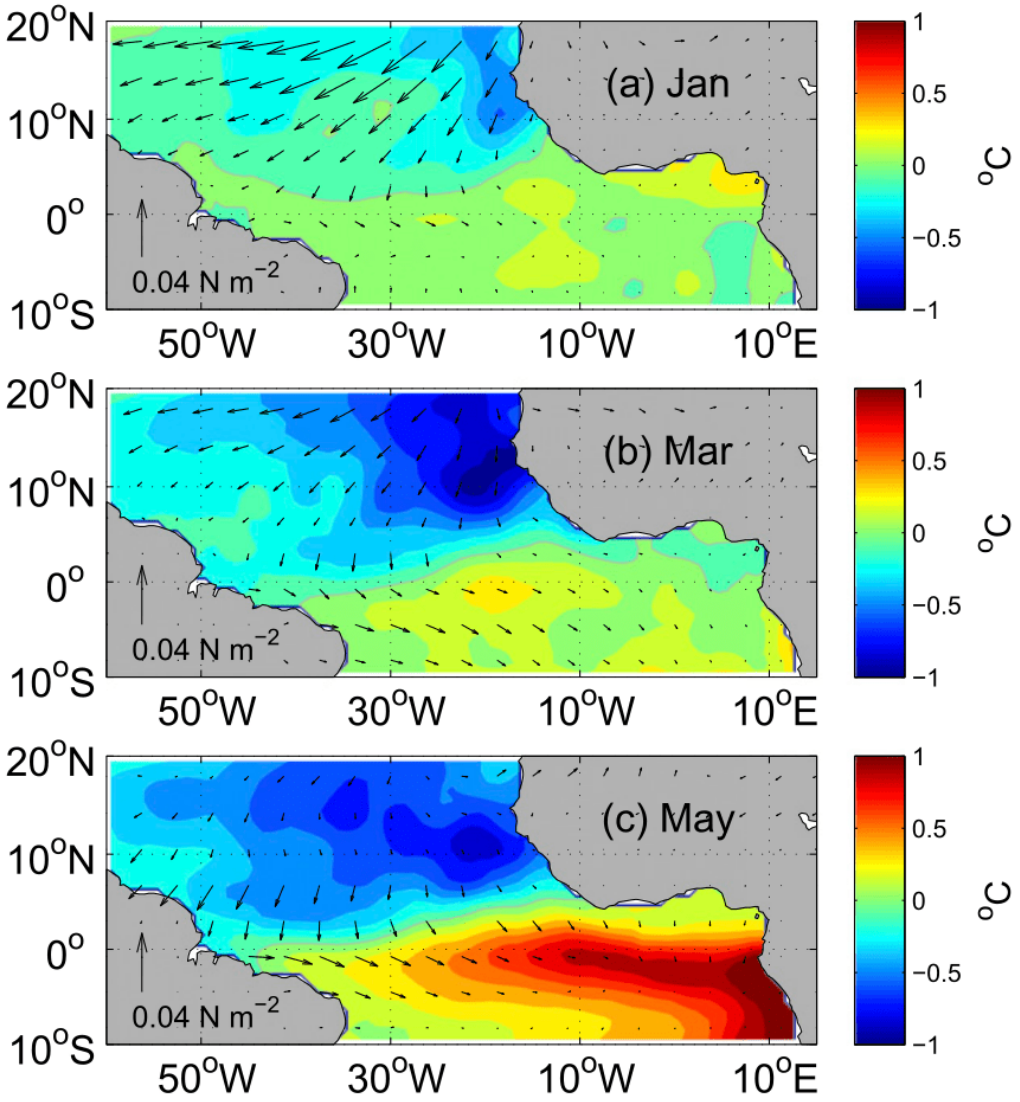

Figure 1.5: Composite maps of AMM events for 1982-2014, SST anomalies (shaded) and wind stress anomalies (vectors) for a) January, b) March and c) May. Signs shown are for typical negative events. Reproduced from Rugg et al. (2016).

northeast Brazil, and can induce floods or droughts in the Amazon watershed (Hastenrath and Greischar, 1993; Nobre and Shukla, 1996; Chiang and Vimont, 2004; Foltz et al., 2012; Marengo and Espinoza, 2016).

The WES feedback is the main mechanism explaining the AMM, but it is not the only one (Tanimoto and Xie, 2002; Mahajan et al., 2010; Rugg et al., 2016; Kataoka et al., 2019). In the following we will describe three more ocean-atmosphere feedbacks participating in the development or damping of the AMM.

1.2.3 Latent heat feedback

With the development of SSTAs, due to the AMM for instance, comes also a change in latent heat flux. Indeed, a SST increase leads usually to an increase in heat loss by latent heat flux (Kumar et al., 2017). Therefore, a negative feedback appears during the AMM: the increase in SST leads to an increase in latent heat flux which decreases the SST (Rugg et al., 2016). Conversely, in the other part of the AMM SST dipole, the decrease in SST leads to a decrease in latent heat flux which increases the SST.

1.2.4 Wind-mixed layer-SST feedbacks

The ML hosts the ocean-atmosphere interactions and can impact the SST (e.g. Miller, 1976). Rugg et al. (2016) first observed that during AMM events, positive SSTAs are associated with a thinner ML, making it more sensitive to the positive surface heat fluxes and heating it further. Later, Kataoka et al. (2019) described two positive feedbacks involving the ML, and named them the wind-induced turbulence–mixed layer–SST (WIMS) feedback and the wind–evaporation–mixed layer–SST (WEMS) feedback.

Analogous to WES feedback, WIMS and WEMS feedback originate from an anomalous cross-equatorial SST gradient that modulates the trade winds. Positive SSTAs are associated with a decrease in wind. In the case of the WIMS feedback, the decrease in wind will cause a thinning of the ML by an inhibition of turbulent mixing. In the case of the WEMS feedback, the decrease in wind will cause a decrease in evaporation and thus a gain in buoyancy, leading to a thinning of the ML. A thinner ML is then more sensitive to the surface heat fluxes and leads to a further warming of the surface. Conversely, negative SSTAs will lead to a deepening of the ML, a ML less sensitive to positive surface heat fluxes and thus a further cooling of the surface.

We can note that these feedbacks are actually sensitive to the sign of the net heat flux. In both Rugg et al. (2016) and Kataoka et al. (2019) studies, the net heat flux is positive, making the feedback positive. But in case of a negative net heat flux, the WIMS and WEMS feedback will become negative feedbacks: a thinner ML - linked with positive SSTAs - will be more reactive to heat loss, which will lead to a decrease in SST; a deeper ML - linked with negative SSTAs - will be less reactive to heat loss, which will lead to an increase in SST (Miller, 1976).

1.2.5 Cloud feedback

Clouds are involved in two different feedbacks: a positive feedback associated with low level clouds, and a negative feedback associated with deep convective clouds.

During AMM events for instance, low level cloud cover increases above the negative SSTAs, and decreases above the positive SSTAs. Clouds are blocking the solar radiation, resulting in

additional positive feedback: areas of negative SSTAs receive less solar radiation, amplifiying the negative SSTAs, whereas areas of positive SSTAs receives more solar radiation, amplifying the positive SSTAs (Tanimoto and Xie, 2002; Hu and Huang, 2006; Xie, 2009; Myers et al., 2018).

However, the clouds associated with deep convection induce a negative feedback. Indeed, deep convection occurs in areas of warm SST, typically over 26-28°C (e.g. Sabin et al., 2013; Evans and Webster, 2014). In these areas, an increase in SST is associated with a densification of deep convective clouds, which in turn decreases the solar flux reaching the ocean surface and thus the SST (Xie, 2009).

1.3 Impact of salinity on the ocean-atmosphere interactions

Salinity can have an influence on the air-sea exchanges of heat, freshwater and momentum. This influence is indirect and the main mechanism is through its impact on the upper ocean stratification and mixed layer depth (MLD). In presence of a strong salinity stratification, the ML becomes thinner. Its heat capacity thus decreases and it is more effectively heated or cooled (depending on the sign of the surface heat fluxes). Moreover, a strong salinity stratification stabilizes the ML, making it less sensitive to wind gusts: in such a case, the ML will not deepen as much and the entrainment of cold water through the base of the ML will decrease (e.g. Miller, 1976). A thinner ML also traps more effectively the wind momentum, enhancing the wind-driven currents (Vialard and Delecluse, 1998).

The strongest salinity stratifications of the tropical Atlantic Ocean are localized in river plumes (Maes and O'Kane, 2014). The impact of the river plumes on the SST has therefore been frequently studied, and is the first topic discussed in this section. Moreover, in the literature, the impact of the river plumes on SST is usually associated with the presence of barrier layers (BLs). We will therefore explain what it is, how they form in the tropical Atlantic Ocean, and the impact that they can have on the SST and on the air-sea heat fluxes. Finally, the presence of BLs might contribute to tropical cyclones (TCs) maintenance and intensification in the northwestern tropical Atlantic (e.g. Grodsky et al., 2012; Balaguru et al., 2020). However, the effect of BLs - and more generally of salinity stratification - on TCs is a long-standing debate, and is thus the last topic of this section.

1.3.1 River plumes

In the tropical Atlantic Ocean, two main river plumes are associated with strong salinity stratification: the Amazon-Orinoco plume, and the Congo plume. The influence of the Amazon and Orinoco plume on SST has been extensively studied, but the results are contradictory. Observational studies suggest a strong impact of the plume on the SST of the region (Pailler et al., 1999; Ffield, 2007; Fournier et al., 2017; Jury, 2019). For instance, Pailler et al. (1999) evaluate that the presence of the river plume conducts to a 1°C increase of SST, while Ffield

(2007) notes that the river plumes are on average 2°C warmer than the open ocean waters. On the other hand, modeling studies do not find any compelling impact on tropical Atlantic SST when removing Amazon runoff, whether conducted with forced ocean models (Huang and Mehta, 2010; Newinger and Toumi, 2015; Hernandez et al., 2016), or coupled ocean-atmosphere models (Jahfer et al., 2017). Nevertheless, Jahfer et al. (2017) suggest that freshwater brought by Amazon runoff has a long-term effect on the North Atlantic climate: shutting down the Amazon for a hundred years would bring saltier water in the northern Atlantic and enhance the sinking of water there, thus strengthening the Atlantic Meridional Overturning Circulation (AMOC) as well as the Gulf Stream and the Guiana Current. These changes in currents then trigger a permanent negative phase of the North Atlantic Oscillation, altering the whole North Atlantic climate.

The impact of the Congo plume on air-sea heat fluxes and on SST has been little studied, and the results are contradictory. Using in-situ measurements of Congo runoff and SST, Materia et al. (2012) found significant - albeit weak - positive correlations between the two along the Angolan coast, in the Gulf of Guinea and in the Cold Tongue area, suggesting that the Congo river was responsible for warming in these areas. On the other hand, Hopkins et al. (2013) used remote sensing data to conduct EOF analysis and found no impact of the Congo river on SST. Furthermore, White and Toumi (2014) conducted modeling experiments with and without Congo river and they also concluded that the Congo has no impact on SST, apart from a slight cooling (up to 0.25°C) off of the Congo mouth.

1.3.2 Barrier layers

1.3.2.1 What is a barrier layer ?

Usually, the tropical oceans can be represented in an idealized way by two layers: the ML, a warm surface layer homogeneous in salinity and temperature - and therefore in density, and the deep ocean, cold and salty (Figure 1.6a). The two layers are separated by a sharp pycnocline that is usually controlled by temperature. However, in areas of strong salinity stratification (river plumes, ITCZ), the pycnocline depth can be driven by salinity. This is a necessary condition of appearance of a BL, but not a sufficient one. For a BL to appear, a decoupling between the thermocline and the halocline is also necessary: the thermocline must be deeper than the halocline, and therefore deeper than the pycnocline (Figure 1.6b). A third layer then appears between the ML and the deep ocean, called the Barrier Layer (Godfrey and Lindstrom, 1989). It is called so because it acts as an insulating barrier between the warm surface waters, interacting with the atmosphere, and the cold waters of the deep ocean. Its thickness is calculated as the difference between the top of the thermocline depth and the pycnocline depth (corresponding to the MLD) (Lukas and Lindstrom, 1991; Sprintall and Tomczak, 1992).

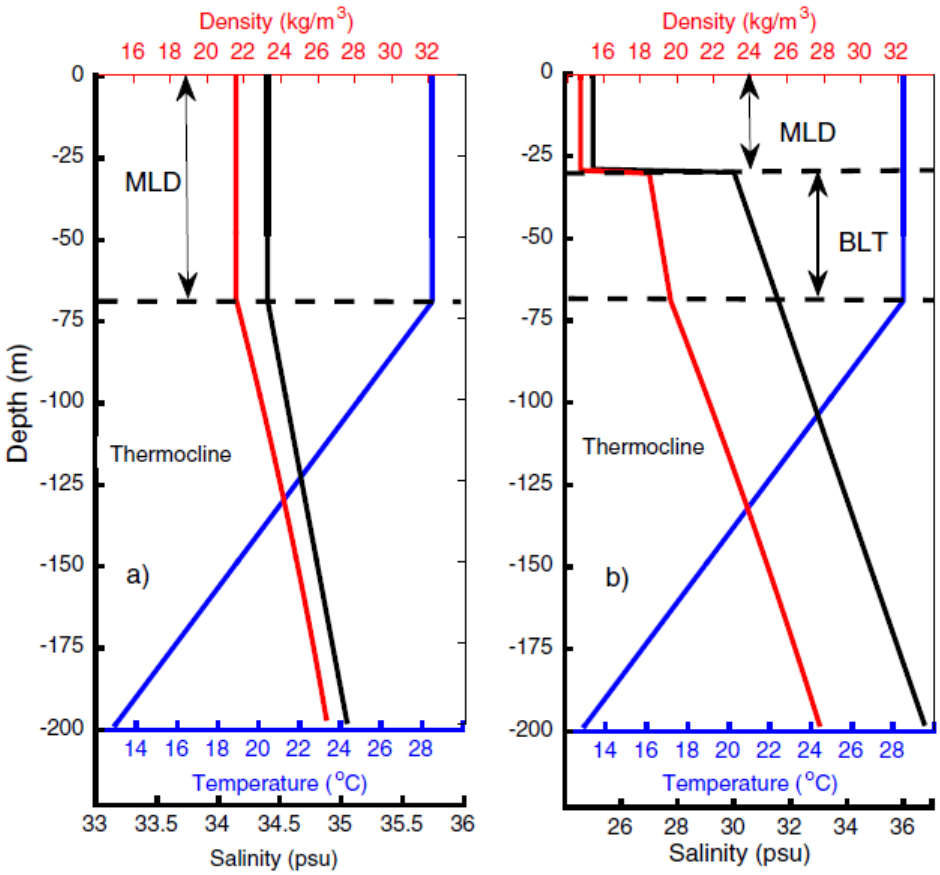

Figure 1.6: Profiles of temperature (blue), salinity (black), and density (red) representing the mixed layer depth (MLD) and the barrier layer thickness (BLT). Two cases are shown: a) no BL and b) thick BL. Reproduced from Yan et al. (2017).

1.3.2.2 Formation mechanisms

In the tropical Atlantic, BLs are mainly present in the northwestern part, and more exactly along the coast between Brazil and Venezuela northwest of the Amazon mouth (Pailler et al., 1999; Masson and Delecluse, 2001; Mignot et al., 2007), in the NBC retroflection and in the NECC in summer (Pailler et al., 1999; Mignot et al., 2007; Saha et al., 2021), near the lesser Antilles, in winter especially (Sprintall and Tomczak, 1992; Mignot et al., 2007, 2012), in the ITCZ (Foltz et al., 2004; Mignot et al., 2007; Tanguy et al., 2010) and equatorward of the northern hemisphere subtropical gyre (Sato et al., 2006; Mignot et al., 2007, 2012; Saha et al., 2021). They are also present equatorward of the southern hemisphere subtropical gyre, close to the Brazilian coast (Sprintall and Tomczak, 1992; Sato et al., 2006; Mignot et al., 2007; Tanguy et al., 2010).

The mechanisms of formation of all these BLs have been thoroughly studied, and are globally similar. Two elements are needed for a barrier layer to develop: a shallow pycnocline and a deeper thermocline (Masson and Delecluse, 2001). The shallow pycnocline is caused by a strong salinity stratification, usually due to the advection at the surface of freshwater from

the Amazon and Orinoco or from the ITCZ (Pailler et al., 1999; Masson and Delecluse, 2001; Mignot et al., 2007). The salinity stratification can be reinforced in some places by the advection of salty water at the subsurface, originating from the subtropical gyres (Sprintall and Tomczak, 1992; Mignot et al., 2007; Tanguy et al., 2010; Balaguru et al., 2012a). In summer, the NBUC also advects salty water of the southern subtropical gyre under the Amazon plume, which helps maintaining the strong salinity stratification there (Masson and Delecluse, 2001). Small scale salinity fronts also play a role in creating strong salinity stratifications locally (Sato et al., 2006; Tanguy et al., 2010; Saha et al., 2021).

The explanation for a deeper thermocline depends on the season and the region. In winter, the thermocline deepens naturally due to a decrease of temperature at the surface inducing a decrease of the temperature gradient, strong mixing and a deepening of the ML. In the area near the lesser Antilles for instance, it deepens faster than the pycnocline, causing very thick BLs (Mignot et al., 2012). In summer, the NBUC advects warm waters from the southern subtropical gyre under the Amazon plume, heating the subsurface. Coupled with the shallow pycnocline, this allows for the development of a BL there (Masson and Delecluse, 2001). Moreover, in spring and summer, solar radiation is maximum, and the ML is very thin in various regions due to the strong salinity stratification. This induces a penetration of the solar flux under the ML, a warming of the subsurface and the development of a BL (Vialard and Delecluse, 1998; Masson and Delecluse, 2001; Mignot et al., 2012).

More recently, BLs have been detected in the northeastern Gulf of Guinea, associated with precipitation in the ITCZ and the Niger river plume (Dossa et al., 2019). Thin BLs (less than 6 m) are also induced by the Congo River (White and Toumi, 2014). However, the exact mechanisms leading to the appearance of barrier layers there have not yet been studied.

1.3.2.3 Impact on SST and air-sea fluxes

BLs have several impacts on SST and on air-sea interactions. First, the trapping of solar flux at the origin of the BLs formation can also lead to the development of temperature inversions (Vialard and Delecluse, 1998). Indeed, the stabilization by the strong salinity stratification allows for the ML to be cooler than the water below without being unstable. These temperature inversions have been observed in the western tropical Atlantic (Miller, 1976; de Boyer Montégut et al., 2007a; Foltz and McPhaden, 2009), and were also reported in models (Miller, 1976; Masson and Delecluse, 2001; Balaguru et al., 2012a; Mignot et al., 2012). They can reach up to 1°C (Mignot et al., 2012). They have been shown to participate to the seasonal and interannual variability of the SST in the tropical Indian Ocean (Durand et al., 2004; Masson et al., 2005; Nagura et al., 2015).

In presence of a BL, there is no cooling by entrainment of cold water at the base of the ML: the water being the same temperature in the BL and in the ML, the deepening of the ML - during a gust a wind for instance - brings water of the same temperature into the ML, or warmer in case of a temperature inversion (Vialard and Delecluse, 1998; Foltz and McPhaden, 2009).

Nevertheless, the impact of BL on SST is controversial. Using in-situ observations, Foltz and McPhaden (2009) suggested that BL presence leads to an increase of SST of 1.3 to 1.9°C in the western tropical Atlantic. The observational studies that noticed an impact of the Amazon plume on SST all linked it to the presence of BLs (Pailler et al., 1999; Ffield, 2007; Fournier et al., 2017). Moreover, modeling studies using a forced ocean model in the tropical Pacific (Vialard and Delecluse, 1998) and a coupled ocean-atmosphere model in the southeastern Arabian sea (Masson et al., 2005) removed the salinity stratification (and therefore the BLs), and each observed an impact of up to 0.5°C on SST. However, similar modeling experiments conducted in the western tropical Atlantic with a forced ocean model (Masson and Delecluse, 2001) and in the Bay of Bengal with a coupled ocean-atmosphere model (Krishnamohan et al., 2019) did not find any impact of salinity stratification on the SST. Moreover, Balaguru et al. (2012a) strengthened the salinity stratification in its coupled model of the tropical Atlantic by increasing the freshening in the Amazon region and increasing the salinity maxima of the subtropical gyres. This resulted in a thicker BL, but no associated change in SST was observed.

Breugem et al. (2008) studied the ability of coupled global General Circulation Models (GCMs) to reproduce the BLs in the tropical Atlantic Ocean, and they observed the development of spurious BLs in the southeastern tropical Atlantic. They linked them with the well-known SST biases of the coupled GCMs in this region. Furthermore, they hypothesized a positive feedback mechanism between BL, SST and ITCZ to explain the persistence of the SST biases. The spurious BLs cause a warm SST bias in the region, which in turn leads to a southward shift of the ITCZ and an increase of precipitation in the area. The latter leads to an increase of freshwater supply, helping to maintain a shallow pycnocline. The warm SST bias also causes a weakening of the easterly winds, leading to a subsurface warm bias that maintains a deep thermocline. The two effects combined cause a persistence of the BL bias, and of the SST bias.

1.3.3 Tropical cyclones

TCs are natural disasters that occur frequently in the tropical Atlantic Ocean (14 tropical storms per year including 7 hurricanes on average over the 1991-2020 period, according to Météo-France). They have strong consequences on the populations, and as such are the subject of intense research and monitoring.

Ffield (2007) was the first to suggest a link between TC intensification and salinity stratification associated with the presence of the Amazon-Orinoco plume. She observed that between 1960 and 2000, 68% of the category 5 hurricanes crossed the Amazon plume. Moreover, relatively strong positive correlation is found between SST in the plume and winds induced by the TCs crossing the area. Coupled with the fact that SSTs are on average 2°C higher in the plume, this seems to indicate an impact of salinity stratification on the TCs intensity.

Subsequently, several studies have focused on this link, but the results are contradictory. Some studies confirmed its existence (e.g. Balaguru et al., 2012b; Grodsky et al., 2012; Androulidakis et al., 2016; Rudzin et al., 2018). For instance, Balaguru et al. (2012b) showed that in the tropical Atlantic Ocean, observations of TC intensification rate are almost 50% higher over regions with BL than over regions without BL. Using also a coupled ocean-atmosphere model, they observed that the surface cooling and the vertical turbulent heat fluxes subsequent to the passage of a TC were reduced by almost 40% in areas with BLs, leading to TC intensification. More recently, Balaguru et al. (2020) studied the rapid intensification of TCs and also found an impact of salinity stratification. Moreover, they observed a slight improvement of the forecast of TC rapid intensification when salinity was included in the predictors.

Yan et al. (2017) refined and nuanced a little this link: they concluded that the impact of BL is complex, and depends on various factors such as ocean stratification and TC intensity. They explain the mechanism behind the impact of strong salinity stratification and BLs on TCs as follows. Under normal circumstances, a surface cooling (1°C on average) appears in the wake of a TC due to the mixing associated with the intense winds. Indeed, the strong winds break through the ML and induce mixing of cooler waters from under the thermocline. Since TCs develop because of high SSTs, this cooling induces a negative feedback on the TC intensity that can reduce the TC intensification by up to 50% (e.g Schade and Emanuel, 1999; Vincent et al., 2012). But in presence of a strong salinity stratification, the pycnocline is sharper and the ML is harder to break through. The ML is also thinner when salinity stratification is strong. This results in less cooling by entrainment of cold water, but more cooling by latent heat flux. The latter is the main process for weak TCs, and the combination of the two processes still results in a decrease of the SST, and an inhibition of the weakest TCs (Vincent et al., 2012; Yan et al., 2017; Hlywiak and Nolan, 2019). In presence of a BL and when the TC is strong enough for the ML to be breached, the water that is mixed is warmer than the surface, previously cooled by the still weak TC. It results in a warming of the surface and a TC intensification. When the TC is strong enough, the induced winds reach the bottom of the BL and the SST begins to decrease. But even then, the presence of a BL induces a higher SST and thus an intensification in comparison with regions without BLs (Yan et al., 2017).

Nevertheless, two modeling studies reported different results (Newinger and Toumi, 2015; Hernandez et al., 2016). By conducing experiments with and without runoff, they have shown that salinity stratification and BLs associated with the Amazon plume have very little impact on SST, on cooling in the wake of TCs, and thus on TC intensification. Newinger and Toumi (2015) studied the separate impact of salinity stratification and bio-optical effects induced by the Amazon. They concluded that salinity stratification alone has a weak impact on TC intensity (modest intensification of -5 to -12 hPa), which is only due to the stabilizing effect of the increased stratification and not to temperature changes. Moreover, the light absorbing particles of the colored plume offset this effect (modest weakening of +6 to +16 hPa), because of a slight increase in SST (+0.1°C) and a slight decrease in subsurface temperature (-0.3°C). The net effect of the plume on TC intensity is therefore negligible.

Hernandez et al. (2016) studied the cooling in TCs wake and confirmed the weak effect of the plume. Like Balaguru et al. (2012b), they observed a lower surface cooling in the wake of TCs in the plume waters than in the open ocean waters (50 to 60%). However, removing runoff - and thus BLs - does not significantly alter this cooling difference (Figure 1.7). Hernandez et al. (2016) concluded that the underlying thermal stratification, incidentally high in the plume area, is the main factor explaining the low TC-induced cooling and the high TC intensification rate in the region.

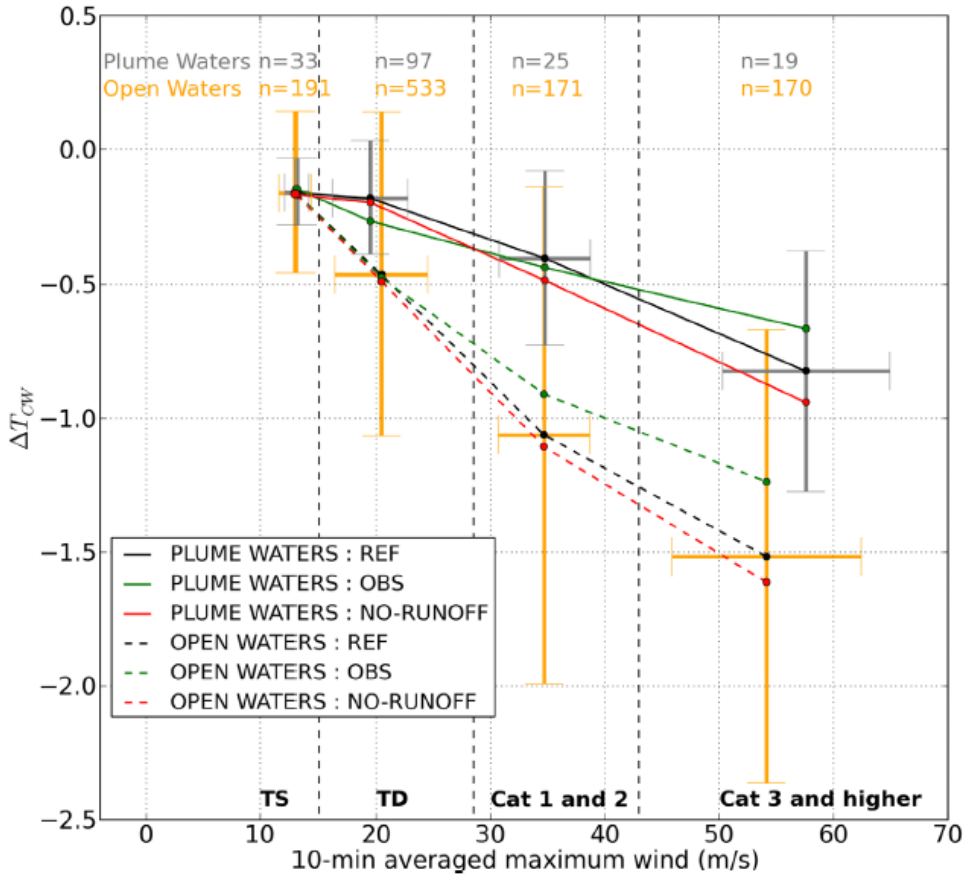

Figure 1.7: Distribution of mean SST maximum cooling (°C) as a function of 10 min averaged maximum wind speed (m/s) obtained from observations and REF and NO-RUNOFF experiments, using data from the period 1998–2012, for open-ocean waters (dashed lines) and plume waters (continuous line). Four categories of the Saffir Simpson scale (rescaled to 10 min averaged maximum wind speed) are considered: TS, TD, Cat 1 and 2, Cat 3 and higher. Vertical bars indicate the standard deviation of the mean cooling in REF experiment. Horizontal bar indicates the standard deviation of the mean winds. Reproduced from Hernandez et al. (2016).

To this date, the debate on the impact of BLs and salinity stratification on the SST and the air-sea interactions is still open. The tropical Atlantic Ocean is an area of particular interest: the salinity structure is especially intense there, and the region is crossed by numerous TCs that affect strongly the population (Carribean islands, southeastern coasts of

Northern America). As most of the modeling studies investigating salinity stratification in the area were conducted with forced ocean models, the need for a high resolution coupled ocean-atmosphere model arises, in order to better understand this peculiar salinity structure and its role on the climate of the tropical Atlantic Ocean. Note however that the impact of salinity stratification on TCs has not been studied in this thesis, despite a detailed review of the literature on the subject. This work can be seen as a preliminary study, that has served to develop the adequate tool and increase our knowledge of the impact of salinity stratification on the mean climate; the study of the TCs would then be the logical continuity of this thesis.

Chapter 2

Materials and methods

Contents

A strong air-sea coupling takes place in the tropical Atlantic Ocean. Ocean-atmosphere feedback processes impact the regional climate and its modes of variability (Section 1.2), and it is necessary to take these processes into account in order to properly understand the role of salinity in the regional climate (Section 1.3). A first part of this thesis consists therefore in developing a coupled ocean-atmosphere configuration of the tropical Atlantic well suited to the study of the impact of salinity on regional oceanic and atmospheric variables.

2.1 Coupled configuration description

The coupled regional configuration relies on the ocean model NEMO v4.0 (Nucleus for European Modeling of the Ocean; Madec and the NEMO team, 2016), the atmospheric model WRF-ARW v3.7.1 (Weather Research and Forecasting; Skamarock and Klemp, 2008), and the coupler OASIS3-MCT v4.0 (Valcke, 2013). A similar configuration has already been used in the Indian Ocean (Samson et al., 2014) and in the tropical belt (Samson et al., 2017; Renault et al., 2019), and to our knowledge, this is its first implementation in the tropical Atlantic. The ocean and the atmospheric model share the same horizontal grid: a Mercator projection that encompasses the tropical Atlantic from 15°S to 35°N, and from 99°W to 20°E, with a resolution of 1/4° ($\sim$ 27 km). Both models use an Arakawa-C grid. Since the grids are identical, no spatial interpolation is required by the coupler. Every hour, heat fluxes, water fluxes and wind stress are sent by WRF to NEMO, and SST and surface currents are sent by NEMO to WRF. All fields exchanged are hourly averages.

2.1.1 Ocean model

The ocean model solves the three-dimensional primitive equations. Its grid has 75 fixed vertical levels (z coordinates), with 12 levels in the upper 20 m and 24 levels in the upper 100 m. The advection scheme used for tracers is the Flux Corrected Transport (FCT) scheme (Zalesak, 1979). The lateral diffusion is parameterized as a bilaplacian isopycnal diffusion. For the vertical mixing, we use the Generic Length Scale (GLS) scheme (Reffray et al., 2015), with a k-ϵ closure. The mixed layer eddy parameterization of Fox-Kemper is also used (Fox-Kemper et al., 2008).

Lateral open boundaries of the model are prescribed using an interannual hindcast from the MERCATOR global daily reanalysis GLORYS2V4 (Ferry et al., 2012), and more specifically temperature, salinity, sea level and horizontal velocities. The solar radiation penetration scheme used is the three-waveband RGB (Red-Green-Blue) model from Lengaigne et al. (2007), a simplified version of the full spectral model of Morel (1988). In order to take into account the ocean color in this scheme, the model is forced with a monthly climatology from 1999 to 2005 of chlorophyll concentrations derived from SeaWiFS (McClain et al., 1998). The empirical parameterization from Morel and Berthon (1989) is used to calculate a vertical profile of chlorophyll from the surface chlorophyll satellite concentrations. Interannual daily runoffs are specified at the river mouths, and were obtained from the ISBA-CTRIP land

surface system (Decharme et al., 2019).

This oceanic configuration has already been used in Giffard et al. (2019), and is very similar to the one used in Jouanno et al. (2017) and in Hernandez et al. (2016, 2017), which gives us confidence in its ability to simulate realistically the dynamics and thermodynamics of the upper tropical Atlantic ocean.

2.1.2 Atmospheric model

The atmospheric model WRF solves the compressible and non-hydrostatic Euler equations, using the Advanced Research WRF dynamical solver (ARW). Its grid has 40 terrain-following vertical levels (sigma coordinates), and the top of the atmosphere is located at 50 hPa.

From the many parameterizations that can be chosen, the best representation of air-sea fluxes was obtained with the Yonsei University planetary boundary layer scheme (Hong et al., 2006) used together with the WSM6 microphysics scheme (Hong and Lim, 2006) modified to take into account the droplet concentration (Jousse et al., 2016). The Rapid Radiative Transfer Model for GCMs (Iacono, 2011) is used for both shortwave and longwave radiation. Convection is represented with the Multi-Scale Kain-Fritsch scheme (Zheng et al., 2016), which allows interaction between parameterized clouds and the radiation schemes. The Noah Land Surface Model (Niu et al., 2011) together with the revised MM5 surface layer scheme (Jiménez et al., 2012) are used. The choice of these parameterizations is explained in Section 2.3.

Lateral boundary conditions are given by 6-hourly fields from ERA-Interim reanalysis (Dee et al., 2011). Following Samson et al. (2017), we prescribed a monthly climatology of albedo derived from MODIS observations (Schaaf et al., 2010).

This coupled configuration is called CONTROL in the rest of this work.

2.2 Observational datasets

In the next two sections, we will present a sensitivity testing of WRF parameterizations and assess the realism of the CONTROL simulation. To this end, several observational datasets are needed. The Optimum Interpolation Sea Surface Temperature (OISST) dataset v2.0 from NOAA (Banzon et al., 2016) is used to assess the model SST. This dataset is a merging of AVHRR satellite data and in situ observations from 2001 to 2015, interpolated on a 1/4° grid. A seasonal climatology of SSS observations at 1/4° resolution was built from Soil Moisture and Ocean Salinity (SMOS) satellite data (Boutin et al., 2020) for the period 2010-2015, the common period between the model simulations and SMOS dataset. A monthly climatology from 2000 to 2014 of the Clouds and the Earth's Radiant Energy System (CERES) Energy Balanced and Filled (EBAF) Surface dataset Ed2.8 (Kato et al., 2013) is used to assess the net longwave and shortwave radiation at the ocean surface. CERES data derives from Terra and Aqua satellite measurements, and has a 1° resolution. The latent heat flux and net heat

flux from the model are compared with those from the Objectively Analyzed air-sea Fluxes (OAFlux) project (Yu et al., 2008). The net heat flux is a combination of radiative downward fluxes (shortwave and infrared fluxes) from the International Satellite Cloud Climatology Project (ISCCP) and turbulent heat fluxes (latent and sensible) from OAFlux, with a spatial resolution of 1° and a temporal resolution of 1 month. Both climatologies were computed using data from 2000 to 2009. Precipitation data are from the Tropical Rainfall Measuring Mission (TRMM; Huffman et al., 2007)), which is a merging of various satellite datasets as well as rain gauges wherever available. The product is provided on a 1/4° grid, and a 2001-2015 climatology is used. To assess the wind speed, the Scatterometer Climatology of Ocean Winds (SCOW) is used (Risien and Chelton, 2008). SCOW is a monthly climatology from 1999 to 2009 based on QuikSCAT scatterometer data and with a 1/4° resolution. To compute the 20°C isotherm depth, we used a climatology from 2002 to 2015 of the ISAS dataset of 3D temperature (Kolodziejczyk et al., 2017; Gaillard et al., 2016). ISAS is based on in-situ measurements, and has a 1/2° resolution. Finally, we compared the model mixed layer depth (MLD) with the climatology from de Boyer Montégut et al. (2004), based on in-situ salinity and temperature profiles. The MLD is computed as the depth where the density is equal to the 10-meter density plus $\Delta\sigma$, with $\Delta\sigma$ a fixed density criterion of 0.03 kg/m^3. Using a density criterion instead of a temperature criterion is critical in regions with strong upper ocean salinity gradients (de Boyer Montégut et al., 2004).

2.3 Parameterization of the atmospheric model

In order to minimize the biases, a large set of sensitivity tests to model parameters was performed. Since the ocean regional configuration has already been extensively validated and used in several studies (Hernandez et al., 2016, 2017; Jouanno et al., 2017; Giffard et al., 2019) adjustment of the NEMO parameters was straightforward. Therefore, the focus was on adjusting the atmospheric model WRF, which to our knowledge has never been coupled to NEMO over a domain encompassing the whole tropical Atlantic Ocean. However, WRF has already been coupled to NEMO in the Indian Ocean (Samson et al., 2014) and in the tropical belt (Samson et al., 2017; Renault et al., 2019). The coupled configuration developed here has benefited from the experience brought by these works, and is a continuation of them.

We started from a set-up based on Meynadier et al. (2015), who conducted sensitivity tests to parameterizations in the Gulf of Guinea with a forced WRF model. We used the Noah land surface model and the WSM6 microphysics scheme that they found to be optimum, especially for precipitation and latent heat flux. Then, we conducted sensitivity tests to determine the best longwave (LW) and shortwave (SW) radiation schemes, convection scheme and planetary boundary layer (PBL) scheme. The choice of the PBL scheme then determines the surface layer scheme. Figure 2.1 summarizes the different schemes included in WRF and how they relate to each other.

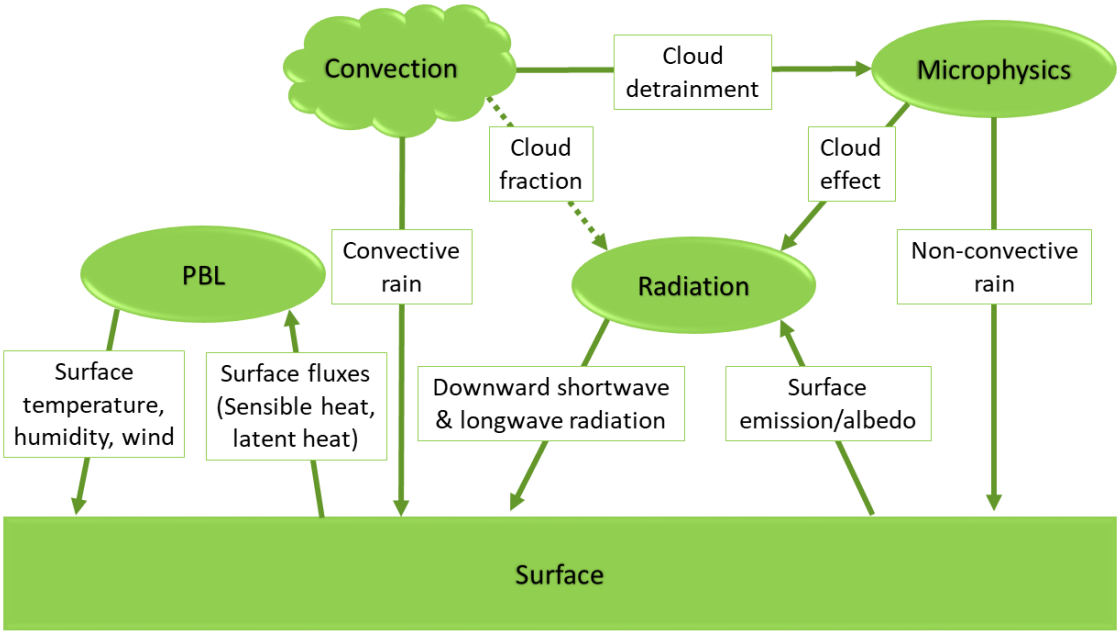

Figure 2.1: Interactions between WRF parameterization schemes. The variables exchanged appear on the arrows. The dotted arrow represent an interaction that is not present in all the sensitivity tests (Run 7 and 8 only, see Table 2.2 for the description of the runs).

The tests were conducted for a 1+3-year period: 1 year of spin-up and 3 years analyzed. Table 2.1 describes the different schemes tested, and Table 2.2 summarize the different tests conducted. The choice of the parameterizations tested is also largely based on Meynadier et al. (2015). Note that the Multi-scale Kain-Fritsch scheme is only available with the Yonsei University PBL scheme, and has only been tested with the two best LW and SW radiation schemes.

To determine the best set of parameters, we observe meridional sections of 8 variables: SST, SSS, precipitation, MLD, wind speed and the three main heat fluxes: the net shortwave and longwave radiations, and the latent heat flux (Figure 2.2). These 8 variables were chosen as indicators of the good representation of the ocean-atmosphere interactions and of the water cycle. Note that precipitation over land do not have impact on the ocean: river runoff is not interactive, but prescribed at the river mouths. These 8 variables show patterns relatively homogeneous zonally, making the meridional sections a good diagnostic to check whether simulations and observations are in agreement. We also analyze the convective processes in the model by plotting the cumulative precipitation as a function of the precipitation intensity (Figure 2.3a), as is done by Samson et al. (2014), and the precipitation intensity as a function of SST (Figure 2.3b) to evaluate the good representation of the SST-convection threshold (Sabin et al., 2013).

Table 2.1: List of the tested schemes and their acronyms

Options	Schemes tested	Reference
Microphysics	WSM6	Hong and Lim (2006)
Land Surface Model	Noah	Niu et al. (2011)
Convection	Betts-Miller-Janjic (BMJ)	Betts and Miller (1986) Janjić (1994)
	Multi-scale Kain-Fritsch (MSKF)	Zheng et al. (2016)
PBL	Yonsei University (YSU)	Hong et al. (2006)
	Assymetric Convective Model 2 (ACM2)	Pleim (2007)
Surface Layer	Revised MM5 Monin-Obukhov (MM5)	Jiménez et al. (2012)
	Pleim-Xiu	Pleim (2006)
LW Radiation	New Goddard	Chou et al. (2001)
	Rapid Radiative Transfer Model (RRTM)	Mlawer et al. (1997)
	RRTM for GCMs (RRTMG)	Iacono (2011)
SW Radiation	New Goddard	Chou and Suarez (1999)
	Goddard	Chou (1992)
	RRTM for GCMs (RRTMG)	Iacono (2011)

Table 2.2: List of the sensitivity tests conducted, with the corresponding combinations of parameterizations

Run	Convection	PBL	Surface Layer	LW / SW Radiation	Conv.-Rad. Feedback
—— 1	BMJ	YSU	MM5	New Goddard	No
- - - 2	BMJ	YSU	MM5	RRTMG	No
..... 3	BMJ	YSU	MM5	RRTM / Goddard	No
—— 4	BMJ	ACM2	Pleim-Xiu	New Goddard	No
- - - 5	BMJ	ACM2	Pleim-Xiu	RRTMG	No
..... 6	BMJ	ACM2	Pleim-Xiu	RRTM / Goddard	No
—— 7	MSKF	YSU	MM5	New Goddard	Yes
- - - 8	MSKF	YSU	MM5	RRTMG	Yes

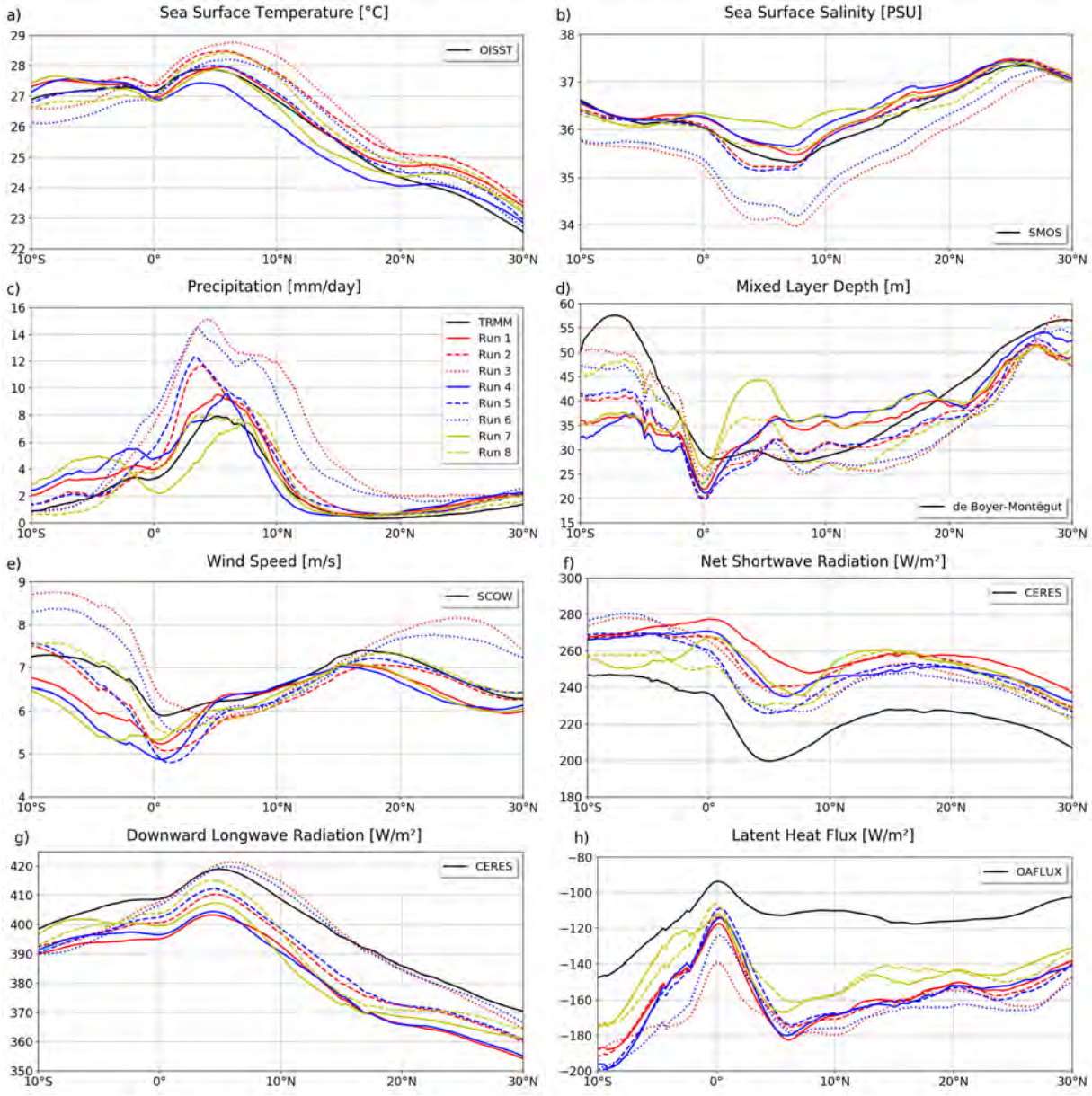

Figure 2.2: South-North sections, 3-years mean between 20°W and 40°W of a) Sea Surface Temperature, b) Sea Surface Salinity, c) Precipitation, d) Mixed Layer Depth, e) Net Shortwave Radiation, f) Net Longwave Radiation and g) Latent Heat Flux

The meridional sections first show us that the model is highly sensitive to the PBL scheme, the convection scheme and the radiative schemes used. But the model has the largest sensitivity to the radiative scheme for most of the variables (comparison between solid, dashed and dotted lines of the same color).

Run 3 and 6 (dotted lines), which use the RRTM and Goddard radiative schemes, can be first eliminated. The precipitation is far too intense with these schemes (Figure 2.2c, Figure 2.3b), and the cumulative precipitation far too high (Figure 2.3a). This impacts the

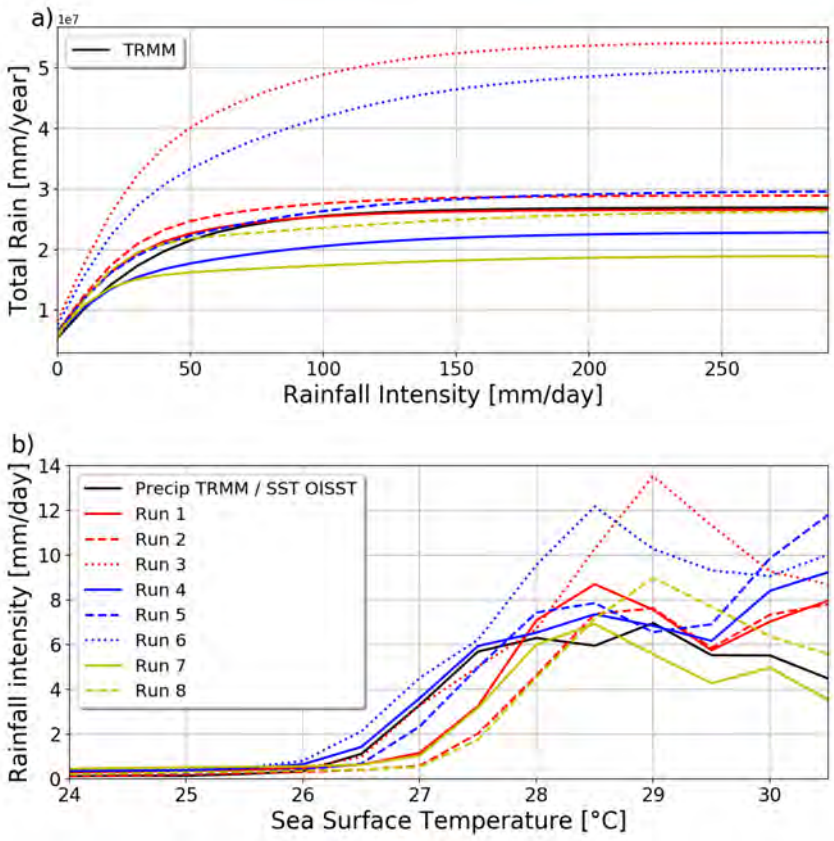

Figure 2.3: a) Total rainfall as a function of rainfall intensity and b) Rainfall intensity as a function of Sea Surface Temperature

SSS, which is consequently much too low. The wind speed is also too high, invalidating further these radiative schemes.

Run 7 can also be eliminated because it presents a double ITCZ bias: a secondary precipitation maxima is present in the southern hemisphere, and the maxima of the northern hemisphere is too far north (Figure 2.2c). SSS is also too high in the ITCZ area.

For Run 1 and 4, SST, SSS and precipitation are in relatively good agreement with the observations, but the MLD, the wind speed and the heat fluxes are not well represented compared to the other simulations. Moreover, they also have a problem representing the convective processes. Indeed, Run 1 has a SST in perfect agreement with the observations in the deep-convective area of the ITCZ (0°N-10°N), but the SST threshold for convection is around 0.5°C too high (Figure 2.3b), which means that there is not enough deep-convection. Similarly, Run 4 has a SST too cold by 0.5°C in the ITCZ area, but a SST threshold in agreement with the observations.

Run 2 and 5 perform good, apart from a slightly too high precipitation. But overall, Run 8 performs better, especially for the heat fluxes. The heat fluxes of this run also present a strong bias, but it is not as large as for the other sets of parameters. The SST-convection

threshold is 0.75°C too high but so is the SST, which leads to a cumulative precipitation close to the observations (Figure 2.3a). Finally, contrary to Run 2 and 5, Run 8 includes a feedback of the parameterized clouds in the radiation schemes (see Figure 2.1, dotted arrow). This is an important process to consider, because at this resolution a large part of the clouds are parameterized. Moreover, Section 1.2.5 showed that the clouds can feedback on the SST due to a modulation of the solar radiation, and we will see in Chapter 3 that this cloud feedback is important for the sensitivity of the coupled system to salinity stratification.

For all these reasons, the set of parameters of Run 8 was chosen and used in the rest of this work.

2.4 Validation of the configuration

2.4.1 Mean state

The CONTROL run is compared with the observational datasets in Figure 2.4. First, our model reproduces fairly well the observed regional patterns of SST, SSS, precipitation, MLD, net heat flux and thermocline depth. However, the model SST is slightly too warm, especially in the ITCZ, with a bias of about 1°C. The SST bias has a magnitude similar to that of the ensemble mean of CMIP5 and CMIP6 coupled GCMs, but is positive everywhere instead of negative in the western part of the basin as usually found in coupled GCMs (Richter and Xie, 2008; Richter et al., 2012,0; Xu et al., 2014). This bias does not appear to have any prominent impact on precipitation nor SSS. Indeed, both are in good agreement with the observations, apart from a slightly too intense precipitation in the ITCZ (about 2 mm/day) and a slighlty too high SSS in the central and northwestern tropical Atlantic (about 0.2-0.4 PSU), and near the Amazon mouth (about 2 PSU). Precipitation is better represented than in state-of-the-art coupled GCMs, except in the Gulf of Guinea (Breugem et al., 2008; Toniazzo and Woolnough, 2014; Siongco et al., 2015). The low salinity band associated with the Amazon plume and the ITCZ are particularly well represented, as is the meridional location of the ITCZ: our model does not show the ITCZ southward extension bias that is so frequent in the coupled GCMs in the tropical Atlantic (Richter et al., 2014; Tian and Dong, 2020; Richter and Tokinaga, 2020). It has therefore a better SSS than in coupled GCMs: in the major part of the basin, the SSS bias is more than twice lower than in the ensemble mean of CMIP6 coupled GCMs (not shown). SSS biases at river mouths may be partly attributed to the different time periods used for the observations and the model, and to the lower accuracy of SMOS near the coast and in areas of high variability such as river plumes, despite an improvement in the latest versions (Boutin et al., 2016, 2018).

The large-scale structure of the MLD is very similar to the observations, apart from the ITCZ and the Amazon plume where it is too thick (5 to 10 m, i.e. 20 to 40% too thick in the ITCZ; 10 to 20 m, i.e. 50 to 100% too thick in the Amazon plume). However, it should be kept in mind that the resolution of the MLD climatology is coarse (2°x2°) and could explain part of the inconsistencies observed. The net heat flux (considered positive downward) is too

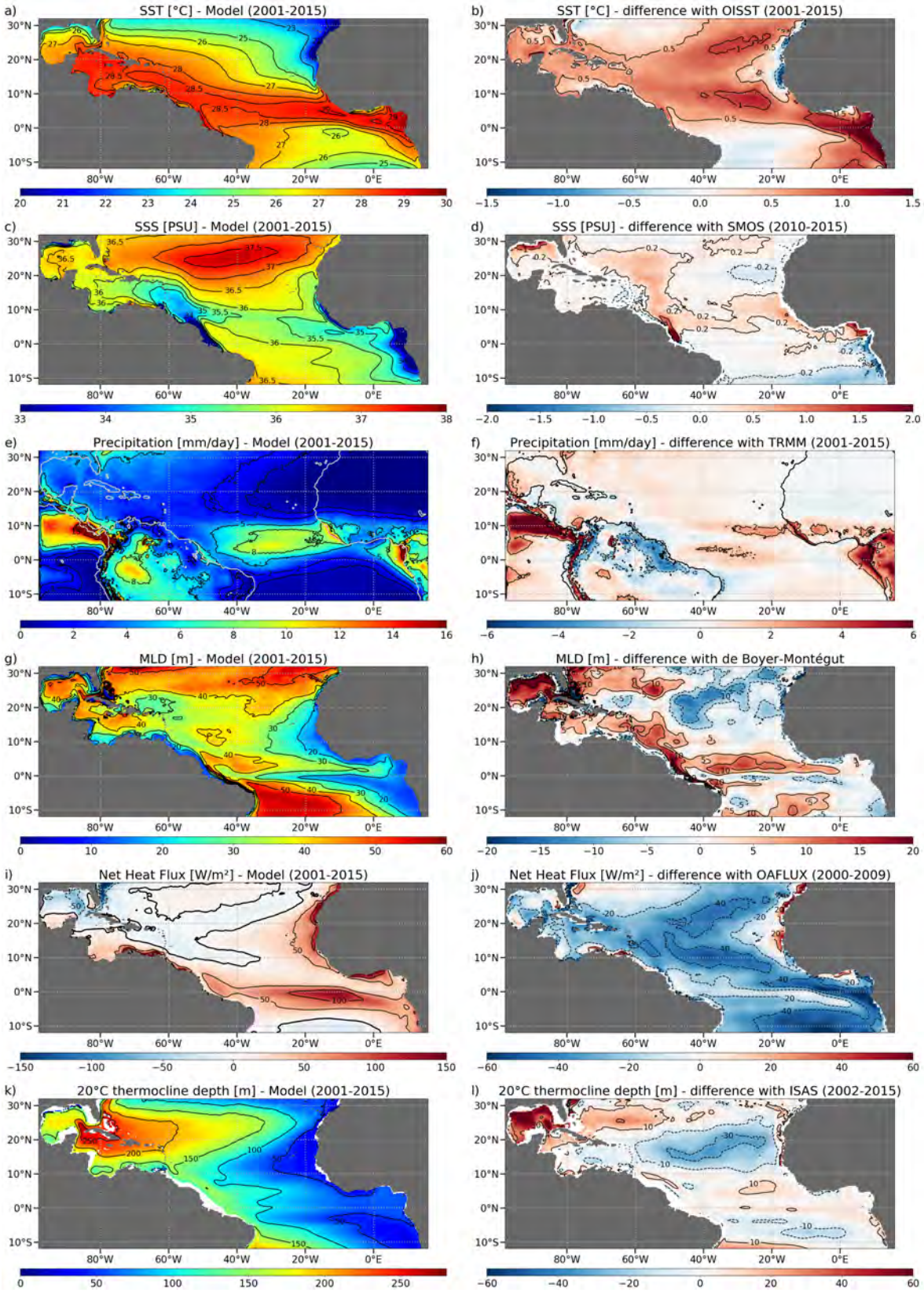

Figure 2.4: 2001–2015 annual climatology of a), b): SST; c), d): SSS; e), f): Precipitation; g), h): MLD; i), j): Net heat flux; k), l): 20°C isotherm depth — model (left column) and difference between the model and the observations (right column)

low, with a bias of -30 to -40 W/m^2 overall. It is caused by too much heat loss by latent heat flux (-40 to -50 W/m^2, not shown) that is partly compensated by a too strong shortwave heat flux (+10 to 20 W/m^2, not shown). While some of these biases undoubtedly fall within the range of the classical biases found in atmospheric and coupled GCMs (Kumar et al., 2012; Xu et al., 2014), OAFlux product is also known to have a positive bias over our region (Kumar et al., 2012), hereby exacerbating the negative bias estimate of our model. The 20°C isotherm depth, a proxy of the thermocline depth, is in good agreement with the observations except in the Gulf of Mexico where it is too deep.

The Gulf of Guinea is the least realistic area in the model, with some zones showing substantial biases of temperature (up to +2°C), salinity (down to -4 PSU) and precipitation (up to +12 mm/day). However, these strong differences occur over small areas and are located nearshore, outside of the areas we are interested in.

2.4.2 Seasonal and interannual variability

We now assess the ability of the model to reproduce the seasonal and interannual variability of the regional salinity (Figure 2.5) and temperature (Figure 2.6), the two main variables of interest. Figure 2.5a and 2.5b show the standard deviations (STD) of monthly SSS from 2010 to 2015 for the CONTROL simulation and for SMOS respectively. The patterns are well reproduced by the model, but the variability near the Amazon mouth is slightly too high in the model. Figure 2.5c shows the SSS seasonal cycle for CONTROL (in red) and SMOS (in black) in the Amazon-Orinoco plume, which is our main region of interest. The Amazon-Orinoco plume is defined as the region where the mean SSS from 2001 to 2015 in CONTROL is under 35 PSU. The phase of the seasonal cycle is well simulated, but the amplitude is a little too strong in the model, with a slighlty too high SSS in boreal winter, and a slightly too low SSS in boreal spring.

Figure 2.5d shows SSS monthly anomalies with respect to their 2010-2015 monthly climatology for CONTROL (in red) and SMOS (in black), averaged in the Amazon-Orinoco plume. The two time series are overall in good agreement from 2012 onwards. There is a SSS peak in 2010 in CONTROL that does not appear in SMOS observations, even though it coincides with one of the most severe Amazon droughts ever recorded (e.g. Barichivich et al., 2018). Some salinity drops are also present in our model but not in the observations (2011, 2014). These discrepancies can be due to the underestimation of SSS on the Amazon shelf in the model due to the too coarse resolution of the model and/or to the absence of tides (Ruault et al., 2020). As before, it can also be caused by a lower accuracy of SMOS data near the coasts and in river plumes (Boutin et al., 2016, 2018).

Temperature variability is very well reproduced by the model (Figure 2.6). STDs are very similar in CONTROL (Figure 2.6a) and OISST (Figure 2.6b), apart from a slightly too high variability in the model near the Amazon mouth, in the Caribbean sea and in the Senegal-Gambia upwelling. The seasonal cycle in the Amazon-Orinoco plume is also rather well reproduced (Figure 2.6c). Even if the bias in mean state described earlier is also present

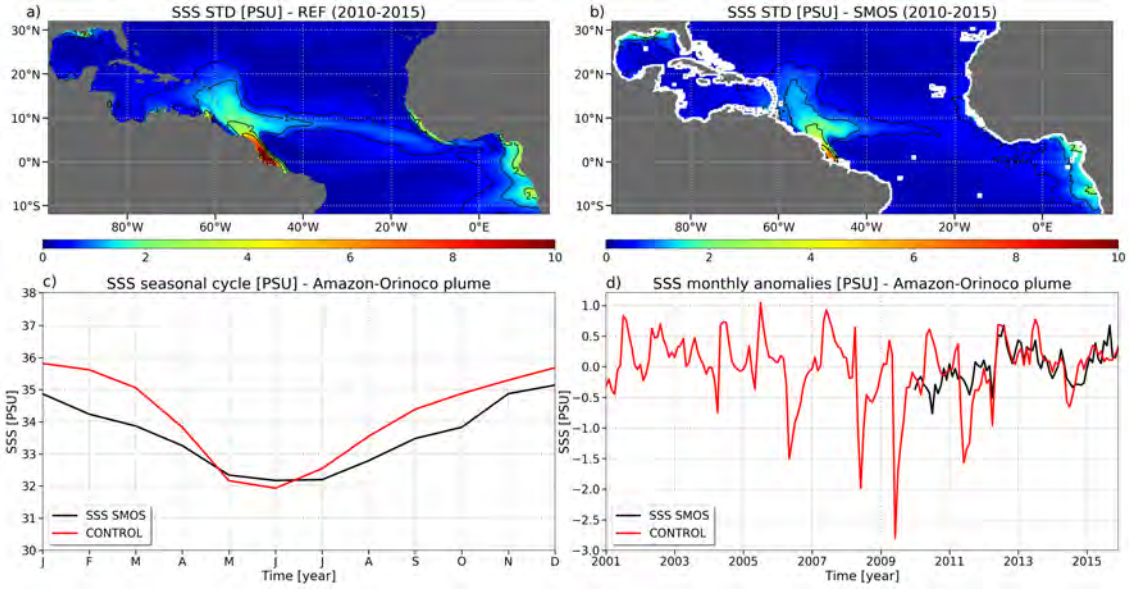

Figure 2.5: 2010–2015 monthly standard deviation of SSS for a) CONTROL run and b) SMOS observations; c) seasonal cycle of SSS and d) monthly anomalies of SSS for CONTROL (red) and SMOS (black). In c) and d), the SSS is averaged over the Amazon-Orinoco plume, defined as the western tropical Atlantic region where the mean SSS from 2001 to 2015 in CONTROL is under 35 PSU.

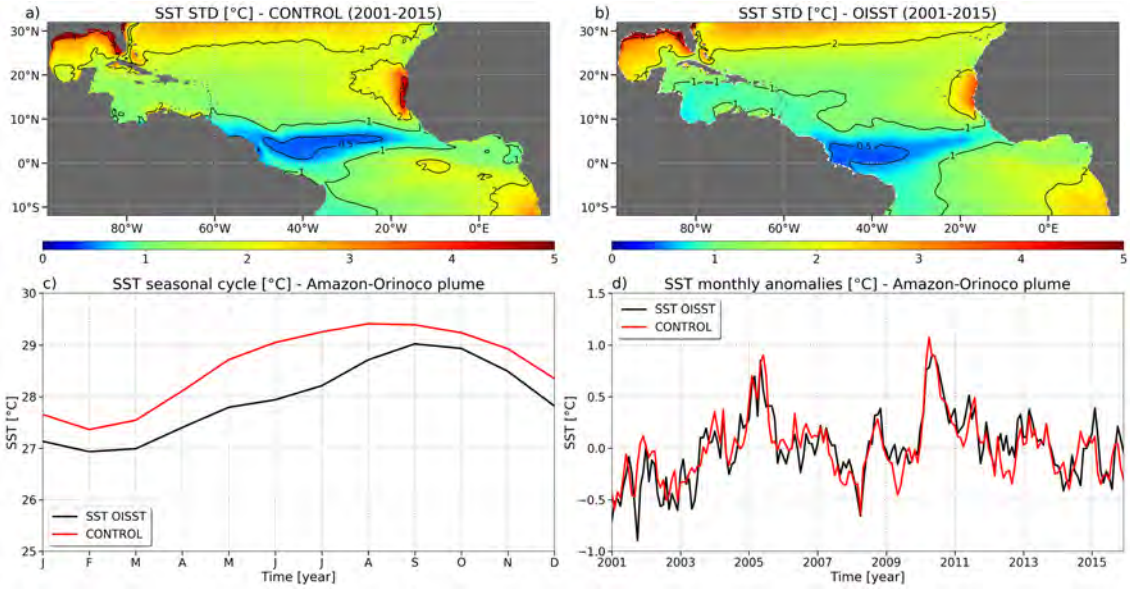

Figure 2.6: 2001–2015 monthly standard deviation of SST for a) CONTROL run and b) OISST observations; c) seasonal cycle of SST and d) monthly anomalies of SST for CONTROL (red) and OISST (black). In c) and d), the SST is averaged over the Amazon-Orinoco plume, defined as the western tropical Atlantic region where the mean SSS from 2001 to 2015 in CONTROL is under 35 PSU.

in this region (0.5 to 1°C), the seasonal amplitude is close to observations, without any prominent phase shift of the seasonal cycle. Finally, the interannual variability of the model in the Amazon plume is in very good agreement with the observations, and all the main variations are properly reproduced (Figure 2.6d). This indicates a strong constraint by the ocean and atmospheric lateral boundary conditions, and a weak internal variability of the coupled model.

In conclusion, the model compares overall fairly well with the observations, apart from a bias in heat fluxes commonly found in GCMs.

2.5 Methods

In the following, we present the methods common to the entire thesis. The methods more specific to each chapter will be presented in each of them.

2.5.1 Mixed layer budgets

2.5.1.1 Heat budget

A mixed layer heat budget was calculated online at each time step, following Vialard and Delecluse (1998). It consists of an integration of the equation of temperature over the ML, expressed as follows:

$$\underbrace{\partial_t T}_{\text{Total tendency}} = \underbrace{< -u\partial_x T - v\partial_y T >_h}_{\text{Horizontal Advection}} + \underbrace{< D_l >_h}_{\text{Lateral Diffusion}} + \underbrace{\frac{Q_s(1-F_{-h})+Q_{ns}}{\rho_0 C_p h}}_{\text{Atmospheric Forcing}} + \underbrace{\underbrace{< -w\partial_z T >_h}_{\text{Vertical Advection}} + \underbrace{\frac{(K_z\partial_z T)_{z=-h}}{h}}_{\text{Vertical Diffusion}} + \underbrace{\frac{\partial_t h}{h}(T_{-h} - < T >_h)}_{\text{Entrainment}}}_{\text{Vertical Processes}} \tag{2.1}$$

with

$$< \bullet >_h = \frac{1}{h}\int_{-h}^{0} \bullet \tag{2.2}$$

where T is the model temperature, u the zonal current, v the meridional current, w the vertical current, K_z the vertical diffusion coefficient and D_l the lateral diffusion. Q_s and Q_{ns} are respectively the solar and non-solar part of the total heat flux, F_{-h} is the fraction of shortwave radiation reaching the base of the ML, and T_{-h} the temperature at the

ML base. Finally, the MLD, h, is calculated using a threshold criterion $\Delta\sigma = 0.01\ kg/m^3$ (de Boyer Montégut et al., 2007b). We chose this criterion, different from the one used previously, for consistency with several dynamical parameterizations in NEMO (Madec and the NEMO team, 2016).

This approach was used in several other studies (Vialard and Delecluse, 1998; Durand et al., 2004; Menkes et al., 2006; Peter et al., 2006; Hernandez et al., 2016; Krishnamohan et al., 2019). It allows to quantify the temperature tendency due to advection, diffusion, atmospheric forcing and entrainment. The entrainment term arises from the integration of the temperature equation over a time-varying ML. In the litterature, however, the entrainment sometimes refers to the processes at the ML base (mixing, vertical advection). In the remainder of the manuscript, to avoid confusion, the only meaning of the term "entrainment" will be that given by Equation 2.1.

2.5.1.2 Salt budget

Similarly, a mixed layer salt budget was calculated online at each time step, and is expressed as follows:

$$\underbrace{\partial_t S}_{\text{Total tendency}} = \underbrace{< -u\partial_x S - v\partial_y S >_h}_{\text{Horizontal Advection}} + \underbrace{< D_l >_h}_{\text{Lateral Diffusion}} + \underbrace{\frac{(E-P)S}{h}}_{\text{Atmospheric Forcing}} + \underbrace{\underbrace{< -w\partial_z S >_h}_{\text{Vertical Advection}} + \underbrace{\frac{(K_z\partial_z S)_{z=-h}}{h}}_{\text{Vertical Diffusion}} + \underbrace{\frac{\partial_t h}{h}(S_{-h} - < S >_h)}_{\text{Entrainment}}}_{\text{Vertical Processes}} \tag{2.3}$$

where S is the model temperature, u the zonal current, v the meridional current, w the vertical current, K_z the vertical diffusion coefficient and D_l the lateral diffusion. $E-P$ is the air-sea freshwater flux, with E the evaporation and P the precipitation. S_{-h} is the salinity at the ML base, and h is the MLD, calculated using the same threshold criterion of $\Delta\sigma = 0.01\ kg/m^3$. Note that the river runoff is imposed as a divergence of the flow at the coastal point closest to the river mouth, and is therefore included in the advection term.

Both budgets were calculated online, at each time step of the ocean model (i.e. every 30 minutes), and averaged monthly afterwards.

2.5.2 Pycnocline depth and barrier layer thickness

The pycnocline depth D_σ is estimated as the depth where a density increase corresponding to a temperature decrease of 0.2°C at 10 m depth is found (de Boyer Montégut et al., 2004, 2007a):

$$D_\sigma = depth\ where\ [\,\sigma_0 = \sigma_0(T_{10m} - 0.2°C, S_{10m}, P_0)\,] \tag{2.4}$$

In areas of intense precipitation or in river plumes, some decoupling may occur between the haline and the thermal stratification of the upper ocean. In such a situation, the low surface salinity limits the pycnocline to the halocline depth, while the thermocline is located deeper: a barrier layer appears (Godfrey and Lindstrom, 1989; Lukas and Lindstrom, 1991). The barrier layer thickness (BLT) is then defined as the difference between the top of the thermocline depth and the pycnocline depth (Sprintall and Tomczak, 1992):

$$BLT = D_{T_{-0.2}} - D_\sigma \tag{2.5}$$

with

$$D_{T_{-0.2}} = depth\ where\ [T = T_{10m} - 0.2°C] \tag{2.6}$$

the top of the thermocline depth (de Boyer Montégut et al., 2004, 2007a).

2.5.3 Salinity contribution to total stratification (OSS_{100m})

To characterize the strength of the salinity stratification, we rely on the OSS_{100m} indicator (Maes and O'Kane, 2014):

$$OSS_{100m} = \frac{< N^2 S >_{100m}}{< N^2 >_{100m}} \tag{2.7}$$

with

$$N^2 = -\frac{g}{\rho_0}\frac{\partial \rho(T,S)}{\partial z} \tag{2.8}$$

the Brunt-Väisälä frequency, where ρ_0 is the sea water density, equal to 1026 kg/m^3, g is the acceleration of gravity, T is the model temperature and S the model salinity. N^2 represents the total stratification, and can be expressed as the sum of the stratification due to temperature N^2T and the stratification due to salinity N^2S:

$$N^2 = N^2S + N^2T \tag{2.9}$$

with

$$N^2S = -\frac{g}{\rho_0}\frac{\partial \rho(T_0,S)}{\partial z} \quad , \quad N^2T = -\frac{g}{\rho_0}\frac{\partial \rho(T,S_0)}{\partial z} \tag{2.10}$$

T_0 and S_0 are constant temperature and salinity values respectively that are representative of the area. Since salinity is more homogeneous than temperature, we chose to calculate N^2S as the difference between N^2 and N^2T (Equation 2.9), as in Hernandez et al. (2016). S_0 is taken equal to 36, which corresponds to the mean value of salinity in the upper 100 m in our

areas of interest (CT, NWTA, ITCZ). We also verified that OSS_{100m} is not sensitive to the chosen value of S_0. N^2, N^2S and N^2T are calculated from the outputs of the CONTROL run. The value of 100 m is chosen as the depth at which salinity stratification becomes close to zero and negligible compared to temperature stratification.

OSS_{100m} is the contribution of salinity stratification N^2S to total stratification N^2, both of which averaged over the first 100 meters. It is expressed as a percentage of N^2.

2.5.4 Significance of the anomalies in simulations intercomparisons

In the rest of this work, the CONTROL simulation is compared with other simulations. The significance of the differences between the two simulations is based on a two-tailed Student's t-test, with a confidence level of 99%. Anomalies considered statistically significant are indicated by dots on the difference maps in Figure 3.1, 3.7, 3.8, 3.10, 4.1, 4.2, 4.4, 6.6, 6.9.

Chapter 3

Impact of salinity stratification

Contents

3.1 Introduction

The aim of this chapter is to study the influence of salinity stratification on the tropical Atlantic Ocean climate. Indeed, as discussed in Section 1.3, the main mechanism by which salinity can influence the air-sea interactions is through changes in ocean stratification. The next step is therefore to assess the impact of salinity stratification on SST and air-sea fluxes. To this end, a twin sensitivity simulation is performed, for which the contribution of salinity stratification in the vertical mixing scheme is included or discarded. Removing salinity stratification also means removing BL, whose impact on SST and air-sea interactions is controversial (see Section 1.3.2).

This idealized approach has already been adopted by several studies, in different regions of the world: in the western tropical Pacific Ocean (Vialard and Delecluse, 1998), in the western tropical Atlantic Ocean (Masson and Delecluse, 2001), in the southeastern Arabian Sea (Masson et al., 2005) and in the northern Bay of Bengal (Krishnamohan et al., 2019). They obtained different results depending on the region: an impact of up to 0.5°C on SST is observed in the tropical Pacific and in the Arabian Sea, while no SST change is observed in the tropical Atlantic and in the Bay of Bengal. Nevertheless, all these studies were conducted using forced ocean models. Here, the use of a coupled ocean-atmosphere model allows us to be confident that the air-sea interactions are well reproduced, and that the response of SST and air-sea fluxes to salinity stratification is as accurate as possible and is not damped artificially by prescribed atmospheric variables used in the computation of the air-sea fluxes.

This chapter is based on the peer-reviewed publication of Gévaudan et al. (2021) (see Appendix A for the published version).

3.2 Methodology

We describe here the methodology specific to this chapter. The rest of the methods are described in Chapter 2, and especially the coupled configuration (Section 2.1) and its validation (Section 2.4), the mixed layer heat budget (Section 2.5.1.1), the definition of barrier layer thickness and pycnocline depth (Section 2.5.2), and the way of defining the anomalies significance (Section 2.5.4).

3.2.1 Simulations

In this chapter, we conducted two ocean-atmosphere coupled simulations: a CONTROL simulation described in Section 2.1, and a sensitivity simulation NOS. In NOS, following Vialard and Delecluse (1998), the salinity gradient is set to zero in the Brunt-Väisälä frequency calculation over the whole domain. The Brunt-Väisälä frequency (N^2), a measure of the ocean stratification, enters as a sink term (or a source term in case of static instability) in the turbulent kinetic energy prognostic equation that is used to derive the vertical diffusion

coefficient K_z (Reffray et al., 2015; Madec and the NEMO team, 2016). Thus, through removing the sensitivity of N^2 to salinity variations, this experiment allows to remove the contribution of salinity stratification to vertical mixing, without direct modification of the model water density. Both sensitivity experiments are conducted from 2000 to 2015, and the analyses conducted hereafter rely on a 15-year period from 2001 to 2015.

3.2.2 Areas of interest

In the following, we will see that two regions show particularly interesting features. We define here two areas in which analyses will be conducted: the northwestern tropical Atlantic (NWTA, 70°W–50°W and 5°N–18°N), and the equatorial cold tongue (CT, 25°W–0°E and 3°S–1°N). The two boxes are drawn on Figure 3.1a.

3.3 Results

3.3.1 Impact of salinity stratification on SST

The impact of salinity stratification on the SST is obtained for summer (June-July-August, JJA) and winter (December-January-February, DJF), as the difference between simulations CONTROL and NOS (Figure 3.1a and 3.1b). The sensitivity to salinity stratification is largest in summer, with a warming of 0.2°C-0.5°C in the NWTA, and a cooling of 0.2°C-0.5°C in the equatorial region, especially in the CT. Over the rest of the basin, the response is not statistically significant. In winter, the response is weaker albeit statistically significant in some localized areas like the ITCZ. It is also worth mentioning that there is a very limited change in SST in the ITCZ throughout the year, despite heavy precipitation in this area.

The seasonal cycle of SST in the NWTA and in the CT (Figure 3.1c) confirms that changes are maximum in summer, and almost null in winter. It shows that the presence of salinity stratification increases the amplitude of the seasonal cycle in both regions (+6% in the NWTA, +9% in the CT). Note finally that the SST seasonal cycles in the NWTA and the CT are opposed.

We will now investigate the causes of this contrasted sensitivity of SST among these regions and seasons.

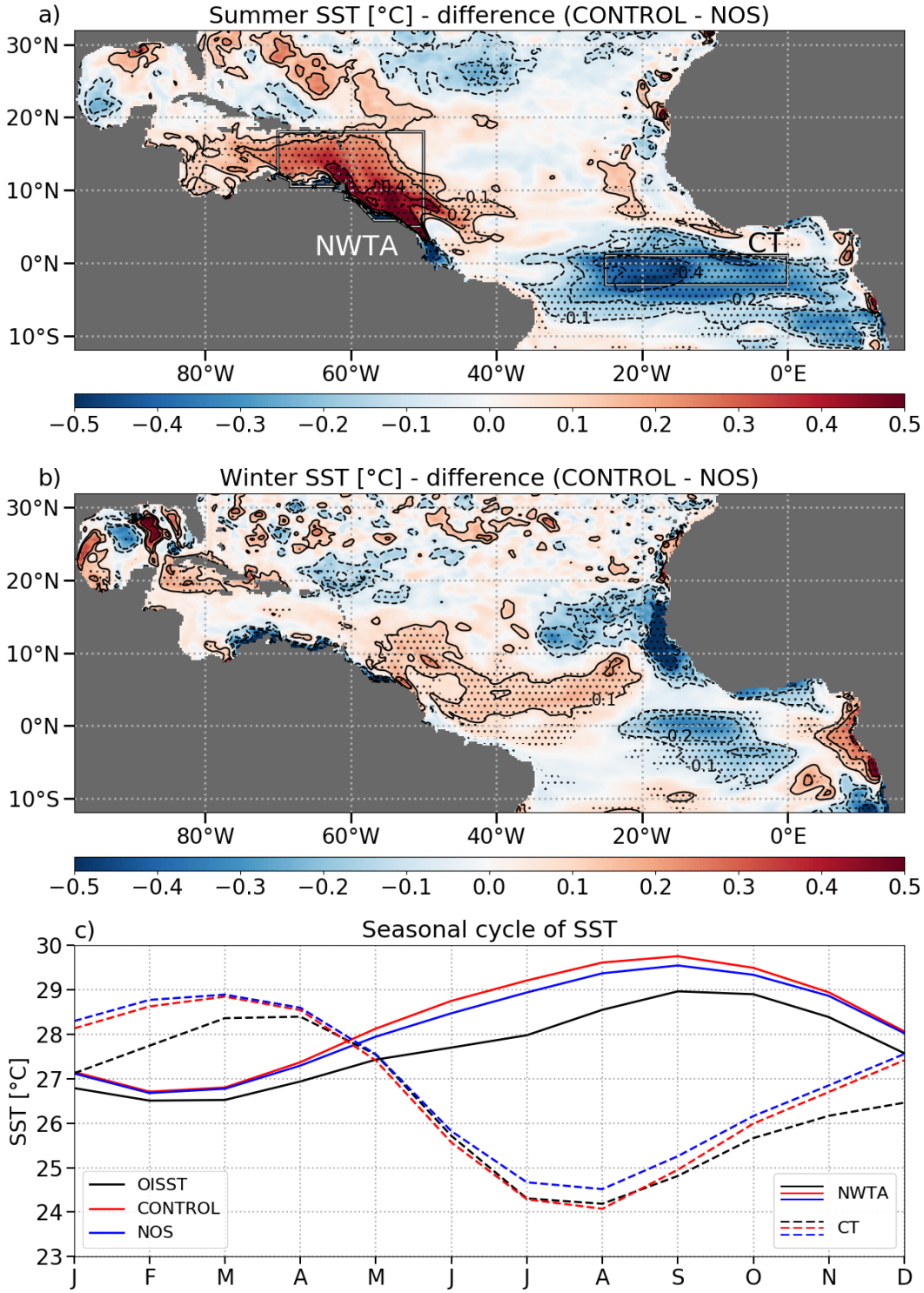

Figure 3.1: SST differences between CONTROL and NOS in a) summer (JJA) and b) winter (DJF), dots indicating the areas where the difference is significant ; c) SST seasonal cycle in the NWTA and the CT (the two boxes are drawn on Figure a);

3.3.2 Northwestern tropical Atlantic SST anomaly

3.3.2.1 Impact of salinity stratification on SST

In summer, the warm anomaly in CONTROL with respect to NOS in the NWTA corresponds to a region with large haline stratification. It is revealed by the OSS_{100m} distribution (Figure 3.2a), which represents the strength of salinity stratification as a percentage of the total stratification. During winter, such a link does not exist (Figure 3.2b). Note that the OSS_{100m} summer map shows patterns very similar to those obtained by Sallée et al. (2021) using observations.

This contrast between summer and winter in terms of sensitivity of the surface temperature to the local haline stratification is confirmed in Figure 3.3a and 3.3c: during summer, the higher the OSS_{100m}, the larger the SST anomalies; it reaches 1.2°C where OSS_{100m} equals 90%. In winter, the SST anomalies between the two simulations are weak and are not related to the strength of the salinity stratification (Figure 3.3c). We relate this seasonal contrast to a

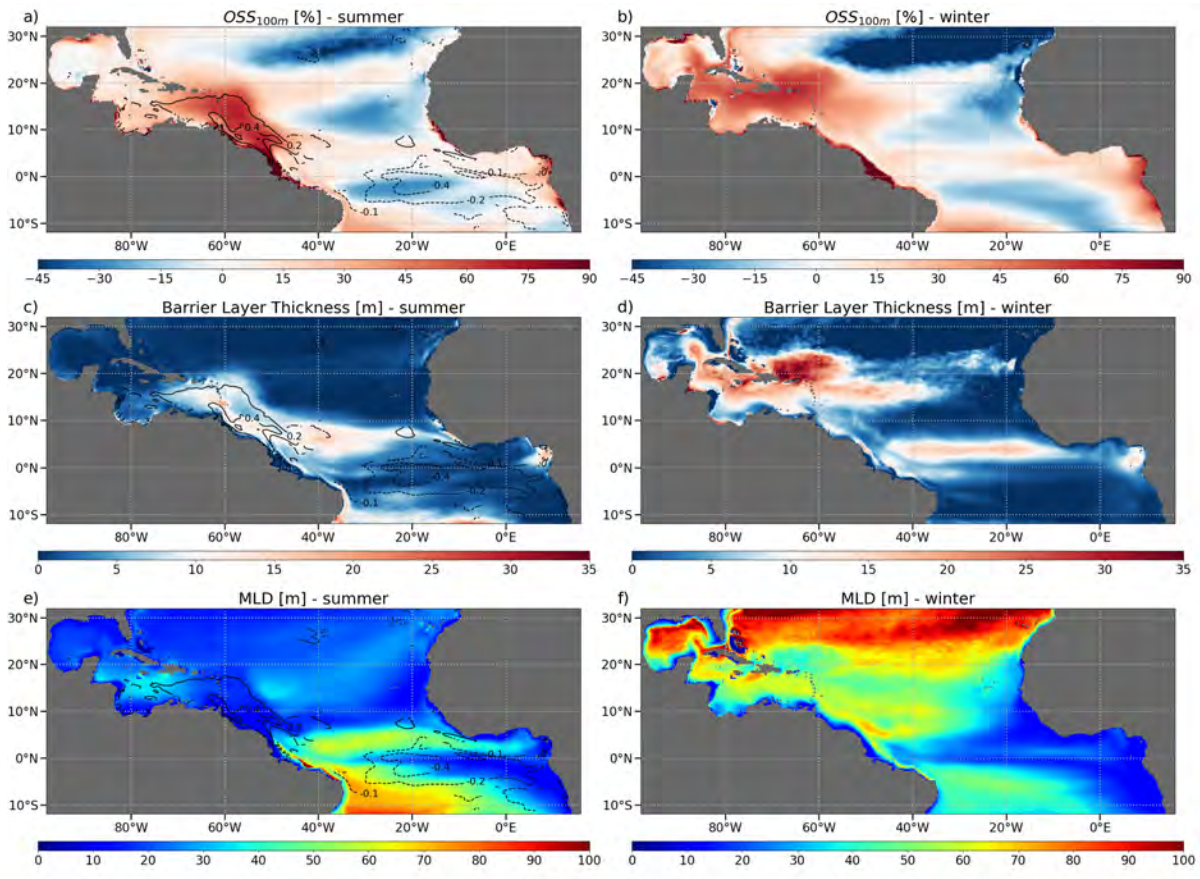

Figure 3.2: Summer (JJA) maps of a) OSS_{100m}, c) BLT and e) MLD for CONTROL simulation; summer SST differences contours are plotted, only where they are statistically significant. b), d), f): same than a), c), e) respectively, but in winter (DJF).

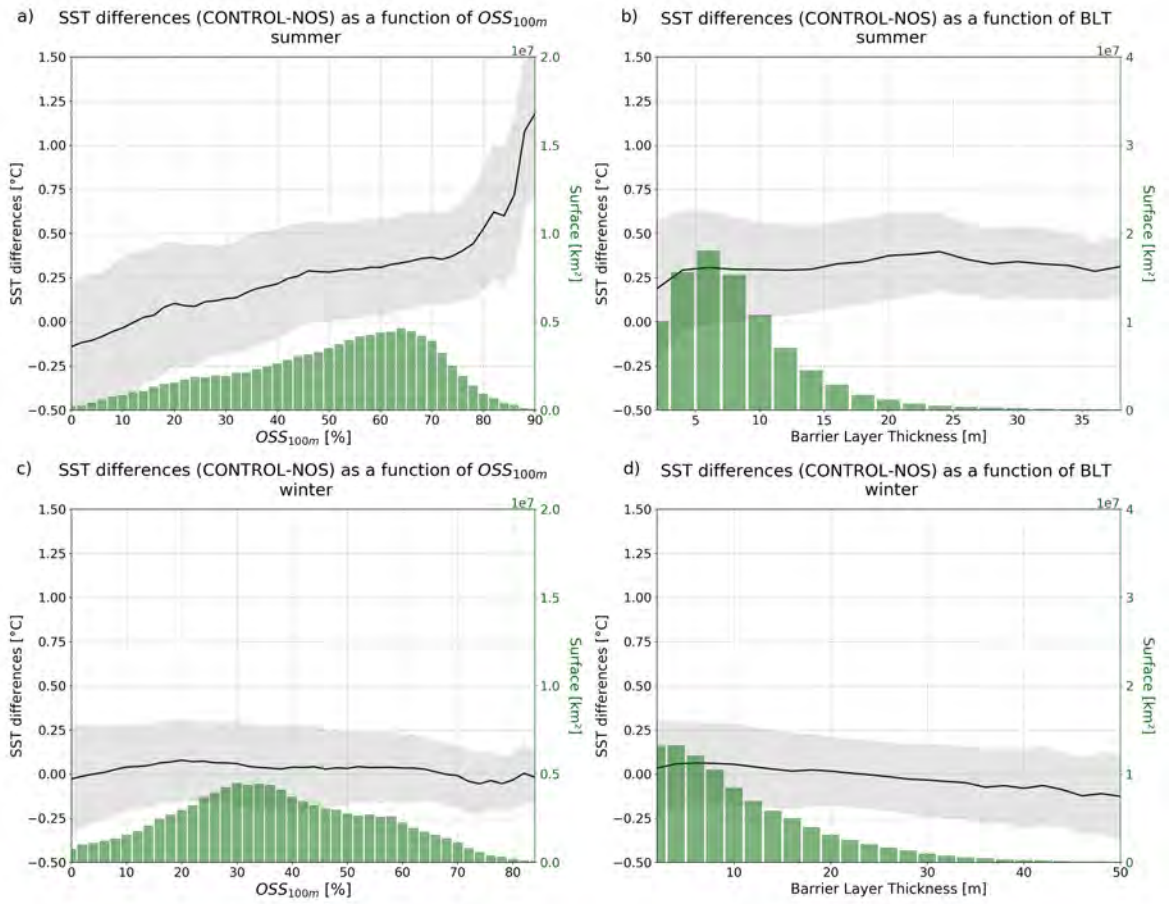

Figure 3.3: Summer (JJA) SST differences as a function of a) OSS_{100m} and b) BLT for CONTROL run, envelope: $\pm\sigma$; coastal areas (i.e. areas where the bathymetry is under 50 m) were removed, as well as values corresponding to less than 100 grid cells. c), d): same than a), b) respectively, but in winter (DJF). For each figure, bins surfaces are represented on a histogram. The analyze is applied on the NWTA box.

much deeper MLD in winter compared to summer (Figure 3.2e and 3.2f). In summer, salinity stratification is maximum in the Amazon plume area, with MLDs between 10 m and 20 m, while in winter, salinity stratification is maximum in the Caribbean Sea, with a mean MLD reaching 60 m to 70 m. This implies that the positive temperature anomaly due to salinity effects is spread over a deeper layer in winter, resulting in a weak SST response regardless of the salinity stratification strength.

3.3.2.2 Mixed layer heat budget

To understand more precisely how salinity stratification impacts SST, we now analyze the seasonal heat budget of the ML (see Section 2.5.1.1) in the NWTA (Figure 3.4a and 3.4c). The ML temperature tendency is controlled at first order by the air-sea fluxes and by two

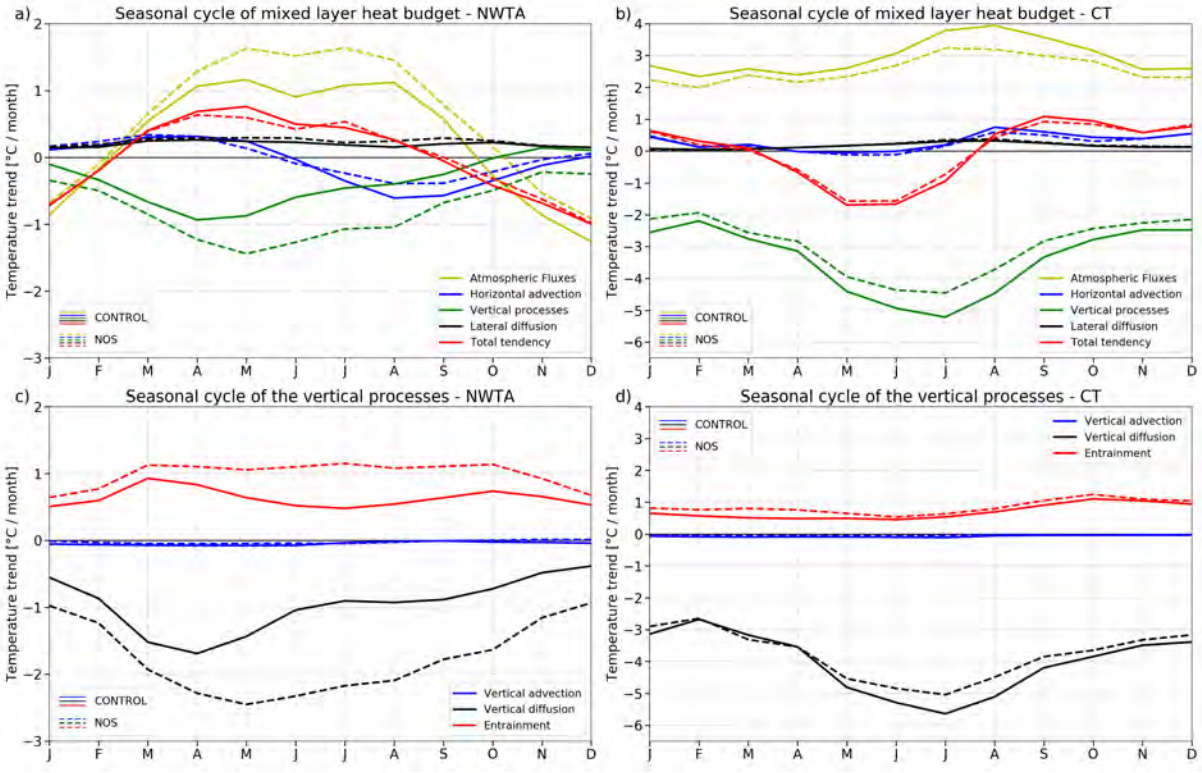

Figure 3.4: Seasonal cycle of mixed layer heat budget in a) NWTA and b) CT ; c) and d): same than a) and b) respectively, but for the vertical processes

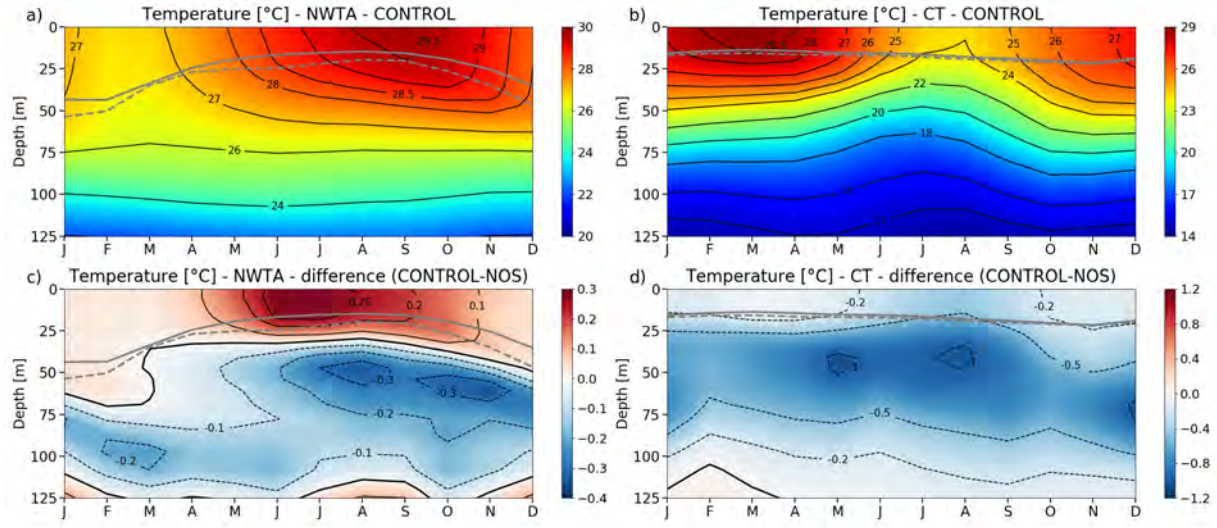

Figure 3.5: Seasonal cycle of temperature section in NWTA for a) CONTROL simulation and c) the difference (CONTROL-NOS) ; b) and d): same than a) and c) respectively, but in the CT. The gray lines represent the ML for CONTROL (solid line) and NOS (dashed line).

vertical processes: the vertical mixing and the entrainment. Moreover, the changes between CONTROL (solid lines) and NOS (dashed lines) mainly concern these three processes. First, a reduction of cooling due to vertical mixing occurs when salinity stratification is considered, because of the stabilizing effect of the salinity stratification. This reduction of the vertical mixing is illustrated by Figure 3.5a and 3.5c, which represent the seasonal evolution of the temperature profile in NWTA: the inclusion of salinity stratification in CONTROL reduces the mixing between the surface and subsurface, leading to a warm anomaly at the surface and a cold anomaly in subsurface. This effect of vertical mixing has already been observed by Deppenmeier et al. (2020). The surface warming happens all year long but is stronger in summer, when salinity stratification is stronger and the ML is at its shallowest.

The reduction of cooling due to vertical mixing reaches 1.2°C/month in summer (Figure 3.4c). It is then partly compensated by a decrease of the warming due to air-sea fluxes and entrainment, each with a contribution of about 0.5°C/month in summer (Figure 3.4a and 3.4c). It results in a 0.1 to 0.2°C/month differential warming between CONTROL and NOS during the summer season, leading to the positive SST anomaly observed in Figure 3.1a. In winter, the changes are much smaller for all the processes and compensate each other so that there is no change in SST.

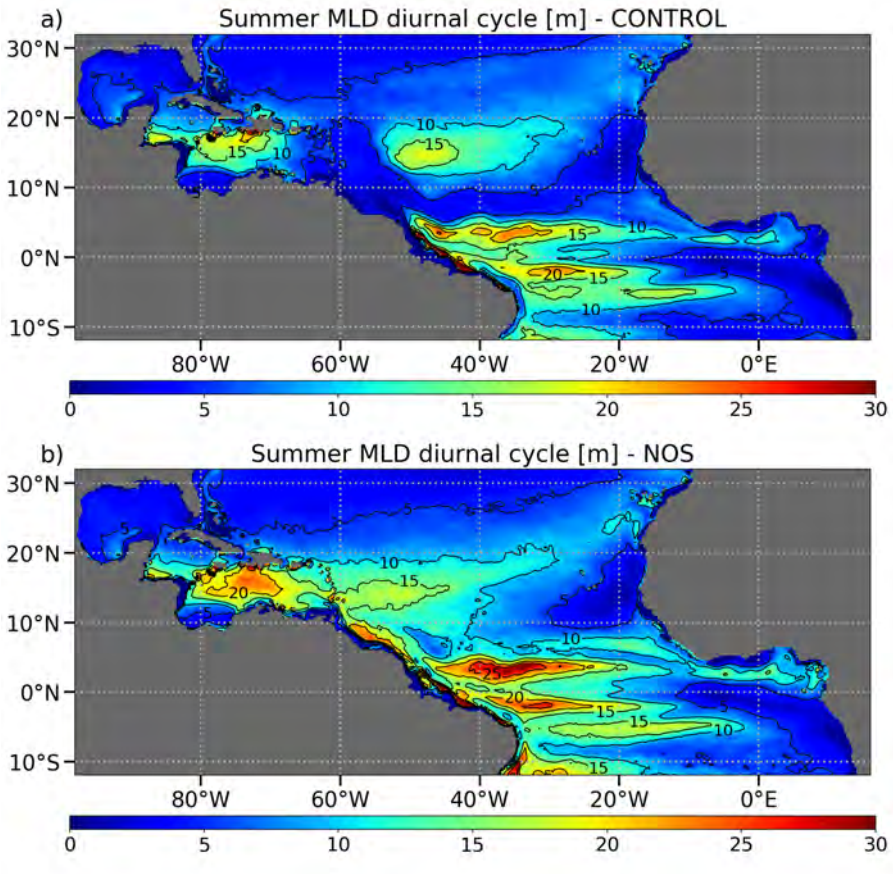

Figure 3.6: Summer (JJA) maps of MLD diurnal cycle for a) CONTROL simulation and b) NOS simulation.

Entrainment is a term that appears when the equation of temperature is integrated on the time-varying ML (see Equation 2.1). During ML deepening events, entrainment is null: in that case, the mean temperature of the ML is equal to the temperature at the base of the ML, which means that the factor $(T_{-h} - < T >_h)$ is equal to zero. Entrainment is therefore controlled by the occurrence of restratification events, and especially those due to the diurnal cycle. In the CONTROL experiment, the MLD diurnal cycle is close to zero in the regions where salinity stratification is strong - and especially the NWTA, while it is important in the NOS experiment due to the absence of salinity stratification (Figure 3.6). As a consequence, the daily restratification is less important in CONTROL than in NOS simulation, leading to a weaker $\partial_t h$ factor and explaining the lower entrainment in the CONTROL simulation.

3.3.2.3 Impact of salinity stratification on the atmosphere

As mentioned previously, the air-sea fluxes also dampen the SST differences between the two simulations. This negative feedback of the atmosphere is now investigated. We focus on summer, as this is the season with the largest changes. Figure 3.7 represents CONTROL-NOS summer differences of the key atmospheric variables. Mean values in summer and NWTA are detailed in Table 3.1 for the heat fluxes, and Table 3.2 for the other atmospheric variables.

The net heat flux (Figure 3.7a) - positive, tending to warm the ocean - is much weaker in CONTROL than in NOS in the NWTA region (decrease of more than 30% on average over the NWTA box; Table 3.1). This is linked to lower net shortwave radiation (Figure 3.7b), responsible for about 29% of the total change in net heat flux, and larger heat loss by latent heat flux (Figure 3.7c), responsible for about 71% of the change. Differences in longwave radiation and sensible heat flux are small (< 1 W/m^2; Table 3.1).

The increase in latent heat loss can be explained by the SST increase, the wind changes being weak in the NWTA (Figure 3.7e, Table 3.2). This leads to a negative feedback of latent heat flux on SST (Section 1.2.3). Over the western tropical Atlantic, the increase in latent heat loss resulting from the SST increase is commonplace in observational air-sea flux databases (Kumar et al., 2017).

The change in net shortwave radiation is due to negative feedback from clouds (see Section 1.2.5). The warm SST anomaly leads to an enhancement of atmospheric deep convection (Sabin et al., 2013) and thus to a more prominent cloud cover (Figure 3.7d). This change in cloud cover is significant (about 15% increase between NOS and CONTROL), and is mainly associated to a change in high clouds (not shown), confirming the enhancement of deep convection. This causes the observed decrease in net shortwave radiation by capturing a part of the incident solar radiation. More extended cloud cover is also consistent with a 19% increase in precipitation between NOS and CONTROL (Figure 3.7f). Moreover, it is worth noting the northward shift of the ITCZ when salinity stratification is considered, which may result from the large scale SST anomaly dipole (Figure 3.1b).

The longwave radiation differences are weak (Table 3.1). This is due to a compensation between the SST increase, leading to more longwave radiation emitted by the ocean, and the

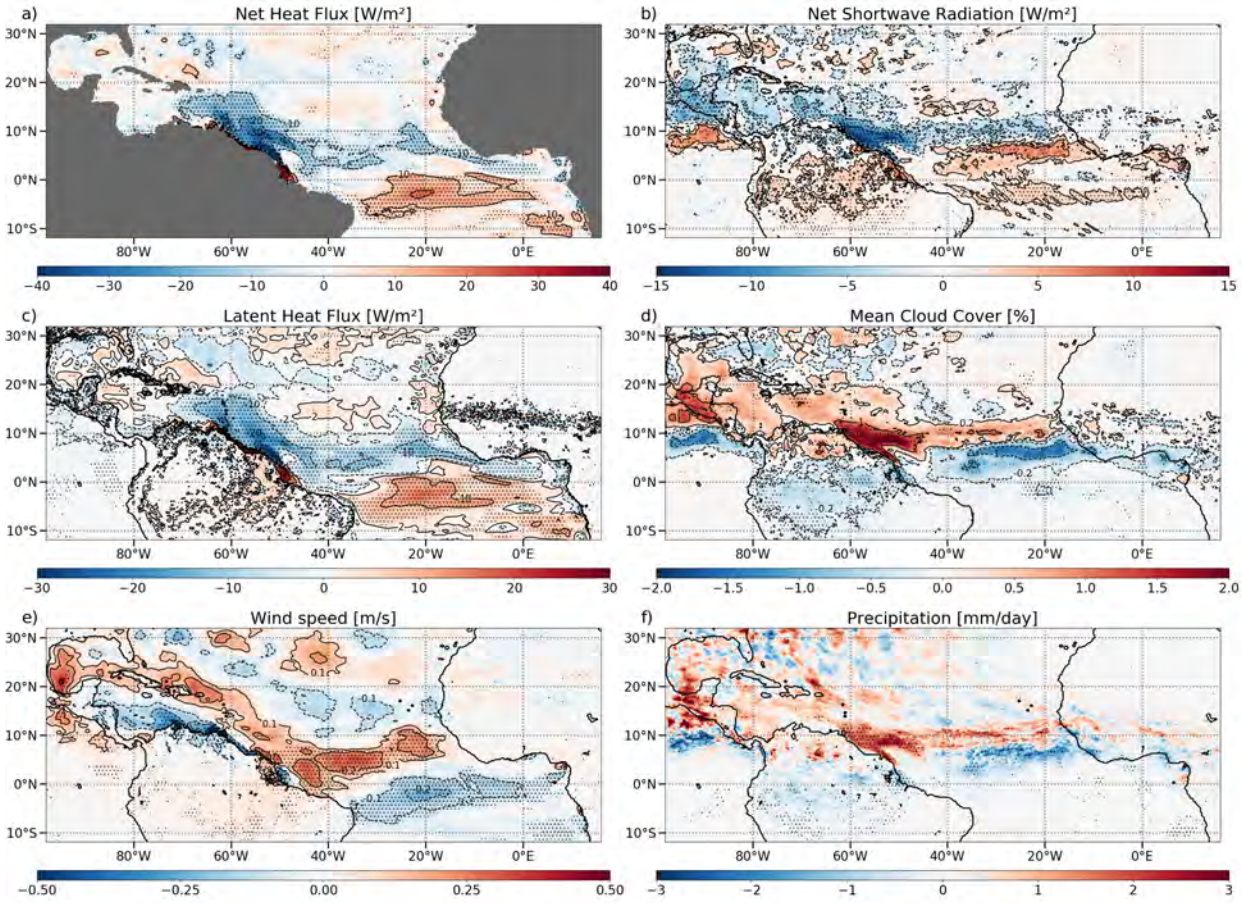

Figure 3.7: Difference between CONTROL and NOS in summer (JJA) of a) Net Heat flux, b) Net Shortwave Radiation, c) Latent Heat Flux, d) Cloud Cover, e) Wind speed and f) Precipitation, dots indicating the areas where the difference is statistically significant

cloud cover increase, leading to more shortwave radiation intercepted by clouds and therefore more longwave radiation emitted by clouds and received by the ocean (not shown).

Finally, the change in MLD can also explain part of the atmospheric negative feedback. First, a thinner ML leads to a higher part of the solar flux penetrating underneath, and therefore less warming by atmospheric fluxes (Lewis et al., 1990; Vialard and Delecluse, 1998; Masson and Delecluse, 2001; Mignot et al., 2012; Krishnamohan et al., 2019). This is especially true in summer, when the ML is thin enough for that process to be significant (Mignot et al., 2012). Moreover, the change in MLD between NOS and CONTROL is substantial in this season (about -36%, see Table 3.2). In winter, the net heat flux is negative and a thinner ML is thus more effectively cooled, leading also to a negative feedback.

Table 3.1: Changes in atmospheric heat fluxes between CONTROL and NOS, in the NWTA box, in summer (JJA), in areas where the SST anomaly is higher than 0.1°C (i.e. where it is significant). CONTROL and NOS values are rounded off to 0.5 W/m^2.

Fluxes	CONTROL value [W/m^2]	NOS value [W/m^2]	Contribution to net heat flux change
Net heat flux	39.5	57	-
Net shortwave radiation	261.5	266.5	29%
Net longwave radiation	-47.5	-48	-3%
Latent heat flux	-163.5	-151	71%
Sensible heat flux	-10	-9	6%

Table 3.2: Changes in several oceanic and atmospheric variables between CONTROL and NOS, in the NWTA box, in summer (JJA), in areas where the SST anomaly is higher than 0.1°C (i.e. where it is significant).

Variables	CONTROL value	NOS value
SST	29.3°C	29°C
SSS	33.6 psu	35.4 psu
Mixed Layer Depth	17.6 m	27.3 m
Cloud cover	6.1%	5.3%
Precipitation	5 mm/day	4.2 mm/day
Wind speed	6.8 m/s	6.7 m/s

3.3.3 Cold tongue SST anomaly

A strong sensitivity of the central equatorial Atlantic Ocean to salinity stratification is also revealed by our set of simulations. We analyze this pattern in the following.

3.3.3.1 A negative SST anomaly

Like in the NWTA, the SST sensitivity to salinity stratification in the equatorial area is greatest in summer, the period of development of the Atlantic CT (Carton and Zhou, 1997), and close to zero in winter (Figure 3.1). However, unlike in the NWTA, the SST anomaly in the CT region is negative: the presence of salinity stratification induces a cooling of the CT. The mixed layer heat budget for the CT region is shown in Figure 3.4b and 3.4d. It indicates that vertical mixing is enhanced when salinity stratification is considered, increasing the ML cooling by about 0.5°C/month in summer. It should be noted that the change in vertical

mixing in the CT is opposite to the one in the NWTA. The increase in vertical mixing in the CT is due to an equatorial adjustment of the thermocline depth, and is discussed in details in the following section.

Entrainment is also decreased in this region, although not to the same extent as in the NWTA. Even so, this leads to an additional cooling of the ML of about 0.2°C/month, bringing down the total to about -0.7°C/month in summer. Again, this is partly compensated by the atmospheric fluxes that show a +0.5°C/month difference in summer. Here the atmospheric feedback is mainly due to the fact that the decrease in SST leads to a decrease in latent heat loss. The atmospheric deep convection is indeed very weak in this region, and the change in SST does not impact the cloud cover nor the shortwave radiation as it does in the NWTA (Figure 3.7b and 3.7d).

3.3.3.2 Strengthening of the CT

The mechanism leading to the CT strengthening is illustrated in Figure 3.8 and 3.9. Figure 3.8a and 3.8b present the annual pycnocline depth for the CONTROL run and for the difference CONTROL-NOS respectively. We can observe a strong shoaling of the pycnocline in the NWTA when salinity stratification is accounted for. This is due to the reduced vertical mixing in the NWTA, which causes a readjustment of the density profile. This density readjustment propagates as baroclinic waves through the equatorial waveguide to adjust the whole equatorial basin up to the eastern part (not shown). The primary indicator of this new state is the change in the equatorial currents: a shoaling and a strengthening of the equatorial undercurrent (EUC) is indeed observed (Figure 3.9b and 3.9d). An impact of salinity stratification on the equatorial currents has already been reported by Vialard and Delecluse (1998): salinity stratification traps the wind momentum over a thinner ML, and therefore enhances the ocean response to wind forcing. But this effect is local and applies to the surface currents, while we observe here a remote effect of salinity stratification on the subsurface currents.

The new equilibrium also exhibits changes in the vertical temperature structure, and in particular a shallower thermocline. This can be observed on Figure 3.8c, where the depth of the 20°C isotherm (D20), a proxy of thermocline, is plotted. The D20 shoals consequently year-round, with a higher response in summer (6 to 7 m) with respect to winter (about 3 m) leading to a larger amplitude of the seasonal cycle. The shoaling of the thermocline is confirmed by Figure 3.9a and 3.9c, which represent summer zonal temperature sections averaged between 3°S and 1°N. The top of the thermocline is clearly seen on Figure 3.9a, zonally tilted from about 100 m at 35°W to 25 m at 0°E. These depths correspond to the depths of the strongest temperature anomalies on Figure 3.9c. The anomalies being negative, this indicates an upward shift of the thermocline occurring across the whole equatorial basin.

The thermocline shoaling leads to an enhancement of the CT (Latif and Grötzner, 2000). However, this happens only when the thermocline is sufficiently shallow and when upwelling occurs, i.e. in summer (Keenlyside and Latif, 2007; Jouanno et al., 2017). Figure 3.5b reveals that the period of the CT development spans from June to October. The temporal evolution

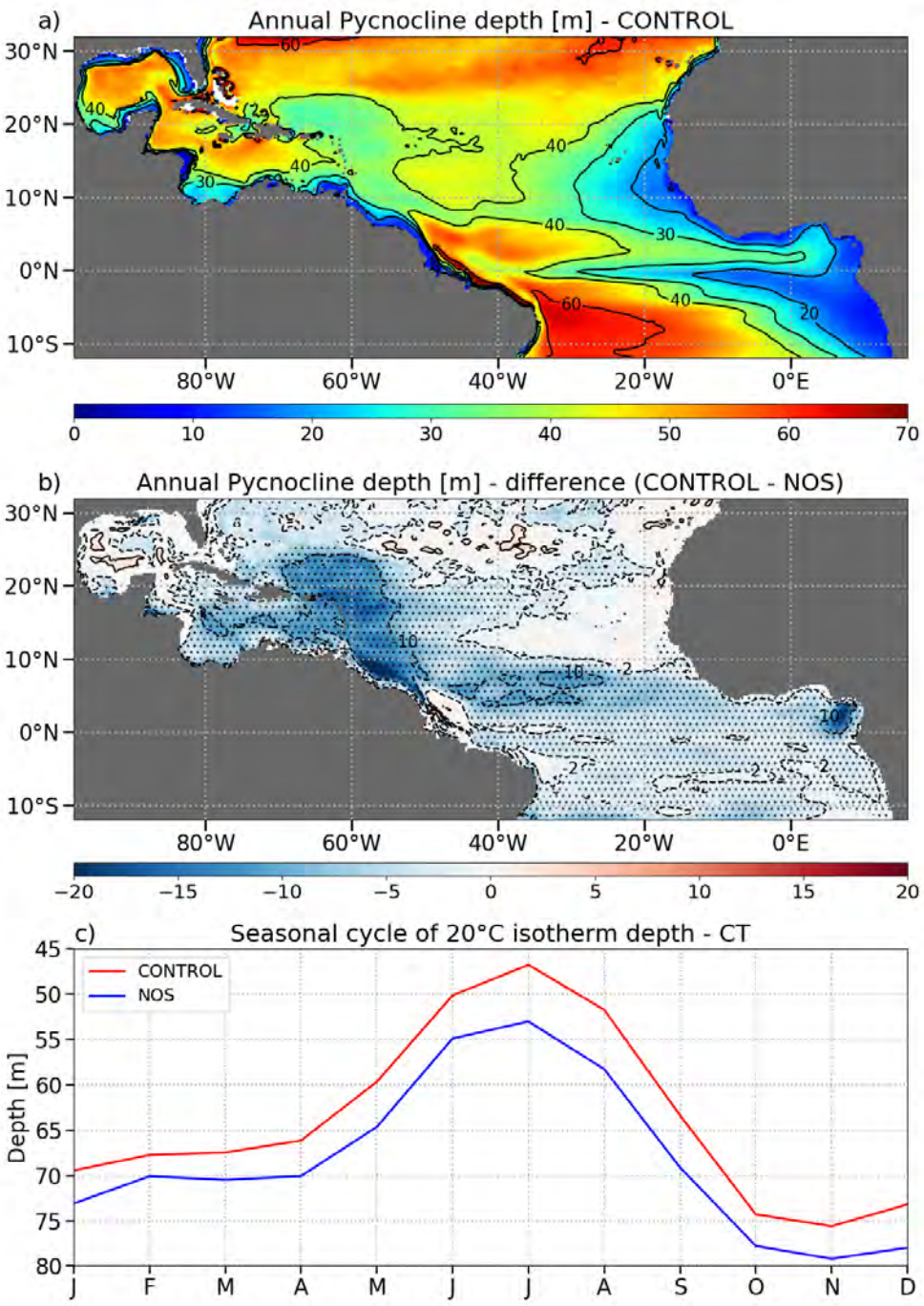

Figure 3.8: Annual pycnocline depth (2001-2015 climatology) for a) CONTROL simulation and b) the difference (CONTROL-NOS), dots indicating the areas where the difference is statistically significant; c) seasonal cycle of 20°C isotherm depth for the 2001-2015 climatology in the CT box

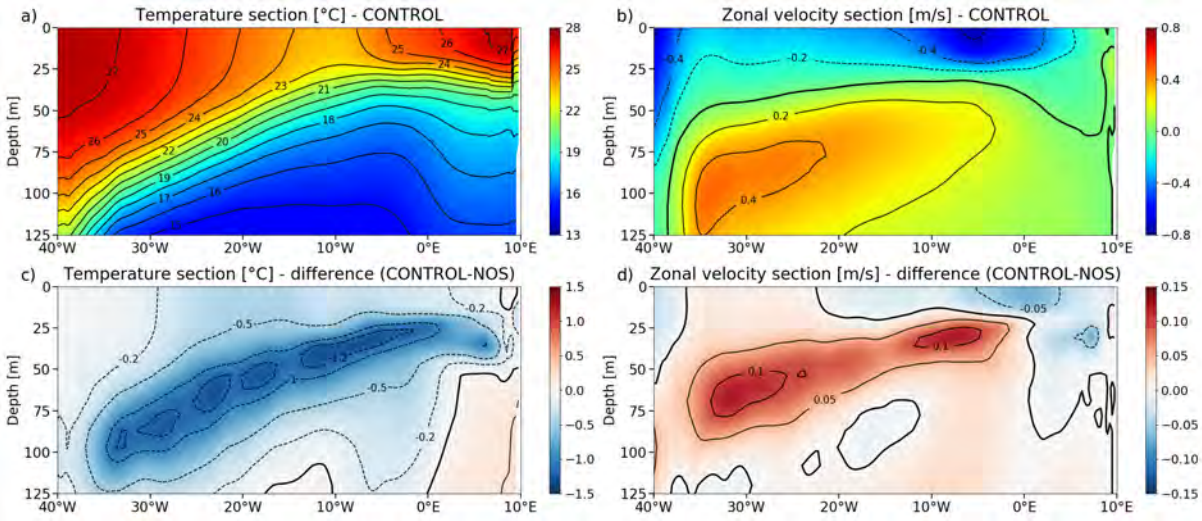

Figure 3.9: a) Temperature section in summer (JJA) for CONTROL simulation, mean between 3°S and 1°N, c) same than a) but for the temperature anomaly (CONTROL-NOS) ; b) and d) : same than a) and c) respectively, but for zonal velocity

of the 15°C to 24°C isotherms also highlights the upwelling period, from May to August, which is consistent with the observations (Wang et al., 2017). Although the adjustment of the thermocline - marked once again by strong temperature anomalies in subsurface - occurs year-round, surface temperature anomalies are only significant from June to October (Figure 3.5d), which coincides with the period of CT development. This also corresponds to the period when the anomaly of temperature trend associated with vertical mixing is largest, suggesting a link between the two. One explanation may be that vertical mixing is more efficient with a shallower thermocline, because it implies the mixing of cooler water and thus a more efficient heat exchange.

3.4 Discussion

3.4.1 Relevance of the coupled approach

A similar experiment was performed by Masson and Delecluse (2001) in the same region, but using an ocean model forced with prescribed air-sea fluxes. They did not find any impact of salinity stratification on SST despite large modifications of the MLD. We reproduced this experiment with our ocean configuration, forced with DFS5.2 atmospheric variables (Dussin et al., 2016) and bulk formulations for the surface fluxes instead of being coupled with WRF. DFS5.2 is based on ERA Interim reanalysis (Dee et al., 2011) and consists of 3-hourly fields of wind speed, atmospheric temperature and humidity, and daily fields of longwave radiation, shortwave radiation and precipitation. In that case, the changes in SST are similar, although weaker than those obtained with the coupled model (Figure 3.10; Figure 3.1). This result differs from Masson and Delecluse (2001), which might be explained

by the use of a different vertical mixing scheme and vertical resolution.

Despite the similar results between the forced model and the coupled model, it is necessary to use the latter. Indeed, not all the processes at stake are represented when using a bulk formulation for air-sea fluxes: the shortwave radiation is prescribed, and the feedback of SST on atmospheric deep convection and precipitation observed in the coupled model is obviously not taken into account. Moreover, using bulk formulations induces by definition an indirect

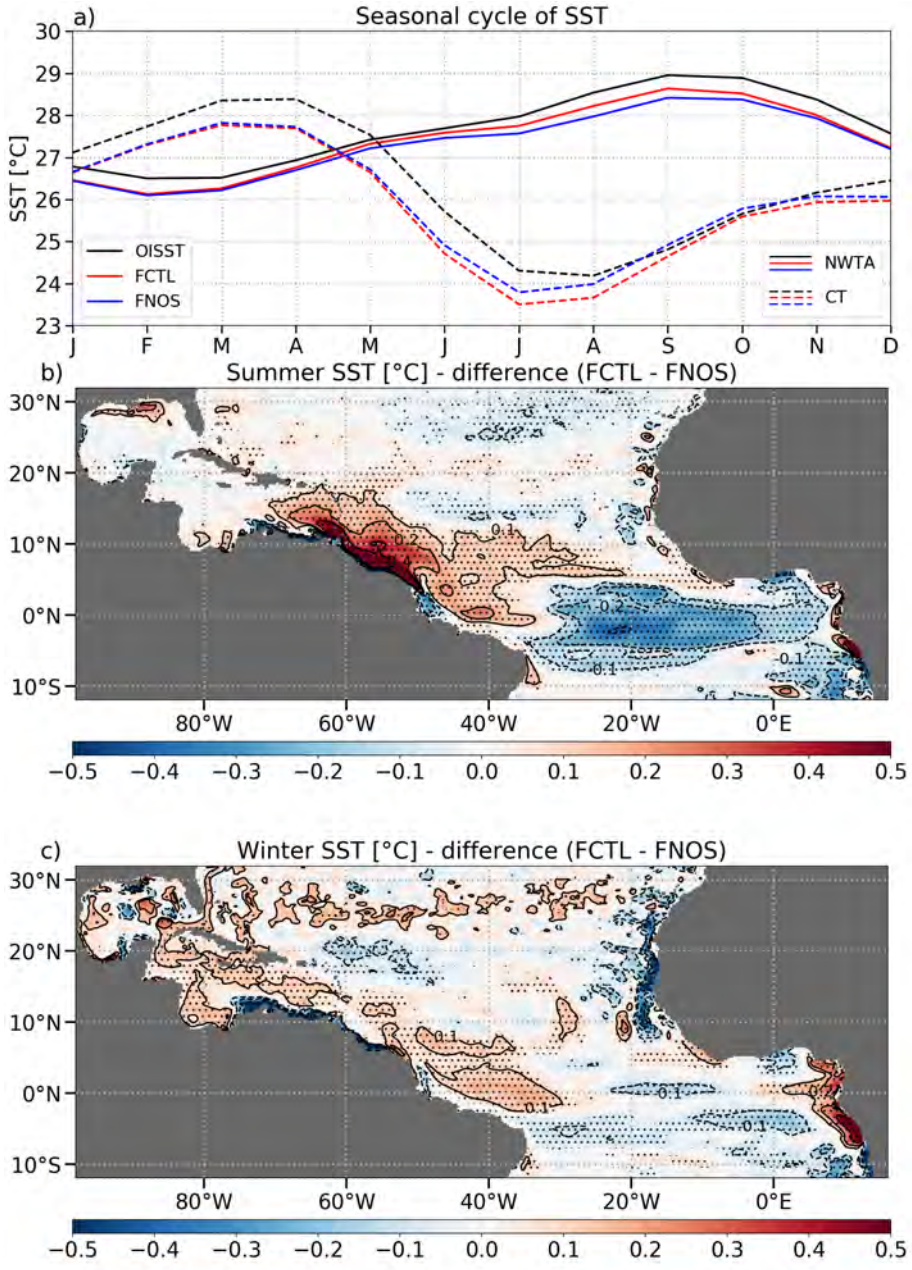

Figure 3.10: Same as Figure 3.1, but for the forced model

nudging toward the surface air temperature, mainly through latent heat flux (not shown). We saw in Figure 3.7 that latent heat fluxes dominate the net air-sea feedback. This can explain why SST changes are very similar in the forced and the coupled models.

The negative feedback of atmospheric fluxes through a decrease in latent heat flux and shortwave radiation is consistent with Krishnamohan et al. (2019), who conducted similar sensitivity simulations to salinity stratification in the Bay of Bengal. However, in their case, the air-sea heat fluxes completely compensate for the decrease in vertical mixing, leading to insignificant SST change in this area: this suggests that the impact of salinity stratification results from a subtle balance whose sign depends on the region considered.

3.4.2 Sensitivity of NWTA SST to salinity stratification: no impact of barrier layer

Previous studies investigating the impact of salinity stratification on SST in the NWTA have all focused on the importance of BL (see Equation 2.5 for the definition of the BLT, and Section 1.3.2.3 for more details on the impact of BL on SST and air-sea fluxes). BL inhibits vertical mixing: thus the presence of a BL can decrease the cooling induced by mixing and warm the surface (Pailler et al., 1999; Foltz and McPhaden, 2009). However, as revealed in Figure 3.2c and 3.2d, such a relationship is not found in our simulations. The simulations reproduce realistically the location and strength of both summer and winter BL (de Boyer Montégut et al., 2007a; Mignot et al., 2007, 2012). Nevertheless, the spatial patterns of summer BLT do not reveal any direct and compelling relationship with the corresponding patterns of SST anomalies. Although the distribution of the SST anomalies in the NWTA is colocalized with thick BLs, this is not true for the ITCZ area (40°W to 20°W and 0°N to 10°N), where there are no SST anomalies despite BL thicker than in the NWTA (Figure 3.1b, Figure 3.2c). This lack of relationship between SST anomalies and BLT is even more marked in winter: SST anomalies are weak and non-significant almost everywhere (Figure 3.1c), whereas the BL is at its thickest. This is furthermore confirmed by the distribution of SST differences as a function of BLT in summer (Figure 3.3b) and winter (Figure 3.3d) that do not exhibit any statistical relationship between the two variables. This result is in contradiction with previous observational studies conducted in the area (Pailler et al., 1999; Foltz and McPhaden, 2009), which concluded to a strong warming caused by BL (about 1°C for Pailler et al., 1999; 1.3 to 1.9°C for Foltz and McPhaden, 2009). However, our result is in line with modeling studies (Breugem et al., 2008; Balaguru et al., 2012a; Hernandez et al., 2016), which did not reveal any impact of BL on SST. Hernandez et al. (2016) also showed with a one-dimensional conceptual mixed layer model that SST cooling primarily depends on vertical salinity gradient rather than on BLT, in the NWTA. This model was applied to ocean cooling due to cyclones, but a parallel can be drawn with cooling occurring at seasonal time scales, and their conclusions may be applied to this case. Moreover, the fact that we do not find any significant relationship between BLT and SST differences, while there is one between salinity stratification and SST differences, reinforces the conclusions drawn by Maes and O'Kane (2014). Indeed, Maes and O'Kane (2014) showed that in several regions without any BL, salinity stratification can still be significant and can play an important role in stabilizing the upper layers of the ocean.

3.5 Conclusion

In this chapter, we used our coupled ocean-atmosphere configuration of the tropical Atlantic to evaluate the impact of salinity stratification on SST and air-sea fluxes. To do so, we performed two simulations: a CONTROL simulation, validated against observations in Section 2.4, and a sensitivity test NOS, where the salinity gradient is removed from the Brünt-Väisälä frequency calculation so that salinity stratification is not taken into account in the computation of the vertical mixing. We investigated the difference (CONTROL minus NOS) of several key variables to assess the impact of salinity stratification, first in the NWTA and then in the CT area.

In the NWTA, seasonal changes of SST are observed: a significant increase is observed in summer (0.2 to 0.5°C) while no change is found in winter. This seasonal warming primarily results from a strong decrease in cooling due to vertical mixing at the ML base. The magnitude of the SST increase then results from a subtle interplay between the decrease in vertical turbulent cooling and a decrease of atmospheric fluxes and entrainment. A negative feedback from the atmosphere mitigates the SST increase, and can be explained as follows. The SST increase leads on the one hand to an increase of latent heat loss (about -12 W/m^2 in summer). On the other hand, it results in an enhancement of atmospheric deep convection, leading to a more prominent cloud cover (about 15% increase in summer) and to a decrease in shortwave radiation received by the ocean (about -5 W/m^2 in summer). This also leads to a strong increase of precipitation over the area (about 19 %), which most likely strengthens the salinity stratification. These two processes (increase in latent heat loss and decrease in shortwave radiation) add up to cause a significant decrease in net heat flux (about -31% in summer), leading to a damping of the SST increase. This damping is total in winter while only partial in summer, explaining the positive SST anomaly observed in summer. A tight relationship between salinity stratification and SST anomalies is found in summer, whereas we could not evidence any relationship between BLT and SST anomalies. It is thus very clear that summer warming in the NWTA is due to the salinity stratification itself, irrespective of the presence of a BL. The impact of salinity stratification on SST in the NWTA revealed here is consistent with historical conceptual studies (e.g. Miller, 1976), although previous studies using forced ocean numerical models reported little effect of it (e.g. Masson and Delecluse, 2001).

Our set of simulations also revealed an important effect of the salinity stratification in the equatorial region: it increases the cooling in the CT, especially in summer during its peak period. This is due to a readjustment of vertical density structure over the whole equatorial basin, leading to a shoaling of the thermocline throughout the year, with larger impact on the SST during summer, when the thermocline is at its shallowest in the CT area.

The salinity structure of interest in the tropical Atlantic Ocean is localized mainly in the river plumes and in the ITCZ, and at the ocean surface. In this respect, NOS experiment is relatively crude, as it removes the salinity stratification on the whole water column and over the whole basin. Moreover, NOS experiment does not allow to differentiate the processes contributing to ocean salinity stratification: the contributions to vertical stratification of

precipitation, river runoff and salinity advection at subsurface by the NBUC (Masson and Delecluse, 2001) are all removed at once. In the following, we will refine the sensitivity experiments in order to study more realistic cases, and understand more in depth the influence of salinity induced by the rivers in the western tropical Atlantic.

Chapter 4

Impact of the Amazon and Orinoco river discharges

Contents

4.1 Introduction

The aim of this chapter is to specifically study the impact of the Amazon and Orinoco rivers on the SSS and the SST of the northwestern tropical Atlantic Ocean. Indeed, as we saw in the previous chapter, salinity stratification of the northwestern tropical Atlantic affects locally the SST. Moreover, salinity stratification in this area is mainly caused by the river discharge from Amazon and Orinoco. The second step of this work is therefore to isolate the effect of salinity stratification induced by river discharge from the other processes (precipitation, subsurface supply of salty water by the NBUC). To do so, we conducted an additional sensitivity experiment in which the freshwater flux from the Amazon and Orinoco is not considered, and we compare this simulation to our reference simulation.

This method has already been extensively used to study the impact of the Amazon and/or Orinoco rivers on the tropical Atlantic Ocean (Masson and Delecluse, 2001; Huang and Mehta, 2010; Coles et al., 2013; Newinger and Toumi, 2015; Hernandez et al., 2016; Jahfer et al., 2017; Giffard et al., 2019; Jahfer et al., 2020). The other usual way is to analyze satellite and in-situ observations (Pailler et al., 1999; Ffield, 2007; Zeng et al., 2008; Fournier et al., 2017). Both observational and modeling studies concluded to a strong impact of Amazon runoff on the sea surface salinity (SSS), the salinity stratification and the plume extent. However, modeling studies revealed that the seasonal cycle of the SSS and the plume extent are not caused by the seasonal cycle of Amazon runoff but by the seasonal cycle of the oceanic circulation (Masson and Delecluse, 2001; Coles et al., 2013). The impact of rivers on the tropical Atlantic SST is controversial, with observational studies suggesting a strong impact on SST (Pailler et al., 1999; Ffield, 2007; Fournier et al., 2017) while modeling studies find a weak impact on SST (e.g Newinger and Toumi, 2015; Hernandez et al., 2016; Jahfer et al., 2017).

Most of the modeling studies are conducted with forced ocean models, which do not reproduce the ocean-atmosphere interactions. Recently, coarse and global ocean-atmosphere coupled models have been used to investigate the role of the Amazon on SST and global climate (Jahfer et al., 2017, 2020). Here we propose to reproduce the experiment with a higher resolution regional coupled model, which is expected to be more accurate in reproducing the regional physics.

4.2 Methodology

4.2.1 Simulations

In this chapter, two ocean-atmosphere coupled simulations are analyzed: the CONTROL simulation already described in Chapter 2 and used in Chapter 3, and a sensitivity simulation called NORiver. In the NORiver experiment, all the rivers of the South American coast from 65°W to 40°W are removed. This corresponds to the Amazon and Orinoco rivers and all the rivers outflowing in between, as well as some rivers to the east of the Amazon, along the Brazilian coast. The parameterization of the thermal effect of ocean color is kept identical to

that of the CONTROL experiment, and we use the same monthly climatology of chlorophyll concentrations in CONTROL and NORiver. This allows to isolate the haline effect of the low salinity plume: the change in ocean color due to river turbidity is not studied here. Note that our coupled simulations do not include any hydrological model: runoff is directly specified as a forcing field at the land-ocean boundary.

A spin-up of 30 years was first conducted with a forced ocean model. This gives the system time to adjust and produce a mean oceanic state consistent with the absence of rivers. The NORiver experiment is then conducted from 2000 to 2010 with the coupled model, and the analyses conducted hereafter are based on the 10-year period from 2001 to 2010.

4.2.2 Areas of interest

The main area of interest of this chapter is the same NWTA domain already defined in Chapter 3 (70°W–50°W and 5°N–18°N, Figure 4.1a). The rivers are indeed removed in this area only, and the main changes are expected there. An analysis is also conducted in the CT (25°W–0°E and 3°S–1°N, Figure 4.4a), to compare with results from the NOS experiment.

4.3 Results

4.3.1 Impact of river discharge on SSS in the NWTA

The first aim of this chapter is to quantify the impact of Amazon and Orinoco rivers on the SSS. To do so, we analyze SSS differences maps between CONTROL and NORiver for summer (Figure 4.1a) and winter (Figure 4.1b). As expected, including the Amazon and the Orinoco into the model forcings decreases significantly the SSS in a large part of the tropical Atlantic, with the strongest signal in the NWTA. Near the Amazon mouth, this decrease is very large year-round (less than -5 PSU). In the rest of the NWTA, the decrease is more important in summer than in winter: around -4 PSU against -1 PSU in the Amazon and Orinoco plume. This can be explained by the seasonal variations of SSS (Figure 4.1c): in CONTROL, SSS is much higher in winter than in summer. In NORiver, the seasonal cycle almost disappears, and the differences are thus larger in summer than in winter. The SSS seasonal cycle is itself linked with the seasonal cycle of the Amazon plume extent, which is mainly driven by currents. In winter, the currents are weak and the Amazon freshwater remains near the river mouth. In spring, NBC starts to advect the freshwater plume northwestward, towards the Lesser Antilles. In summer, the NBC retroflection advects the plume eastward in the NECC (e.g. Coles et al., 2013, see Section 1.1.3 for more details).

It is also interesting to note that the SSS signal crosses the tropical Atlantic basin and reaches as far as the Gulf of Guinea, with a difference still significant there albeit weak (0.1 to 0.2 PSU).

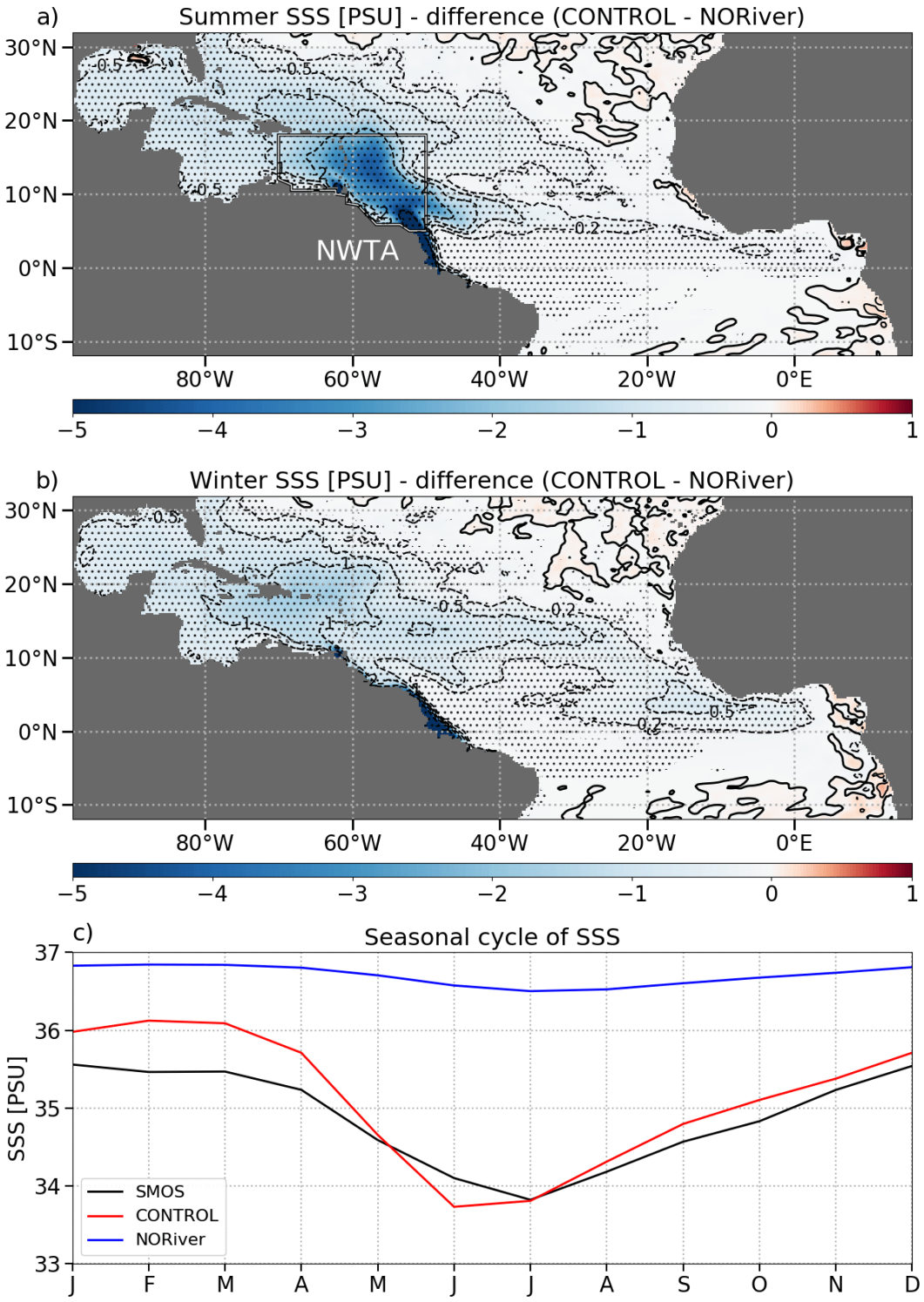

Figure 4.1: SSS differences between CONTROL and NORiver in a) summer and b) winter, dots indicating the areas where the difference is significant

4.3.2 Impact of river discharge on SST in the NWTA

We now assess the impact of Amazon and Orinoco discharge on the SST by analyzing SST differences maps between CONTROL and NORiver for summer (Figure 4.2a) and winter (Figure 4.2b). In both seasons, SST changes are weak in the whole basin: there are almost no significant changes, apart from a small SST increase of about 0.1°C in the NWTA and in the CT. This means that there is a weak SST signature associated with the strong SSS change in the NWTA.

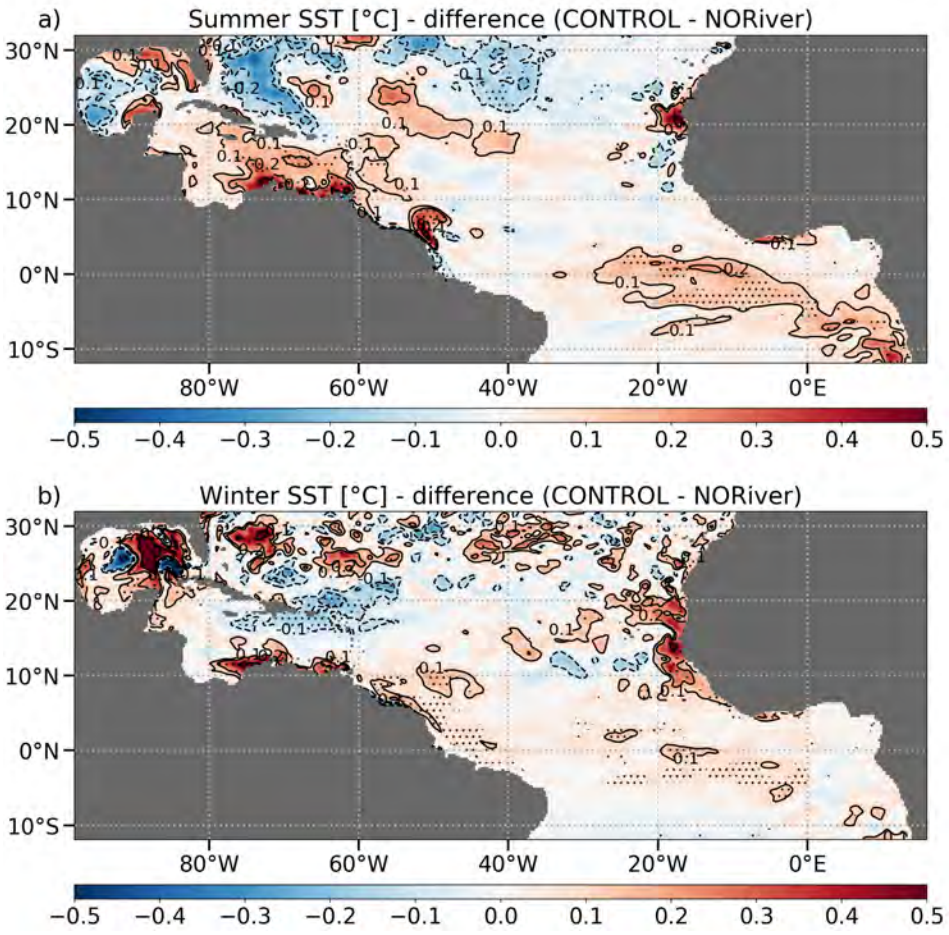

Figure 4.2: SST differences between CONTROL and NORiver in a) summer and b) winter, dots indicating the areas where the difference is significant ; c) SST seasonal cycle in NWTA

This result is surprising at first considering what we learned in Chapter 3. Indeed, we saw previously that salinity stratification has a significant impact on SST in summer in the NWTA (Figure 3.1a). Furthermore, removing Amazon and Orinoco (as in NORiver) or removing salinity stratification (as in NOS) results in changes in total stratification in the NWTA of relatively similar magnitude (not shown). Thus, similar changes in SST in the two experiments would be expected, which is not the case.

This discrepancy can be understood through the analysis of the mixed layer heat budget in CONTROL and NORiver in the NWTA (Figure 4.3). The heat budget shows that three main processes are at stake in this region: the air-sea heat fluxes, the vertical mixing and the entrainment.

In presence of Amazon and Orinoco plumes, the vertical mixing is less efficient to cool the ML. But this is compensated by weaker warming by air-sea fluxes and entrainment. These processes balance each other almost perfectly, resulting in a very small SST change in the NWTA.

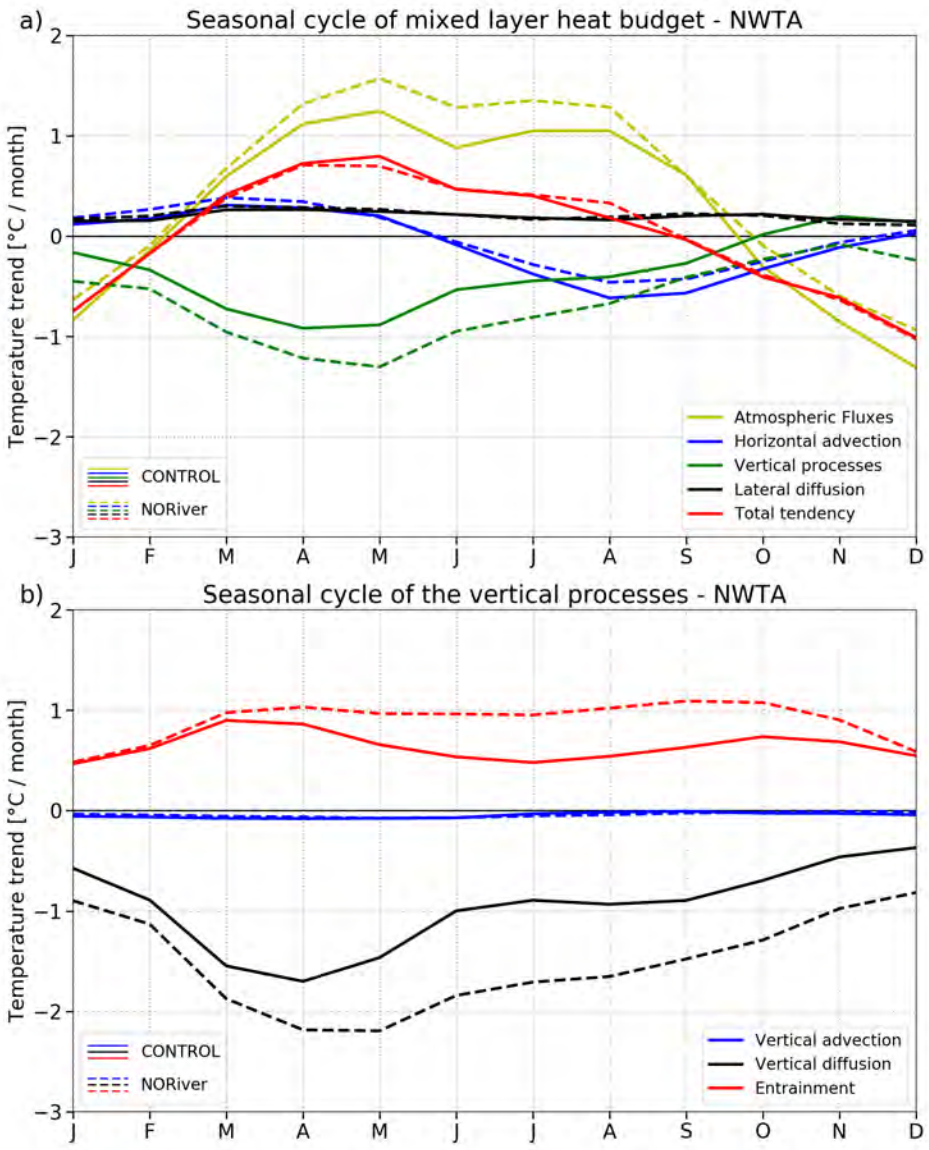

Figure 4.3: Seasonal cycle of the mixed layer heat budget in NWTA: a) main terms of the budget and b) vertical processes

Table 4.1: Changes in atmospheric heat fluxes between CONTROL and NOS and between CONTROL and NORiver, in the NWTA box, in summer. CONTROL and differences values are rounded off to 0.5 W/m^2.

Fluxes	CONTROL [W/m^2]	CONTROL-NOS [W/m^2]	CONTROL-NORiver [W/m^2]
Net heat flux	44	-15	-6.5
Net shortwave radiation	263.5	-4.5	-2
Net longwave radiation	-48	0.5	0
Latent heat flux	-161	-10.5	-4.5
Sensible heat flux	-9.5	-1	-0.5

This change in the heat balance is similar to what was found for the NOS simulation (Figure 3.4a and 3.4c). However, the temperature change due to vertical mixing is stronger in the NOS experiment than in the NORiver experiment. This is most likely due to the fact that removing the whole salinity stratification destabilizes more the ML than removing only the rivers. The negative atmospheric and entrainment feedbacks are also stronger in the NOS experiment than in the NORiver experiment. Nevertheless, the change in vertical mixing in the NOS experiment is too strong to be fully compensated by the negative atmospheric and entrainment feedbacks: an imbalance remains, resulting in SST anomalies. In contrast, the change in vertical mixing in the NORiver experiment is weak enough to be almost fully compensated by the negative atmospheric and entrainment feedbacks: equilibrium is nearly reached, and there are weak SST anomalies.

The negative feedback mechanisms of entrainment and atmospheric heat fluxes have already been explained in the previous chapter (see Section 3.3.2.2 and Section 3.3.2.3), and will not be detailed further. Yet, we noticed that the atmospheric changes are much weaker for the NORiver experiment than for the NOS experiment (Table 4.1). Therefore, the intensity of the change in atmospheric trend for NORiver is likely due primarily to strong ML changes, and to a lesser extent to the feedback of atmospheric heat fluxes.

4.4 Discussion

4.4.1 Comparison with previous studies

Several studies have investigated the impact of the Amazon and Orinoco rivers on the tropical Atlantic, and here we compare their results with ours. First, the SSS response obtained here is faithful to what has been observed previously. All studies investigating SSS found a strong impact of the Amazon and/or Orinoco rivers, with a decrease of -2 to -4 PSU in the Amazon-Orinoco plume (Masson and Delecluse, 2001; Coles et al., 2013; Newinger and Toumi, 2015;

Giffard et al., 2019; Varona et al., 2019). A strong decrease was reported year-round near the Amazon mouth (Newinger and Toumi, 2015; Varona et al., 2019), very similar in magnitude to the one found here (Figure 4.1a and 4.1b). Moreover, the winter difference map (Figure 4.1b) compares very well in magnitude and patterns with the January map of Coles et al. (2013) (Figure 1.2). The main difference is that the maps are smoother in this study, due to the different periods of time used for the average (3-month mean over 15 years here against 1-month mean for Coles et al., 2013). The response is also a little stronger in the west in our model, probably due to the fact that they only removed Amazon and Tocantins while we also removed the Orinoco.

Regarding the SST response in the NWTA, our findings are in agreement with the other modeling studies conducted in the region (Huang and Mehta, 2010; Newinger and Toumi, 2015; Hernandez et al., 2016; Jahfer et al., 2017), which all concluded to a very weak effect of Amazon and/or Orinoco on SST. In particular, the magnitude and patterns of SST response are very similar to Newinger and Toumi (2015) and Hernandez et al. (2016), who both studied a similar period of time (from 2000 to 2010 for Newinger and Toumi, 2015, from 1998 to 2012 for Hernandez et al., 2016, from 2001 to 2010 in this work). However, observational studies in the region concluded to a very strong effect of Amazon-Orinoco plume on SST of 1 to 2 °C (Pailler et al., 1999; Ffield, 2007; Fournier et al., 2017). This conclusion is based on the fact that the low SSS plume (characterized by SSS under 35 to 35.5 PSU depending on the study) is colocalized with high SSTs, while waters presenting SSS higher than this threshold are cooler. But Ffield (2007) also notes that the highest SSTs can be observed in the Caribbean Sea; yet, the Caribbean Sea exhibits SSS that is higher than the SSS threshold used to characterized plume waters (Figure 2.4c). As a matter of fact, none of these studies include the Caribbean Sea, and taking it into account could alter the results obtained. This is emphasized by Hernandez et al. (2016), who showed that the colocalization of Amazon plume and high SSTs is a mere coincidence: high SSTs in the region are due to the presence of the Atlantic Warm Pool (Wang and Enfield, 2001), and removing the Amazon and Orinoco weakly affects thermal stratification and SST.

4.4.2 Distinct responses between NOS and NORiver in the cold tongue region

The CT region exhibits SST changes in the NORiver experiment that are opposite to the NOS experiment. Indeed, a strong SST decrease occurs in summer in the NOS experiment (Figure 3.1a), while a slight SST increase is observed in the NORiver experiment (Figure 4.2a). In winter, the changes are much weaker but of the same sign than in summer.

These distinct changes are related to a response of the pycnocline that is different depending on the experiment. Indeed, the NOS experiment present a strong shoaling of the pycnocline in the whole basin (Figure 3.8b). On the other hand, the shoaling of pycnocline in the NORiver experiment is confined to the northern hemisphere, and the pycnocline even shows a slight deepening in the southern hemisphere, especially in the CT region (Figure 4.4a). It is associated with a slight deepening of the 20°C isotherm depth – a proxy of the thermo-

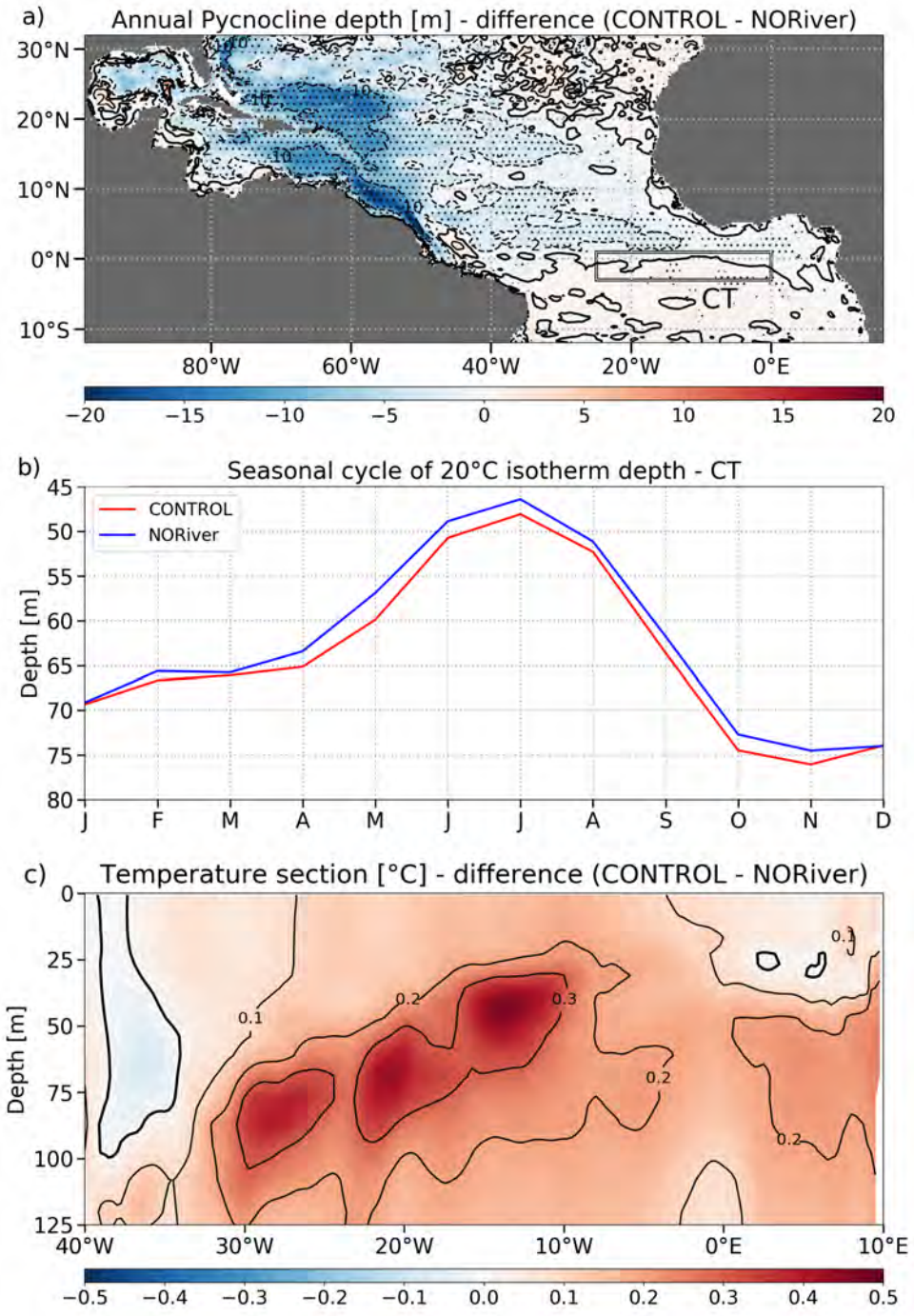

Figure 4.4: a) Annual pycnocline depth (2001-2010 climatology) for the difference (CONTROL-NORiver), dots indicating the areas where the difference is statistically significant; b) seasonal cycle of 20°C isotherm depth for the 2001-2010 climatology in the CT box; c) Section of temperature anomaly (CONTROL-NOS) in summer, mean between 3°S and 1°N.

cline – year-round in the CT (Figure 4.4b). The underlying mechanism is the exact opposite to what was observed in the NOS experiment: the deepening of the thermocline leads to an increase of the subsurface temperature (Figure 4.4c), which is then upwelled and leads to an increase in SST. As for the NOS experiment, the deepening of the thermocline happens year-round, but the impact on SST is particularly marked during the CT development, when upwelling occurs, i.e in summer.

The reason for this different response in pycnocline depth (strong shoaling in NOS experiment, slight deepening in NORiver experiment) remains unclear. This is probably linked with the fact that removing the Amazon and Orinoco rivers is less drastic and has a more local effect (primarily restricted to the north of the equatorial waveguide) than removing the whole salinity stratification (which affects both hemispheres).

4.5 Conclusion

In this chapter, we used our coupled ocean-atmosphere configuration of the tropical Atlantic Ocean to quantify the impact of Amazon and Orinoco rivers on the SSS and the SST of the NWTA. To this end, we compared two simulations: a CONTROL simulation as close to observations as possible (see Section 2.4), and a NORiver simulation, where all the rivers from 65°W to 40°W are removed, corresponding mainly to the Amazon and Orinoco rivers. We analyzed the difference (CONTROL minus NORiver), which corresponds to the response when Amazon and Orinoco rivers are included to the model.

A very large SSS decrease is observed year-round near the Amazon mouth. In the NWTA, the decrease is stronger in summer than in winter. This is well explained by the seasonal variations of the Amazon-Orinoco plume, linked with the seasonal cycle of currents. In the rest of the basin, the SSS signal is weak but significant over much of the area: it crosses the tropical Atlantic from west to east to reach the Gulf of Guinea.

Despite a strong salinity response, the SST changes are very weak year-round in the NWTA. This is due to a compensation between vertical mixing, atmospheric heat fluxes and entrainment. Indeed, adding the rivers limits the cooling by vertical mixing, causing an increase in SST. However, this increase is balanced by a decrease in the warming from the atmospheric heat fluxes and from entrainment. The combination of all these processes results in a slight SST increase. This mechanism is the same as for the NOS experiment (Section 3.3.2.2). The negative feedback of the atmosphere is also similar, albeit much weaker, to what is observed in the NOS experiment (Section 3.3.2.3).

The results obtained are coherent with previous modeling studies for both SSS and SST (e.g. Newinger and Toumi, 2015; Hernandez et al., 2016; Giffard et al., 2019). But here, the use of a coupled ocean-atmosphere model ensures that all ocean-atmosphere interactions are included, and thus that the SST response is well represented.

NORiver experiment allows to isolate the effect of Amazon and Orinoco rivers on salinity

and temperature, but some studies also justified conducting this experiment on the grounds that the Amazon should dry up in the future. Nevertheless, even studies predicting a strong decrease of runoff in the Amazon and Orinoco basins do not forecast a drying up of the rivers (e.g. Brêda et al., 2020). Moreover, other studies present more nuanced findings: Sorribas et al. (2016) show for instance that the future tendencies are not the same across the Amazon basin, wetter conditions being found in the west and drier conditions in the east. Conflicting results are also observed among the GCMs from the CMIP intercomparison studies, which disagree on whether there will be an increase or decrease in precipitation (Li et al., 2006; Sorribas et al., 2016). Therefore, NORiver may not be considered as a fully plausible situation.

Current consensus is rather that the hydrological cycle is intensifying, with an increase in extreme droughts and floods, especially in the Amazon basin (Espinoza et al., 2009a; Gloor et al., 2013; Marengo and Espinoza, 2016; Barichivich et al., 2018). This trend is expected to persist in the future (Skliris et al., 2016; Allan et al., 2020). It therefore seems important to assess the impact of these extreme events on the tropical Atlantic Ocean, which is the next step of this work.

Chapter 5

Impact of the interannual variability of river discharge

Contents

5.1 Introduction

The purpose of this chapter is to quantify the impact of the interannual variability of river discharge – and especially the Amazon – on the SSS and the SST of the northwestern tropical Atlantic Ocean. In the previous chapter, we assessed the impact of Amazon and Orinoco rivers on SSS and SST, and we now want to refine our understanding of the impact of the rivers by investigating the impact of floods.

The Amazon basin is regularly affected by extreme droughts and floods, which have a strong impact on the population and the ecosystems of the region (e.g. Marengo et al., 2013; Filizola et al., 2014; Espinoza et al., 2016). The cause of these extreme hydrological events is well documented: they are mainly associated with two modes of tropical variability, ENSO and the AMM, which explain most of the last events (Drumond et al., 2014; Marengo and Espinoza, 2016; Towner et al., 2020). Both ENSO and the AMM have a similar influence on these extreme events (Zeng et al., 2008; Yoon and Zeng, 2010), and the mechanism by which they influence precipitation and runoff is also well understood (see Section 1.2.1 and Section 1.2.2). Nevertheless, the impact of the resulting interannual variability of river discharge has been little studied, and the published results can appear contradictory. Several studies have found a link between the variability of Amazon runoff and the SSS variability of different areas: Barbados (Hellweger and Gordon, 2002), the Antilles (Jury, 2019), the NECC (Gouveia et al., 2019a), and along the Amazon plume trajectory (Salisbury et al., 2011). However, Grodsky et al. (2014) observed that the ocean surface was saltier in 2012, despite a stronger Amazon runoff this year, and Fournier et al. (2017) found no evidence of an influence of SSS by river discharge east of the lesser Antilles. Moreover, the modeling study of Grodsky et al. (2015) found a variability of SSS in the Caribbean very close to observations when their model considered a climatological runoff, leading them to conclude that the interannual variability of Amazon does not significantly impact the SSS interannual variability in this area. Regarding SST, a positive correlation is found between the interannual variability of the Lesser Antilles SST and the Amazon runoff (Jury, 2019), and between the SST and the SSS to the east of the Lesser Antilles (Fournier et al., 2017). However, Fournier et al. (2017) also mention a strong interannual variability of SST linked with the AMM that could impact these results.

The studies on the interannual variability of the Amazon discharge were usually conducted with ocean observations, which present several problems. One of them is that the correlations found are highly dependent on the discharge estimates used (Reeves Eyre and Zeng, 2021), and that the Obidos stream gauge commonly used to estimate the Amazon discharge at the river mouth misrepresents the seasonal cycle (Salisbury et al., 2011; Reeves Eyre and Zeng, 2021). Another one is that the oceanic impact of runoff variability cannot be separated from the impact of ocean and atmospheric variability (mixing, advection, atmospheric fluxes), something that can be done with a model. To our knowledge, no sensitivity test has ever been conducted with a model to isolate the impact of runoff interannual variability on the Amazon plume region. Therefore, we conducted two simulations with our coupled configuration, forced alternatively with daily interannually-varying runoff and a daily runoff climatology. The use of a coupled model is once again essential since we want to assess changes in the ocean

thermodynamics as a whole, including SST. Composite analysis of the lowest and highest floods years for both simulations allows us to isolate and quantify precisely the effect of the extreme floods that occurred in the last decades, and separate the effect of runoff interannual variability from the effects of ocean and atmospheric interannual variability.

5.2 Methodology

5.2.1 Simulations

In this chapter, two coupled simulations of 16 years each are conducted, with the last 15 years – from 2001 to 2015 - being analyzed. The aim of these twin experiments is to assess the impact of the runoff interannual variability. Thus, the first simulation, REF, has interannual daily runoff forcing while the second simulation, CLIM, has a daily climatological runoff forcing averaged from 2001 to 2015. Runoff data were obtained from the ISBA-CTRIP land surface model (Decharme et al., 2019). Moreover, according to Newinger and Toumi (2015), the ocean color is of great importance in the good representation of the impact of Amazon plume on the air-sea heat fluxes. Therefore, we decided to use chlorophyll fields consistent with the runoff forcing: we used interannual monthly fields of chlorophyll for the REF experiment, and a monthly climatology averaged from 2001 to 2015 for the CLIM experiment. Note that in these simulations, the ocean color forcing of the solar radiation penetration scheme has been modified. Following Hernandez et al. (2017), we use chlorophyll data from Globcolour, which is based on a merging of several satellite products (Maritorena et al., 2010), together with the empirical parameterization from Morel and Berthon (1989) to calculate a vertical profile of chlorophyll from surface chlorophyll satellite concentration.

5.2.2 Composites

5.2.2.1 Composites calculation

Composite analysis is conducted in the rest of the chapter to analyze the consequences of the anomalous Amazon discharges, resulting either from high floods or low floods, on the tropical Atlantic Ocean. Since the Amazon river yields the first discharge of the global ocean, and it accounts for around 70% of the total discharge received by the NWTA, we based our composite analysis on the Amazon runoff, shown on Figure 5.1a. The 4 years with the highest floods, 2006, 2008, 2009 and 2014, are averaged to give the highest floods composite or HF, while the 4 years with the lowest floods, 2003, 2004, 2007 and 2010, are averaged to give the lowest floods composite, or LF. The years of highest and lowest floods are chosen by comparing the maximum discharge value of each year. Moreover, we chose to study the flood season because the seasonal cycle of interannual discharge standard deviation peaks at this time (not shown), indicating that variability is greater during this season. The composite analysis is performed on both REF and CLIM simulations. In the following, $\mathrm{REF_{HF}}$ and

$CLIM_{HF}$ refer to the two composites for the highest floods years, and REF_{LF} and $CLIM_{LF}$ refer to the two composites for the lowest floods years. The seasonal maxima of runoff is around 345,000 m3/s for REF_{HF}, around 267,000 m3/s for REF_{LF}, and around 305,000 m3/s for the CLIM experiment, giving a 25% relative change between the peak runoff of the REF_{HF} and REF_{LF} composites.

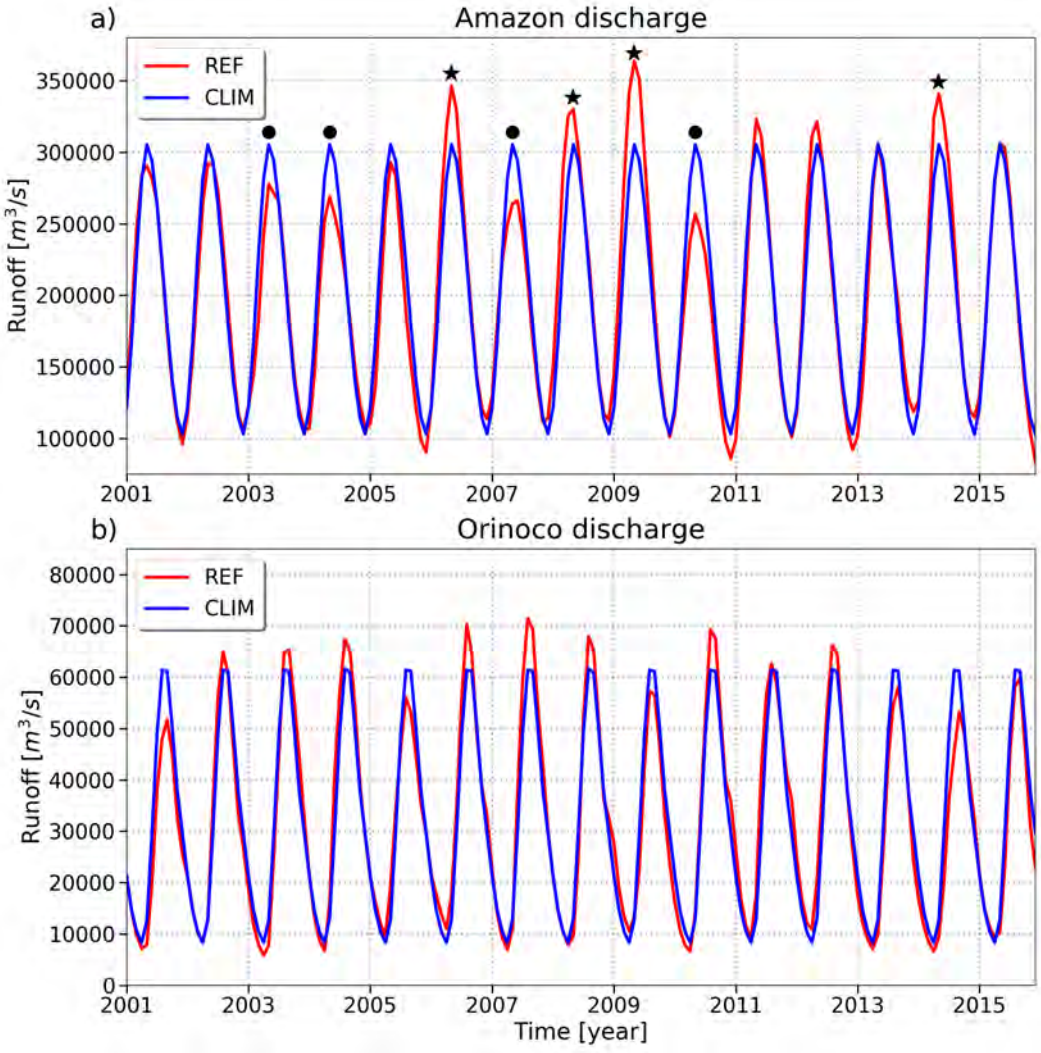

Figure 5.1: Time series of a) Amazon discharge and b) Orinoco discharge for the REF and CLIM experiments. The dots indicate the years with the lowest Amazon floods while the stars indicate the years with the highest Amazon floods.

5.2.2.2 Differences between composites

In the following, differences between composites are being analyzed. This allows to assess the impact of runoff interannual variability independently of the ocean and atmospheric variability (mixing, advection, atmospheric water and heat fluxes). The difference between REF_{HF}

and REF_{LF} represents the sum of all variabilities: river runoff, ocean dynamics and atmospheric fluxes. The difference between $CLIM_{HF}$ and $CLIM_{LF}$ represents the impact of ocean and atmospheric variability only. Indeed, the river runoff is climatological in the CLIM experiment, which means that the runoff interannual variability is removed, leaving only the ocean and atmospheric variability. Therefore, the difference between REF and CLIM composites – that is (REF_{HF} - REF_{LF}) - ($CLIM_{HF}$ - $CLIM_{LF}$) – represents the sole runoff variability.

5.2.3 Definition of Amazon-Orinoco plume

In the following, some analyses are conducted in the low salinity plume associated with the Amazon and Orinoco rivers. Following Coles et al. (2013), the plume is defined as the area where the annual SSS averaged from 2001 to 2015 is under 35 PSU (see gray contour in Figure 5.3a). The area used is therefore fixed in time, and does not vary with the seasons.

5.3 Results

5.3.1 Impact of runoff interannual variability on SSS

The first aim of this study is to investigate the impact of the runoff interannual variability on SSS. Figure 5.2 represents the seasonal cycle of SSS in the Amazon-Orinoco plume in REF (solid lines) and CLIM (dashed lines) for the highest floods (blue lines) and lowest floods (red lines) composites. At the beginning of the year, SSS is similar for all composites. Then, as the flood season peaks, anomalies develop. For both REF and CLIM, the differences between highest floods and lowest floods years are the largest from May to July. They subside afterwards and have completely disappeared by October: the anomalies vanish in a few months only.

To quantify the impact of the runoff interannual variability on SSS, we now observe differences between composites of SSS seasonal cycle (Figure 5.2, bar chart). As explained in Section 5.2.2.2, these differences allow to disentangle the different forcing driving the SSS anomalies. First, we can see that the change between the highest and lowest floods years when all the variability is considered is very important in spring and summer: up to 1.7 PSU in June (Figure 5.2, black bars). This change is due almost equally to runoff interannual variability (Figure 5.2, green bars) and to ocean and atmospheric variability (Figure 5.2, gray bars), with nonetheless a larger share of the variability explained by runoff in May-June-July. This indicates that the interannual variability of the Amazon does not explain all of SSS variability in the region: other factors such as the surface currents (and especially the NBC), the precipitation and the wind-induced mixing and currents influence the SSS variability in the same way as the runoff, inducing fresh anomalies during the years of excess runoff (Masson and Delecluse, 2001; Molleri et al., 2010; Coles et al., 2013; Fournier et al., 2017). This result is however in disagreement with Grodsky et al. (2014) and Grodsky et al. (2015), who suggested that runoff interannual variability has no impact on SSS variability,

and therefore in agreement with the studies observing a correlation between SSS and runoff variabilities (Hellweger and Gordon, 2002; Salisbury et al., 2011; Gouveia et al., 2019a; Jury, 2019).

In order to better understand the changes in salinity distribution, SSS maps of difference between REF composites are shown for spring (Figure 5.3a) and summer (Figure 5.3b), the two seasons of greatest change. A strong SSS decrease is observed in spring close to the river mouth and along the Guiana coast. In summer, the decrease has already partially vanished and has moved towards the lesser Antilles, while an increase in SSS is observed to the east, at the location of the NBC retroflection and the NECC.

To quantify the part of SSS variability that can be attributed to runoff interannual variability, we now observe SSS maps of difference between REF and CLIM composites for spring (Figure 5.3c) and summer (Figure 5.3d). In spring, the runoff interannual variability leads to important changes in salinity near the Amazon mouth (less than -3 PSU), and anomalies in the whole Amazon plume decreasing with the distance from the mouth (-1 PSU up to 9°N and -0.2 PSU in the Lesser Antilles). In summer, the changes are still noticeable but their magnitude has diminished by a factor of 2 to 3.

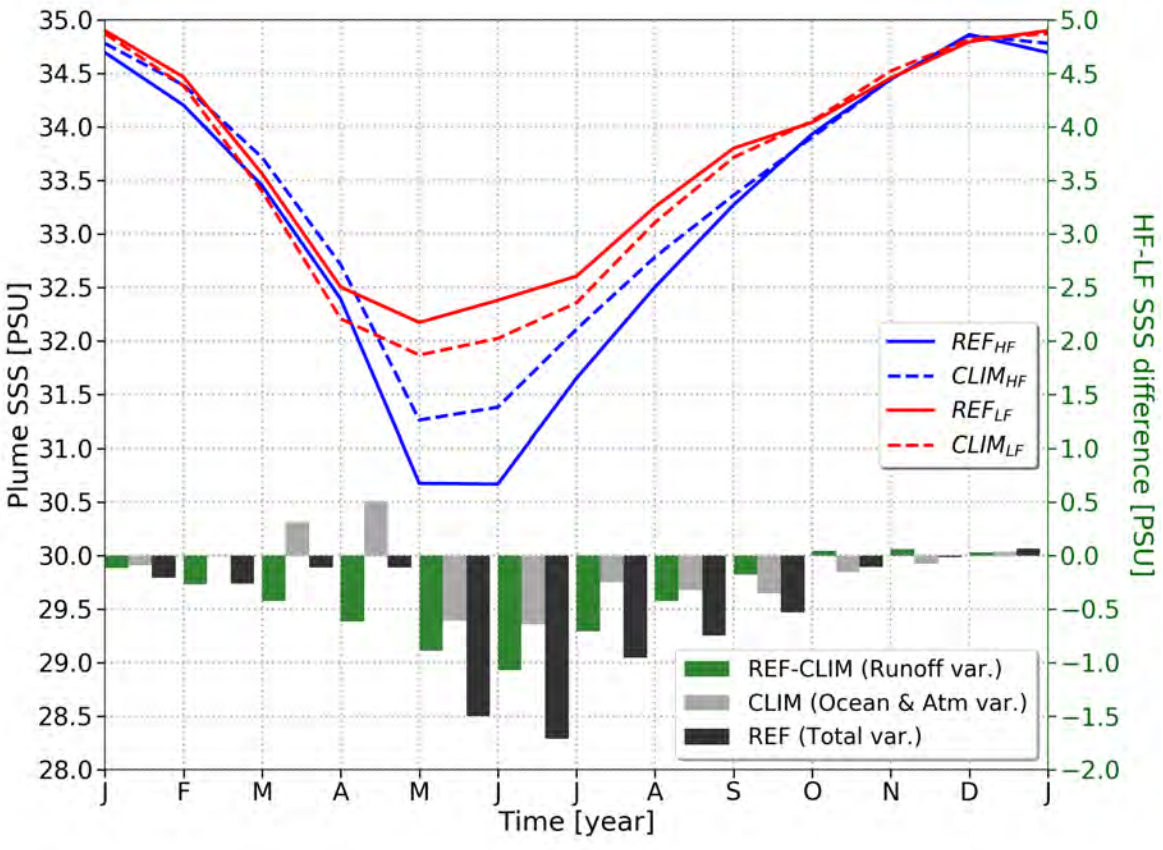

Figure 5.2: SSS seasonal cycle in the Amazon-Orinoco plume of each composite (curves) and of the differences between composites (bar chart).

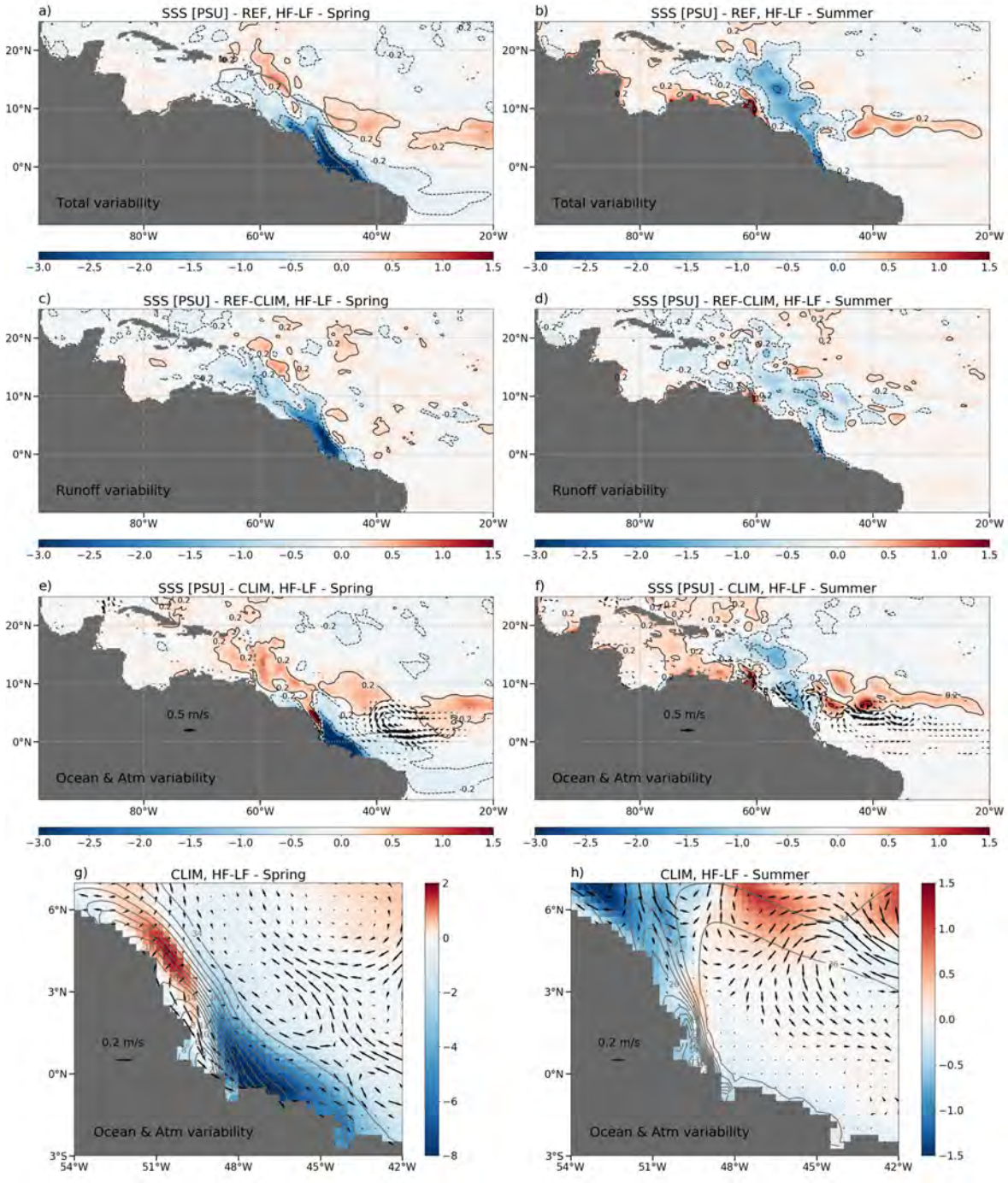

Figure 5.3: Spring (April-May-June, AMJ) maps of SSS differences between highest floods and lowest floods for a) REF, c) REF - CLIM and e) CLIM; b), d), f): same as a), c), e) respectively but for the summer season (July-August-September, JAS); the arrows on e) and f) represent the current anomalies with a norm greater than 0.1 m/s. g), h): zoom at the Amazon mouth of e) and f) respectively. The contours represent the SSS of $\mathrm{CLIM_{HF}}$ and the arrows represent the currents anomalies of ($\mathrm{CLIM_{HF}}$ - $\mathrm{CLIM_{LF}}$) for each season.

The patterns of SSS differences driven by ocean and atmospheric variability are captured by the CLIM experiment (Figure 5.3e and 5.3f). In spring, the SSS map of difference between years of highest floods and years of lowest floods shows a dipole with positive anomalies near Guiana and in the Lesser Antilles and a strong negative anomaly near the Amazon mouth. These anomalies are consistent with changes in the currents, as can be seen in Figure 5.3g. At this time of the year, the Amazon plume is mainly advected northwestward along the coast by the NBC and the Guiana current (Coles et al., 2013). Figure 5.3g shows a weakening of these currents in highest floods years compared to lowest floods years, leading on the one hand to an accumulation of freshwater near the Amazon mouth, and on the other hand to a lesser northwestward along-shore freshwater transport and thus a positive SSS anomaly along the Guiana coast. Furthermore, these changes occur in the region of Amazon plume front, an area of very strong SSS gradients (see contours of Figure 5.3g), which explains the high amplitude of the negative anomaly (down to -9 PSU). A southward shift of NECC can also be observed (see arrows on Figure 5.3e). In summer, the changes in currents near the Amazon mouth disappear (Figure 5.3h), as well as the SSS anomaly dipole. A strengthening of the NBC and a weakening of the NBC retroflection are observed (see arrows on Figure 5.3f), leading to an increase of freshwater transport towards the Lesser Antilles and a decrease of freshwater transport by the north-equatorial countercurrent (NECC). Finally, we note here again that the contribution of runoff interannual variability is similar in magnitude to the contribution of ocean and atmospheric variability.

To understand more precisely the changes in salinity observed, and especially the fast disappearance of the SSS anomaly (Figure 5.2), we analyze the seasonal cycle of mixed layer salt budget averaged over the Amazon-Orinoco plume (Figure 5.4). Two main processes dominate this salt budget: the horizontal advection and the vertical diffusion. The atmo-

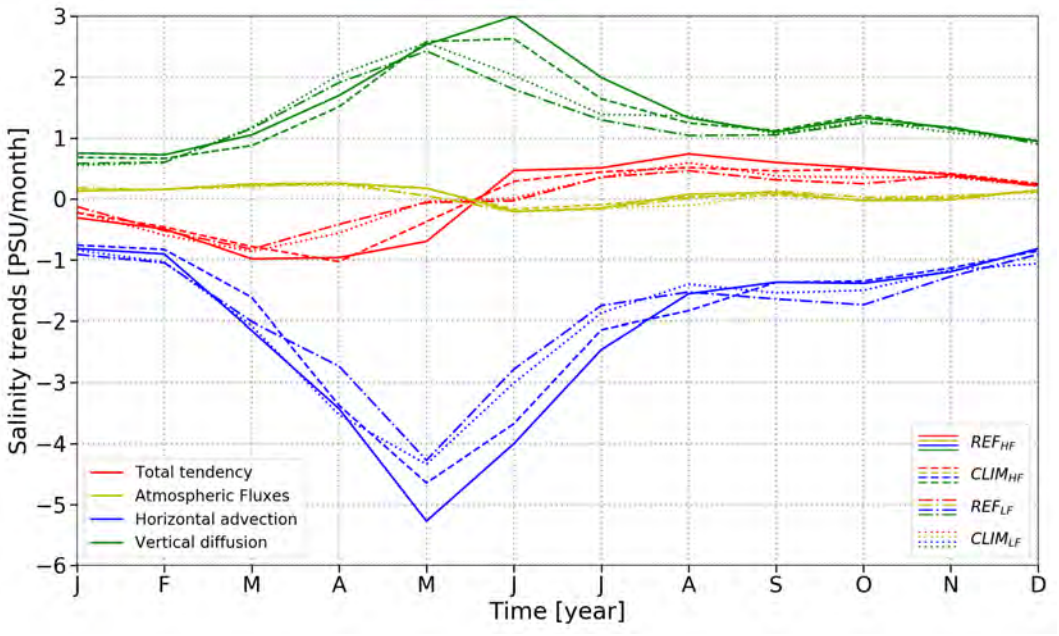

Figure 5.4: Seasonal cycle of the mixed layer salt budget in the Amazon-Orinoco plume

spheric fluxes (evaporation and precipitation) are negligible. The horizontal advection term is strongly negative since it corresponds to the transport of freshwater from the river runoff, and it dominates the total tendency at the beginning of the year. However, it is immediately counterbalanced by a strongly positive vertical diffusion term that mixes the underlying salty water into the ML. Therefore, the total tendency becomes positive as early as June. These results are consistent with Ferry and Reverdin (2004), who also found a strong contribution of horizontal advection at the beginning of the year, followed by a damping by vertical mixing and entrainment. It is also consistent with Foltz et al. (2004), who found that horizontal advection was an important component of the salt budget in the northwestern tropical Atlantic due to strong SSS gradients. Camara et al. (2015) found a more prominent effect of the vertical mixing year-round and lesser impact of horizontal advection, but their analysis domain lies further east and is not representative of the whole plume. The detail of the curves on Figure 5.4 shows that the runoff interannual variability can impact the salt budget. The horizontal advection and vertical diffusion are stronger in $\mathrm{REF_{HF}}$ (solid lines) than in $\mathrm{CLIM_{HF}}$ (dashed lines): adding the runoff interannual variability exacerbates the response during the highest floods years. Conversely, $\mathrm{REF_{LF}}$ (dashed-dotted lines) shows weaker horizontal advection and weaker vertical diffusion than $\mathrm{CLIM_{LF}}$ (dotted lines), but differences are not as strong as for the highest floods composites.

5.3.2 Impact of runoff interannual variability on the plume area

Another commonly studied feature is the plume extent, whose seasonal cycle is shown in Figure 5.5 for the two simulations, and for the lowest and highest floods years. The plume extent is at its lowest in winter, increases during spring and reaches its highest values in

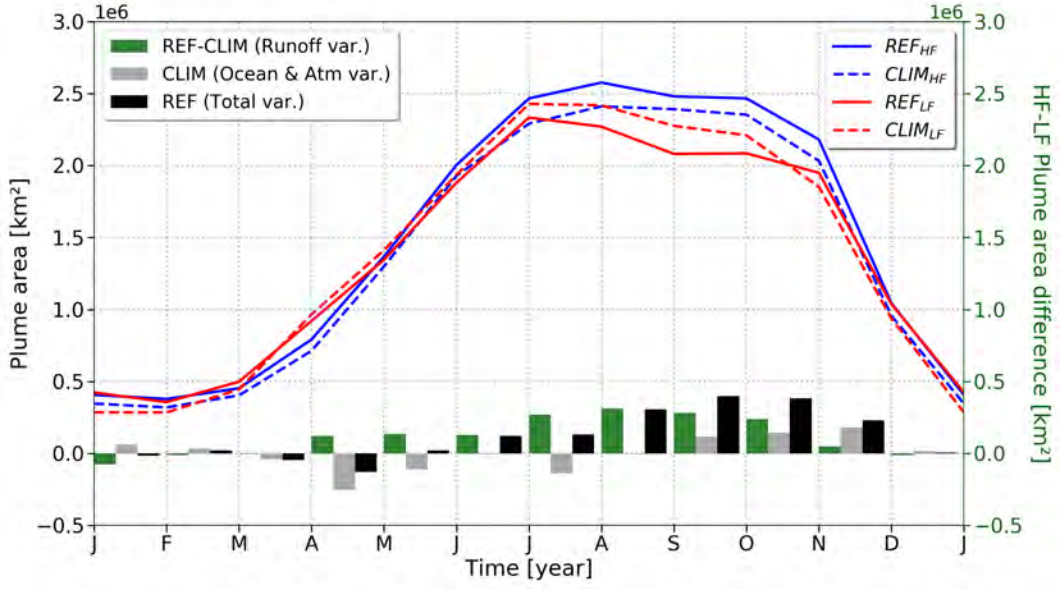

Figure 5.5: Seasonal cycle of the plume extent of each composite (curves), and of the differences between composites (bar chart).

summer and fall. This is consistent with Coles et al. (2013), but not exactly with Molleri et al. (2010), who found smaller values of plume extent, and a seasonal cycle peaking in July and decreasing shortly after. However, Molleri et al. (2010) used a different threshold value for the plume (34 instead of 35 PSU) and their area of analysis is smaller. We obtain a comparable seasonal cycle by using the same criterion as them (not shown).

The impact of the runoff interannual variability on the plume extent is also substantial. During the season of largest plume extent, that is August-September-October (ASO), the total change in plume extent (i.e. the difference between REF composites, Figure 5.5, black bars) is around 16%. Around three quarters of this change is explained by runoff interannual variability (i.e. the difference between REF and CLIM composites, Figure 5.5, gray bars). This is in perfect agreement with Molleri et al. (2010), who found that runoff interannual variability explained 74% of the plume extent variability. This is also in agreement with Zeng et al. (2008), who did not quantify the impact of runoff variability on the plume extent, but found a strong correlation between Amazon runoff and plume extent interannual anomalies.

It is interesting to note that in April, the plume in $\mathrm{CLIM_{LF}}$ is much larger (around 35%) than the plume in $\mathrm{CLIM_{HF}}$. This might be related to the weakening of the along-shore currents observed in spring during years of highest floods (Figure 5.3g).

5.3.3 Impact of runoff interannual variability on SST

As done for the SSS, we isolate the effect of the runoff interannual variability on the SST (Figure 5.6a and 5.6b) from the changes due to the other forcing factors (Figure 5.6c and 5.6d). Despite a strong impact on SSS (Figure 5.3c), the runoff interannual variability leads to very weak changes in SST in spring (Figure 5.6a). More importantly, these changes are completely negligible compared to the very strong changes in SST induced by ocean and atmospheric variability (Figure 5.6c), which can most likely be related to the AMM (see Section 5.4.1). From July onwards, the SST anomalies linked with AMM tend to disappear (Foltz et al., 2012). This explains the weaker summer anomalies due to ocean and atmospheric variability (Figure 5.6d). The impact of interannual runoff variability remains weak (Figure 5.6b), which was expected since the salinity anomaly is already fading in summer (Figure 5.3d).

The fact that SST anomalies induced by runoff interannual variability are weak despite a strong SSS change can be explained by the same compensation mechanism as in the two previous chapters. Indeed, if we observe the differences in mixed layer heat budget caused by runoff interannual variability (Figure 5.7), we can see that the temperature trend in vertical mixing increases from April to June. This is due to an increase in salinity stratification caused by the extreme floods, which inhibits the cooling by vertical mixing. On the other hand, the temperature trend due to the atmospheric fluxes decreases, most likely due to a decrease in net heat flux. In fall, the changes are reversed, in link probably with a salinization of the surface at this time (not shown).

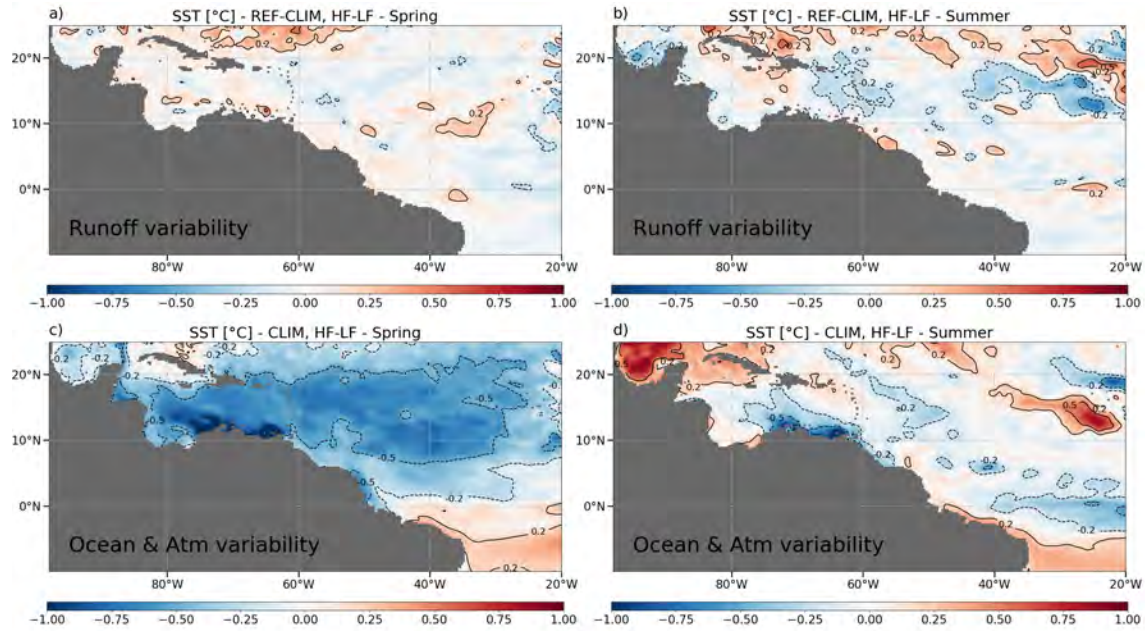

Figure 5.6: Spring (AMJ) maps of SST differences between highest floods and lowest floods for a) CLIM and c) REF minus CLIM; b), d): same as a), c) respectively but in summer (JAS)

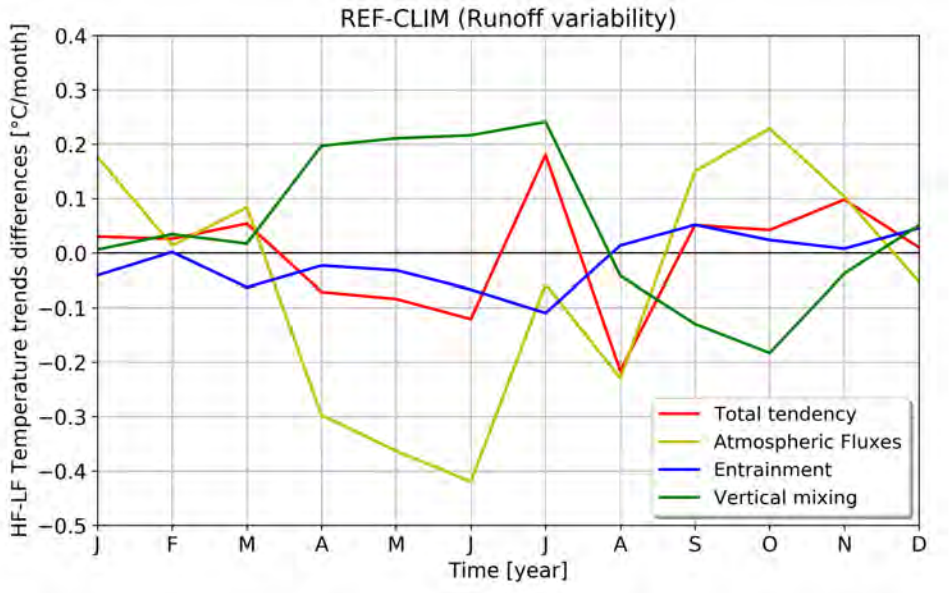

Figure 5.7: Seasonal cycle of the different contributions to the mixed layer heat budget for the difference between REF and CLIM composites in the NWTA box.

5.4 Discussion

5.4.1 Influence of the Atlantic Meridional Mode

A large part of the variability captured by the chosen composites is likely caused by the AMM. First of all, runoff interannual variability can be linked to AMM. Indeed, several Amazon droughts are related to positive AMM phase, while several Amazon floods are related to negative AMM phase (Foltz et al., 2012; Marengo and Espinoza, 2016). The difference between highest floods and lowest floods composites can therefore be associated with a negative AMM phase. And indeed, some patterns that emerge are very characteristic of a negative AMM event.

AMM is primarily characterized by a dipole of SST anomalies, generated and enhanced by WES feedback (see Section 1.2.2), which peaks in spring. For a negative AMM event, the SST anomalies are negative in the northern hemisphere, and positive in the southern hemisphere (Figure 1.5). This pattern is identical to what is observed in spring in the SST map of difference between the REF composites (not shown, but very similar to Figure 5.6c). This is also consistent with results from Fournier et al. (2017), who found strong negative SST anomalies in 2014 (one of the year composing our highest floods composite), and strong positive anomalies in 2010 (one of the year composing our lowest floods composite).

The SST dipole generates a southward shift of the ITCZ during negative AMM phase, and therefore an increase in precipitation over the Amazon basin (Xie and Carton, 2004; Rugg et al., 2016; Grodsky et al., 2018), leading to higher Amazon floods in the process. This ITCZ shift is clearly observed in the precipitation map of difference between the REF composites (Figure 5.8), and is similar to what observe Jury (2019) when doing a difference between fresh and salty years .

The SSS signature of AMM has been extracted by Awo et al. (2018), and is similar to what is obtained here (Figure 5.3a). Moreover, the changes in currents previously identified as drivers of SSS variability are likely caused by AMM (Hormann et al., 2012; Jury, 2019), and especially the southward shift of NECC in spring (Hormann et al., 2012) and the increase in NBC and decrease in NBC retroflection in summer (Jury, 2019).

Finally, it is interesting to note that MLD is also strongly impacted by AMM: during negative AMM events, a deepening of the ML is observed in the northwestern part of the basin (including the Amazon plume), despite the strong SSS decrease and the increase in salinity stratification induced by Amazon extreme floods (Rugg et al., 2016, ; see also Figure 5.8). This shows that the Amazon extreme floods does not have a strong impact on the vertical dynamics in the Amazon plume. This ML deepening is most likely related to a wind increase (not shown, see Rugg et al., 2016), but also to the SST decrease previously discussed, which suggests that temperature changes linked to AMM have a stronger control on stratification than salinity changes due to extreme floods.

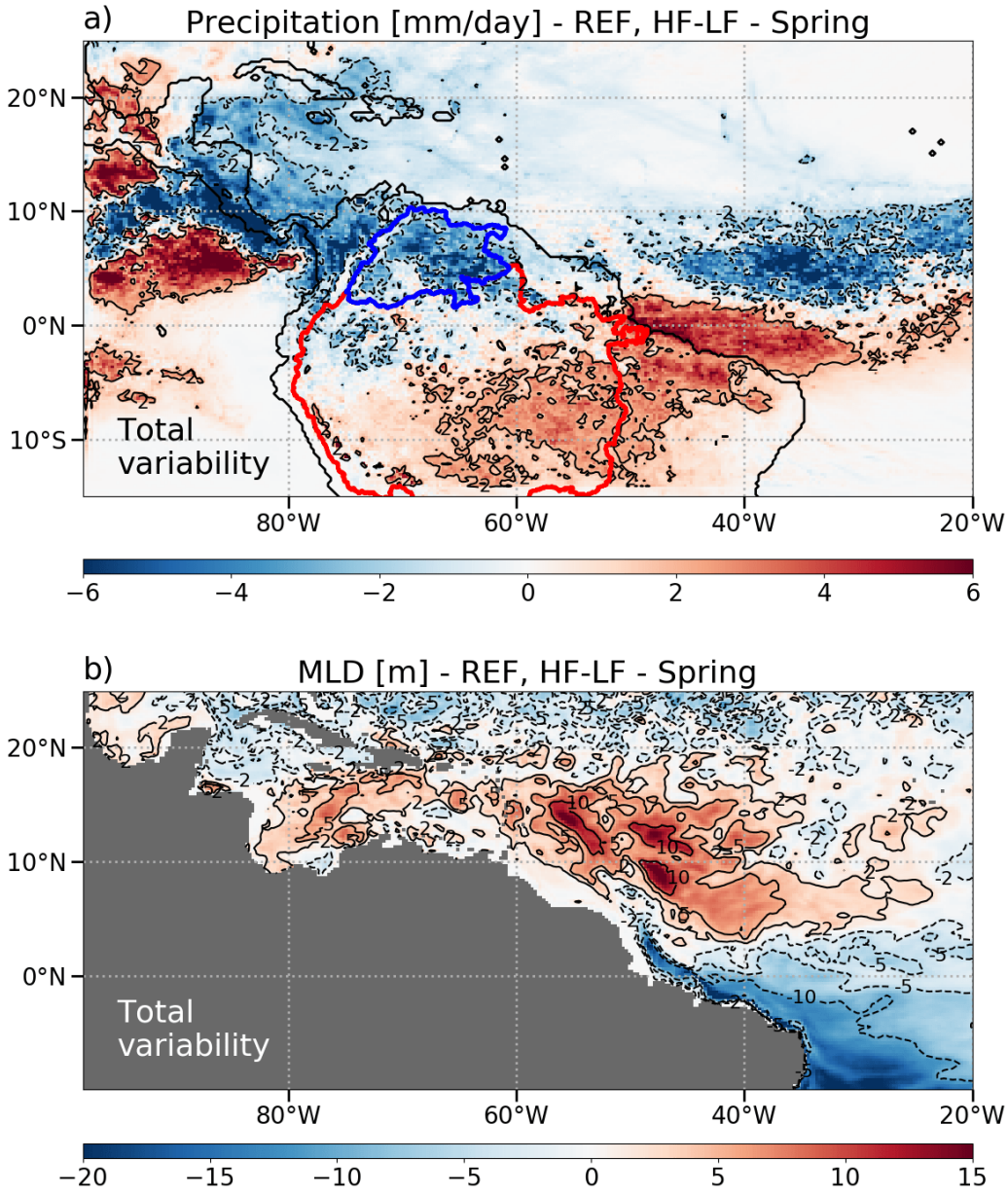

Figure 5.8: Map of a) precipitation and b) mixed layer depth in spring (AMJ), difference between the REF composites. The contours of the Orinoco (in blue) and Amazon (in red) watersheds are represented on a).

5.4.2 SSS changes in the Orinoco plume

A strong positive anomaly near 62°W and 10°N can be observed in Figure 5.3d and 5.3f, which corresponds to the location of the Orinoco river mouth. Indeed, the variability of the

Orinoco is generally opposite to that of the Amazon: years of low floods of the Amazon correspond to years of extreme floods for the Orinoco, and some of the major Amazon floods coincides with years of low floods for the Orinoco (see Figure 5.1a and 5.1b). This is driven by ITCZ interannual variability. Indeed, Amazon floods usually occur when the ITCZ is anomalously far south. This ITCZ shift, usually due to a negative AMM phase, then leads to a lack of precipitation in the north of the Amazon watershed and in the Orinoco watershed (see Figure 5.8a). Moreover, the effect of the Orinoco is not observed in spring but only in summer, the time of the year where the Orinoco discharge is the highest (Müller-Karger et al., 1989). Both processes combined probably explain part of the salinization that drives the change in mixed layer heat budget in fall (Figure 5.7).

5.5 Conclusion

In this study, we used a coupled ocean-atmosphere model at a 1/4° resolution to assess the impact of runoff interannual variability on the SSS, the plume extent and the SST in the western tropical Atlantic. To this end, we conducted two 15-years experiments: a REF experiment with interannual variability of river runoff and ocean color, and a CLIM experiment forced with 2001-2015 monthly climatologies of runoff and ocean color. To investigate the effect of the extreme floods observed in the last decades, we calculated composites of the four years with the highest floods and the four years with the lowest floods. The runoff change between highest and lowest floods years is about 25%. Finally, we calculated differences maps of the two composites, for the REF minus CLIM difference and for the CLIM experiment. This allows us to isolate the effect of runoff interannual variability from other processes (mixing, advection, atmospheric water and heat fluxes) whose variability can impact the salinity and temperature properties in the western tropical Atlantic.

Runoff interannual variability has a strong impact on the SSS of the Amazon plume in spring (less than -3 PSU near the Amazon mouth), but this effect fades rapidly under the action of the vertical mixing and has completely disappeared by fall. Moreover, the ocean and atmospheric variability impacts the SSS to a similar magnitude as runoff. In spring, a decrease in NBC and in coastal currents leads to an accumulation of freshwater near the Amazon mouth and a salty anomaly downstream, near the Guiana coast. In summer, a decrease in NBC retroflection leads to a stronger northwestward freshwater transport into the Lesser Antilles, and less freshwater transport into the NECC. These currents changes can be associated with AMM.

The plume area is also affected by extreme floods in summer and fall, the period when it is the most extended. In ASO, a change of 16% in plume area is observed, and runoff interannual variability explains 75% of it .

Finally, we show that years with high and low floods are associated with strong SST anomalies in spring in the north tropical Atlantic. This anomaly is linked with a negative phase of the AMM and therefore a southward shift of the ITCZ, which in turn causes Amazon floods. But our simulations do not reveal any clear impact of the runoff interannual variability

on the SST, neither in spring nor in summer. Nevertheless, a mechanism similar – albeit much weaker – to what is observed in the simulations without salinity stratification (Chapter 3) and without rivers (Chapter 4) is observed: the increase in stratification due to extreme floods leads to a decrease in cooling by vertical mixing, more than compensated by a decrease in heat brought by atmospheric fluxes.

One limitation of this chapter is the lack of relevant indicator to assess the statistical significance of the differences between composites. Having 4-year composites already makes the study robust, but one way to make the study even more robust would be to have a longer simulation, in order to compute composites with more high floods and low floods events. Another way would be to compute an ensemble of several members (5 to 10 for instance) for REF and CLIM simulations: averaging these members would allow to smooth the intrinsic variability and retain only the significant signal (Bessières et al., 2017). Nevertheless, the intrinsic variability in the tropics and in the tropical Atlantic is relatively low, especially at the ocean surface (e.g. Sérazin et al., 2017), and we can be reasonably confident in the results obtained here.

Chapter 6

Impact of salinity stratification in a future climate

Contents

6.1 Introduction

In Chapter 3, a link between salinity stratification and SST has been identified in the present climate. The aim of this chapter is to investigate the evolution of this link in the future: will it be exacerbated under climate change, or on the contrary will it be damped?

Indeed, several parameters influencing this link are expected to be affected by climate change. The MLD plays an important role in the relationship between salinity stratification and SST, and it is well known that the increase in temperature due to climate change will strengthen thermal stratification and impact the MLD, especially in the tropics (Capotondi et al., 2012; Bindoff et al., 2019). In the tropical Atlantic Ocean, the increase in SST could locally reach up to 4.5°C above the present value by 2100 under the RCP 8.5 scenario (Deppenmeier et al., 2020). This SST increase is likely to affect the atmospheric deep convection, which is bound to modify the atmospheric feedbacks revealed in Chapter 3. The water cycle is also expected to amplify in the future (Durack, 2015; Skliris et al., 2016), which could induce changes in runoff and therefore in salinity stratification, leading to a possible feedback on SST. Finally, the vertical mixing also influences the response of SST and precipitation to future climate in the tropical Atlantic, and the way vertical mixing will evolve in the future remains unclear (Deppenmeier et al., 2020). Some changes are counteracting, and the way the relationship between salinity stratification and SST will evolve cannot be easily guessed and needs a proper study.

6.2 Methodology

To study the link between salinity stratification and SST in a future climate, a dynamical downscaling is conducted. This consists in using one model or a multi-model ensemble mean of the Coupled Model Intercomparison Project (CMIP) to force a regional model. This dynamical downscaling approach first allows to limit the computational costs inherent to a global model. A regional model is also expected to reproduce more accurately the regional physics, since an appropriate set of parameterizations is chosen specifically for the region of study. Finally, using dynamical downscaling allows to increase the model resolution compared to global models, which generally gives better results (e.g. Siongco et al., 2017; Cabos et al., 2018) and might modify the response to climate change (van Westen et al., 2020).

6.2.1 Simulations

In this chapter, four ocean-atmosphere coupled simulations are analyzed. The twin sensitivity experiments with and without stratification, CONTROL and NOS, are used as present state (see Chapter 2 and Chapter 3), and two more simulations of a future climate with and without salinity stratification are computed: CTLf and NOSf.

The simulations of a future climate need some new boundary conditions and a new initial state that take climate change into account. The scenario chosen is SSP5–8.5 of CMIP6, which is similar to the RCP8.5 scenario of CMIP5. It represents a high economic growth and an extensive use of fossil fuels (Gidden et al., 2019), and is known as the "business as usual" scenario, even if this statement is debated (Hausfather and Peters, 2020). The method used to obtain the new forcings is described in the following. 15 years of simulation were conducted, corresponding approximately to the last 15 years of the 21st century (2086 to 2100). New values for the atmospheric concentrations of greenhouse gases (GHG) were also set, corresponding to the year 2090 for the RCP8.5 scenario (see IPCC, 2013).

6.2.2 CMIP6 multi-model ensemble mean

The first step to construct the new boundaries was to compute a multi-model ensemble mean (MMEM) of 25 CMIP6 models. The criterion for the choice of the CMIP6 models is the availability of all the atmospheric and oceanic variables that we need, for both the historical and the SSP5-8.5 scenarios. Some CMIP6 models have multiple members available, but to avoid giving too much weight to these models with respect to the other CMIP6 models, we chose to use only the first available member. All the models and the chosen members are listed in Table 6.1.

We computed 30-years monthly climatologies of the MMEM for the historical run (1985 to 2014) and the SSP5-8.5 scenario (2071 to 2100). Then, we calculated the monthly anomalies between future and present climatologies, which will be called "CMIP6 MMEM anomaly" in the following.

Table 6.1: CMIP6 models used for the MMEM

Model name	Member used
ACCESS-CM2	r1i1p1f1
ACCESS-ESM1-5	r1i1p1f1
CMCC-CM2-SR5	r1i1p1f1
CNRM-CM6-1	r1i1p1f2
CNRM-CM6-1-HR	r1i1p1f2
CNRM-ESM2-1	r1i1p1f2
CanESM5	r1i1p1f1
CanESM5-CanOE	r1i1p2f1
EC-Earth3	r1i1p1f1
EC-Earth3 Veg	r1i1p1f1
FGOALS-f3-L	r1i1p1f1
GFDL-CM4	r1i1p1f1
GISS-E2-1-G	r1i1p1f2
HadGEM3-GC31-LL	r1i1p1f3
HadGEM3-GC31-MM	r1i1p1f3
INM-CM4-8	r1i1p1f1
INM-CM5-0	r1i1p1f1
IPSL-CM6A-LR	r1i1p1f1
MCM-UA-1-0	r1i1p1f2
MIROC-ES2L	r1i1p1f2
MIROC6	r1i1p1f1
MPI-ESM1-2-HR	r1i1p1f1
MPI-ESM1-2-LR	r1i1p1f1
MRI-ESM2-0	r1i1p1f1
UKESM1-0-LL	r1i1p1f2

6.2.3 Pseudo-global warming approach

To simulate the future climate, we used the Pseudo-Global Warming (PGW) approach (e.g. Schär et al., 1996; Rasmussen et al., 2011; Liu et al., 2016; Dai et al., 2017b; Dutheil et al., 2019). This method of dynamical downscaling consists in adding the CMIP6 MMEM anomaly to the lateral boundaries and to the initial state of the oceanic and atmospheric model. To initialize the oceanic model, a 30 years spin-up is conducted using a forced ocean model: the CMIP6 MMEM anomaly is thus also added to the atmospheric bound-

Table 6.2: Variables modified using the CMIP6 MMEM anomaly

Variables	Dimension	Unit	Model
Air temperature	3D	[K]	WRF
Relative humidity	3D	[%]	WRF
Zonal and meridional wind	3D	[m/s]	WRF
Geopotential height	3D	[m]	WRF
Sea level pressure	2D	[Pa]	WRF and NEMO forced
Surface pressure	2D	[Pa]	WRF
Sea surface temperature	2D	[K]	WRF
Ocean temperature	3D	[K]	NEMO coupled and forced
Salinity	3D	[PSU]	NEMO coupled and forced
Zonal and meridional currents	3D	[m/s]	NEMO coupled and forced
Precipitation	2D	[kg/m^2/s]	NEMO forced
Specific humidity at the surface	2D	[kg/kg]	NEMO forced
Surface air temperature	2D	[K]	NEMO forced
Zonal and meridional surface winds	2D	[m/s]	NEMO forced
Surface longwave radiation	2D	[W/m^2]	NEMO forced
Surface shortwave radiation	2D	[W/m^2]	NEMO forced

aries of the forced model. The detail of the modified variables can be found in Table 6.2. Runoff is kept identical in the present and the future simulations because precipitation changes are very different in our model and in the CMIP6 MMEM (see Section 6.3.1): including the future changes in runoff to the model would mean including changes in runoff corresponding to very distinct changes in precipitation, which would lead to inconsistency.

The PGW approach is robust: doing downscalings of several individual CMIP models and taking the ensemble mean afterwards gives results very similar to one downscaling of the ensemble mean of these models (Kawase et al., 2009; Lauer et al., 2013). Moreover, the mean state biases of the GCMs are removed, since we are using the difference between future and present MMEM added to reanalyses instead of the MMEM itself (Liu et al., 2016). But with this method, the only changes taken into account are the seasonal mean changes due to the increase in GHG: the internal climate variability imposed on the boundaries is the same in the future and present simulations (Dai et al., 2017a), and corresponds to the variability of the reanalyses (ERA-Interim for the atmosphere and GLORYS2V4 for the ocean). This is illustrated on Figure 6.1: the present and future SST variability are really close from one another, and the small changes observed (a slight decrease of SST extremes in the future)

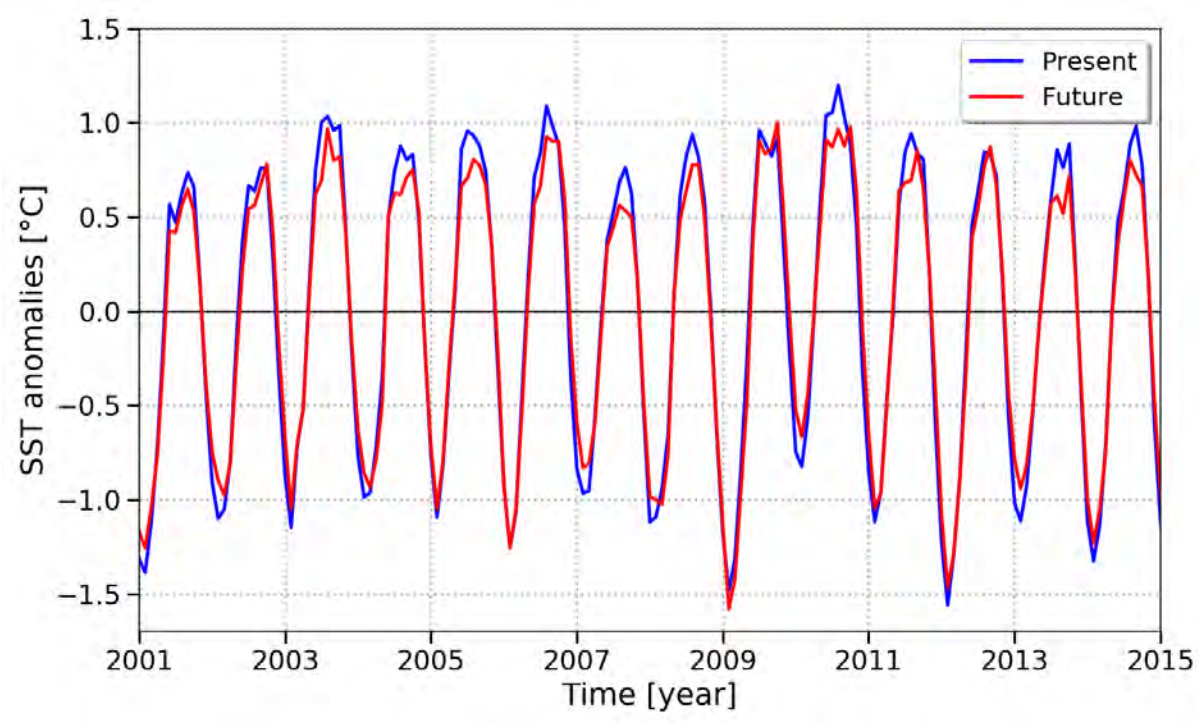

Figure 6.1: SST anomaly averaged over the whole domain, for the present (blue) and the future (red). The anomaly is calculated as the difference between the monthly SST and the 15-year average. Note that the SST anomaly does not have any trend: our model is not in a transient state like for instance the CMIP models that simulate climate between 2000 and 2100. On the contrary, it has reached a stable state.

are due solely to the impact of the mean warming on the internal temperature variability. Since the future variability is highly uncertain, this can be considered as an advantage (Deser et al., 2016; Liu et al., 2016). Moreover, this allows the use of shorter simulations (Kawase et al., 2009). However, this also implies that the PGW approach is not suited for studying the interannual and decadal changes (Xu et al., 2018; Adachi and Tomita, 2020).

6.3 Results

6.3.1 Changes in the tropical Atlantic Ocean induced by the increase in GHG concentrations

The present simulation CONTROL has been validated in Section 2.4, and is globally faithful to the observations. We now assess the impact of climate change on the tropical Atlantic Ocean, and the difference between what is obtained with the MMEM of CMIP6 global models (Figure 6.2) and what is obtained with our downscaled model (Figure 6.3).

The variable most characteristic of climate change is SST. In this scenario, the SST

increase is very strong: up to 3.5°C in the GCMs (Figure 6.2a and 6.2b), and up to 4°C in our model (Figure 6.3a and 6.3b). An overall increase in temperature is observed, but the CT area and the ITCZ exhibit stronger SST changes, while the Canary upwelling system shows weaker changes. The patterns of SST changes are very similar in the CMIP6 MMEM and in our model, despite a slightly higher amplitude of warming in our model. This suggests that the PGW approach is successfully implemented: the warming trend induced by climate change is effectively input into our model.

The changes in SSS and precipitation are really different in our model compared to CMIP6 MMEM. Indeed, an increase in SSS is found in the main part of the basin in the MMEM, except in the western tropical Atlantic (Figure 6.2c and 6.2d), while a decrease is found in most of the basin in our model (Figure 6.3c and 6.3d). This is partly due to the very distinct changes in precipitation. In the MMEM, changes in precipitation are small: a slight increase (around +1 mm/day) is observed in the ITCZ while there is a slight decrease in the rest of the basin (locally up to -1 mm/day) (Figure 6.2e and 6.2f). On the other hand, a strong, widespread precipitation increase is observed in our model (up to +6 mm/day),

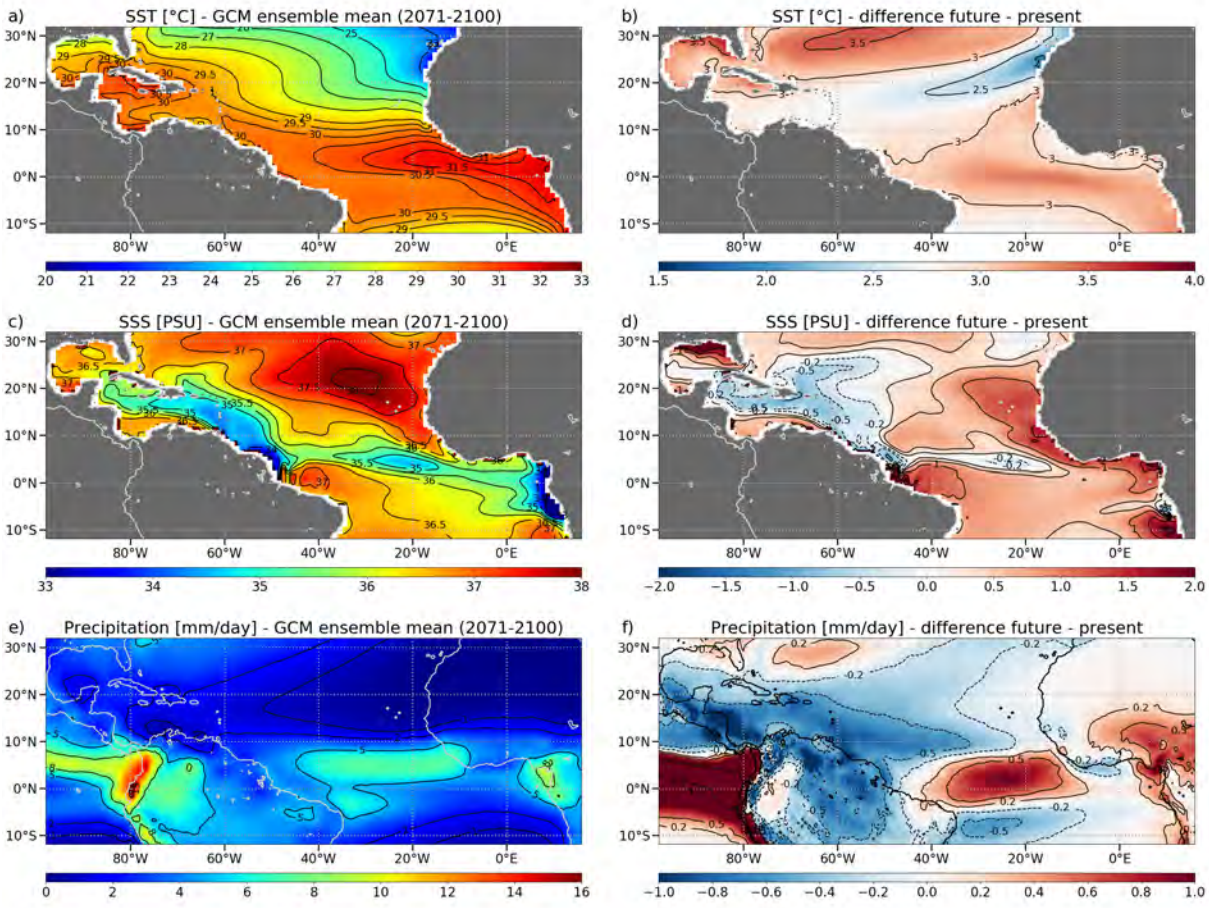

Figure 6.2: Maps of a), b): SST ; c), d): SSS and e), f): precipitation for the future (2071-2100) CMIP6 MMEM on the left, and the CMIP6 MMEM anomaly on the right.

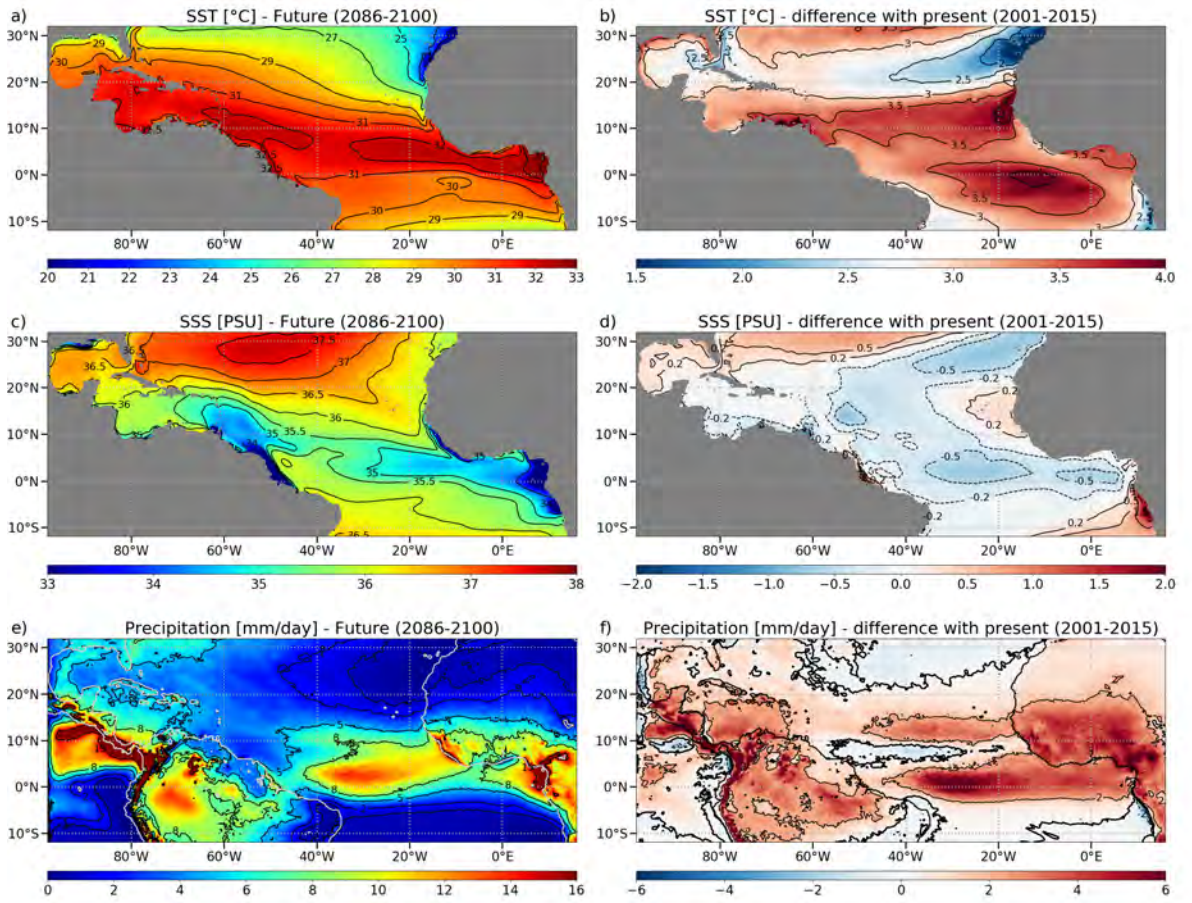

Figure 6.3: Maps of a), b): SST ; c), d): SSS ; e), f): precipitation ; g), h): MLD and i), j): net heat flux for the future downscaled simulation CTLf (2086-2100) on the left, and the difference between CTLf and present simulation CONTROL (2001-2015) on the right.

due to a broadening of the ITCZ toward the south mainly and toward the north a little (Figure 6.3e and 6.3f). Note that the color scales of Figure 6.2f and Figure 6.3f are different. Nevertheless, our model has a better representation of the ITCZ than the GCMs in the present climate (Figure 6.4). Indeed, the CMIP6 MMEM exhibits a double ITCZ bias: a secondary precipitation maximum is observed in the southern hemisphere. Furthermore, the maximum in the northern hemisphere is too low compared to the TRMM observations. This problem was already documented in CMIP3 and CMIP5, and is still present in CMIP6 (e.g. Tian and Dong, 2020). Having a better representation of precipitation in the present could indicate that the precipitation changes in the future may also be better represented in our model.

MLD is an important feature when studying the impact of salinity stratification on SST. In our model, a strong thinning of the ML is observed in the future in most of the basin, together with two small areas of increase in the north and the south of the domain (Figure 6.5a and 6.5b, see also Figure 2.4g for the present MLD). The thinning of the ML occurs in an area where it is already very thin, and the decrease in MLD reaches -25% in the NWTA, making

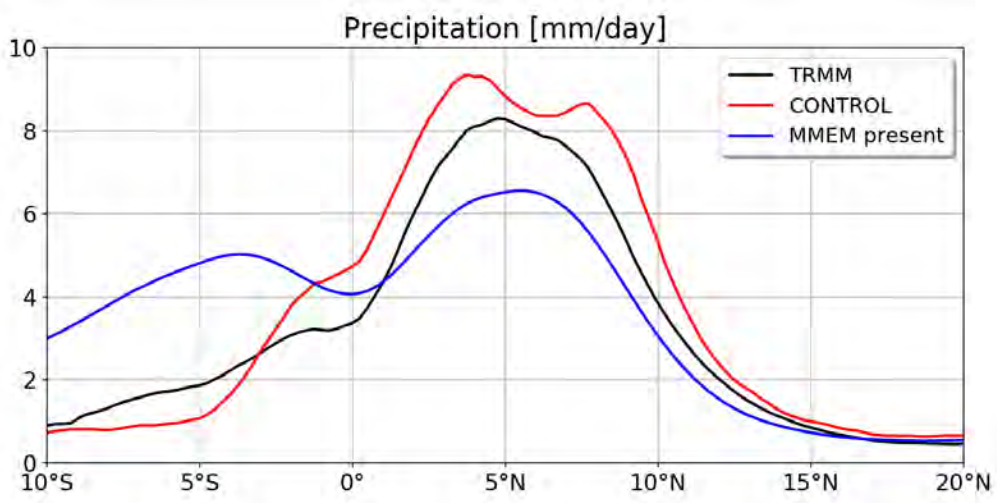

Figure 6.4: South-North sections of precipitation averaged between 20°W and 40°W: TRMM (2001-2015) in black, CONTROL (2001-2015) in red and CMIP6 MMEM (1985-2014) in blue.

the ML even more sensitive to the atmospheric fluxes. The change in ML is associated with a change in total stratification (Figure 6.5c and 6.5d). Indeed, the patterns of both variables are very similar, with a strong increase in total stratification in areas where the ML thinning is the most intense, and a weaker increase or even a decrease in stratification in areas where the ML is deepening. Note that the link between the two is not straightforward: an increase of stratification has been observed over the past 50 years, and is associated with a deepening of the ML (Sallée et al., 2021).

Salinity stratification shows an increase in our main areas of interest (NWTA, ITCZ, CT; Figure 6.5e and 6.5f), consistent with the overall decrease in SSS (Figure 6.3d). However, the patterns of salinity stratification changes match the patterns of SSS changes in only a portion of the basin. Indeed, an increase in SSS is observed in the southeast of the domain, destabilizing the water column and leading to a decrease in salinity stratification. On the other hand, a decrease in SSS is observed in the main part of the domain, but this leads to an increase in salinity stratification south of 15°N only. In the northern part of the basin, a SSS decrease is not systematically associated with an increase in salinity stratification. This discrepancy is likely due to subsurface processes, combined with the fact that salinity stratification is very weak in this part of the basin.

The part of density stratification driven by salinity increases much less than the total density stratification. This means that total stratification change is mainly driven by a strong thermal stratification increase. As a consequence, OSS_{100m} (see definition in Section 2.5.3) is decreasing in some part of the basin where salinity stratification is increasing (Figure 6.5g and 6.5h): even though salinity stratification increases, the greater increase in thermal stratification results in a smaller contribution of salinity stratification to total stratification. This is especially the case in NWTA, where the OSS_{100m} decrease is quite important (about -20% on average in the NWTA box).

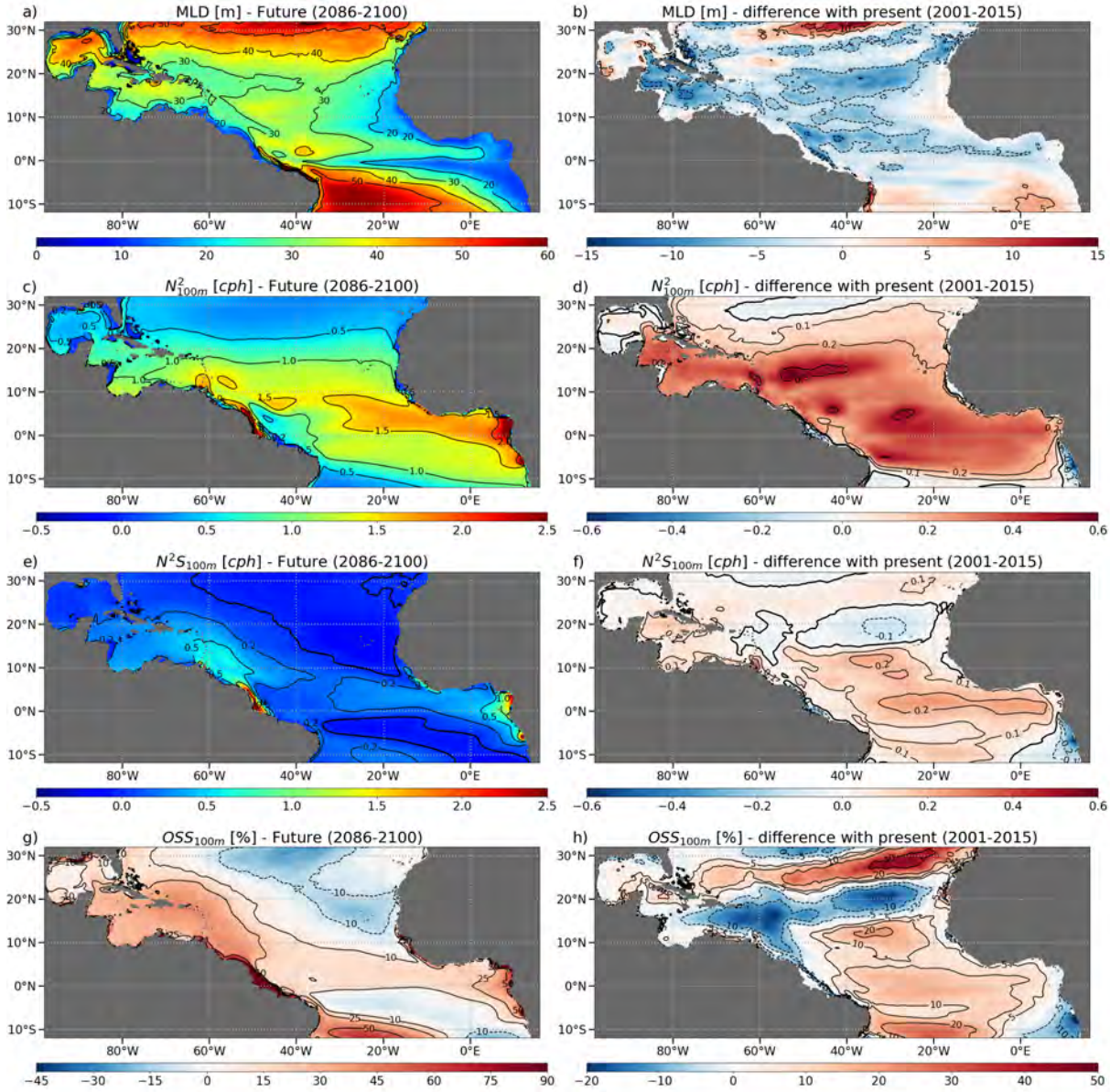

Figure 6.5: Maps of a), b): MLD ; c), d): total stratification N^2 averaged over 100 m, e), f): salinity stratification N^2S averaged over 100 m and g), h) OSS_{100m} for the future downscaled simulation CTLf (2086-2100) on the left, and the difference between CTLf and present simulation CONTROL (2001-2015) on the right.

6.3.2 Changes in the relationship between salinity stratification and SST induced by the increase in GHG concentrations

The difference between CTLf and NOSf simulations is now analyzed, in order to evaluate the impact of salinity stratification in a future climate. SST differences are calculated for the present simulations (Figure 6.6a and 6.6c) and the future simulations (Figure 6.6b and 6.6d) in summer and winter. The sensitivity of SST to salinity stratification exhibits very similar patterns in the present and in the future, with a SST increase in the NWTA in summer, a SST decrease in the CT in summer, and lesser changes in winter. Nevertheless, small changes in the response appear: in the NWTA, the response in the future climate is weaker than in the current climate in summer and slightly stronger in winter ; in the CT, the response is stronger in summer (down to -0.8°C in the future simulations, but down to -0.5°C only in the present simulations), and weaker in winter. In winter, a new pattern of response develops in the future in the central tropical Atlantic: a slight increase between 10°N and 20°N and between 50°W and 30°W. A decrease in SST can also be observed in winter in the upwelling off the Senegalese coast; it was already there in the present climate, but it is stronger and encompasses a wider area in the future simulations.

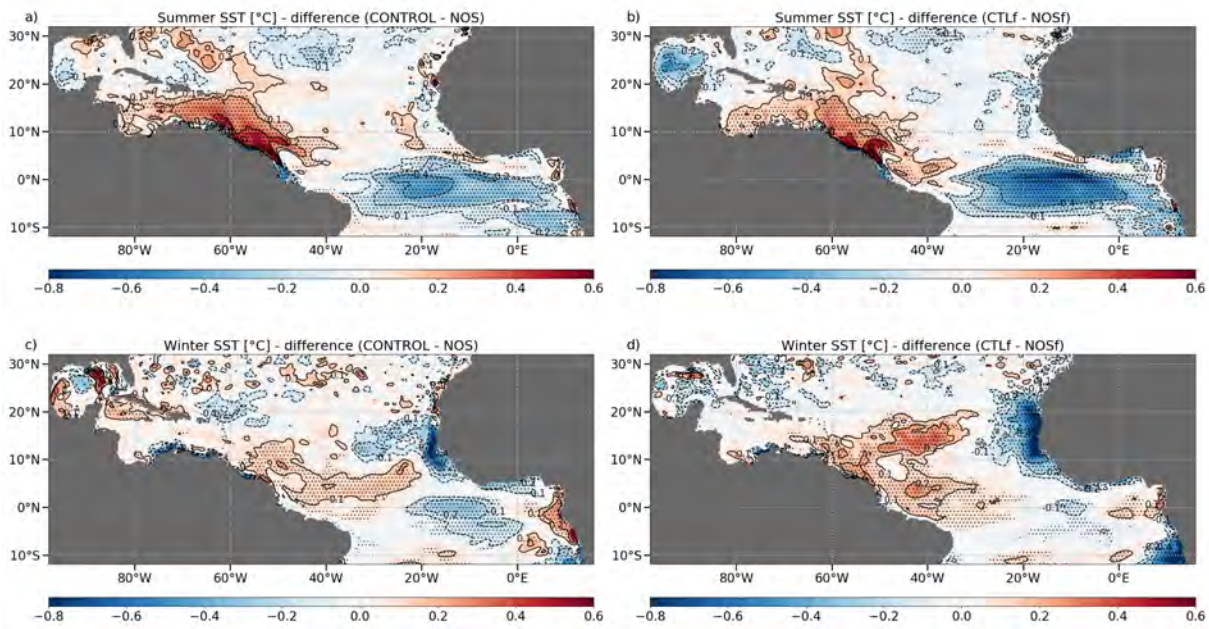

Figure 6.6: SST differences between CONTROL and NOS in a) summer and c) winter, dots indicating the areas where the difference is significant. b), d): same as a), c) respectively, but for the difference between CTLf and NOSf.

6.3.2.1 Changes in the northwestern tropical Atlantic SST anomaly

In the NWTA, the temperature response is very similar in the present and future climate, with an increase in surface temperature and a decrease in subsurface of same magnitude (Figure 6.7a and 6.7b). Nevertheless, some modulations can be observed: the sensitivity of SST to salinity stratification is decreased in summer in a future climate, but increased in winter. This can be related to a change in the seasonal cycle of the salinity stratification, N^2S (Figure 6.7c). First, a stronger salinity stratification is observed in winter in the future, which could explain the greater SST difference in this season. Then, N^2S becomes lower in July and August in the future, explaining the weaker response compared to the present. Finally, a secondary maximum in SST difference is observed in the future in November (Figure 6.7b), corresponding to a secondary peak in N^2S during this month.

The ML heat budget (see Section 2.5.1.1) of the area is now analyzed (Figure 6.8). First, the ML heat budgets of CTLf and CONTROL show strong similarities (Figure 6.8a and 6.8b, dashed and solid lines): the three main processes influencing it are the vertical diffusion, the atmospheric fluxes and the entrainment, roughly compensating each other to give smaller changes in the total tendency. The total tendency is close for CTLf and CONTROL, meaning that climate change does not alter much the amplitude of the SST seasonal cycle in the NWTA. However, other terms of the heat budget are impacted by climate change, and especially the atmospheric fluxes and the vertical diffusion. The atmospheric fluxes warm more intensely the ML in the future and particularly in summer. This is due to an increase in net heat flux (not shown), combined with a thinning of the ML in the future (Figure 6.4) that makes the ML more responsive to heat fluxes. It is then balanced by an increase in cooling by vertical diffusion. This increase is likely linked to the strong increase in stratification in the future. It is a competition between two processes. On the one hand, the increase in total stratification stabilizes the water column and decreases the mixing. On the other hand, the strong increase in thermal stratification leads to a much sharper thermocline, enhancing the mixing efficiency. This second process seems to prevail over the first, leading to a more efficient cooling by vertical diffusion in the future.

The changes in ML heat budget due to salinity stratification are similar in the present and the future (Figure 6.8c and 6.8d). The same processes and feedbacks are at stake, with 1) a decrease in the cooling by vertical diffusion when taking salinity stratification into account, leading to a warming of the ML, and 2) a damping of this warming by the entrainment and the atmospheric fluxes. Nevertheless, some variations can be observed in the future, especially in AMJ, which is the period of development of the SST anomaly due to salinity stratification (see for instance Figure 6.7a). Vertical diffusion is more sensitive to salinity stratification, (1.2°C/month in the future in AMJ, i.e. +20% compared to the present climate), but this higher sensitivity is more effectively compensated by the atmospheric fluxes (-0.7°C/month in the future in AMJ, i.e. +55% compared to the present climate), which gives in the end a weaker change in total tendency in the future (0.05°C/month in the future in AMJ instead of 0.1°C/month). Finally, the new secondary SST maximum observed previously in November can be related to the peak in CTLf-NOSf total tendency in October. The latter is due mainly to a secondary maximum in vertical diffusion trend, which can be related to the secondary

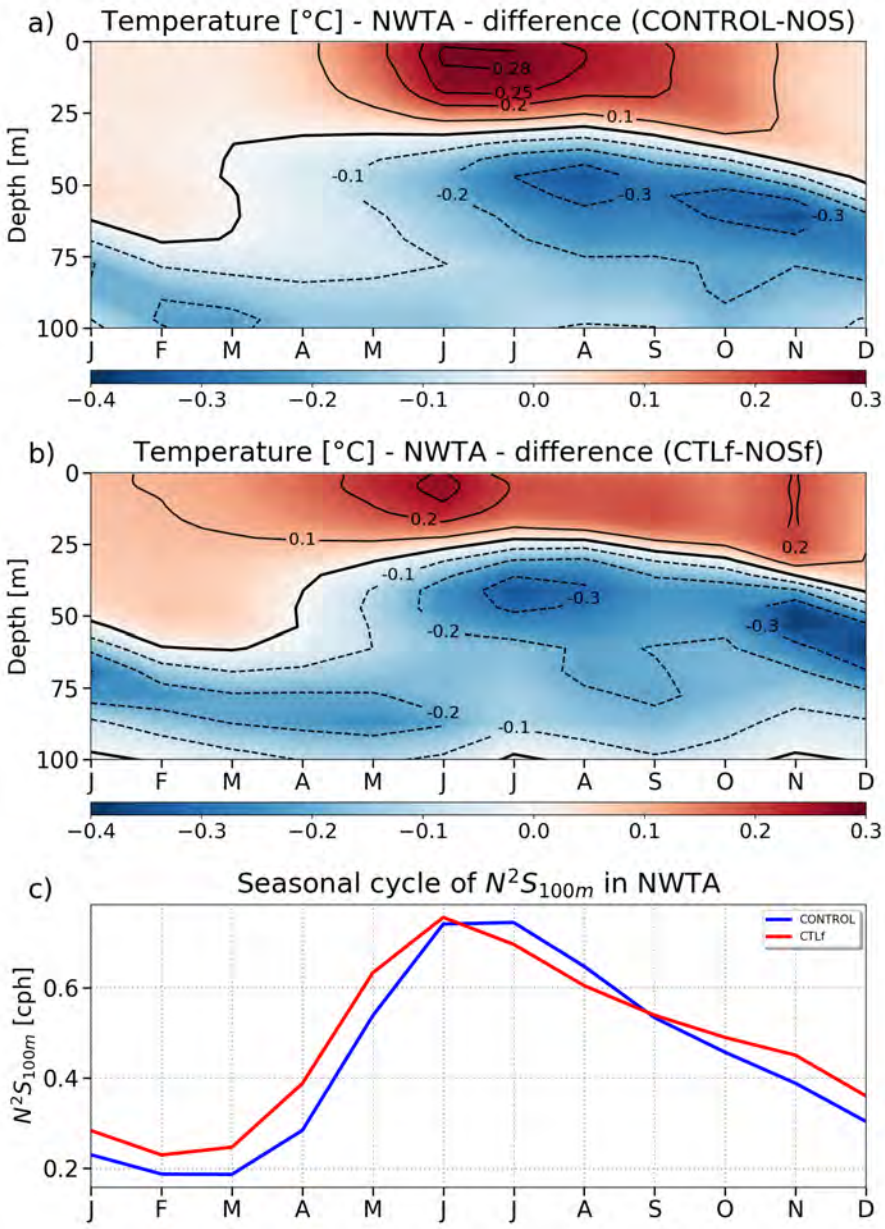

Figure 6.7: Seasonal cycle of temperature difference in the NWTA as a function of depth for a) the present simulations (CONTROL-NOS), b) the future simulations (CTLf-NOSf); c) Seasonal cycle of N^2S_{100m} (i.e. salinity stratification averaged over 100 m depth) in the NWTA for CONTROL (blue) and CTLf (red).

peak in N^2S (Figure 6.7c). More generally, the differences in vertical diffusion (Figure 6.8d, black curves) are very well correlated to N^2S (Figure 6.7c), suggesting that the increased sensitivity of vertical diffusion to salinity stratification in the future is directly linked to the change in N^2S seasonal cycle.

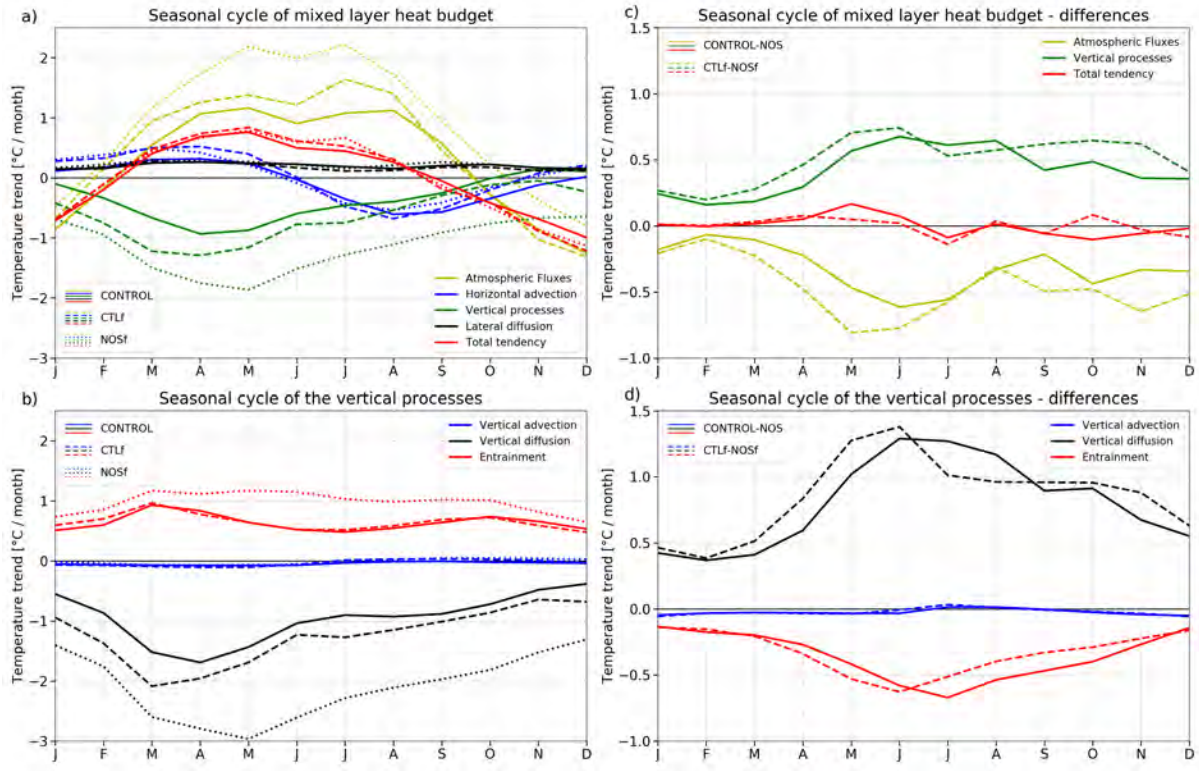

Figure 6.8: Seasonal cycle of the mixed layer heat budget in NWTA for CONTROL, CTLf and NOSf simulations (left) and differences CONTROL-NOS and CTLf-NOSf (right): a), c) main terms of the budget and b), d) vertical processes

The mechanism behind the damping by the atmospheric heat fluxes is similar to what is found in the present climate (Section 3.3.2.3). In the NWTA, the increase in SST induced by the decrease in vertical mixing strengthens the latent heat flux, and leads to a more important heat loss (Figure 6.9a) that mitigates the SST increase. As in the present climate, this is the main feedback mechanism and it drives most of the changes in net heat flux (not shown). A secondary feedback loop occurs through the solar heat flux: the increase in SST enhances the deep-convection in the NWTA, and leads to an increase of cloud cover (Figure 6.9b). Clouds block solar radiation, leading to a decrease in solar heat flux reaching the ocean surface, and thus a decrease in SST.

However, some small changes in the atmospheric response to salinity stratification in the future are worth noting. First, the northward shift of the ITCZ observed in the present does not appear in the future (Figure 3.7d and Figure 6.9b). It is replaced by a stronger decrease in cloud cover in the ITCZ and over the West African coast. The associated decrease in precipitation mitigates therefore the increase in precipitation induced by climate change, especially over the coasts of Liberia and Nigeria. In addition, in the NWTA, the area of strongest increase in cloud cover is shifted to the northwest in the future. Yet, the area of high SST increase is located in the same place, and a decrease in SST response to the northwest is even observed in the future. This discrepancy might be related to a decrease in

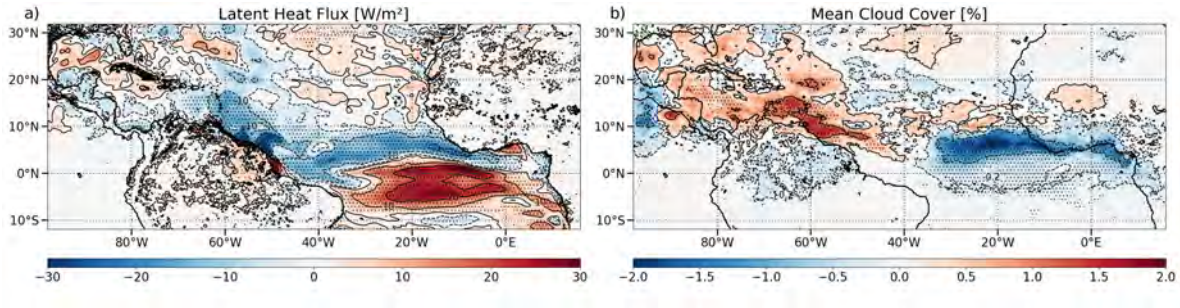

Figure 6.9: Difference between CTLf and NOSf in summer of a) Latent Heat Flux and b) Cloud Cover, dots indicating the areas where the difference is statistically significant

precipitation there due to climate change (Figure 6.3f): deep convection is less likely to be triggered there, and is thus less sensitive to a change in SST.

The overall similarity of the SST sensitivity to salinity stratification in a present and a future climate strengthens the conclusions of Chapter 3: the response is robust, even in a very different climate. However, so little change in the link between salinity stratification and SST in NWTA can be surprising given the intensity of the changes induced by the increase in GHG.

6.3.2.2 Changes in the cold tongue SST anomaly

In the CT region, the sensitivity of surface and subsurface temperature to salinity stratification is increased in summer in a future climate, but decreased in winter (Figure 6.10a and 6.10b). In summer, all the changes observed in the present are enhanced in a future climate: the decrease in surface and subsurface temperature due to salinity stratification is almost twice as important in the future (Figure 6.10c and 6.10d), and so is the strengthening of the EUC (Figure 6.10e and 6.10f).

The reason for the enhanced sensitivity in summer is probably twofold. In Chapter 3, we observed that the SST decrease in the CT is due to a shoaling of the thermocline. This shoaling causes a decrease in subsurface temperature that impacts the surface during the season of upwelling and CT development, i.e. in summer. In a future climate, the 20°C isotherm depth, proxy of the thermocline depth, is much more sensitive to salinity stratification: when averaging over the CT box, the D20 shoals by 9 m in CTLf-NOSf, and only by 6 m in CONTROL-NOS. Moreover, a strong increase in thermal stratification is observed in the region (Figure 6.5). This means that the temperature gradient is stronger, and that a change in the thermocline depth has more impact on the subsurface temperature. The stronger decrease in subsurface temperature is then upwelled in summer, leading to a stronger SST decrease in the future. In winter however, the stabilizing effect of the enhanced stratification prevails, and the subsurface temperature anomaly does not reach the surface at all, unlike in the present climate.

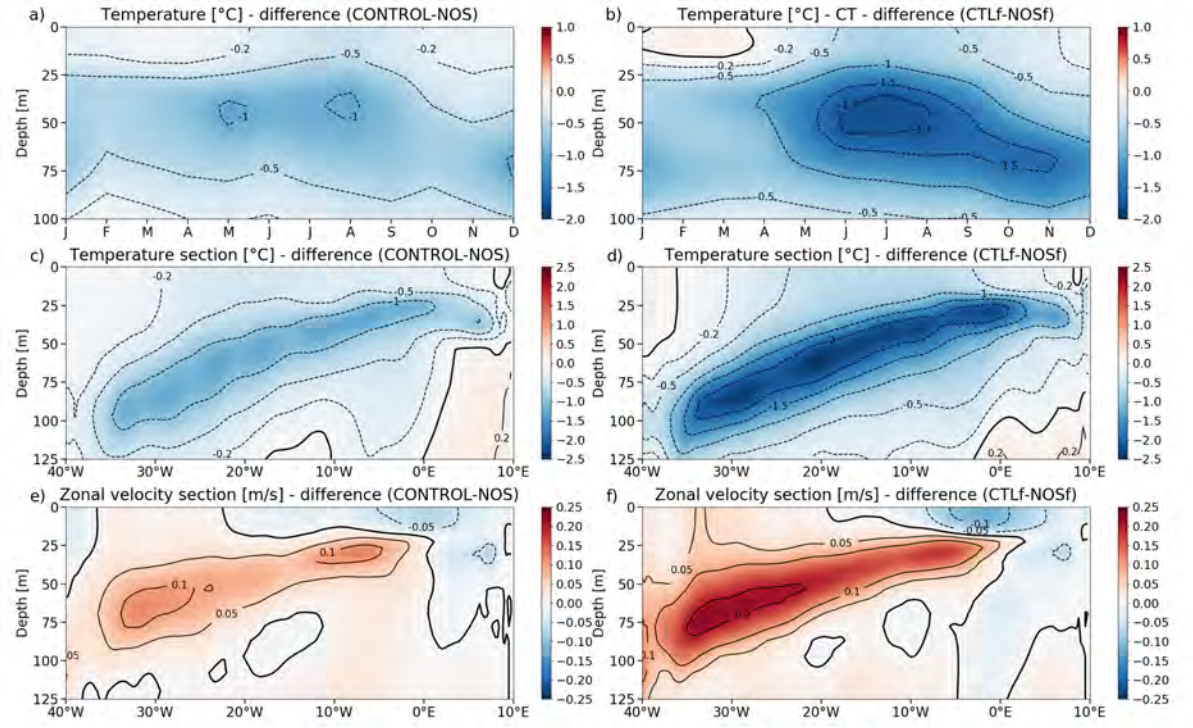

Figure 6.10: a), b): Seasonal cycle of temperature difference in the CT as a function of depth; Summer section averaged between 1°N and 3°S of c), d) temperature difference and e), f) zonal velocity. The difference CONTROL-NOS is on the left, and CTLf-NOSf is on the right.

6.4 Discussion

Several studies have investigated the influence of climate change, the main source of information on this subject being the IPCC. Studies concerning the tropical Atlantic Ocean are not as frequent, but global studies can already allow us to compare with the results from our downscaling.

The SST in our model has patterns and magnitude of changes very similar to CMIP5 and CMIP6 models (e.g. Stocker et al., 2013; Arias et al., 2021). The exception is the southeastern tropical Atlantic, near the coast of Angola, where our model predicts a lower change in SST than the globel models do (around 2°C instead of 3 to 4 °C). However, this area is poorly described in the CMIP models and exhibits a strong SST bias (e.g. Richter and Xie, 2008; Richter and Tokinaga, 2020), while our model has a better representation of the SST in this area. The stronger increase observed in the CT is consistent with other studies (Deppenmeier et al., 2020) and seems to indicate a decrease in upwelling, as found by Terada et al. (2020), but unlike Seo and Xie (2011). A stronger SST increase is also observed in the Senegalo-Mauritanian upwelling, suggesting a decrease in upwelling, as reported by Sylla et al. (2019) and Mignot et al. (2020).

Regarding salinity, Capotondi et al. (2012) found that a salinity stratification decrease was to be expected in the tropical Atlantic due to an increase in SSS, whereas we observe a decrease in SSS (Figure 6.3d) and an increase in salinity stratification (Figure 6.5f) in most of the basin. However, total stratification is expected to increase drastically (e.g Capotondi et al., 2012; Bindoff et al., 2019), which we also observe (Figure 6.5d). This increase is mainly driven by the increase of thermal stratification: even in areas where salinity stratification decreases, the total stratification increases strongly. This phenomenon is already observed in the present climate, due to the increase in temperature linked with the climate change already at stake (Sallée et al., 2021).

The precipitation changes show a strong increase in our model (Figure 6.3f), which is consistent with some studies and inconsistent with others. Precipitation changes are uncertain in the tropics (Kent et al., 2015) due to a weakening of the tropical atmospheric circulation (Vecchi and Soden, 2007; Chadwick et al., 2013; Ma et al., 2018) balanced with an amplification of the hydrological cycle (Durack, 2015; Skliris et al., 2016). Moreover, the models disagree on the spatial changes of precipitation, leading to non-significant and usually weak changes in the MMEM (Stocker et al., 2013; McSweeney and Jones, 2013; Chadwick et al., 2015). But individually, most of the models exhibit strong precipitation changes (Chadwick et al., 2015) that are for some of them relatively similar to what we observe, and for some others opposite (Cook et al., 2012; Dufresne et al., 2013; Brêda et al., 2020; Deppenmeier et al., 2020).

Despite these uncertain changes, two other precipitation-related variables are validated. A southward shift of the ITCZ is found in several studies (Skliris et al., 2020; Mamalakis et al., 2021) while we observe instead a widening of the ITCZ, mostly to the south and a little to the north. An increase in the SST-convection threshold is also observed in our model (Figure 6.11), consistent with what found Johnson and Xie (2010) in the whole tropics. However, an increase in rainfall rate occurs in our model, while Johnson and Xie (2010) observed no change in this variable, but this could be due to the difference in scenario studied (A1B, equivalent to RCP6.0 for them ; SSP5-8.5, equivalent to RCP8.5 for us).

Regarding the modulation of the link between salinity stratification and SST, no study addressed this specific topic. However, an experiment relatively close has been made by Deppenmeier et al. (2020): they examined the impact of increased vertical mixing in a present and a future climate. Removing salinity stratification as is done in NOS experiment means increasing the vertical mixing. Contrary to Deppenmeier et al. (2020), the increase in vertical mixing is not uniform in NOS experiment as it affects more strongly the areas of high salinity stratification. Nevertheless, a qualitative comparison of the SST patterns obtained by this study and ours can be made. The changes in the relationship between salinity stratification and SST induced by the increase of GHG (Figure 6.6) are globally consistent with the results of Deppenmeier et al. (2020). In summer, an increase in SST response is observed in the CT area, while a decrease is observed in NWTA. This is similar to what we observe. However, the decrease in NWTA is such that the sign of the anomaly is switching, which is not the case in our model. In winter, an increase in the SST response occurs in the Senegalo-Mauritanian upwelling, as well as in the central tropical Atlantic, in the area where the new pattern

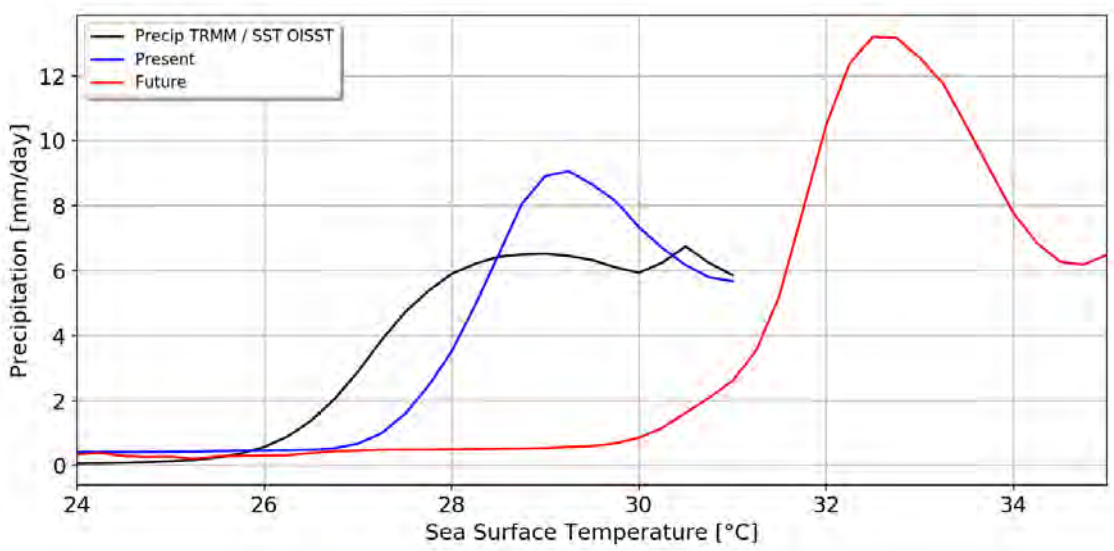

Figure 6.11: Rainfall intensity as a function of SST representative of the SST-convection threshold for TRMM in black, CONTROL run (2001-2015) in blue and CTLf (2086-2100) in red.

response develops in our model. This gives us more confidence in the results obtained here.

Finally, it is interesting to note that the CT and the Senegalo-Mauritanian upwelling show an impact of salinity stratification enhanced in the future during their period of development. Indeed, the CT appears in summer, and this region exhibits a stronger SST decrease in the future than in the present in this season (Figure 6.6a and 6.6b). Similarly, the Senegalo-Mauritanian upwelling shows a stronger decrease in the future in winter, its period of occurence (Figure 6.6c and 6.6d). These two upwelling regions are highly impacted by climate change, more than the rest of the basin: a warming of up to 4°C is observed in both areas, while the mean warming over the whole basin is around 3°C. This suggests that salinity stratification has an important role in mitigating climate change in these two upwelling regions.

6.5 Conclusion

In this Chapter, we studied the changes in the relationship between salinity stratification and SST induced by climate change. To do so, we modified the boundaries of our coupled configuration to model the end of the 21st century climate under the "business as usual" scenario from CMIP6, the SSP5-8.5 scenario. The new boundaries are created using the PGW approach with a MMEM of 25 CMIP6 models. This approach allows to study the impact of a mean climate change, with the internal variability being identical in the future and the present simulations.

According to our model, the tropical Atlantic will undergo substantial changes in the future. The most important one concerns SST: a warming of up to 4°C in the CT, and more than 3.5°C in the ITCZ. The SSS decreases from -0.2 to -0.5 PSU in a large part of the basin, mainly related to a very strong increase in precipitation (up to 6 mm/day). The MLD also shows an important thinning, associated with a strong increase in stratification driven mainly by thermal stratification changes. The increase in thermal stratification is so great that total stratification increases even in areas where salinity stratification decreases, and that OSS_{100m} – the contribution of salinity stratification to total stratification – decreases in areas where the salinity stratification increases.

Despite these strong changes in the tropical Atlantic climate, salinity stratification is expected to have a similar impact on SST in the future and in the present climate in terms of patterns. In winter, the changes remain small in a future climate. In summer, an increase of SST in the NWTA and a decrease in the CT is still observed when salinity stratification is taken into account. However, the amplitude of the SST changes varies. In the NWTA, a more moderate SST sensitivity is seen in summer. It is caused by a change in the ML heat budget balance: the inclusion of salinity stratification leads to a stronger increase of the vertical diffusion trend in the future, but an even stronger decrease of the trend in atmospheric fluxes. In winter, the SST response is slightly more important in the future, likely linked with a stronger salinity stratification in this season. In general, changes in vertical mixing sensitivity seem closely related to changes in stratification. In the CT, the response is stronger in the future: the SST and subsurface temperature decrease is almost twice stronger, as is the strengthening of EUC. It is due to a stronger change in subsurface temperature, linked with the strong strengthening of thermal stratification and with a more important sensitivity of the thermocline depth to salinity stratification in the future.

One of the limitation of this study is that runoff is prescribed in our coupled model, and we kept it identical between the future and the present run. We saw in Chapter 4 that the absence of runoff can modify some ocean variables, and especially the heat balance in the ML. The strong precipitation increase observed in our model, especially in the Amazon and Orinoco basin (about +50%), could impact the runoff, assuming that the increase in evaporation linked with the strong surface temperature increase does not counteract it. An increase in runoff could modify a little the results obtained here, by increasing the salinity stratification in the Amazon and Orinoco plume for instance, which in turn may further enhance the warming response of the NWTA. Yet, the changes in precipitation are highly uncertain in the future in the Amazon basin (Vera et al., 2006; Boisier et al., 2015; Guimberteau et al., 2017; Brêda et al., 2020), and keeping the runoff identical to present climate is also a valid hypothesis.

Conclusion and perspectives

Conclusion

The tropical Atlantic Ocean exhibits a unique salinity structure, largely due to the presence of the ITCZ and the Amazon and Orinoco rivers. This salinity structure is characterized in particular by a strong salinity stratification in the northwestern part of the basin, whose impact on the tropical Atlantic climate is poorly understood and remains controversial. This work aimed at a better understanding of this salinity stratification. It improved the knowledge of the key processes underlying its impact on the mean state of the region, including SST.

To this end, a coupled ocean-atmosphere general circulation model of the tropical Atlantic Ocean has been developed. It is based on NEMO and WRF models, which exchange information through the OASIS coupler, and has a resolution of $1/4°$ for both ocean and atmosphere. The use of a coupled model is essential for our study, because the ocean-atmosphere interactions are at the heart of the processes studied. A series of sensitivity experiments was then conducted, from the most idealized to the most realistic. First, salinity stratification was removed from the ocean model, to understand its impact on the SST and the atmosphere. Then, South American rivers, and notably the Amazon and Orinoco, were removed from the model. These rivers are indeed a major contributor to salinity stratification in the tropical Atlantic. Interannual variability of river runoff was then studied to assess the impact of Amazon extreme floods. Finally, the experiment without salinity stratification has been conducted in a future climate, where several of the key variables identified in the present climate are very distinct from their present state. This allows to better discriminate the effect of each of these variables.

From this hierarchy of sensitivity experiments, a consistent mechanism emerges. It is identified in summer in the northwestern tropical Atlantic, the season and region of strongest salinity stratification. Salinity stratification first impacts vertical diffusion. Indeed, the inclusion of salinity stratification (or part of it) in the model results in a less efficient cooling of the mixed layer by vertical mixing. The resulting warming is substantial, but is then mitigated by a negative feedback from the atmosphere and the entrainment. The balance between these three processes is subtle, and the outcome – an increase or a decrease in SST – depends on the sensitivity test considered (Figure 7.1). Overall, the response of the three processes decreases as the tests become more realistic, that is from including salinity control on vertical mixing to including the interannual variability of the Amazon runoff. This is due to the fact that a smaller fraction of the stratification is added when assessing the impact of Amazon interannual variability than when assessing the impact of the whole salinity stratification. But this does not reflect on the SST: for instance, the response of vertical diffusion, atmospheric fluxes and entrainment to salinity stratification is stronger in the future (CTLf-NOSf) than in the present (CONTROL-NOS), and yet the change in total tendency (i.e. in SST) is weaker in the future due to a better compensation between the three processes. The SST changes are

therefore hard to anticipate, and cannot be predicted without a coupled ocean-atmosphere model taking into account all the air-sea interactions. Moreover, the sensitivity test to Amazon extreme floods shows weak changes that fade quickly in time and space, suggesting that the variability of Amazon discharge has little impact on the tropical Atlantic SST and climate.

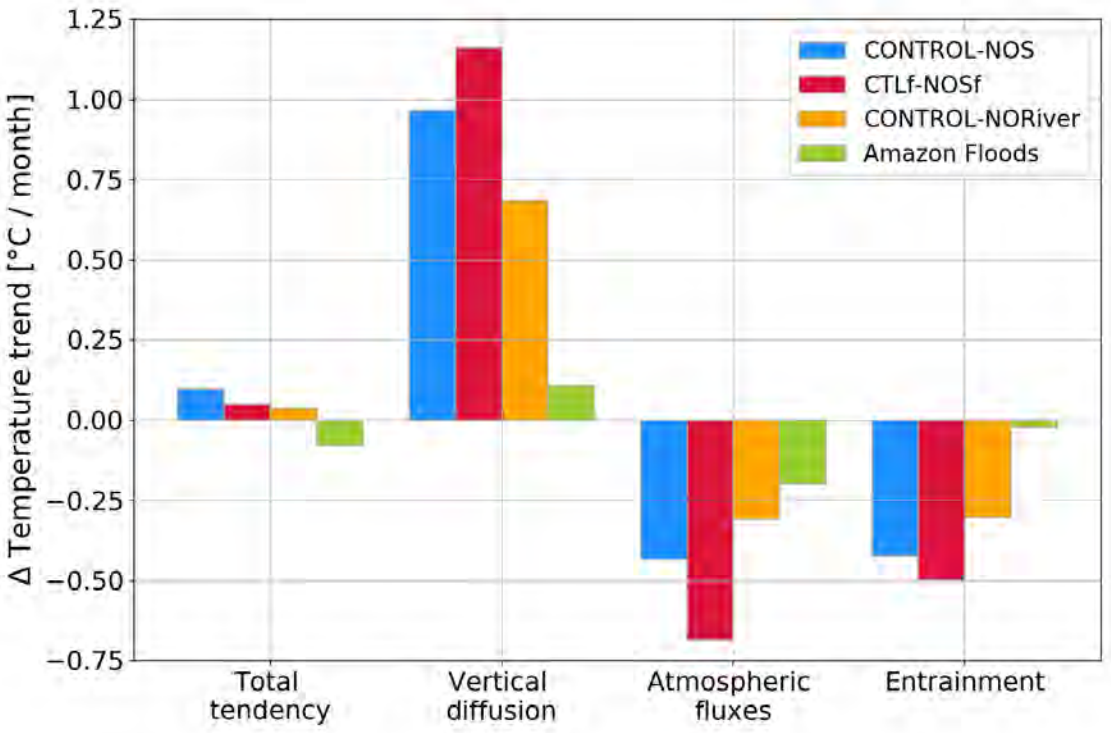

Figure 7.1: Sensitivity to salinity stratification of the different contributions to the mixed layer heat budget, averaged between April and June and over the NWTA, for all the different sensitivity tests. CONTROL-NOS represents the impact of adding salinity stratification in the present climate, CTLf-NOSf is the same, but for a future climate. CONTROL-NORiver represents the impact of the inclusion of the rivers in the present climate. Finally, the "Amazon Floods" test shows the impact of the Amazon extreme floods in the present climate (see Section 5.2.2 for methodological details). Note that the total tendency is representative of the SST anomaly.

As mentioned earlier, the results point to a mitigation by the atmosphere of the surface warming induced by salinity stratification. The processes at play have been investigated in detail. It consists of two negative feedback loops that reduce the net heat flux received by the ocean. First, the SST increase leads to an increase in heat loss by latent heat flux, which reduces the SST anomaly. This is the main feedback loop, accounting for around 70% of the net heat flux change in the northwestern tropical Atlantic. Second, the SST increase enhances the atmospheric deep convection, and thus the cloud cover, which then masks the solar radiation. This results in a decrease in the shortwave radiation reaching the ocean surface, and the further damping of the SST anomaly. This second process accounts

for around 30% of the net heat flux change. It is worth noting that the deep convection enhancement also causes a significant increase in precipitation (around 15%), which could have a positive feedback effect by further increasing salinity stratification. Finally, the SST increase leads to more longwave radiation emitted by the ocean, but the increase in cloud cover results in more longwave radiation emitted by the clouds and absorbed by the ocean. The resultant is close to zero.

Significant SST changes are also observed in the equatorial region in summer. The inclusion of salinity stratification in the model causes a decrease in SST in the cold tongue area in the present, a response exacerbated in the future. However, the sensitivity test to river discharges shows on the contrary a slight increase in SST in this area. The mechanism behind these SST changes is nevertheless the same, and is related to a modulation of the thermocline depth. In the two sensitivity tests to salinity stratification (present and future), the thermocline shoals substantially year-round, leading to an intense subsurface cooling throughout the year, and a surface cooling in summer – the period of the CT development. On the contrary, the thermocline deepens slightly in the sensitivity test to rivers, leading to a moderate subsurface warming year-round and a slight surface warming in summer. The reason for these opposite responses remains unclear.

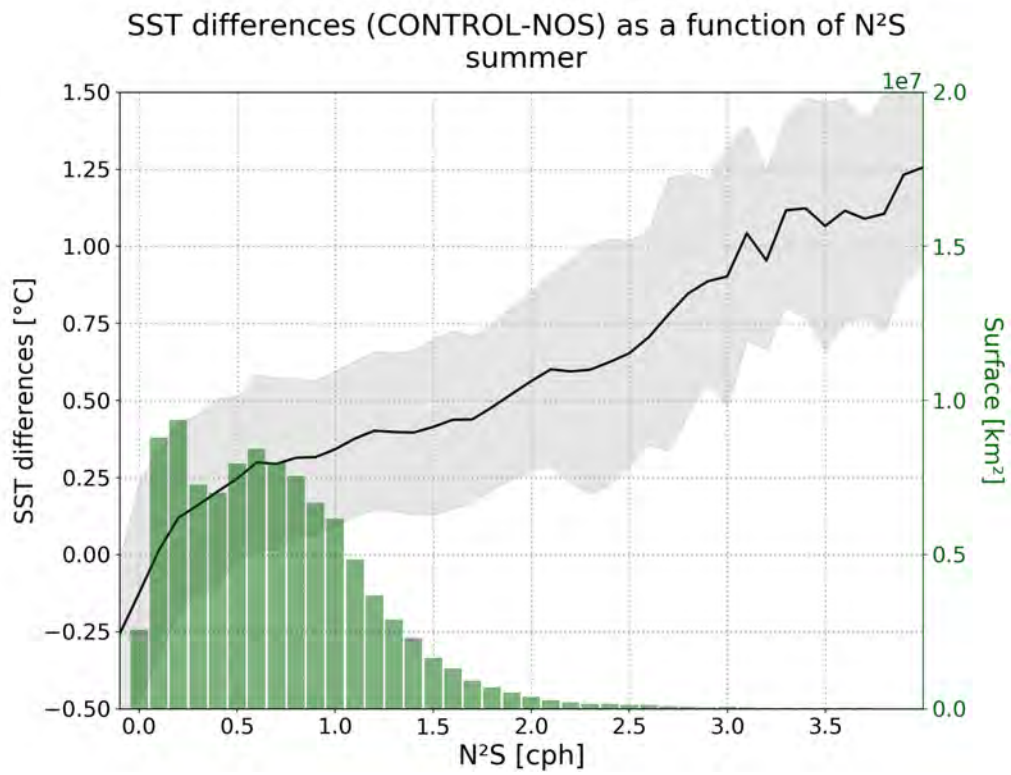

Figure 7.2: Summer SST differences as a function of N^2S for CONTROL run, envelope: $\pm\sigma$; coastal areas (i.e. areas where the bathymetry is under 50 m) where removed, as well as values corresponding to less than 20 grid cells. Bins surfaces are represented on a histogram. The analyze is applied on the NWTA box.

One of the limitations of this work, common to all modeling studies, is that the magnitude of the SST responses obtained might depend on the numerical choices and on the model configuration used. We expect the mechanism of compensation between vertical diffusion, atmospheric fluxes and entrainment to be robust, given that it is identical in all sensitivity tests independently of the strength of the salinity stratification, and independently of the mean state of the ocean-atmosphere system (present or future). However, the balance between all the processes, which ultimately determines the magnitude and the sign of the SST response, is expected to depend to some extent on the choice of parameterizations. Nevertheless, we showed here the importance of cloud feedback on SST, and the set of parameterizations chosen is the only one that includes a feedback of the parameterized clouds in the radiation schemes while comparing satisfactorily with observations.

Another limitation is the difficulty in selecting the appropriate indicator to assess the sensitivity of SST to salinity stratification. For a long time, the barrier layer depth has been used, but it has been shown in this work that it is not relevant (Figure 3.3b). The variable OSS_{100m} – the contribution of salinity stratification to total stratification – has then been chosen instead, and seemed to serve its purpose well (Figure 3.3a). Nevertheless, the climate change study has shown that it is not really the case when the upper ocean is significantly warmer than today: variation of OSS_{100m} in the future poorly explains the changes in SST sensitivity to salinity stratification. N^2S finally seems to be the right indicator: it explains well the changes in the future (Figure 6.7c) and in the present as well (Figure 7.2).

Perspectives

Impact of salinity stratification on the tropical cyclones

In this thesis, we studied the impact of salinity stratification in the western tropical Atlantic on the mean state of the basin. But historically, salinity stratification has also been studied for its potential impact on TCs, which are numerous in this region. This issue is still under debate, with some studies showing that cyclones intensify more in the area of strong Amazon-induced salinity stratification, while other studies suggest that the intensification in this area may be sustained by a large heat content, independently of the presence of the Amazon plume (Section 1.3.3). Most of these studies rely on observations or forced ocean models to draw conclusions, whereas we have shown that air-sea interactions are critical to understand the processes involved. Therefore, the coupled ocean-atmosphere configuration developed here could provide new insights into the subject.

A first step would be to evaluate the ability of our model to correctly reproduce TCs. Indeed, our coupled configuration has a resolution of 1/4°, which is theoretically sufficient to simulate the number and trajectory of TCs, but does not allow to reproduce accurately the intensity of the most powerful cyclones (e.g. Lengaigne et al., 2018; Roberts et al., 2020; Vannière et al., 2020). An example of cyclones generated by our model is shown in Figure 7.3. The sensitivity tests to salinity stratification, river freshwater supply and Amazon extreme

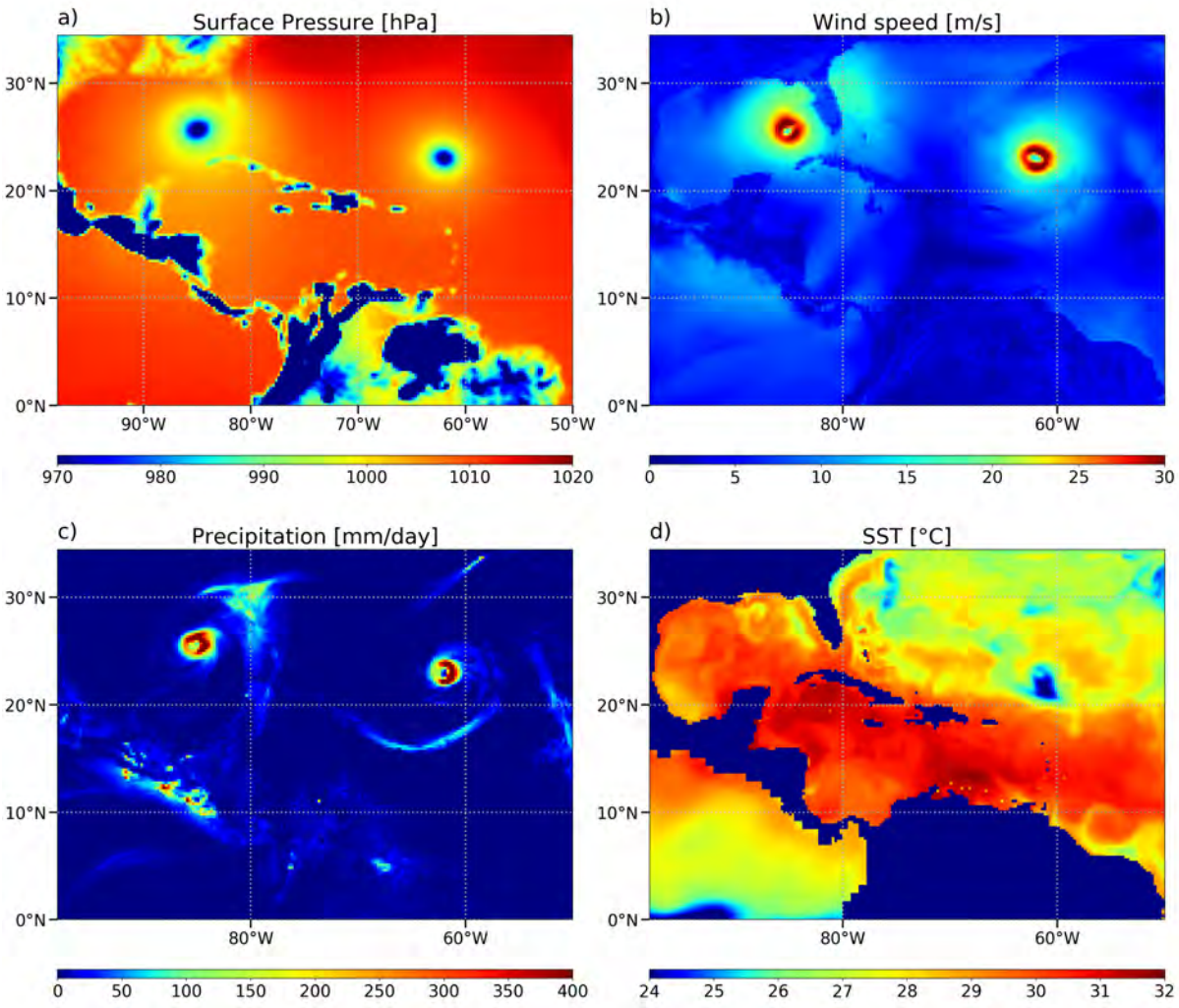

Figure 7.3: Daily snapshot of a) surface pressure, b) wind speed, c) precipitation and d) SST showing two TCs in the tropical Atlantic Ocean.

floods performed for this thesis could then be analyzed to assess their impact on the trajectory, number and intensity of TCs. Finally, increasing the resolution of the configuration (from 1/4° to 1/12° for instance) could be interesting in order to simulate more realistically the most intense TCs.

In addition, it would be interesting to study the impact of climate change on the different metrics of TCs. The simulation of climate change conducted in this thesis does not take into account future interannual variability, but has the advantage of a fairly high horizontal and vertical resolution in the ocean and the atmosphere, as well as better SST, which may be lacking in the global CMIP models. Moreover, despite the progress made in the last IPCC report (Seneviratne et al., 2021), the question of the impact of climate change on cyclones remains open, particularly in the tropical Atlantic (e.g. Roberts et al., 2020).

Impact of salinity stratification on biogeochemistry

Stratification has been shown to influence biological productivity: enhanced stratification reduces the nutrient supply brought at the surface by vertical mixing, especially in areas already strongly stratified such as the tropics (Behrenfeld et al., 2006; Boyce et al., 2010). Climate change induces a strengthening of the stratification, and a decreasing trend in primary production and phytoplankton in the tropics has already been observed in the last decades (e.g. Behrenfeld et al., 2006; Polovina et al., 2008; Boyce et al., 2010) and is consistently predicted by the CMIP models for the end of the century (e.g. Bopp et al., 2013; Kwiatkowski et al., 2020).

In the tropical Atlantic, several regions are of particular interest in this regard. The Amazon plume is a region of high biological productivity due to riverine input of nutrients (e.g. Smith and Demaster, 1996). Moreover, three upwelling systems are located in the tropical Atlantic: the Benguela upwelling, the Senegalo-Mauritanian upwelling and the equatorial upwelling in the CT region. Upwellings are areas where a particular wind structure induces a rise of cold and nutrient-rich subsurface waters, driving a high biological productivity. The impact of vertical mixing on productivity has been shown in at least two of these regions: the CT (Jouanno et al., 2011; Radenac et al., 2020) and the Amazon plume (Gouveia et al., 2019b). Therefore, it could be interesting to investigate the impact of salinity stratification on these high productivity areas by coupling a biogeochemical model (for instance PISCES) to our configuration.

Impact of salinity stratification on the ocean dynamics

Few studies have investigated the impact of the Amazon and its associated salinity stratification on the ocean currents and dynamics (Masson and Delecluse, 2001; Coles et al., 2013). However, they have revealed that it is significant. Indeed, when Amazon is included in their model, a weakening of the NBC retroflection is observed by Masson and Delecluse (2001), while Coles et al. (2013) find a broadening of the NBC. Coles et al. (2013) also mention an increase of the vertical velocity shear, due to the trapping of the wind momentum in the shallower mixed layer (see also Vialard and Delecluse, 1998) and to the horizontal salinity gradient (Cronin and McPhaden, 2002).

Comparison of the Eddy Kinetic Energy (EKE) between the CONTROL and NOS experiments reveals an enhancement of the EKE when salinity stratification is included (Figure 7.4). A strong response is observed in the Amazon and Niger plumes, as well as a significant increase in the central tropical Atlantic, suggesting an impact of salinity stratification on tropical instability waves (see also Olivier et al., 2020). The processes involved in these sensitivities would deserve to be examined and would complement our understanding of the importance of salinity stratification on ocean dynamics. Furthermore, unlike the studies of Masson and Delecluse (2001) and Coles et al. (2013) mentioned above, our coupled configuration would allow to investigate how the "current feedback" (Renault et al., 2016; Jullien et al., 2020) and the mesoscale "thermal feedback" are altered by salinity stratification.

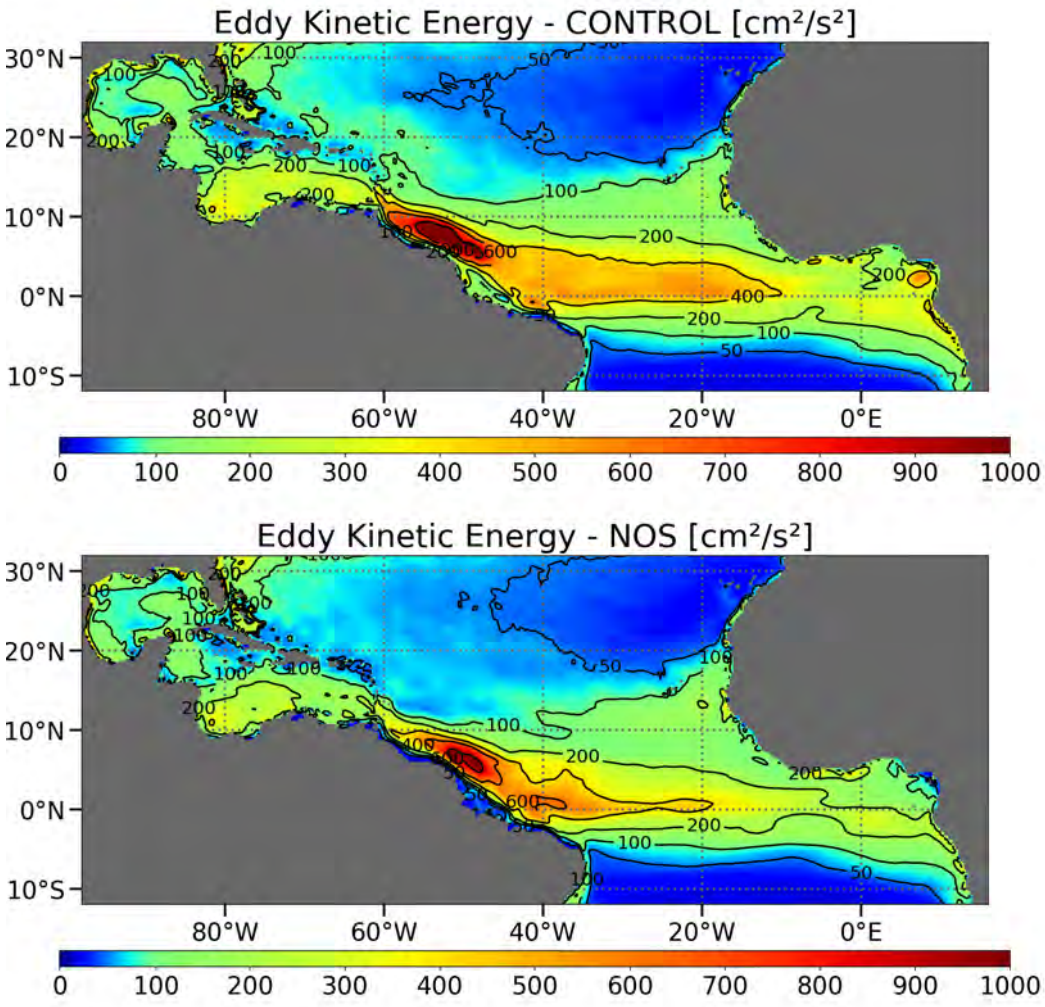

Figure 7.4: Impact of salinity stratification on the EKE $[cm^2/s^2]$.

Other perspectives

Several other perspectives that arise from this work could be investigated.

- **Feedback of continental freshwater on salinity stratification:** A statistically significant decrease in precipitation is observed in a large part of the Amazon basin when salinity stratification is included in the model (Figure 3.7f). A similar signal, albeit weaker, is also observed when the rivers are included to the model (not shown). This leads to a negative feedback on salinity stratification: including salinity stratification causes a decrease in precipitation over the Amazon basin, a decrease in runoff (evaporation change is weak, not shown) and therefore a decrease in salinity stratification. On the other hand, an increase in precipitation in the NWTA is observed, leading this time to a positive feedback on salinity stratification. Since runoff is prescribed, our

model includes only the positive feedback. It could therefore be of interest to couple a hydrological model to our configuration, in order to assess the impact of precipitation change over the Amazon basin on salinity stratification and on tropical Atlantic climate.

- **Ocean color:** The Amazon brings very turbid waters to the ocean due to high load of sediments and colored dissolved organic matter (Vecchio, 2004; Hu et al., 2004). It is also a source of nutrients, leading to high biological productivity in the plume (Smith and Demaster, 1996). All these processes color the plume and alter the light absorption, impacting the ocean temperature in the NWTA (Newinger and Toumi, 2015; Hernandez et al., 2017), with a temperature increase at the surface and a decrease in subsurface. These results have been obtained with forced ocean models, and this topic has not yet been studied with a coupled ocean-atmosphere model in the tropical Atlantic. Our current configuration is forced with a monthly climatology of chlorophyll concentrations in order to include ocean color. It might therefore be interesting to perform a sensitivity test where the the influence of chlorophyll and suspended matter on solar flux penetration is removed (clear waters), as we have shown in this work that among the air-sea interactions, the shortwave radiation is an important process to consider.

- **Congo river plume:** The Congo is the second largest river in the world in terms of discharge, and therefore strong salinity stratification is also present in the Congo plume. As for the Amazon, its impact on the SST is controversial (Materia et al., 2012; Hopkins et al., 2013; White and Toumi, 2014), and it has been studied with observations or forced ocean models only. It could be worth verifying whether the mechanism identified for the Amazon plume is also valid in another river plume. Moreover, the Congo plume is particularly interesting to study because despite the large freshwater input, no barrier layer is observed in the region (Figure 3.2c and 3.2d). This work hints that barrier layer have a weak impact on SST, contrary to salinity stratification. Finding the same mechanism in areas with and without barrier layers would therefore support this hypothesis.

Conclusion et perspectives

Conclusion

L'océan Atlantique tropical présente une structure en salinité unique, due en grande partie à la présence de la ZCIT et des fleuves Amazone et Orénoque. Cette structure en salinité est notamment caractérisée par une forte stratification en sel dans la partie nord-ouest du bassin, dont l'impact sur le climat de l'Atlantique tropical est mal compris et reste controversé. Ce travail visait à mieux comprendre cette stratification en sel. Il a permis d'améliorer la connaissance des processus clés qui sous-tendent son impact sur l'état moyen de la région, et notamment la TSM.

Pour ce faire, un modèle couplé océan-atmosphère de l'océan Atlantique tropical a été développé. Il est basé sur les modèles NEMO et WRF, qui échangent des informations via le coupleur OASIS, et a une résolution de 1/4° pour l'océan et l'atmosphère. L'utilisation d'un modèle couplé est essentielle pour notre étude, car les interactions océan-atmosphère sont au cœur des processus étudiés. Une série d'expériences de sensibilité a ensuite été menée, de la plus idéalisée à la plus réaliste. Tout d'abord, la stratification en sel a été enlevée du modèle océanique, afin de comprendre son impact sur les TSM et l'atmosphère. Ensuite, les fleuves sud-américains, et notamment l'Amazone et l'Orénoque, ont été retirés du modèle. Ces fleuves sont en effet un contributeur majeur à la stratification en sel dans l'Atlantique tropical. La variabilité interannuelle du débit des fleuves a ensuite été étudiée pour évaluer l'impact des crues extrêmes de l'Amazone. Enfin, l'expérience sans stratification en sel a été menée dans un climat futur, où plusieurs des variables clés identifiées dans le climat actuel sont très distinctes de leur état actuel. Cela permet de mieux discriminer l'effet de chacune de ces variables.

De cette hiérarchie d'expériences de sensibilité, un mécanisme émerge. Il est identifié en été dans l'Atlantique tropical nord-ouest, saison et région où la stratification en sel est la plus forte. La stratification en sel a d'abord un impact sur la diffusion verticale. En effet, l'inclusion de la stratification en sel (ou d'une partie de celle-ci) dans le modèle entraîne un refroidissement moins efficace de la couche mélangée par le mélange vertical. Le réchauffement qui en résulte est important, mais il est ensuite atténué par une rétroaction négative de l'atmosphère et de l'entraînement. L'équilibre entre ces trois processus est subtil, et le résultat – une augmentation ou une diminution de la TSM – dépend du test de sensibilité considéré (Figure 7.1). Dans l'ensemble, la réponse des trois processus diminue à mesure que les tests deviennent plus réalistes. Cela est dû au fait qu'une plus petite fraction de la stratification est ajoutée lorsque l'on étudie les crues extrêmes de l'Amazone que lorsque l'on étudie la stratification en sel totale. Mais cela ne se répercute pas sur la TSM : par exemple, la réponse de la diffusion verticale, des flux atmosphériques et de l'entraînement à la stratification en sel est plus forte dans le futur (CTLf-NOSf) que dans le présent (CONTROL-NOS), et pourtant le changement de la tendance totale (c'est-à-dire de la TSM) est plus faible dans le futur en raison

d'une meilleure compensation entre les trois processus. Les changements de SST sont donc difficiles à anticiper, et impossibles à prévoir sans un modèle couplé océan-atmosphère prenant en compte toutes les interactions air-mer. De plus, le test de sensibilité aux inondations extrêmes de l'Amazone montre de faibles changements qui s'estompent rapidement dans le temps et l'espace, ce qui suggère que l'Amazone a peu d'impact sur la TSM et le climat de l'Atlantique tropical.

Comme mentionné précédemment, on constate une atténuation par l'atmosphère du réchauffement de la surface induit par la stratification en sel. Les processus en jeu ont été étudiés en détail. Ils consistent en deux boucles de rétroaction négative qui réduisent le flux de chaleur net reçu par l'océan. Premièrement, l'augmentation de la TSM entraîne une augmentation de la perte de chaleur par flux de chaleur latente, ce qui réduit l'anomalie de TSM. Il s'agit de la principale boucle de rétroaction, qui représente environ 70 % de la variation du flux thermique net dans l'Atlantique tropical nord-ouest. Deuxièmement, l'augmentation de la TSM renforce la convection atmosphérique profonde, et donc la couverture nuageuse, qui masque alors le rayonnement solaire. Il en résulte une diminution du rayonnement solaire atteignant la surface de l'océan, et une atténuation supplémentaire de l'anomalie de TSM. Ce deuxième processus représente environ 30 % de la variation du flux thermique net. Il convient de noter que le renforcement de la convection profonde entraîne également une augmentation significative des précipitations (environ 15 %), qui pourrait avoir un effet de rétroaction positif en augmentant davantage la stratification en sel. Enfin, l'augmentation de la TSM entraîne une augmentation du rayonnement infrarouge émis par l'océan, mais l'augmentation de la couverture nuageuse entraîne une augmentation du rayonnement infrarouge émis par les nuages et absorbé par l'océan. La résultante est proche de zéro.

Des changements significatifs de la TSM sont également observés dans la région équatoriale en été. L'inclusion de la stratification en sel dans le modèle entraîne une diminution de la TSM dans la zone de la langue d'eau froide dans le climat présent, une réponse exacerbée dans le futur. Cependant, le test de sensibilité aux débits des fleuves montre au contraire une légère augmentation de la TSM dans cette zone. Le mécanisme à l'origine de ces changements de TSM est néanmoins le même, et est lié à une modulation de la profondeur de la thermocline. Dans les deux tests de sensibilité à la stratification en sel (présent et futur), la thermocline remonte de manière significative tout au long de l'année, entraînant un refroidissement intense de la subsurface tout au long de l'année et un refroidissement de la surface en été – la période de développement de la langue d'eau froide. Au contraire, la thermocline s'approfondit légèrement dans le test de sensibilité aux fleuves, conduisant à un réchauffement modéré de la subsurface tout au long de l'année et à un léger réchauffement de la surface en été. La raison de ces réponses opposées reste incertaine.

Une des limites de ce travail, commune à toutes les études de modélisation, est que l'ampleur des changements de TSM observés pourrait dépendre des choix numériques et de la configuration du modèle utilisée. Nous nous attendons à ce que le mécanisme de compensation entre la diffusion verticale, les flux atmosphériques et l'entraînement soit robuste, étant donné qu'il est identique dans tous les tests de sensibilité indépendamment de la force de la stratification en sel, et indépendamment de l'état moyen du système océan-atmosphère

(présent ou futur). En revanche, l'équilibre entre tous les processus, qui détermine finalement l'ampleur et le signe du changement de TSM, est susceptible de dépendre dans une certaine mesure du choix des paramétrisations. Néanmoins, nous avons montré ici l'importance de la rétroaction des nuages sur la TSM, et l'ensemble de paramétrisations choisi est le seul qui inclut une rétroaction des nuages paramétrés dans les schémas de rayonnement tout en se comparant de manière satisfaisante aux observations.

Une autre limite est la difficulté quant au choix de l'indicateur correct pour évaluer la sensibilité de la TSM à la stratification en sel. Pendant longtemps, la profondeur de la couche barrière a été utilisée, mais il a été démontré dans ce travail qu'elle n'est pas adéquate (Figure 3.3b). La variable OSS_{100m} – la contribution de la stratification en sel à la stratification totale – a alors été choisie à la place, et a semblé bien remplir son rôle (Figure 3.3a). Néanmoins, l'étude dans un climat futur a montré que ce n'est pas vraiment le cas lorsque l'océan est nettement plus chaud qu'aujourd'hui : la variation d'OSS_{100m} dans le futur explique mal les changements de sensibilité de la TSM à la stratification en sel. La variable N^2S semble finalement être le bon indicateur : elle explique bien les changements dans le futur (Figure 6.7c) et dans le présent également (Figure 7.2).

Perspectives

Impact de la stratification en sel sur les cyclones tropicaux

Dans cette thèse, nous avons étudié l'impact de la stratification en sel de l'ouest de l'Atlantique tropical sur l'état moyen du bassin. Mais historiquement, la stratification en sel a été étudiée pour son impact potentiel sur les cyclones tropicaux, nombreux dans cette région. Cette question est toujours en débat, certaines études montrant que les cyclones s'intensifient plus dans la zone de forte stratification en sel induite par l'Amazone, et d'autres études suggérant que l'intensification dans cette zone semble être favorisée par un important contenu thermique, indépendamment de la présence du panache de l'Amazone (Section 1.3.3). La plupart de ces études s'appuient sur des observations ou des modèles océaniques forcés pour tirer des conclusions, alors que les interactions air-mer sont essentielles à la compréhension des processus en jeu. De ce fait, la configuration couplée océan-atmosphère développée ici pourrait apporter de nouveaux éléments sur le sujet.

Une première étape serait d'évaluer la capacité de notre modèle à reproduire correctement les cyclones tropicaux. En effet, notre configuration couplée a une résolution de 1/4°, ce qui est théoriquement suffisant pour simuler le nombre et la trajectoire des cyclones tropicaux, mais ne permet pas de reproduire l'intensité des cyclones les plus puissants (e.g. Lengaigne et al., 2018; Roberts et al., 2020; Vannière et al., 2020). Un exemple de cyclones générés par notre modèle est représenté sur la Figure 7.3. Les tests de sensibilité à la stratification en sel, à l'apport d'eau douce des fleuves et aux crues de l'Amazone effectués pour cette thèse pourraient ensuite être analysés pour évaluer leur impact sur la trajectoire, le nombre et l'intensité des cyclones. Enfin, l'augmentation de la résolution de la configuration pourrait

être envisagée afin de simuler de manière plus réaliste les cyclones les plus intenses.

Parallèlement, il serait intéressant d'étudier l'impact du changement climatique moyen sur les différentes métriques des cyclones tropicaux. La simulation de changement climatique réalisée dans cette thèse ne prend pas en compte la variabilité interannuelle future, mais présente l'avantage d'avoir une assez haute résolution verticale et horizontale ainsi qu'une meilleure TSM, ce qui peut faire défaut aux modèles globaux CMIP. De plus, malgré les progrès réalisés dans le dernier rapport du GIEC (Seneviratne et al., 2021), la question de l'impact du changement climatique sur les cyclones reste ouverte, notamment dans l'Atlantique tropical (e.g. Roberts et al., 2020).

Impact de la stratification en sel sur la biogéochimie

Il a été démontré que la stratification influe sur la productivité biologique : une stratification renforcée réduit l'apport de nutriments à la surface par le mélange vertical, en particulier dans les zones déjà fortement stratifiées comme les tropiques (Behrenfeld et al., 2006; Boyce et al., 2010). Le changement climatique induit un renforcement de la stratification, et une tendance à la baisse de la production primaire et du phytoplancton dans les tropiques a déjà été observée au cours des dernières décennies (e.g. Behrenfeld et al., 2006; Polovina et al., 2008; Boyce et al., 2010) et est systématiquement prédite par les modèles CMIP pour la fin du siècle (e.g. Bopp et al., 2013; Kwiatkowski et al., 2020).

Dans l'Atlantique tropical, plusieurs régions présentent un intérêt particulier à cet égard. Le panache de l'Amazone est une région de forte productivité biologique due à l'apport fluvial de nutriments (e.g. Smith and Demaster, 1996). Par ailleurs, trois systèmes d'upwelling sont situés dans l'Atlantique tropical : l'upwelling du Benguela, l'upwelling sénégalo-mauritanien et l'upwelling équatorial dans la région de la langue d'eau froide. Les upwellings sont des zones où une structure de vent particulière induit une montée des eaux de subsurface froides et riches en nutriments, entraînant une forte productivité biologique. L'impact du mélange vertical sur la productivité a été démontré dans au moins deux de ces régions : la langue d'eau froide (Jouanno et al., 2011; Radenac et al., 2020) et le panache de l'Amazone (Gouveia et al., 2019b). Par conséquent, il pourrait être intéressant d'étudier l'impact de la stratification en sel sur ces zones de haute productivité en couplant un modèle biogéochimique (par exemple PISCES) à notre configuration.

Impact de la stratification en sel sur la dynamique océanique

Peu d'études se sont penchées sur l'impact de l'Amazone et de la stratification en sel qui lui est associée sur les courants et la dynamique de l'océan (Masson and Delecluse, 2001; Coles et al., 2013). Cependant, elles ont révélé qu'il est significatif. En effet, lorsque l'Amazone est incluse dans leur modèle, un affaiblissement de la rétroflexion du NBC est observé par Masson and Delecluse (2001), alors que Coles et al. (2013) trouvent un élargissement du NBC. Coles et al. (2013) mentionnent également une augmentation du cisaillement vertical de vitesse, due

au piégeage de la quantité de mouvement du vent dans la couche mélangée moins profonde (voir aussi Vialard and Delecluse, 1998) et au gradient horizontal de salinité (Cronin and McPhaden, 2002).

La comparaison de l'énergie cinétique turbulente (Eddy Kinetic Energy, EKE) entre les expériences CONTROL et NOS révèle une augmentation de l'EKE lorsque la stratification en sel est incluse (Figure 7.4). Une forte réponse est observée dans les panaches de l'Amazone et du Niger, ainsi qu'une augmentation significative dans le centre de l'Atlantique tropical, ce qui suggère un impact de la stratification en sel sur les ondes d'instabilité tropicales (voir aussi Olivier et al., 2020). Les processus impliqués mériteraient d'être étudiés et viendraient compléter notre compréhension de l'importance de la stratification en sel sur la dynamique océanique. En outre et contrairement aux études de Masson and Delecluse (2001) et Coles et al. (2013) mentionnées ci-dessus, notre configuration couplée permettrait d'étudier comment la "rétroaction du courant" (Renault et al., 2016; Jullien et al., 2020) et la "rétroaction thermique" à méso-échelle sont modifiées par la stratification en sel.

Autres perspectives

Plusieurs autres perspectives découlant de ce travail pourraient être explorées.

- **Rétroaction de l'apport d'eau douce sur la stratification en sel :** Une diminution statistiquement significative des précipitations est observée dans une grande partie du bassin de l'Amazone lorsque la stratification en sel est incluse dans le modèle (Figure 3.7f). Un signal similaire, bien que plus faible, est également observé lorsque les fleuves sont inclus dans le modèle (non illustré). Cela conduit à une rétroaction négative sur la stratification en sel : l'inclusion de la stratification en sel entraîne une diminution des précipitations sur le bassin de l'Amazone, une diminution du débit (les changements d'évaporation sont faibles, non illustré) et donc une diminution de la stratification en sel. D'autre part, une augmentation des précipitations est observée dans l'ouest de l'Atlantique tropical, conduisant cette fois à une rétroaction positive sur la stratification en sel. Comme le débit est prescrit, notre modèle n'inclut que la rétroaction positive. Il pourrait donc être intéressant de coupler un modèle hydrologique à notre configuration, afin d'évaluer l'impact du changement des précipitations dans le bassin amazonien sur la stratification en sel et sur le climat de l'Atlantique tropical.
- **Couleur de l'eau :** L'Amazone déverse dans l'océan des eaux très turbides, en raison d'une forte charge en sédiments et en matière organique dissoute colorée (Vecchio, 2004; Hu et al., 2004). L'eau douce apportée est également riche en nutriments, ce qui entraîne une forte productivité biologique dans le panache (Smith and Demaster, 1996). Tous ces processus colorent le panache et modifient l'absorption du rayonnement solaire, ce qui a un impact sur la température de l'océan dans l'ouest de l'océan Atlantique tropical (Newinger and Toumi, 2015; Hernandez et al., 2017), avec une augmentation de la température en surface et une diminution en subsurface. Ces résultats ont été obtenus avec des modèles océaniques forcés, et ce sujet n'a pas encore été étudié dans

l'Atlantique tropical avec un modèle couplé océan-atmosphère. Notre configuration actuelle est forcée avec une climatologie mensuelle des concentrations en chlorophylle afin d'inclure la couleur de l'océan. Il pourrait donc être intéressant de réaliser un test de sensibilité où l'influence de la chlorophylle et des matières en suspension sur la pénétration du flux solaire est supprimée (eaux claires), car nous avons montré dans ce travail que parmi les interactions air-mer, le rayonnement solaire est un processus important à considérer.

- **Panache du Congo :** Le Congo est le deuxième plus grand fleuve du monde en termes de débit, et son panache présente donc lui aussi une forte stratification en sel. Comme pour l'Amazone, son impact sur la SST est controversé (Materia et al., 2012; Hopkins et al., 2013; White and Toumi, 2014), et il n'a été étudié qu'avec des observations ou des modèles océaniques forcés. Il pourrait être intéressant de vérifier si le mécanisme identifié pour le panache de l'Amazone est également valable dans un autre panache fluvial. De plus, le panache du Congo est particulièrement intéressant à étudier car malgré l'important apport d'eau douce, aucune couche barrière n'est observée dans la région (Figure 3.2c et 3.2d). Cette thèse suggère que la couche barrière a un faible impact sur la TSM, contrairement à la stratification en sel. Le fait de trouver le même mécanisme dans des zones avec et sans couches barrières confirmerait donc cette hypothèse.

Appendix A

Publication in Climate Dynamics

Climate Dynamics
https://doi.org/10.1007/s00382-021-05713-z

Influence of ocean salinity stratification on the tropical Atlantic Ocean surface

Manon Gévaudan[1] · Julien Jouanno[1] · Fabien Durand[1] · Guillaume Morvan[1] · Lionel Renault[1] · Guillaume Samson[2]

Received: 23 July 2020 / Accepted: 2 March 2021

Abstract
The tropical Atlantic Ocean receives an important freshwater supply from river runoff and from precipitation in the inter-tropical convergence zone. It results in a strong salinity stratification that may influence vertical mixing, and thus sea surface temperature (SST) and air–sea fluxes. The aim of this study is to assess the impact of salinity stratification on the tropical Atlantic surface variables. This is achieved through comparison among regional 1/4° coupled ocean–atmosphere simulations for which the contribution of salinity stratification in the vertical mixing scheme is included or discarded. The analysis reveals that the strong salinity stratification in the northwestern tropical Atlantic induces a significant increase of SST (0.2 °C–0.5 °C) and rainfall (+ 19%) in summer, hereby intensifying the ocean–atmosphere water cycle, despite a negative atmospheric feedback. Indeed, the atmosphere dampens the oceanic response through an increase in latent heat loss and a reduction of shortwave radiation reaching the ocean surface. In winter, the impacts of salinity stratification are much weaker, most probably because of a deeper mixed layer at this time. In the equatorial region, we found that salinity stratification induces a year-round shoaling of the thermocline, reinforcing the cold tongue cool anomaly in summer. The concept of barrier layer has not been identified as relevant to explain the SST response to salinity stratification in our region of interest.

Keywords Ocean vertical mixing · Air–sea coupling · Regional modeling · Mixed layer heat budget · Atlantic cold tongue · Barrier layer

1 Introduction

Air-sea coupling in the tropical Atlantic drives the regional climate and its modes of variability, which affect continental rainfall over Africa and South America (Caniaux et al. 2011; Giannini et al. 2004; Meynadier et al. 2016; Lübbecke et al. 2018; Crespo et al. 2019), tropical cyclone formation (Vimont and Kossin 2007; Wang et al. 2008), and biological productivity (Christian and Murtugudde 2003; Radenac et al. 2020). The region shows warm surface waters throughout the year, sustaining the development of atmospheric deep convection and associated precipitation at large scale. It is also the recipient of Amazon freshwater supply, the most powerful fluvial system in the world (50% of the total Atlantic river runoff). The surface salinity distribution, which largely results from these freshwater fluxes, can have indirect but important impacts on the upper ocean temperatures and thus on the air–sea heat and freshwater fluxes. Nevertheless, the impact of salinity distribution on the regional climate remains controversial (Balaguru et al. 2012b; Hernandez et al. 2016).

Salinity can affect sea surface temperature (SST) through its contribution to stratification, with changes that are often complex and not straightforward to interpret. With a 1D model of the mixed layer (ML), Miller (1976) showed that strong salinity stratification inhibits the entrainment of cold water by vertical mixing at the base of the ML: since stratification is stronger, the ML thickness is less reactive to wind anomalies for instance, and the ML does not deepen as much. This reduced entrainment leads to positive SST anomalies. But in case of surface heat loss events, in winter or during the night for instance, a thinner ML results in an increased cooling of the ML. In some areas, salinity stratification can be so strong that it allows the ML to be colder than the water below without being unstable. These

✉ Manon Gévaudan
manon.gevaudan@gmail.com

[1] LEGOS, Université de Toulouse, CNES-CNRS-IRD-UPS, 14 Avenue Edouard Belin, 31400 Toulouse, France

[2] Mercator Océan, 10 Rue Hermès, 31520 Ramonville Saint-Agne, France

so-called temperature inversions have been reported in both observations (Anderson et al. 1996; de Boyer Montégut et al. 2007a; Foltz and McPhaden 2009) and models (Miller 1976; Vialard and Delecluse 1998; Mignot et al. 2012; Krishnamohan et al. 2019). They have been shown to participate to the seasonal and interannual variability of the SST in the tropical Indian Ocean (Durand et al. 2004; Masson et al. 2005; Nagura et al. 2015).

These temperature inversions are due to the presence of barrier layers (BL): these are salt-stratified layers embedded within the warm upper layer (Godfrey and Lindstrom 1989; Lukas and Lindstrom 1991). The presence of a BL implies that the mixing at the base of the ML does not cool the ML, since the temperature of the water in the BL is the same as in the ML (or even higher than it, if there is a temperature inversion): the result is an insulation of the warm ML from the cooler subsurface (Sprintall and Tomczak 1992). BL have been observed in the tropical Atlantic, in the western part (Pailler et al. 1999; de Boyer Montégut et al. 2007a; Mignot et al. 2009), and more recently in the northeastern Gulf of Guinea (Dossa et al. 2019). Moreover, studies have been conducted in the western tropical Atlantic to evaluate the impact of BL on the SST and the air–sea fluxes, but their conclusions diverge. Observational studies suggest a strong impact of BL on the SST (Pailler et al. 1999; Foltz and McPhaden 2009), whereas modeling studies show weak impact of BL (Breugem et al. 2008; Balaguru et al. 2012a; Hernandez et al. 2016). This controversy also underlies the issue of cyclones intensification in the western tropical Atlantic, with some studies concluding that BL play a significant role in this intensification (Balaguru et al. 2012b; Grodsky et al. 2012; Reul et al. 2014; Androulidakis et al. 2016), and other studies showing the opposite (Newinger and Toumi 2015; Hernandez et al. 2016). Yan et al. (2017) tend to reconcile both perspectives: they concluded that the impact of BL is complex, and depends on various factors such as ocean stratification and cyclone intensity.

The tropical Atlantic Ocean exhibits a very contrasted surface salinity distribution, with (1) low SSS due to large amounts of freshwater, supplied by four of the world's largest rivers in terms of discharge (Amazon, Congo, Orinoco and Niger), and high precipitation associated with the Intertropical Convergence Zone (ITCZ), and (2) high SSS in the subtropical gyres, linked with strong evaporation and low precipitation in these zones. The surface freshwater distribution presents a marked seasonal variability in response to seasonal variations of the ITCZ (Tchilibou et al. 2015; Foltz et al. 2015), transport by the large-scale currents (Masson and Delecluse 2001; Da-Allada et al. 2013; Foltz et al. 2015; Coles et al. 2013), or variability of the Amazon discharge (Masson and Delecluse 2001). The PIRATA observing system (Foltz et al. 2019) fostered significant advances on the identification and understanding of the modes of upper ocean variability occurring in the tropical Atlantic, and also on the processes that control the ML properties. Nevertheless, local observations alone could not provide a clear picture of the impact of salinity distribution on the regional climate, nor on its seasonal variability.

The aim of this paper is to identify the influence of salinity stratification in the tropical Atlantic on SST, air–sea fluxes and regional climate. To tackle these questions, we performed a set of interannual 1/4° resolution simulations using a regional tropical Atlantic ocean–atmosphere coupled model. This choice allows the identification of regional ocean–atmosphere feedback processes while limiting the computational cost inherent to coupled modeling. Following Vialard and Delecluse (1998), we performed a twin sensitivity simulation for which the impact of salinity stratification on the vertical mixing is removed. We focused on the northwestern part of the basin (5° N–18° N and 70° W–50° W) and on the cold tongue region (3° S–1° N and 25° W–0° E), both showing interesting features.

2 Methodology

2.1 Coupled model description

The coupled regional configuration relies on the ocean model NEMO v4.0 (Nucleus for European Modeling of the Ocean; Madec and the NEMO team 2016), the atmospheric model WRF-ARW v3.7.1 (Weather Research and Forecasting; Skamarock and Klemp 2008), and the coupler OASIS3-MCT v4.0 (Valcke 2013). A similar configuration has already been used in the Indian Ocean (Samson et al. 2014) and in the tropical channel (Samson et al. 2017; Renault et al. 2019), and to our knowledge, this is its first implementation in the tropical Atlantic. The ocean and the atmospheric model share the same horizontal grid: a Mercator projection that encompasses the tropical Atlantic from 15° S to 35° N, and from 99° W to 20° E, with a resolution of 1/4° (∼ 27 km). Both models use an Arakawa-C grid. Since the grids are identical, no spatial interpolation is required by the coupler. Every hour, heat fluxes, water fluxes and wind stress are sent by WRF to NEMO, and SST and surface currents are sent by NEMO to WRF. All fields exchanged are hourly averages.

2.1.1 Ocean model

The ocean model solves the three-dimensional primitive equations. Its grid has 75 fixed vertical levels (z coordinates), with 12 levels in the upper 20 m and 24 levels in the upper 100 m. Lateral open boundaries of the model are prescribed using an interannual hindcast from the MERCATOR global daily reanalysis GLORYS2V4 (Ferry et al.

2012), and more specifically temperature, salinity, sea level and horizontal velocities. In order to take into account the ocean color in the solar radiation penetration scheme, the model is forced with a monthly climatology from 1999 to 2005 of chlorophyll concentrations derived from SeaWiFS (McClain et al. 1998). Interannual daily runoffs are specified at the river mouths and were obtained from the ISBA-CTRIP land surface system (Decharme et al. 2019). This oceanic configuration has already been used in Giffard et al. (2019). We refer the reader to this paper for further details on the configuration parameters and for a comprehensive validation of the sea level and surface salinity fields. It is worth mentioning that the ocean model configuration is very similar to the one used in Jouanno et al. (2017) and in Hernandez et al. (2016, 2017), which gives us confidence in its ability to simulate realistically the dynamics and thermodynamics of the upper tropical Atlantic ocean.

2.1.2 Atmospheric model

The atmospheric model WRF solves the compressible and non-hydrostatic Euler equations, using the Advanced Research WRF dynamical solver (ARW). Its grid has 40 terrain-following vertical levels (sigma coordinates), and the top of the atmosphere is located at 50 hPa. From the many parameterizations that can be chosen, the best representation of air–sea fluxes was obtained with the Yonsei University planetary boundary layer scheme (Hong et al. 2006) used together with the WSM6 microphysics scheme (Hong and Lim 2006) modified to take into account the droplet concentration (Jousse et al. 2016), and the Rapid Radiative Transfer Model for GCMs (Iacono 2011) for both shortwave and longwave radiation. Convection is represented with the Multi-Scale Kain–Fritsch scheme (Zheng et al. 2016), which allows interaction between parameterized clouds and the radiation schemes. The Noah Land Surface Model (Niu et al. 2011) together with the revised MM5 surface layer scheme (Jiménez et al. 2012) were used. The choice of these parameterizations is mainly based on Meynadier et al. (2015), who conducted sensitivity tests to parameterizations in the Gulf of Guinea with a forced WRF model. Lateral boundary conditions are given by 6-hourly fields from ERA-Interim reanalysis (Dee et al. 2011). Following Samson et al. (2017), we prescribed a monthly climatology of albedo derived from MODIS observations (Schaaf et al. 2011).

2.2 Simulations

The ocean model, initialized from the World Ocean Atlas 1998 climatology, was first spun up alone for 30 years (1970 to 1999) using DFS5.2 atmospheric forcing (Dussin et al. 2016), and bulk formulation (Large and Yeager 2009). Then, from 2000 onwards, two ocean–atmosphere coupled simulations are conducted: a CONTROL simulation as described in the previous section, and a sensitivity simulation NOS. In NOS, following Vialard and Delecluse (1998), Masson and Delecluse (2001) or Krishnamohan et al. (2019), the salinity gradient is set to zero in the Brunt–Väisälä frequency calculation over the whole domain. The Brunt–Väisälä frequency (N^2), a measure of the ocean stratification, enters as a sink term (or a source term in case of static instability) in the turbulent kinetic energy prognostic equation that is used to derive the vertical diffusion coefficient K_z (Reffray et al. 2015; Madec and the NEMO team 2016). Thus, through removing the sensitivity of N^2 to salinity variations, this experiment allows to remove the contribution of salinity stratification to vertical mixing, without direct modification of the model water density. Both sensitivity experiments are conducted from 2000 to 2015, and the analyses conducted hereafter rely on a 15-year period from 2001 to 2015.

2.3 Observations

Several observational datasets are used to assess the realism of the CONTROL simulation. The Optimum Interpolation Sea Surface Temperature (OISST) dataset v2.0 from NOAA (Banzon et al. 2016) is used to assess the model SST. This dataset is a merging of AVHRR satellite data and in situ observations from 2001 to 2015, interpolated on a 1/4° grid. A seasonal climatology of SSS observations at 1/4° resolution was built from SMAP satellite data for the period 2015–2018 (Meissner et al. 2019). Our model net heat flux is compared with the net heat flux from the Objectively Analyzed air–sea Fluxes (OAFlux) project (Yu et al. 2008). More precisely, it is a combination of radiative downward fluxes (shortwave and infrared fluxes) from the International Satellite Cloud Climatology Project (ISCCP) and turbulent heat fluxes (latent and sensible) from OAFlux, with a spatial resolution of 1° and a temporal resolution of 1 month. A climatology was computed using data from 2000 to 2009. Precipitation data are from the Tropical Rainfall Measuring Mission (TRMM; Huffman et al. 2007), which is a merging of various satellite datasets as well as rain gauges wherever available. The product is provided on a 1/4° grid, and a 2001–2015 climatology is used. To compute the 20 °C isotherm depth, we used a climatology from 2002 to 2015 of the ISAS dataset of 3D temperature (Kolodziejczyk et al. 2017; Gaillard et al. 2016). ISAS is based on in-situ measurements, and has a 1/2° resolution. Finally, we compared the model mixed layer depth (MLD) with the climatology from de Boyer Montégut et al. (2004), based on in-situ salinity and temperature profiles. The MLD is computed as the depth where the density is equal to the 10-meter density plus $\Delta\sigma$, with $\Delta\sigma$ a fixed density criterion of 0.03 kg/m^3. Using a

density criterion instead of a temperature criterion is critical in regions with strong upper ocean salinity gradients.

2.4 Validation

The CONTROL run is compared with the observational datasets in Fig. 1. First, our model reproduces fairly well the observed regional patterns of SST, SSS, precipitation, MLD, net heat flux and thermocline depth. The model SST is slightly too warm, especially in the ITCZ zone, with a bias of the order of 1 °C. The SST bias has a magnitude similar to that of the ensemble mean of CMIP5 and CMIP6 coupled general circulation models (GCMs), but is positive everywhere instead of negative in the western part of the basin as usually found in coupled GCMs (Richter and Xie 2008; Richter et al. 2012, 2014; Xu et al. 2014). This bias does not appear to have any prominent impact on SSS nor precipitation. Indeed, both are in good agreement with the observations, with the exception of a slightly too high SSS in the northern subtropical gyre (about 0.2 PSU) and slightly too intense precipitation in the ITCZ zone (about 2 mm/day). Precipitation is better represented than in state-of-the-art coupled GCMs, except in the Gulf of Guinea (Breugem et al. 2008; Toniazzo and Woolnough 2014; Siongco et al. 2015). The low salinity band associated with the Amazon plume and the ITCZ are particularly well represented, as is the meridional location of the ITCZ: our model does not show the ITCZ southward extension bias that is so frequent in the coupled GCMs in the tropical Atlantic (Richter et al. 2014; Tian and Dong 2020; Richter and Tokinaga 2020). It has therefore a better SSS than in coupled GCMs: in the main part of the basin, the SSS bias is more than twice lower than in the ensemble mean of CMIP6 coupled GCMs (not shown). SSS biases at river mouths may be partly attributed to the different time periods used for the observations and the model, and to the lower accuracy of SMAP at the coast (Grodsky et al. 2018). The large-scale structure of the MLD is very similar to the observations, apart from the Amazon plume and the ITCZ where it is slightly too thick (by 5–10 m). However, it should be kept in mind that the resolution of the MLD climatology is coarse (2°× 2°) and could explain part of the inconsistencies observed. The net heat flux (considered positive downward) is too low, with a bias of − 30 to − 40 W/m^2 overall. It is caused by too much heat loss by latent heat flux (− 40 to − 50 W/m^2, not shown) that is partly compensated by a too strong shortwave heat flux (+ 10 to 20 W/m^2, not shown). While some of these biases undoubtedly fall within the range of the classical biases found in atmospheric and coupled GCMs (Kumar et al. 2012; Xu et al. 2014), OAFlux product is also known to have a positive bias over our region (Kumar et al. 2012), hereby exacerbating the negative bias estimate of our model. The 20 °C isotherm depth, a proxy of the thermocline depth, is in good agreement with the observations except in the Gulf of Mexico where it is too deep.

The Gulf of Guinea is the least realistic area in the model, with some zones showing substantial biases of temperature (up to + 2 °C), salinity (down to − 4 PSU) and precipitation (up to + 12 mm/day). However, these strong differences occur over small areas and are located nearshore, outside of the areas we are interested in. Finally, Fig. 2a shows the SST seasonal cycle in two areas of importance for the rest of the study: the cold tongue (CT, 25° W–0° E and 3° S–1° N) and the northwestern tropical Atlantic (NWTA, 70° W–50° W and 5° N–18° N). We can see that the model (in red) matches well the OISST observations (in black): the SST is too high in winter in the CT and too high in summer in the NWTA, but the seasonal amplitude is close from observations in both regions, without any prominent phase shift of the seasonal cycle.

2.5 Methods

2.5.1 Salinity contribution to total stratification (OSS_{100m})

To characterize the strength of the salinity stratification, we rely on the OSS_{100m} indicator (Maes and O'Kane 2014):

$$OSS_{100m} = \frac{\langle N^2 S \rangle_{100m}}{\langle N^2 \rangle_{100m}} \tag{1}$$

with

$$N^2 = -\frac{g}{\rho_0}\frac{\partial \rho(T,S)}{\partial z} \tag{2}$$

the Brunt–Väisälä frequency, where ρ_0 is the sea water density, equal to 1026 kg/m^3, g is the acceleration of gravity, T is the model temperature and S the model salinity. N^2 represents the total stratification, and can be expressed as the sum of the stratification due to temperature N^2T and the stratification due to salinity N^2S:

$$N^2 = N^2S + N^2T \tag{3}$$

with

$$N^2S = -\frac{g}{\rho_0}\frac{\partial \rho(T_0,S)}{\partial z} \quad , \quad N^2T = -\frac{g}{\rho_0}\frac{\partial \rho(T,S_0)}{\partial z} \tag{4}$$

T_0 and S_0 are constant temperature and salinity values respectively that are representative of the area. Since salinity is more homogeneous than temperature, we chose to calculate N^2S as the difference between N^2 and N^2T (Eq. (3)), as in Hernandez et al. (2016). S_0 is taken equal to 36, which corresponds to the mean value of salinity in the upper 100 m in our areas of interest (CT, NWTA, ITCZ). We also verified that OSS_{100m} is not sensitive to the chosen value of S_0. N^2, N^2S and N^2T are calculated from the outputs of the CONTROL run.

Finally, we have

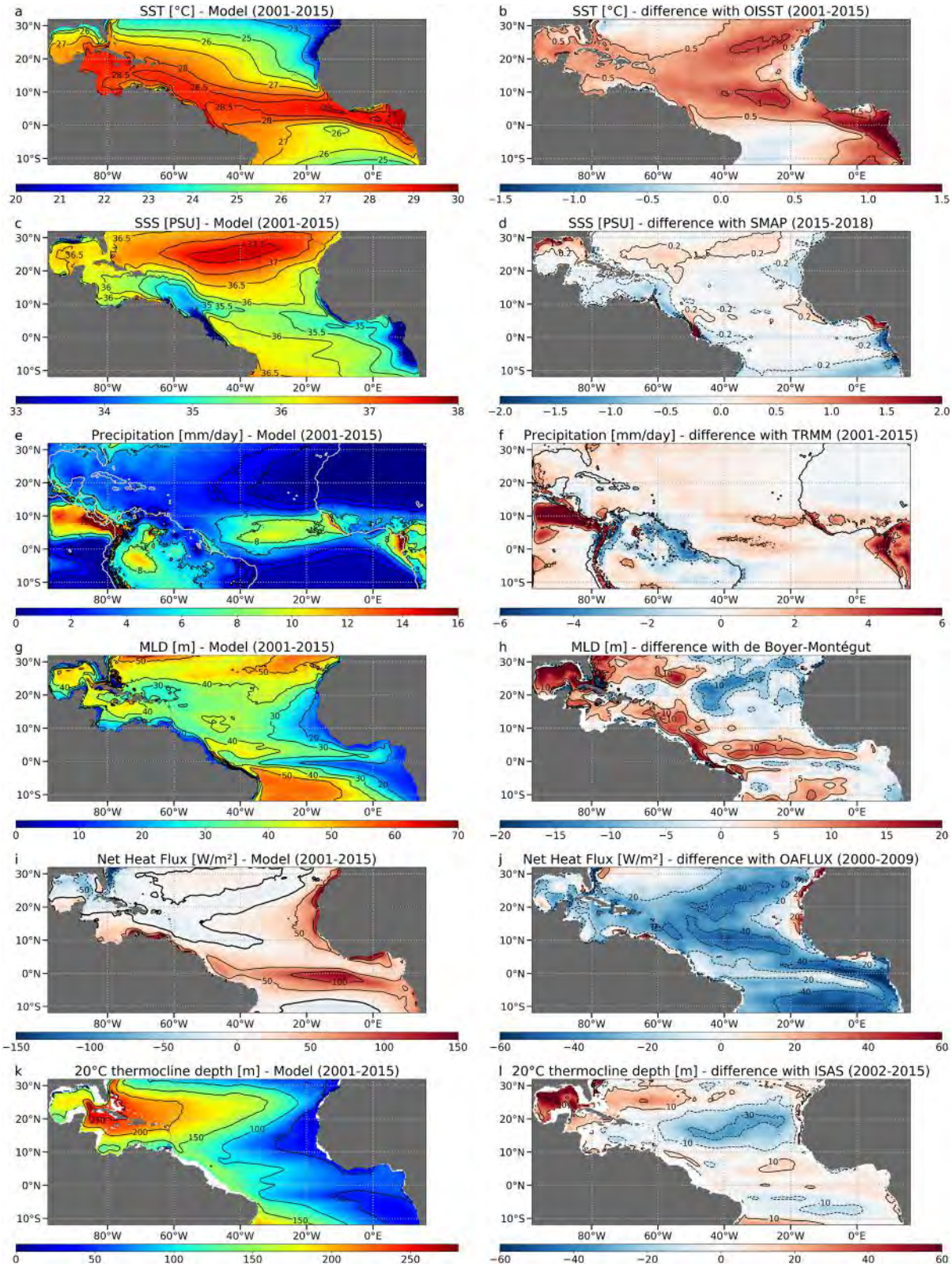

Fig. 1 2001–2015 annual climatology of **a**, **b**: SST; **c**, **d**: SSS; **e**, **f**: Precipitation; **f**, **g**: MLD; **i**, **j**: Net heat flux; **k**, **l**: 20 °C isotherm depth—model (left column) and difference between the model and the observations (right column)

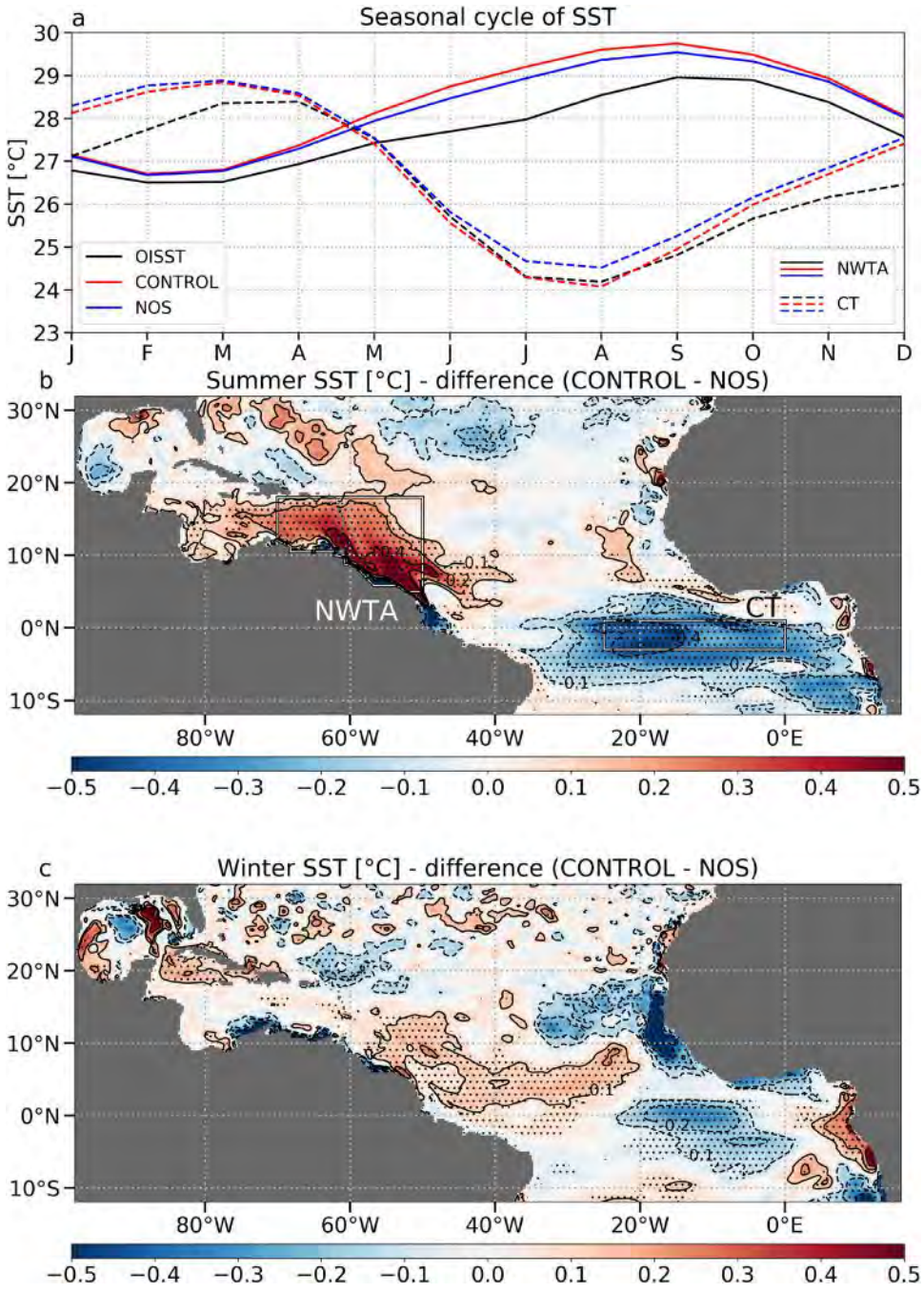

Fig. 2 **a** SST seasonal cycle in NWTA and CT (the two boxes are drawn on figure **b**; SST differences between CONTROL and NOS in **b** summer and **c** winter, dots indicating the areas where the difference is significant

$$\langle \bullet \rangle_h = \frac{1}{h} \int_{-h}^{0} \bullet \tag{5}$$

OSS_{100m} is the contribution of salinity stratification N^2S to total stratification N^2 averaged over the first 100 m to total stratification N^2, also averaged over the first 100 m, expressed as a percentage of N^2.

2.5.2 Mixed layer heat budget

A mixed layer heat budget was calculated online, following Vialard and Delecluse (1998). This consists of an integration of the equation of temperature over the ML, expressed as follows:

$$\underbrace{\partial_t T}_{\text{Total tendency}} = \underbrace{< -u\partial_x T - v\partial_y T >_h}_{\text{Horizontal Advection}} + \underbrace{< D_l >_h}_{\text{Lateral Diffusion}} + \underbrace{\frac{Q_s(1-F_{-h})+Q_{ns}}{\rho_0 C_p h}}_{\text{Atmospheric Forcing}} + \underbrace{\underbrace{< -w\partial_z T >_h}_{\text{Vertical Advection}} + \underbrace{\frac{(K_z \partial_z T)_{z=-h}}{h}}_{\text{Vertical Diffusion}} + \underbrace{\frac{\partial_t h}{h}(T_{-h} - < T >_h)}_{\text{Entrainment}}}_{\text{Vertical Processes}} \quad (6)$$

where T is the model temperature, u the zonal current, v the meridional current, w the vertical current, K_z the vertical diffusion coefficient and D_l the lateral diffusion. Q_s and Q_{ns} are respectively the solar and non-solar part of the total heat flux, F_{-h} is the fraction of shortwave radiation reaching the base of the ML, and T_{-h} the temperature at the ML base. Finally, the MLD, h, is calculated using a threshold criterion $\Delta\sigma = 0.01$ kg/m^3 (de Boyer Montégut et al. 2007b). We chose this criterion, different from the one used previously, for consistency with several dynamical parameterizations in NEMO (Madec and the NEMO team 2016). This approach was used in several other studies (Vialard and Delecluse 1998; Durand et al. 2004; Menkes et al. 2006; Peter et al. 2006; Hernandez et al. 2016; Krishnamohan et al. 2019). It allows to quantify the temperature tendency due to advection, diffusion, atmospheric forcing and entrainment. The entrainment term arises from the integration of the temperature equation over a time-varying ML.

2.5.3 Pycnocline depth

The pycnocline depth D_σ is estimated as the depth where a density increase corresponding to a temperature decrease of 0.2 °C at 10 m depth is found (de Boyer Montégut et al. 2004, 2007a):

$$D_\sigma = depth\ where\ \left[\sigma_0 = \sigma_0(T_{10m} - 0.2°C, S_{10m}, P_0)\right] \quad (7)$$

2.5.4 Definition of the barrier layer thickness (BLT)

In areas of intense salinity precipitation or in river plumes, some decoupling may occur between the haline and the thermal stratification of the upper ocean. In such a situation, the low surface salinity limits the pycnocline to the halocline depth, while the thermocline is located deeper: a barrier layer (BL) appears (Godfrey and Lindstrom 1989; Lukas and Lindstrom 1991). The BLT is then defined as the difference between the top of the thermocline depth and the pycnocline depth (Sprintall and Tomczak 1992):

$$BLT = D_{T_{-0.2}} - D_\sigma \quad (8)$$

with

$$D_{T_{-0.2}} = depth\ where\ \left[T = T_{10m} - 0.2°C\right] \quad (9)$$

the top of the thermocline depth (de Boyer Montégut et al. 2004, 2007a). The pycnocline depth D_σ is defined in paragraph 2.5.3.

2.5.5 Significance of the anomalies in simulation intercomparison

In the rest of the study, the CONTROL simulation is compared with the NOS simulation over a fifteen year period. The significance of the differences between the two simulations is based on a two-tailed Student's t-test, with a confidence level of 99%. Anomalies considered statistically significant are indicated by dots on the difference maps in Figs. 2, 8, 9 and 11.

3 Results

3.1 Impact of salinity stratification on SST

The impact of salinity stratification on the SST is obtained for summer (June–July–August, JJA) and winter (December–January–February, DJF), as the difference between simulations CONTROL and NOS (Fig. 2b, c). The sensitivity to salinity stratification is largest in summer, with a warming of 0.2 °C–0.5 °C in the NWTA, and a cooling of 0.2 °C–0.5 °C in the equatorial region, especially in the CT. Over the rest of the basin, the response is not statistically significant. In winter, the response is weaker albeit statistically significant in some localized areas like the ITCZ. Moreover, it is interesting to note that there is a very limited change in SST under the ITCZ throughout the year, despite heavy precipitation in this area. The seasonal cycle of SST in the NWTA and in the CT (Fig. 2a) confirms that changes are maximum in summer, and almost null in winter. It shows that the presence of salinity stratification increases the amplitude of the seasonal cycle in both regions (+ 6% in the NWTA, + 9% in the CT). It is worth mentioning that the SST seasonal cycles of NWTA and CT are opposed.

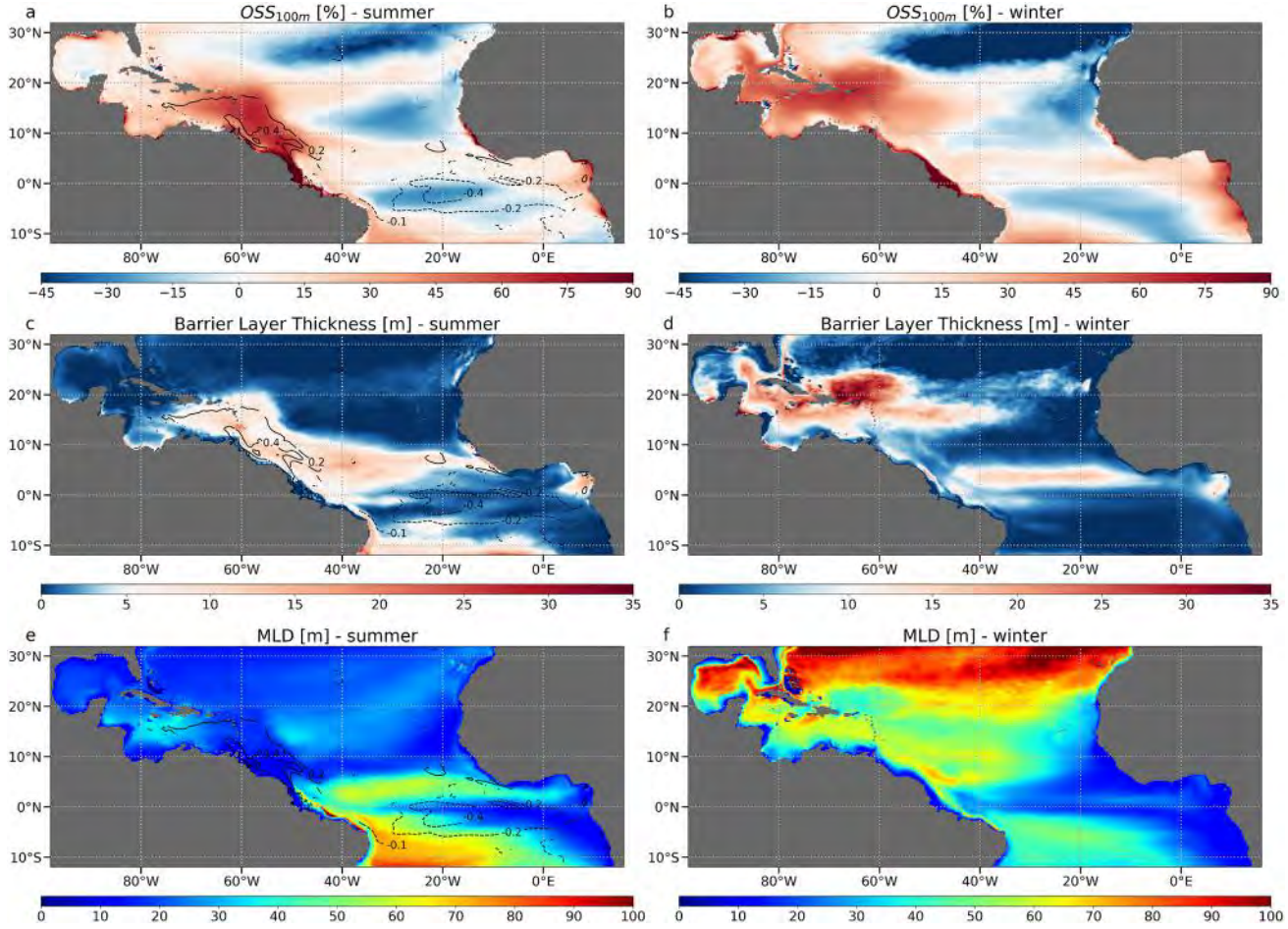

Fig. 3 Summer maps of **a** OSS_{100m}, **c** BLT and **e** MLD for CONTROL simulation; summer SST differences contours are plotted, only where they are statistically significant. **b**, **d**, **f**: same than **a**, **c**, **e** respectively, but in winter

We will now investigate the causes of this contrasted sensitivity of SST among these regions and seasons.

3.2 Northwestern tropical Atlantic SST anomaly

3.2.1 Impact of salinity stratification on SST

In summer, the warm anomaly in CONTROL with respect to NOS in the NWTA corresponds to a region with large haline stratification. It is revealed by the OSS_{100m} distribution (Fig. 3a), which represents the strength of salinity stratification as a percentage of the total stratification. During winter, such a link does not exist (Fig. 3b). This contrast between summer and winter in terms of sensitivity of the surface temperature to the local haline stratification is confirmed in Fig. 4a, c: during summer, the higher the OSS_{100m}, the larger the SST anomalies; it reaches 1.2 °C where OSS_{100m} equals 90%. In winter, the SST anomalies between the two simulations are weak and are not related to the strength of the salinity stratification (Fig. 4c). We relate this seasonal contrast to a much deeper MLD in winter compared to summer (Fig. 3e, f). In summer, salinity stratification is maximum in the Amazon plume area, with MLDs between 10 and 20 m, while in winter, salinity stratification is maximum in the Caribbean Sea, with a mean MLD reaching 60–70 m. This implies that the positive temperature anomaly due to salinity effects is spread over a deeper layer in winter, resulting in a weak SST response regardless of the salinity stratification strength.

3.2.2 Mixed layer heat budget

To understand more precisely how salinity stratification impacts the SST, we now analyze the seasonal heat budget of the ML (see Sect. 2.5.2) over the NWTA area (Fig. 5a, c). The ML temperature tendency in the NWTA is controlled at first order by the air–sea fluxes and by two vertical processes: the vertical mixing and the entrainment. The changes between CONTROL (solid line) and NOS (dashed line) mainly concern these three processes. There is a reduction of cooling due to vertical mixing when salinity stratification

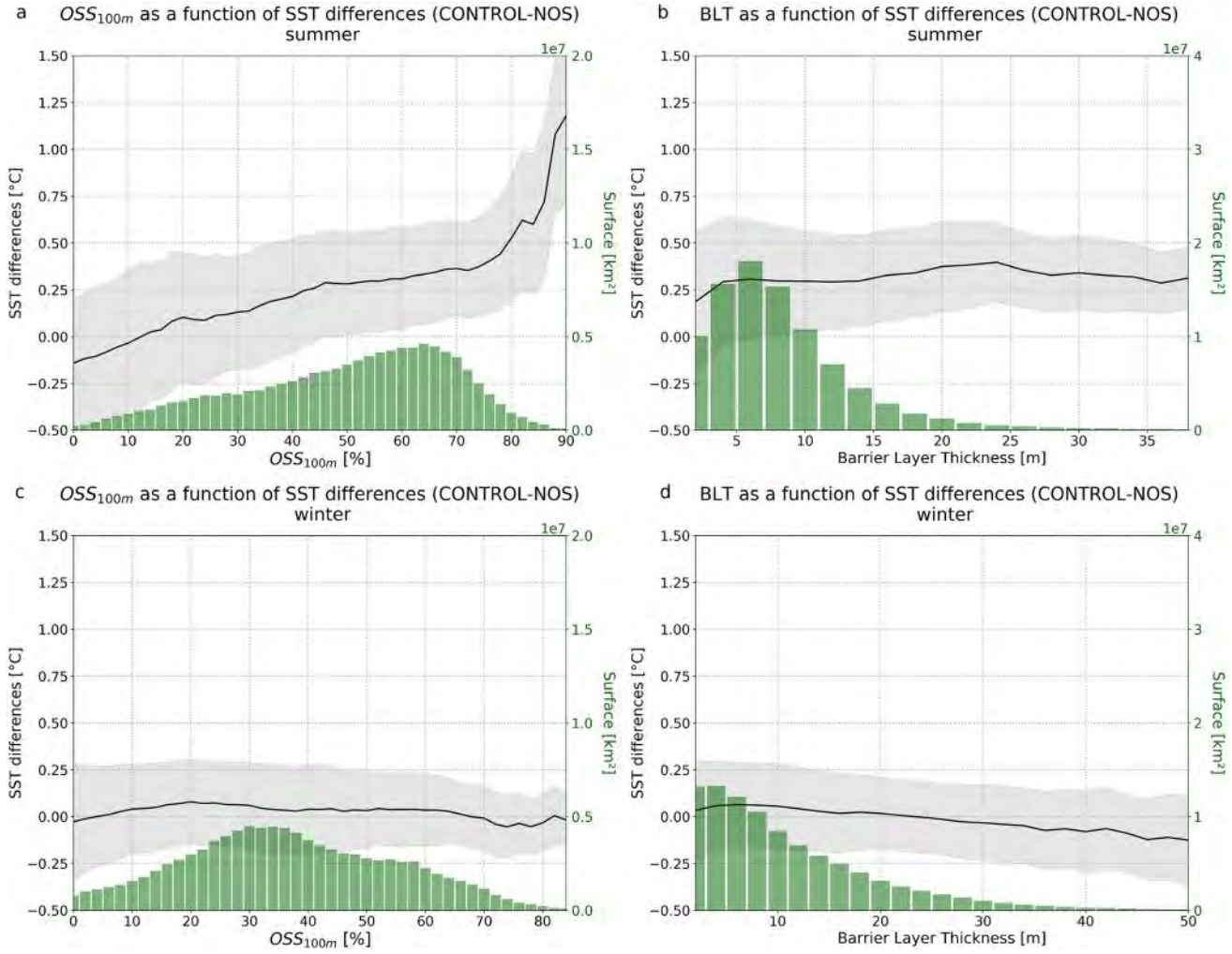

Fig. 4 Summer SST differences as a function of **a** OSS_{100m} and **b** BLT for CONTROL run, envelope: $\pm\sigma$; coastal areas (i.e. areas where the bathymetry is under 50 m) where removed, as well as values corresponding to less than 100 grid cells. **c**, **d**: same than **a**, **b** respectively, but in winter. For each figure, bins surfaces are represented on a histogram. The analyze is applied on the NWTA box

is considered, because of the stabilizing effect of the salinity stratification. This reduction of the vertical mixing is illustrated by Fig. 6a, c, which represent the seasonal evolution of the temperature profile in NWTA. In CONTROL, the salinity stratification reduces the mixing between the surface and subsurface, leading to a warm anomaly at the surface and a cold anomaly in subsurface. This effect of vertical mixing has already been observed by Deppenmeier et al. (2020). The surface warming happens all year long but is stronger in summer, when salinity stratification is stronger and the ML is at its shallowest. In summer, when considering the salinity stratification, the decrease of the ML cooling by vertical mixing reaches 1.2 °C/month. It is partly compensated by a decrease of the warming due to air–sea fluxes and entrainment, each with a contribution of about 0.5 °C/month in summer (Fig. 5a, c). It results in a 0.1–0.2 °C/month differential warming between NOS and CONTROL during the summer season, leading to the positive SST anomaly observed in Fig. 2b. In winter, the changes are much smaller for all the processes and compensate each other so that there is no change in SST.

Entrainment is a term that appears when the equation of temperature is integrated on the time-varying ML (see Eq. 6). During ML deepening events, entrainment is null: in that case, the mean temperature of the ML is equal to the temperature at the base of the ML, which means that the factor $(T_{-h} - \langle T \rangle_h)$ is equal to zero. Entrainment is therefore controlled by the occurrence of restratification events, and especially those due to the diurnal cycle. In the CONTROL experiment, the MLD diurnal cycle is close to zero in the regions where salinity stratification is strong—and especially the NWTA, while it is important in the NOS experiment due to the absence of salinity stratification (Fig. 7). As a consequence, the daily restratification is less important in

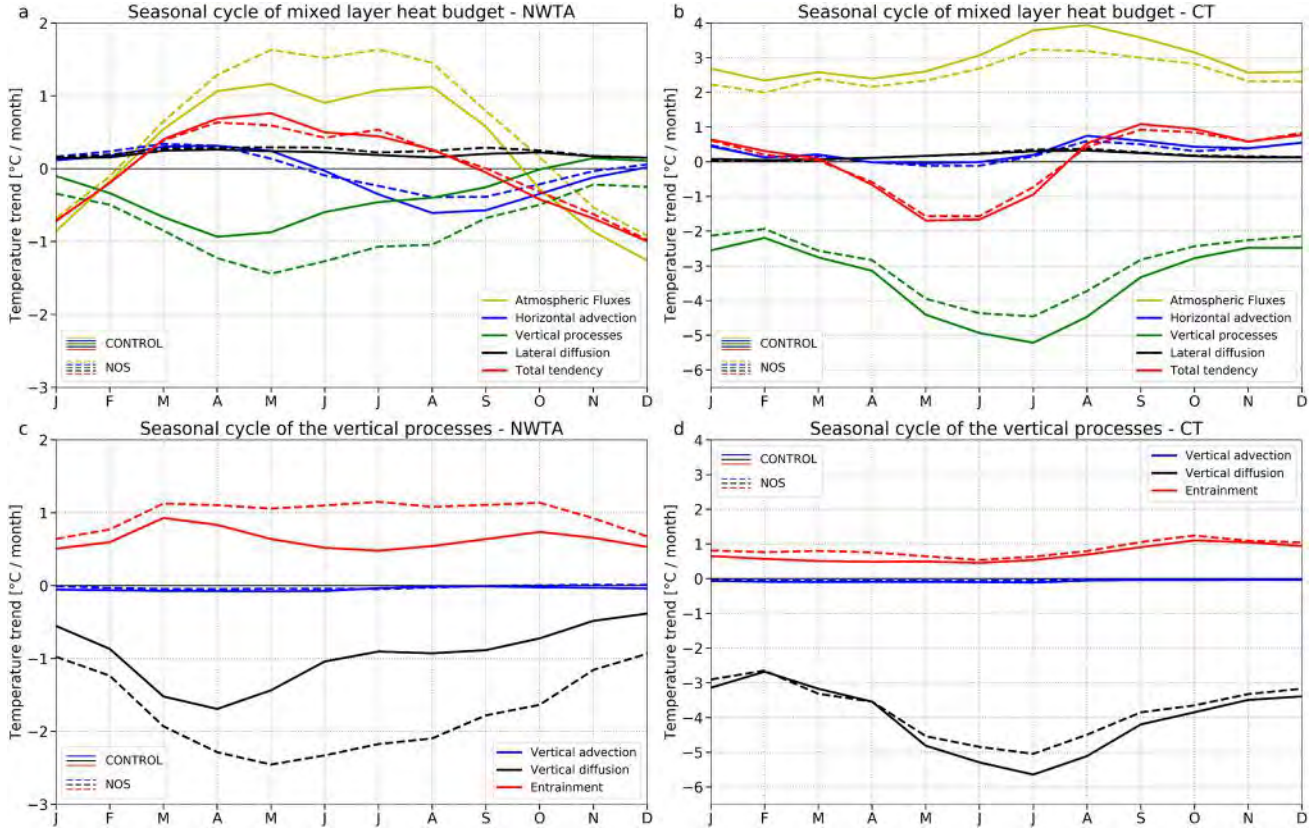

Fig. 5 Seasonal cycle of mixed layer heat budget in **a** NWTA and **b** CT; **c**, **d** are same than **a**, **b** respectively, but for the vertical processes

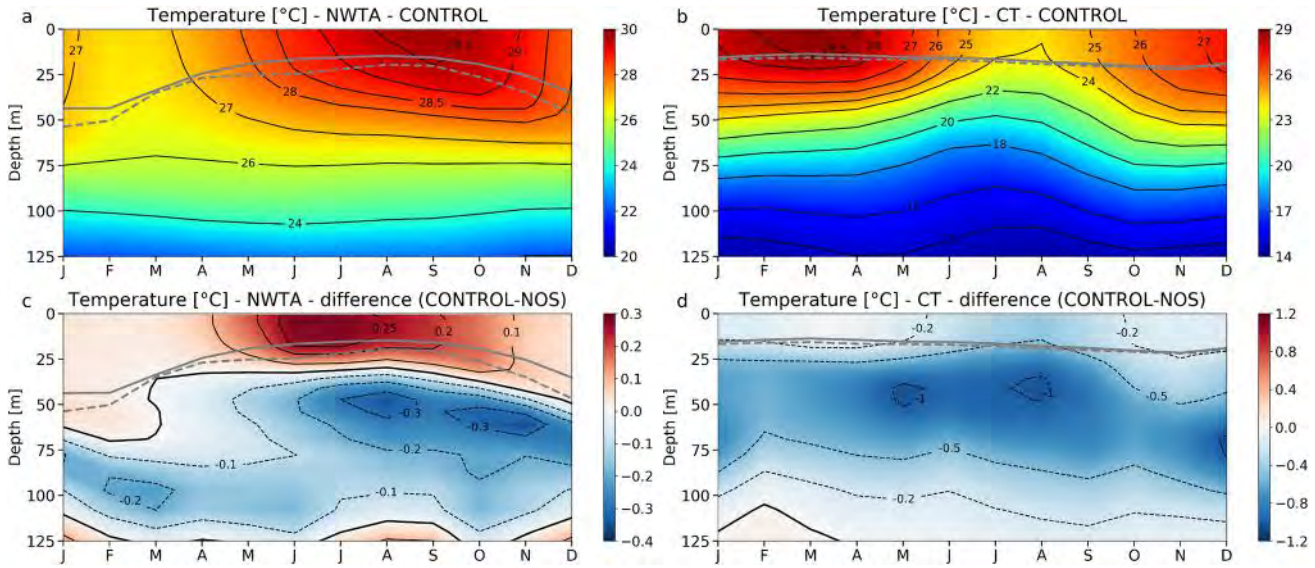

Fig. 6 Seasonal cycle of temperature section in NWTA for **a** CONTROL simulation and **c** the difference (CONTROL-NOS); **b** and **d**: same than **a**, **c** respectively, but in CT. The grey lines represent the ML for CONTROL (solid line) and NOS (dashed line)

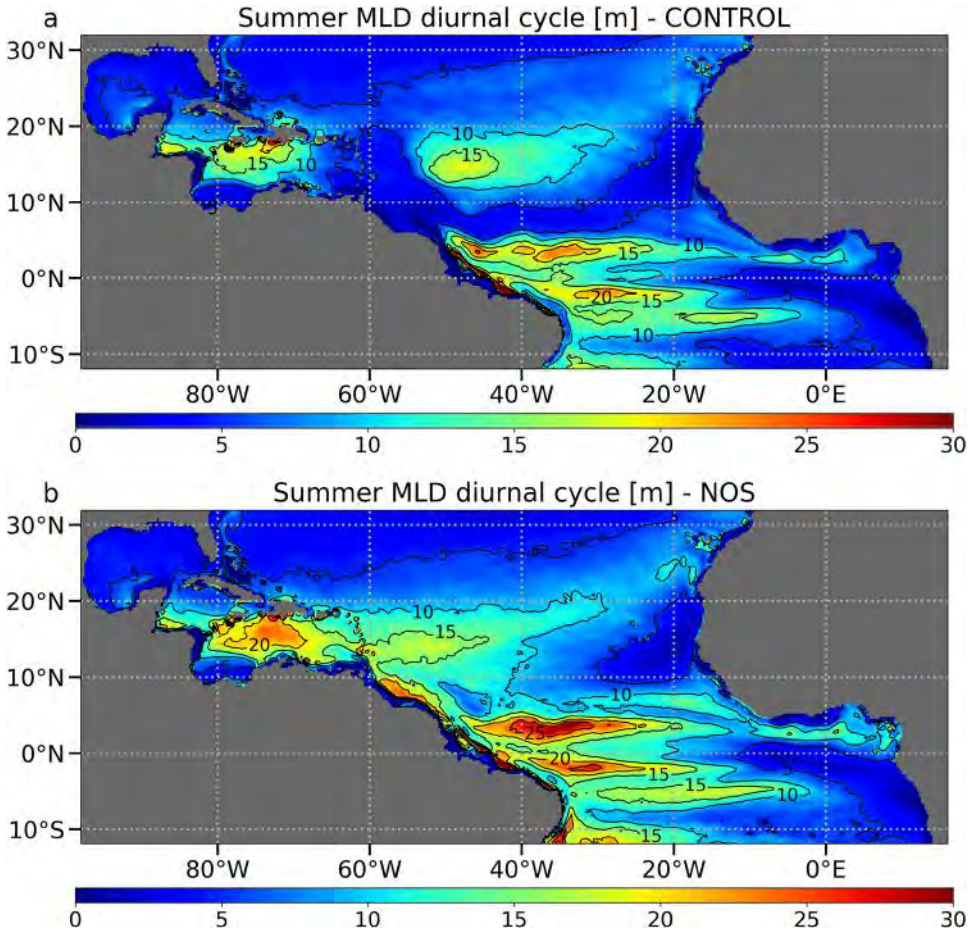

Fig. 7 Summer maps of MLD diurnal cycle for **a** CONTROL simulation and **b** NOS simulation

CONTROL than in NOS simulation, leading to a weaker $\partial_t h$ factor and explaining the lower entrainment in the CONTROL simulation.

3.2.3 Impact of salinity stratification on the atmosphere

As mentioned previously, the air–sea fluxes also dampen the differences between the two simulations. This negative feedback of the atmosphere is now investigated. We focus on summer, since this is the season with the largest changes. Figure 8 represents CONTROL-NOS summer differences of the key atmospheric variables. Mean values in summer and NWTA are detailed in Table 1 for the heat fluxes, and Table 2 for the other atmospheric variables. The net heat flux (Fig. 8a) is much weaker in CONTROL respective to NOS in the NWTA region (down to − 40 W m^2, corresponding to a decrease of more than 50%). This is linked to lower net shortwave radiation (Fig. 8b), responsible for about 29% of the total change in net heat flux, and larger heat loss by latent heat flux (Fig. 8c), responsible for about 71% of the change. Differences in longwave radiation and sensible heat flux are small (< 1 W/m^2; Table 1). We can also notice in Table 1 that the differences between CONTROL and NOS values are rather low for all fluxes composing the net heat flux. For instance, the change in latent heat flux is − 8%, and the change in shortwave radiation is − 2%. But all these small changes add up to give a significant change in net heat flux (more than 30%).

The increase in latent heat loss can be explained by the SST increase, the wind changes being weak in the NWTA (Fig. 8e, Table 2). Over the western tropical Atlantic, the increase in latent heat loss resulting from the SST increase is commonplace in observational air–sea flux databases (Kumar et al. 2017).

The changes in net shortwave radiation involve a more complex feedback loop, which can be synthesized as follows. The warm SST anomaly leads to an enhancement of atmospheric deep convection (Sabin et al. 2013) and thus to a more prominent cloud cover (Fig. 8d). This change in cloud cover is significant (about 15% increase between NOS and CONTROL), and is mainly associated to a change in high clouds (not shown), confirming the enhancement of deep convection. This causes the observed decrease in net shortwave radiation by capturing a part of the incident solar radiation. This mechanism is in agreement with Xie (2009), who described this negative cloud-SST feedback over warm

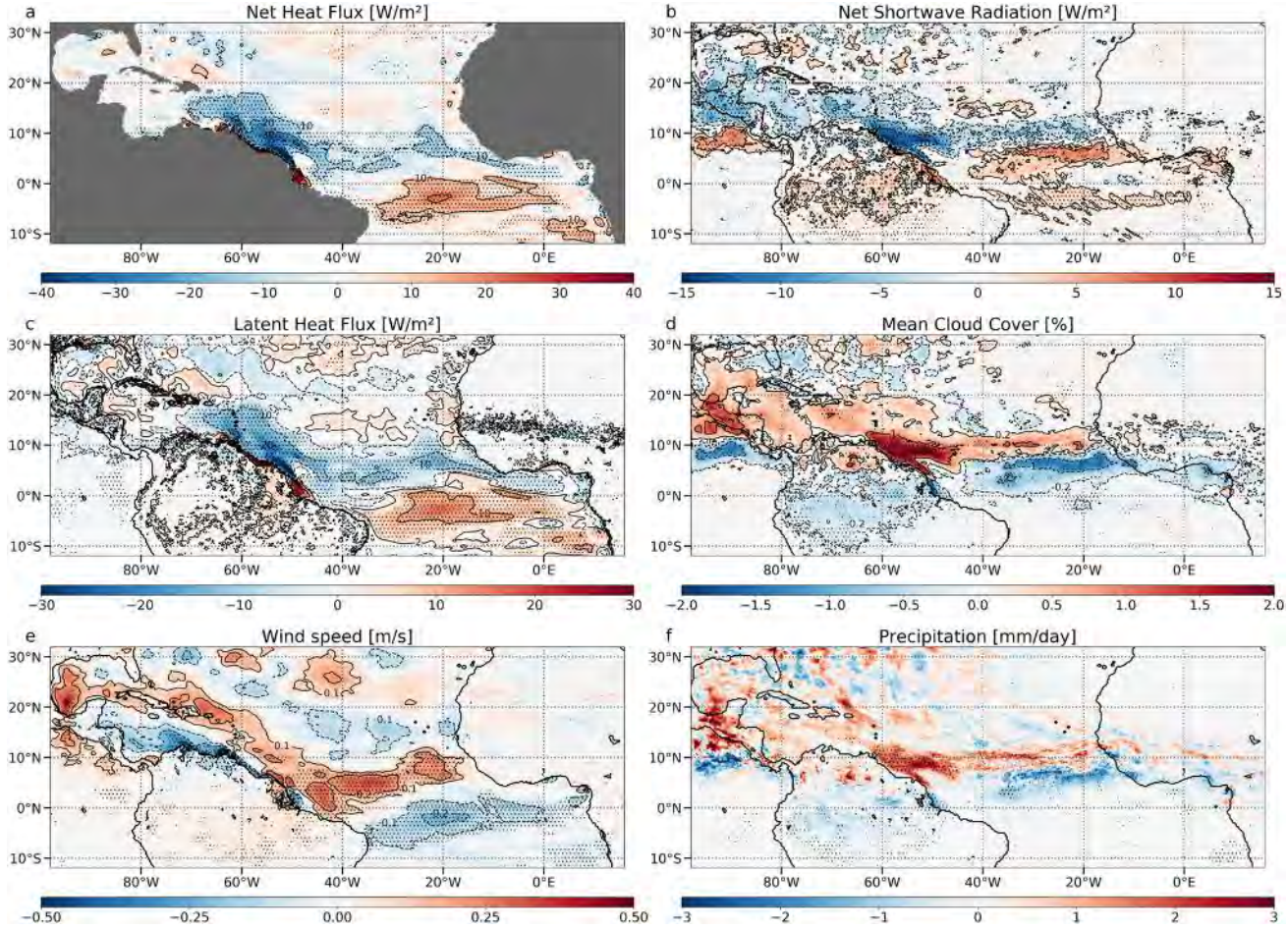

Fig. 8 Difference between CONTROL and NOS in summer of **a** Net Heat flux, **b** Net Shortwave Radiation, **c** Latent Heat Flux, **d** Cloud Cover, **e** Wind speed and **f** Precipitation, dots indicating the areas where the difference is statistically significant

areas where deep convection develops. More extended cloud cover is also consistent with a 19% increase in precipitation between NOS and CONTROL (Fig. 8f). Moreover, it is worth noting the northward shift of the ITCZ when salinity stratification is considered, which may result from the large scale SST anomaly dipole (Fig. 2b).

The longwave radiation differences are weak (Table 1). This is due to a compensation between the SST increase, leading to more longwave radiation emitted by the ocean, and the cloud cover increase, leading to more shortwave radiation intercepted by clouds and therefore more longwave radiation emitted by clouds and received by the ocean (not shown).

Finally, the change in MLD can also explain part of this atmospheric negative feedback: a thinner ML leads to a higher part of the solar flux penetrating underneath, and therefore less warming by atmospheric fluxes (Lewis et al. 1990; Vialard and Delecluse 1998; Masson and Delecluse 2001; Mignot et al. 2012; Krishnamohan et al. 2019). This is especially true in summer, when the ML is thin enough for that process to be significant (Mignot et al. 2012). Moreover, the change in MLD between NOS and CONTROL is substantial in this season (about − 36%, see Table 2).

Table 1 Changes in atmospheric heat fluxes between CONTROL and NOS, in the NWTA box, in summer, in areas where the SST anomaly is higher than 0.1 °C (i.e. where it is significant)

Fluxes	CONTROL value [W/m^2]	NOS value [W/m^2]	Contribution to net heat flux change
Net heat flux	39.5	57	–
Net shortwave radiation	261.5	266.5	29%
Net longwave radiation	− 47.5	− 48	− 3%
Latent heat flux	− 163.5	− 151	71%
Sensible heat flux	− 10	− 9	6%

CONTROL and NOS values are rounded off to 0.5 W/m^2

Table 2 Changes in several oceanic and atmospheric variables between CONTROL and NOS, in the NWTA box, in summer, in areas where the SST anomaly is higher than 0.1 °C (i.e. where it is significant)

Variables	CONTROL value	NOS value
SST	29.3 °C	29 °C
SSS	33.6 psu	35.4 psu
Mixed layer depth	17.6 m	27.3 m
Cloud cover	6.1%	5.3%
Precipitation	5 mm/day	4.2 mm/day
Wind speed	6.8 m/s	6.7 m/s

3.3 Cold tongue SST anomaly

A strong sensitivity of the central equatorial Atlantic Ocean to salinity stratification also appears, as mentioned in Sect. 3.1. We analyze this pattern in the following.

3.3.1 A negative SST anomaly

Like in the NWTA, the SST sensitivity to salinity stratification in the equatorial area is greatest in summer, and close to zero in winter (Fig. 2). Summer season corresponds to

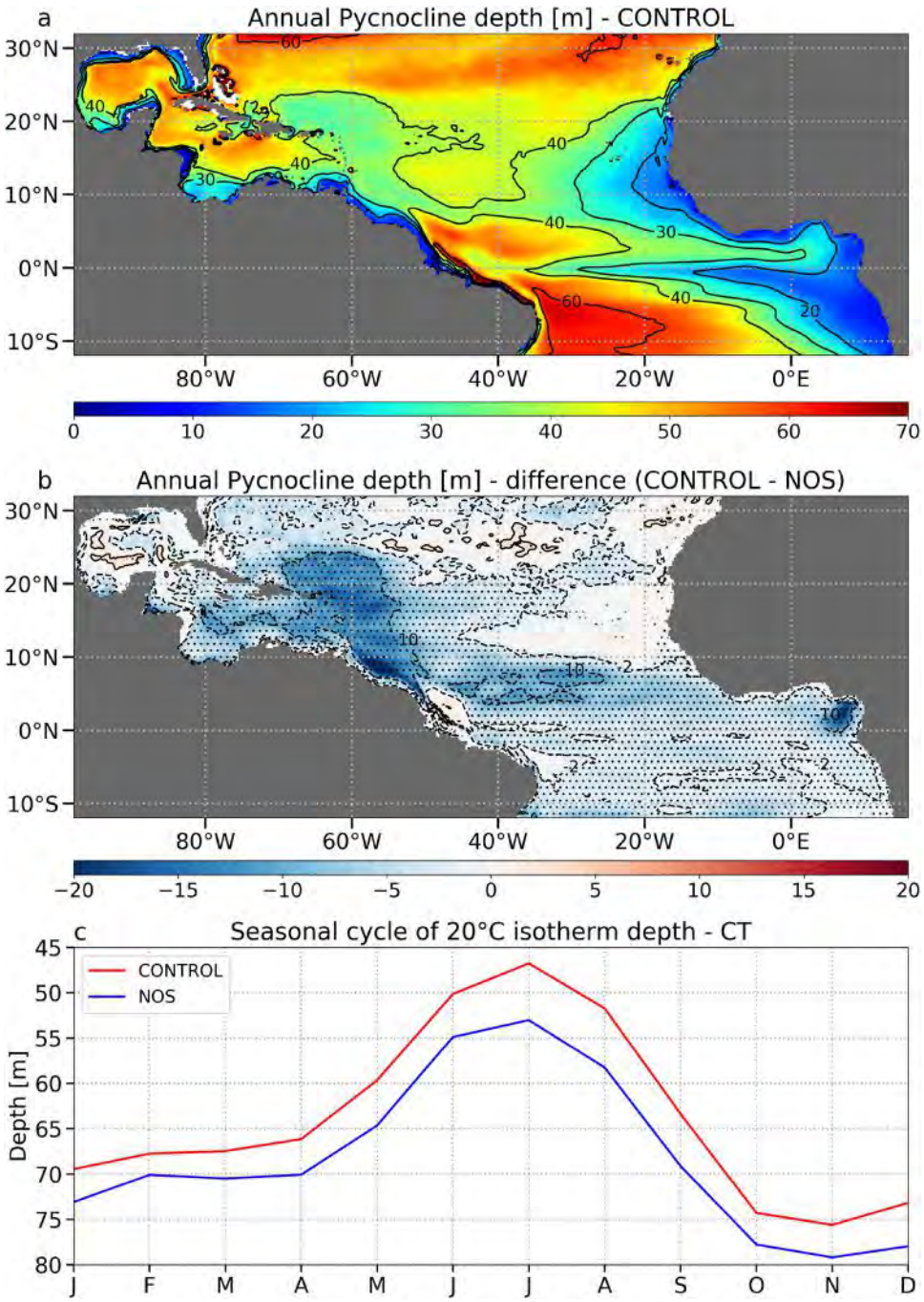

Fig. 9 **a** Annual turbocline depth (2001–2015 climatology) for **a** CONTROL simulation and **b** the difference (CONTROL-NOS), dots indicating the areas where the difference is statistically significant; **c** seasonal cycle of 20 °C isotherm depth for the 2001–2015 climatology in the CT box

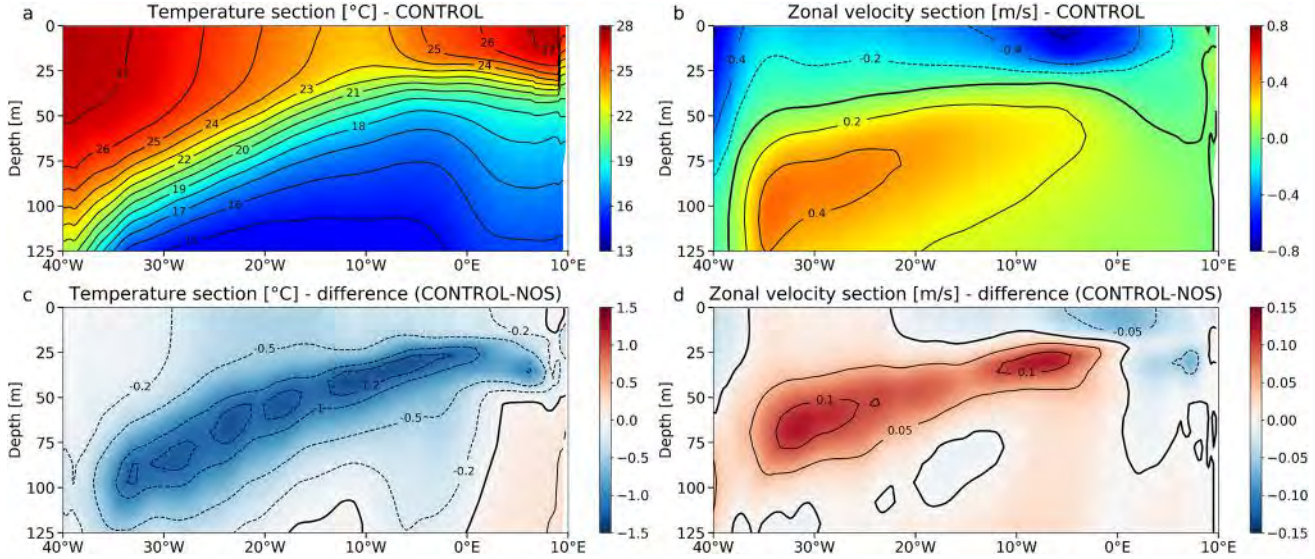

Fig. 10 **a** Temperature section in summer for CONTROL simulation, mean between 3° S and 1° N, **c** same than **a** but for the temperature anomaly (CONTROL-NOS); **b** and **d**: same than **a** and **c** respectively, but for zonal velocity

the period of development of the Atlantic CT (Carton and Zhou 1997). However, unlike the NWTA, the SST anomaly in the CT region is negative: the presence of salinity stratification induces a cooling of the CT. The mixed layer heat budget for the CT region is shown in Fig. 5b, d. It indicates that vertical mixing is enhanced when salinity stratification is considered, increasing the ML cooling by about 0.5 °C/month in summer. It should be noted that the change in vertical mixing in the CT is opposite to the one in the NWTA. The increase in vertical mixing in the CT is due to an equatorial adjustment of the thermocline depth, and is discussed in details in the following section. Entrainment is also decreased in this region, although not to the same extent as in the NWTA. Even so, this leads to an additional cooling in the contribution of the vertical processes of about 0.2 °C/month, bringing down the total to about − 0.7 °C/month in summer. Again, this is partly compensated by the atmospheric fluxes that show a + 0.5 °C/month difference in summer. Here the atmospheric feedback is mainly due to the fact that the decrease in SST leads to a decrease in latent heat loss. The atmospheric deep convection is indeed very weak in this region, and the change in SST does not impact the cloud cover nor the shortwave radiation as it does in the NWTA (Fig. 8b, d).

3.3.2 Strengthening of the CT

The mechanism leading to the CT strengthening is illustrated in Figs. 9 and 10. Figure 9a, b present the annual pycnocline depth for the CONTROL run and for the difference CONTROL-NOS respectively. We can observe a strong shoaling of the pycnocline in the NWTA when salinity stratification is accounted for. This is due to the reduced vertical mixing in the NWTA, which causes a readjustment of the density profile. This density readjustment propagates as baroclinic waves through the equatorial waveguide to adjust the whole equatorial basin up to the eastern part (not shown). The primary indicator of this new state is the change in the equatorial currents: a shoaling and a strengthening of the equatorial undercurrent (EUC) is indeed observed (Fig. 10b, d). An impact of salinity stratification on the equatorial currents has already been reported by Vialard and Delecluse (1998): salinity stratification traps the wind momentum over a thinner ML, and therefore enhances the ocean response to wind forcing. But this effect is local and applies to the surface currents, while we observe here a remote effect of salinity stratification on the subsurface currents.

The new equilibrium also exhibits changes in the vertical temperature structure, and in particular a shallower thermocline. This can be observed on Fig. 9c, where the depth of the 20 °C isotherm (D20), a proxy of thermocline, is plotted. The D20 shoals consequently year-round, with a higher response in summer (6–7 m) with respect to winter (about 3 m) leading to a larger amplitude of the seasonal cycle. The shoaling of the thermocline is confirmed by Fig. 10a, c, which represent summer zonal temperature sections averaged between 3° S and 1° N. The top of the thermocline is clearly seen on Fig. 10a, zonally tilted from about 100 m at 35° W to 25 m at 0° E. These depths correspond to the depths of the strongest temperature anomalies on Fig. 10c. The anomalies being negative, this indicates an upward shift of the thermocline occurring across the whole equatorial basin. The thermocline shoaling leads to an enhancement of the CT (Latif and Grötzner 2000). However, this happens

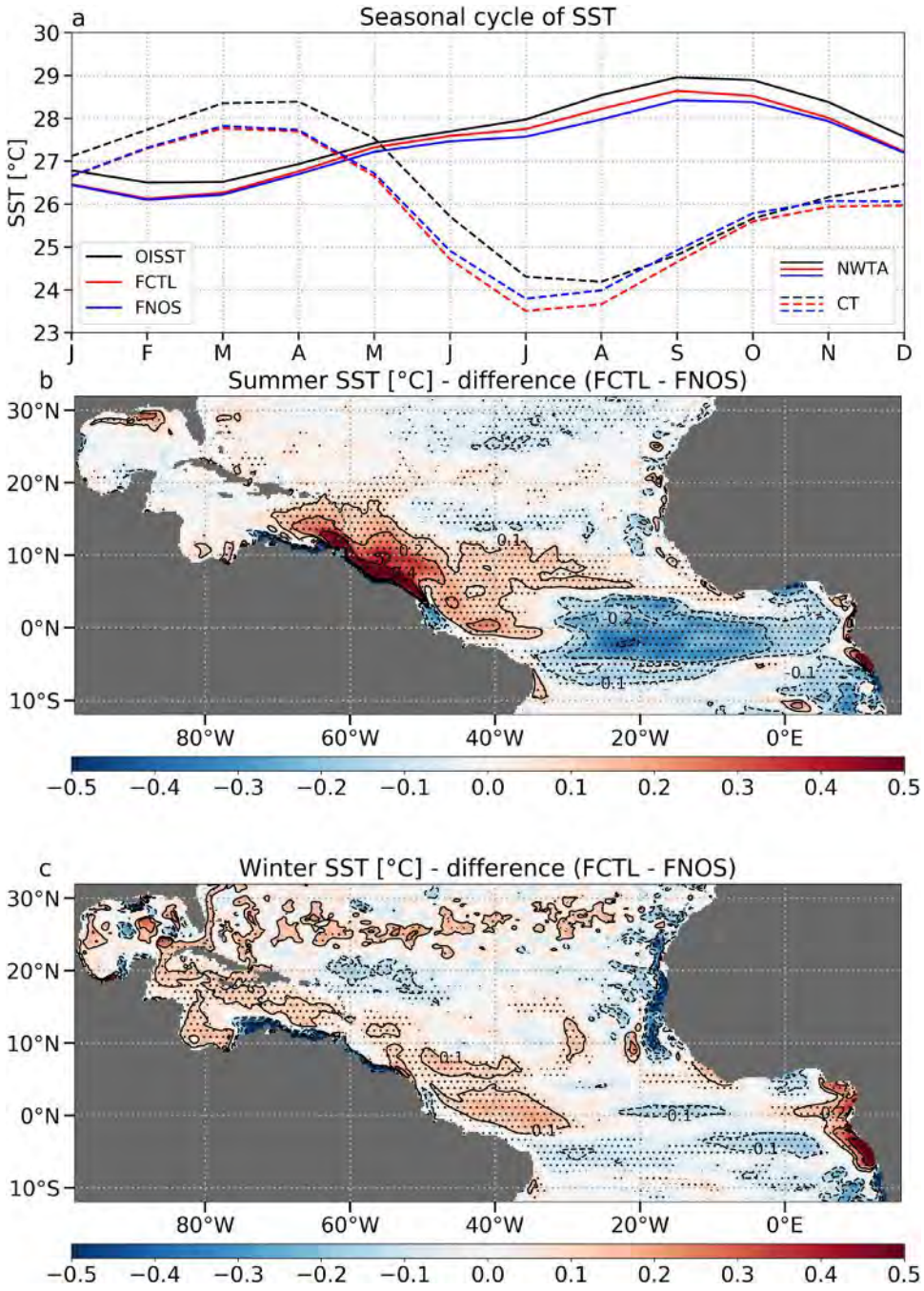

Fig. 11 Same as Fig. 2, but for the forced model

only when the thermocline is sufficiently shallow and when upwelling occurs, i.e. in summer (Keenlyside and Latif 2007; Jouanno et al. 2017). Figure 6b reveals that the period of the CT development spans from June to October. The temporal evolution of the 15 °C–24 °C isotherms also highlights the upwelling period, from May to August, which is consistent with the observations (Wang et al. 2017). Although the adjustment of the thermocline—marked by strong temperature anomalies in subsurface— occurs year-round, temperature anomalies at the surface are important only from June to October, which coincides with the period of the CT development (Fig. 6d). This also corresponds to the period during which the anomaly of temperature trend associated with vertical mixing is the most important, suggesting a connection between the two. One explanation may be that vertical mixing is more efficient with a shallower thermocline, because it implies the mixing of colder water and thus a more efficient heat exchange.

4 Discussion

4.1 Relevance of the coupled approach

A similar experiment was performed by Masson and Delecluse (2001) in the same region, but using an ocean model forced with prescribed air–sea fluxes. They did not find any impact of salinity stratification on SST despite large modifications of the MLD. We reproduced this experiment with our ocean configuration, forced with DFS5.2 atmospheric variables (Dussin et al. 2016) and bulk formulations for the surface fluxes instead of being coupled with WRF. DFS5.2 is based on ERA Interim reanalysis (Dee et al. 2011) and consists of 3-hourly fields of wind speed, atmospheric temperature and humidity, and daily fields of longwave radiation, shortwave radiation and precipitation. In that case, the changes in SST are similar, although weaker than those obtained with the coupled model (Figs. 2, 11). This result differs from Masson and Delecluse (2001), which might be explained by the use of a different vertical mixing scheme and vertical resolution.

Despite the similar results between the forced model and the coupled model, it is necessary to use the latter. Indeed, not all the processes at stake are represented when using a bulk formulation for air–sea fluxes: the shortwave radiation is prescribed, and the feedback of SST on atmospheric deep convection observed in the coupled model is obviously not taken into account. Moreover, using bulk formulations induces by definition an indirect nudging toward the surface air temperature, mainly through latent heat flux (not shown). We saw in Fig. 8 that latent heat fluxes dominate the net air–sea feedback. This can explain why SST changes are very similar in the forced and the coupled models.

The negative feedback of atmospheric fluxes through a decrease in latent heat flux and shortwave radiation is consistent with Krishnamohan et al. (2019), who conducted similar sensitivity simulations to salinity stratification in the Bay of Bengal. However, in their case, the air–sea heat fluxes completely compensate for the decrease in vertical mixing, leading to insignificant SST change in this area: this suggests that the impact of salinity stratification results from a subtle balance whose sign depends on the region considered.

4.2 Sensitivity of NWTA SST to salinity stratification: no impact of the barrier layer

Previous studies investigating the impact of salinity stratification on SST in the NWTA have all focused on the importance of BL (see paragraph 2.5.4 for the definition of the BLT). A BL inhibits vertical mixing: thus the presence of a BL can decrease the cooling induced by mixing and warm the surface (Pailler et al. 1999; Foltz and McPhaden 2009). However, as revealed in Fig. 3c, d, such a relationship is not found in our simulations. The simulations reproduce realistically the location and strength of both summer and winter BL (de Boyer Montégut et al. 2007a; Mignot et al. 2007, 2012). Nevertheless, the spatial patterns of summer BLT do not reveal any direct and compelling relationship with the corresponding patterns of SST anomalies. Although the distribution of the SST anomalies in the NWTA is colocalized with thick BL, this is not true for the ITCZ area (40° W–20° W and 0° N–10° N), where there are no SST anomalies despite BL thicker than in the NWTA (Figs. 2b, 3c). This lack of relationship between SST anomalies and BLT is even more marked in winter: SST anomalies are weak and non-significant almost everywhere (Fig. 2c), whereas the BL is at its thickest. This is furthermore confirmed by the distribution of SST differences as a function of BLT in summer (Fig. 4b) and winter (Fig. 4d) that do not exhibit any statistical relationship between the two variables. This result is in contradiction with previous observational studies conducted in the area (Pailler et al. 1999; Foltz and McPhaden 2009), which concluded to a strong warming caused by BL (about 1 °C for Pailler et al. (1999); 1.3 to 1.9 °C for Foltz and McPhaden (2009)). However, our result is in line with modeling studies (Breugem et al. 2008; Balaguru et al. 2012a; Hernandez et al. 2016), which did not reveal any impact of BL on SST. Hernandez et al. (2016) had also shown with a one-dimensional conceptual mixed layer model that SST cooling primarily depends on vertical salinity gradient rather than on BLT, in the NWTA. This model was applied to ocean cooling due to cyclones, but a parallel can be drawn with cooling occurring at seasonal time scales, and their conclusions may be applied to this case. Moreover, the fact that we do not find any significant relationship between BLT and SST differences, while there is one between salinity stratification and SST differences, reinforces the conclusions drawn by Maes and O'Kane (2014). Indeed, Maes and O'Kane (2014) showed that in several regions without any BL, salinity stratification can still be significant and can play an important role in stabilizing the upper layers of the ocean.

5 Summary

In this study, we used a 1/4° coupled ocean–atmosphere model of the tropical Atlantic to evaluate the impact of salinity stratification on the SST. To do so, we performed two simulations: a CONTROL simulation, validated against observations, and a sensitivity test NOS, where the salinity gradient is removed from the Brünt–Väisälä frequency calculation so that salinity stratification is not taken into account in the computation of the vertical mixing. We investigated

the difference (CONTROL minus NOS) of several key variables to assess the impact of salinity stratification, first in the NWTA and then in the CT area. In the NWTA, seasonal changes of SST are observed: a strong increase is observed in summer (0.2–0.5 °C) while no change is found in winter. This seasonal warming primarily results from a strong decrease in cooling due to vertical mixing at the ML base. It affects significantly the tropical Atlantic climate as revealed by a 19% increase of precipitation over the area. The magnitude of the SST increase results from a subtle interplay between a decrease in vertical turbulent cooling and a decrease of atmospheric fluxes and entrainment. A negative feedback from the atmosphere mitigates the SST increase, and can be explained as follows. The SST increase leads on the one hand to an increase of latent heat loss (about − 12 W/m^2 in summer). On the other hand, it results in an enhancement of atmospheric deep convection, leading to a more prominent cloud cover (about 15% increase in summer) and to a decrease in shortwave radiation received by the ocean (about − 5 W/m^2 in summer). These two processes add up to cause a significant decrease in net heat flux (about − 31% in summer), leading to a damping of the SST increase. This damping is total in winter while only partial in summer, explaining the positive SST anomaly observed in summer. A tight relationship between salinity stratification and SST anomalies is found in summer, whereas we could not evidence any relationship between BLT and SST anomalies. It is thus very clear that summer warming in the NWTA is due to the salinity stratification itself, irrespective of the presence of a BL. The impact of salinity stratification on SST in the NWTA revealed by our study is consistent with historical conceptual studies (e.g. Miller 1976), although previous studies using forced ocean numerical models reported little effect of it (e.g. Masson and Delecluse 2001).

Our set of simulations also revealed an important effect of the salinity stratification in the equatorial region: it increases the cooling in the CT, especially in summer during its peak period. This is due to a readjustment of vertical density structure over the whole equatorial basin, leading to a shoaling of the thermocline throughout the year, with larger impact on the SST during summer when the thermocline shoals in the CT area.

One of the limitations of our study is that the magnitude of the responses observed may depend on the numerical choices and on the model configuration used. While we expect the processes at stake to be robust, the balance between all the processes (shown on Fig. 5) which ultimately determine the SST response is expected to be modulated by the use of different sets of parameterizations. A systematic assessment of these sensitivities might deserve further attention.

An interesting lead to dig into is the evolution of the link between salinity stratification and SST in the future: will it be exacerbated under climate change, or on the contrary will it be damped? Several key-parameters of the present study will indeed be affected by climate change. The MLD plays an important role in the relationship between salinity stratification and SST, and it is well known that the increase in temperature due to climate change will impact the MLD through its effect on thermal stratification, especially in the tropics (Bindoff et al. 2019; Capotondi et al. 2012). Besides, the increase in SST, which could locally reach up to 4.5 °C above the present value by 2100 in the tropical Atlantic under the RCP 8.5 scenario (Deppenmeier et al. 2020), is likely to affect the atmospheric deep convection, which is bound to modify the atmospheric feedbacks revealed in this study. The water cycle is expected to amplify in the future (Durack 2015; Zika et al. 2018), even if changes in precipitation remain unclear in the tropics, due to changes in the atmospheric circulation (Chadwick et al. 2013; Huang et al. 2017; Skliris et al. 2020). This could induce changes in runoff, and therefore in salinity stratification, leading to a feedback on SST. Finally, the vertical mixing also influences the response of SST and precipitation to future climate in the tropical Atlantic (Deppenmeier et al. 2020). The way vertical mixing will evolve in the future remains unclear. Our study provides the baseline mechanism, against which the future projections may be investigated.

Acknowledgements We warmly thank Sébastien Masson for the countless fruitful discussions and ideas, as well as for his invaluable advice on the implementation and parameterization of the coupled model. We also thank the two anonymous reviewers for their constructive comments on the manuscript. Computing facilities were provided by GENCI (project GEN7298). NODC (Levitus) WOA98 data are provided by the NOAA/OAR/ESRL PSL, Boulder, Colorado, USA, from their web site at https://psl.noaa.gov/data/gridded/data.nodc.woa98.html.

Data Availability Statement The datasets generated and analysed during the current study are available from the corresponding author on reasonable request.

Declarations

Conflict of interest The authors declare that they have no conflict of interest.

References

Anderson SP, Weller RA, Lukas RB (1996) Surface buoyancy forcing and the mixed layer of the western Pacific warm pool: observations and 1D model results. J Clim 9(12):3056–3085. https://doi.org/10.1175/1520-0442(1996)009<3056:SBFATM>2.0.CO;2

Androulidakis Y, Kourafalou V, Halliwell G, Le Hénaff M, Kang H, Mehari M, Atlas R (2016) Hurricane interaction with the upper ocean in the Amazon-Orinoco plume region. Ocean Dyn 66(12):1559–1588. https://doi.org/10.1007/s10236-016-0997-0

Balaguru K, Chang P, Saravanan R, Jang CJ (2012a) The barrier layer of the Atlantic warmpool: formation mechanism and influence on the mean climate. Tellus A Dyn Meteorol Oceanogr 64(1):18162. https://doi.org/10.3402/tellusa.v64i0.18162

Balaguru K, Chang P, Saravanan R, Leung LR, Xu Z, Li M, Hsieh JS (2012b) Ocean barrier layers effect on tropical cyclone intensification. Proc Nat Acad Sci 109(36):14343–14347. https://doi.org/10.1073/pnas.1201364109

Banzon V, Smith TM, Chin TM, Liu C, Hankins W (2016) A long-term record of blended satellite and in situ sea-surface temperature for climate monitoring, modeling and environmental studies. Earth Syst Sci Data 8(1):165–176. https://doi.org/10.5194/essd-8-165-2016, https://www.earth-syst-sci-data.net/8/165/2016/

Bindoff N, Cheung WW, Kairo J, Arstegui J, Guinder V, Hallberg R, Hilmi N, Jiao N, Karim M, Levin L et al (2019) Changing ocean, marine ecosystems, and dependent communities. In: IPCC special report on the ocean and cryosphere in a changing climate

Breugem WP, Chang P, Jang C, Mignot J, Hazeleger W (2008) Barrier layers and tropical Atlantic SST biases in coupled GCMs. Tellus A Dyna Meteorol Oceanogr 60(5):885–897. https://doi.org/10.1111/j.1600-0870.2008.00343.x

Caniaux G, Giordani H, Redelsperger JL, Guichard F, Key E, Wade M (2011) Coupling between the Atlantic cold tongue and the West African monsoon in boreal spring and summer. J Geophys Res Oceans. https://doi.org/10.1029/2010JC006570

Capotondi A, Alexander MA, Bond NA, Curchitser EN, Scott JD (2012) Enhanced upper ocean stratification with climate change in the CMIP3 models. J Geophys Res Oceans. https://doi.org/10.1029/2011JC007409

Carton JA, Zhou Z (1997) Annual cycle of sea surface temperature in the tropical Atlantic Ocean. J Geophys Res Oceans 102(C13):27813–27824. https://doi.org/10.1029/97JC02197

Chadwick R, Boutle I, Martin G (2013) Spatial patterns of precipitation change in CMIP5: why the rich do not get richer in the tropics. J Clim 26(11):3803–3822. https://doi.org/10.1175/JCLI-D-12-00543.1

Christian JR, Murtugudde R (2003) Tropical Atlantic variability in a coupled physical-biogeochemical ocean model. Deep Sea Res Part II 50(22):2947–2969. https://doi.org/10.1016/j.dsr2.2003.07.005

Coles VJ, Brooks MT, Hopkins J, Stukel MR, Yager PL, Hood RR (2013) The pathways and properties of the Amazon river plume in the tropical North Atlantic Ocean. J Geophys Res Oceans 118(12):6894–6913. https://doi.org/10.1002/2013JC008981

Crespo LR, Keenlyside N, Koseki S (2019) The role of sea surface temperature in the atmospheric seasonal cycle of the equatorial Atlantic. Clim Dyn 52(9–10):5927–5946. https://doi.org/10.1007/s00382-018-4489-4

Da-Allada CY, Alory G, du Penhoat Y, Kestenare E, Durand F, Hounkonnou NM (2013) Seasonal mixed-layer salinity balance in the tropical Atlantic Ocean: mean state and seasonal cycle. J Geophys Res Oceans 118(1):332–345. https://doi.org/10.1029/2012JC008357

de Boyer Montégut C, Madec G, Fischer AS, Lazar A, Iudicone D (2004) Mixed layer depth over the global ocean: An examination of profile data and a profile-based climatology. J Geophys Res Oceans. https://doi.org/10.1029/2004JC002378

de Boyer Montégut C, Mignot J, Lazar A, Cravatte S (2007a) Control of salinity on the mixed layer depth in the world ocean: 1. General description. J Geophys Res Oceans. https://doi.org/10.1029/2006JC003953

de Boyer Montégut C, Vialard J, Shenoi SSC, Shankar D, Durand F, Ethé C, Madec G (2007b) Simulated seasonal and interannual variability of the mixed layer heat budget in the Northern Indian Ocean. J Clim 20(13):3249–3268. https://doi.org/10.1175/JCLI4148.1

Decharme B, Delire C, Minvielle M, Colin J, Vergnes JP, Alias A, Saint-Martin D, Séférian R, Sénési S, Voldoire A (2019) Recent changes in the ISBA-CTRIP land surface system for use in the CNRM-CM6 climate model and in global off-line hydrological applications. J Adv Model Earth Syst 11(5):1207–1252. https://doi.org/10.1029/2018MS001545

Dee DP, Uppala SM, Simmons A, Berrisford P, Poli P, Kobayashi S, Andrae U, Balmaseda M, Balsamo G, Bauer DP et al (2011) The ERA-Interim reanalysis: configuration and performance of the data assimilation system. Q J R Meteorol Soc 137(656):553–597. https://doi.org/10.1002/qj.828

Deppenmeier AL, Haarsma RJ, LeSager P, Hazeleger W (2020) The effect of vertical ocean mixing on the tropical Atlantic in a coupled global climate model. Clim Dyn 54(11–12):5089–5109. https://doi.org/10.1007/s00382-020-05270-x

Dossa A, Da-Allada C, Herbert G, Bourlès B (2019) Seasonal cycle of the salinity barrier layer revealed in the northeastern Gulf of Guinea. Afr J Mar Sci 41(2):163–175. https://doi.org/10.2989/1814232X.2019.1616612

Durack PJ (2015) Ocean salinity and the global water cycle. Oceanography 28(1):20–31. https://doi.org/10.2307/24861839

Durand F, Shetye SR, Vialard J, Shankar D, Shenoi SSC, Ethe C, Madec G (2004) Impact of temperature inversions on SST evolution in the South-Eastern Arabian Sea during the pre-summer monsoon season. Geophys Res Lett. https://doi.org/10.1029/2003GL018906

Dussin R, Barnier B, Brodeau L, Molines J (2016) The making of the Drakkar forcing set DFS5. DRAKKAR/MyOcean Rep pp 01–04

Ferry N, Parent L, Garric G, Bricaud C, Testut C, Le Galloudec O, Lellouche J, Drevillon M, Greiner E, Barnier B et al (2012) GLORYS2V1 global ocean reanalysis of the altimetric era (1992–2009) at mesoscale. Mercator Ocean Q Newsl 44

Foltz GR, McPhaden MJ (2009) Impact of barrier layer thickness on SST in the central tropical North Atlantic. J Clim 22(2):285–299. https://doi.org/10.1175/2008JCLI2308.1

Foltz GR, Schmid C, Lumpkin R (2015) Transport of surface freshwater from the equatorial to the subtropical North Atlantic Ocean. J Phys Oceanogr 45(4):1086–1102. https://doi.org/10.1175/JPO-D-14-0189.1

Foltz GR, Brandt P, Richter I, Rodriguez-fonseca B, Hernandez F, Dengler M, Rodrigues RR, Schmidt JO, Yu L, Lefevre N et al (2019) The tropical Atlantic observing system. Front Mar Sci 6:206. https://doi.org/10.3389/fmars.2019.00206

Gaillard F, Reynaud T, Thierry V, Kolodziejczyk N, von Schuckmann K (2016) In situ-based reanalysis of the global ocean temperature and salinity with ISAS: variability of the heat content and steric height. J Clim 29(4):1305–1323. https://doi.org/10.1175/JCLI-D-15-0028.1

Giannini A, Saravanan R, Chang P (2004) The preconditioning role of tropical Atlantic variability in the development of the ENSO teleconnection: Implications for the prediction of Nordeste rainfall. Clim Dyn 22(8):839–855. https://doi.org/10.1007/s00382-004-0420-2

Giffard P, Llovel W, Jouanno J, Morvan G, Decharme B (2019) Contribution of the Amazon river discharge to regional sea level in the tropical Atlantic Ocean. Water 11(11):2348. https://doi.org/10.3390/w11112348

Godfrey JS, Lindstrom EJ (1989) The heat budget of the equatorial western Pacific surface mixed layer. J Geophys Res Oceans 94(C6):8007–8017. https://doi.org/10.1029/JC094iC06p08007

Grodsky SA, Reul N, Lagerloef G, Reverdin G, Carton JA, Chapron B, Quilfen Y, Kudryavtsev VN, Kao HY (2012) Haline hurricane wake in the Amazon/Orinoco plume: AQUARIUS/SACD and SMOS observations. Geophys Res Lett. https://doi.org/10.1029/2012GL053335

Grodsky SA, Vandemark D, Feng H (2018) Assessing coastal SMAP surface salinity accuracy and its application to monitoring Gulf of Maine circulation dynamics. Remote Sens 10(8):1232. https://doi.org/10.3390/rs10081232

Hernandez O, Jouanno J, Durand F (2016) Do the Amazon and Orinoco freshwater plumes really matter for hurricane-induced ocean surface cooling? J Geophys Res Oceans 121(4):2119–2141. https://doi.org/10.1002/2015JC011021

Hernandez O, Jouanno J, Echevin V, Aumont O (2017) Modification of sea surface temperature by chlorophyll concentration in the Atlantic upwelling systems. J Geophys Res Oceans 122(7):5367–5389. https://doi.org/10.1002/2016JC012330

Hong SY, Lim JOJ (2006) The WRF single-moment 6-class microphysics scheme (WSM6). Asia Pac J Atmos Sci 42(2):129–151

Hong SY, Noh Y, Dudhia J (2006) A new vertical diffusion package with an explicit treatment of entrainment processes. Mon Weather Rev 134(9):2318–2341. https://doi.org/10.1175/MWR3199.1

Huang P, Chen D, Ying J (2017) Weakening of the tropical atmospheric circulation response to local sea surface temperature anomalies under global warming. J Clim 30(20):8149–8158. https://doi.org/10.1175/JCLI-D-17-0171.1

Huffman GJ, Bolvin DT, Nelkin EJ, Wolff DB, Adler RF, Gu G, Hong Y, Bowman KP, Stocker EF (2007) The TRMM multisatellite precipitation analysis (TMPA): quasi-global, multiyear, combined-sensor precipitation estimates at fine scales. J Hydrometeorol 8(1):38–55. https://doi.org/10.1175/JHM560.1

Iacono MJ (2011) Application of improved radiation modeling to general circulation models. https://doi.org/10.2172/1010861

Jiménez PA, Dudhia J, Gonzélez-Rouco JF, Navarro J, Montávez JP, García-Bustamante E (2012) A revised scheme for the WRF surface layer formulation. Mon Weather Rev 140(3):898–918. https://doi.org/10.1175/MWR-D-11-00056.1

Jouanno J, Hernandez O, Sanchez-Gomez E (2017) Equatorial Atlantic interannual variability and its relation to dynamic and thermodynamic processes. Earth Syst Dyn 8(4):1061. https://doi.org/10.5194/esd-8-1061-2017

Jousse A, Hall A, Sun F, Teixeira J (2016) Causes of WRF surface energy fluxes biases in a stratocumulus region. Clim Dyn 46(1–2):571–584. https://doi.org/10.1007/s00382-015-2599-9

Keenlyside NS, Latif M (2007) Understanding equatorial Atlantic interannual variability. J Clim 20(1):131–142. https://doi.org/10.1175/JCLI3992.1

Kolodziejczyk N, Prigent-Mazella A, Gaillard F (2017) ISAS-15 temperature and salinity gridded fields. https://doi.org/10.17882/52367

Krishnamohan K, Vialard J, Lengaigne M, Masson S, Samson G, Pous S, Neetu S, Durand F, Shenoi S, Madec G (2019) Is there an effect of Bay of Bengal salinity on the northern Indian Ocean climatological rainfall? Deep Sea Res Part II 166:19–33. https://doi.org/10.1016/j.dsr2.2019.04.003

Kumar BP, Vialard J, Lengaigne M, Murty V, Mcphaden MJ (2012) Tropflux: Air-sea fluxes for the global tropical oceans - description and evaluation. Clim Dyn 38(7–8):1521–1543. https://doi.org/10.1007/s00382-011-1115-0

Kumar BP, Cronin MF, Joseph S, Ravichandran M, Sureshkumar N (2017) Latent heat flux sensitivity to sea surface temperature: regional perspectives. J Clim 30(1):129–143. https://doi.org/10.1175/JCLI-D-16-0285.1

Large WG, Yeager SG (2009) The global climatology of an interannually varying air-sea flux data set. Clim Dyn 33(2–3):341–364. https://doi.org/10.1007/s00382-008-0441-3

Latif M, Grötzner A (2000) The equatorial Atlantic oscillation and its response to ENSO. Clim Dyn 16(2–3):213–218. https://doi.org/10.1007/s003820050014

Lewis MR, Carr ME, Feldman GC, Esaias W, McClain C (1990) Influence of penetrating solar radiation on the heat budget of the equatorial Pacific Ocean. Nature 347(6293):543–545. https://doi.org/10.1038/347543a0

Lukas R, Lindstrom E (1991) The mixed layer of the western equatorial Pacific Ocean. J Geophys Res Oceans 96(S01):3343–3357. https://doi.org/10.1029/90JC01951

Lübbecke JF, Rodríguez-Fonseca B, Richter I, Martín-Rey M, Losada T, Polo I, Keenlyside NS (2018) Equatorial Atlantic variability–Modes, mechanisms, and global teleconnections. WIREs Clim Change 9(4): https://doi.org/10.1002/wcc.527

Madec G, the NEMO team (2016) NEMO ocean engine. Note du Pôle de modélisation, Institut Pierre-Simon Laplace (IPSL). France 27:1288–1619

Maes C, O'Kane TJ (2014) Seasonal variations of the upper ocean salinity stratification in the tropics. J Geophys Res Oceans 119(3):1706–1722. https://doi.org/10.1002/2013JC009366

Masson S, Delecluse P (2001) Influence of the Amazon river runoff on the tropical Atlantic. Phys Chem Earth Part B 26(2):137–142. https://doi.org/10.1016/S1464-1909(00)00230-6

Masson S, Luo JJ, Madec G, Vialard J, Durand F, Gualdi S, Guilyardi E, Behera S, Delecluse P, Navarra A, Yamagata T (2005) Impact of barrier layer on winter-spring variability of the southeastern Arabian Sea. Geophys Res Lett. https://doi.org/10.1029/2004GL021980

McClain CR, Cleave ML, Feldman GC, Gregg WW, Hooker SB, Kuring N (1998) Science quality SeaWiFS data for global biosphere research. Sea Technol 39:10–16

Meissner T, Wentz FJ, Manaster A, Lindsley R (2019) Remote sensing system SMAP level 3 sea surface salinity standard mapped image monthly v4.0 validated dataset. https://doi.org/10.5067/SMP40-3SMCS; https://podaac.jpl.nasa.gov/dataset/SMAP_RSS_L3_SSS_SMI_MONTHLY_V4

Menkes CER, Vialard JG, Kennan SC, Boulanger JP, Madec GV (2006) A modeling study of the impact of tropical instability waves on the heat budget of the Eastern Equatorial Pacific. J Phys Oceanogr 36(5):847–865. https://doi.org/10.1175/JPO2904.1

Meynadier R, de Coëtlogon G, Bastin S, Eymard L, Janicot S (2015) Sensitivity testing of WRF parameterizations on air-sea interaction and its impact on water cycle in the Gulf of Guinea. Q J R Meteorol Soc 141(690):1804–1820. https://doi.org/10.1002/qj.2483

Meynadier R, de Coëtlogon G, Leduc-Leballeur M, Eymard L, Janicot S (2016) Seasonal influence of the sea surface temperature on the low atmospheric circulation and precipitation in the eastern equatorial Atlantic. Clim Dyn 47(3–4):1127–1142. https://doi.org/10.1007/s00382-015-2892-7

Mignot J, de Boyer Montégut C, Lazar A, Cravatte S (2007) Control of salinity on the mixed layer depth in the world ocean: 2 Tropical areas. J Geophys Res Oceans. https://doi.org/10.1029/2006JC003954

Mignot J, de Boyer Montégut C, Tomczak M (2009) On the porosity of barrier layers. Ocean Sci 5(3):379–387. https://doi.org/10.5194/os-5-379-2009

Mignot J, Lazar A, Lacarra M (2012) On the formation of barrier layers and associated vertical temperature inversions: a focus on the northwestern tropical Atlantic. J Geophys Res Oceans. https://doi.org/10.1029/2011JC007435

Miller JR (1976) The salinity effect in a mixed layer ocean model. J Phys Oceanogr 6(1):29–35. https://doi.org/10.1175/1520-0485(1976)006<0029:TSEIAM>2.0.CO;2

Nagura M, Terao T, Hashizume M (2015) The role of temperature inversions in the generation of seasonal and interannual SST variability in the far northern bay of Bengal. J Clim 28(9):3671–3693. https://doi.org/10.1175/JCLI-D-14-00553.1

Newinger C, Toumi R (2015) Potential impact of the colored Amazon and Orinoco plume on tropical cyclone intensity. J Geophys Res Oceans 120(2):1296–1317. https://doi.org/10.1002/2014JC010533

Niu GY, Yang ZL, Mitchell KE, Chen F, Ek MB, Barlage M, Kumar A, Manning K, Niyogi D, Rosero E et al (2011) The community Noah land surface model with multiparameterization options (Noah-MP): 1 Model description and evaluation with local-scale measurements. J Geophys Res Atmos. https://doi.org/10.1029/2010JD015139

Pailler K, Bourlès B, Gouriou Y (1999) The barrier layer in the western tropical Atlantic Ocean. Geophys Res Lett 26(14):2069–2072. https://doi.org/10.1029/1999GL900492

Peter AC, Le Hénaff M, du Penhoat Y, Menkes CE, Marin F, Vialard J, Caniaux G, Lazar A (2006) A model study of the seasonal mixed layer heat budget in the equatorial Atlantic. J Geophys Res Oceans. https://doi.org/10.1029/2005JC003157

Radenac MH, Jouanno J, Tchamabi CC, Awo M, Bourles B, Arnault S, Aumont O (2020) Physical drivers of the nitrate seasonal variability in the Atlantic cold tongue. Biogeosciences. https://doi.org/10.5194/bg-17-529-2020

Reffray G, Bourdalle-Badie R, Calone C (2015) Modelling turbulent vertical mixing sensitivity using a 1-D version of NEMO. Geosci Model Dev. https://doi.org/10.5194/gmd-8-69-2015

Renault L, Masson S, Oerder V, Jullien S, Colas F (2019) Disentangling the mesoscale ocean-atmosphere interactions. J Geophys Res Oceans 124(3):2164–2178. https://doi.org/10.1029/2018JC014628

Reul N, Fournier S, Boutin J, Hernandez O, Maes C, Chapron B, Alory G, Quilfen Y, Tenerelli J, Morisset S et al (2014) Sea surface salinity observations from space with the SMOS satellite: a new means to monitor the marine branch of the water cycle. Surv Geophys 35(3):681–722. https://doi.org/10.1007/s10712-013-9244-0

Richter I, Tokinaga H (2020) An overview of the performance of CMIP6 models in the tropical Atlantic: mean state, variability, and remote impacts. Clim Dyn 55(9):2579–2601. https://doi.org/10.1007/s00382-020-05409-w

Richter I, Xie SP (2008) On the origin of equatorial Atlantic biases in coupled general circulation models. Clim Dyn 31(5):587–598. https://doi.org/10.1007/s00382-008-0364-z

Richter I, Xie SP, Wittenberg AT, Masumoto Y (2012) Tropical Atlantic biases and their relation to surface wind stress and terrestrial precipitation. Clim Dyn 38(5–6):985–1001. https://doi.org/10.1007/s00382-011-1038-9

Richter I, Xie SP, Behera SK, Doi T, Masumoto Y (2014) Equatorial Atlantic variability and its relation to mean state biases in CMIP5. Clim Dyn 42(1–2):171–188. https://doi.org/10.1007/s00382-012-1624-5

Sabin TP, Babu CA, Joseph PV (2013) SST-convection relation over tropical oceans. Int J Climatol 33(6):1424–1435. https://doi.org/10.1002/joc.3522

Samson G, Masson S, Lengaigne M, Keerthi MG, Vialard J, Pous S, Madec G, Jourdain NC, Jullien S, Menkès C et al (2014) The NOW regional coupled model: Application to the tropical Indian Ocean climate and tropical cyclone activity. Journal of Advances in Modeling Earth Systems 6(3):700–722. https://doi.org/10.1002/2014MS000324

Samson G, Masson S, Durand F, Terray P, Berthet S, Jullien S (2017) Roles of land surface albedo and horizontal resolution on the Indian summer monsoon biases in a coupled ocean-atmosphere tropical-channel model. Clim Dyn 48(5–6):1571–1594. https://doi.org/10.1007/s00382-016-3161-0

Schaaf C, Liu J, Gao F, Strahler AH (2011) MODIS albedo and reflectance anisotropy products from Aqua and Terra. Land Remote Sens Glob Environ Change NASA Earth Observ Syst Sci ASTER MODIS 11:549–561. https://doi.org/10.1007/978-1-4419-6749-7

Siongco AC, Hohenegger C, Stevens B (2015) The Atlantic ITCZ bias in CMIP5 models. Clim Dyn 45(5–6):1169–1180. https://doi.org/10.1007/s00382-014-2366-3

Skamarock WC, Klemp JB (2008) A time-split nonhydrostatic atmospheric model for weather research and forecasting applications. J Comput Phys 227(7):3465–3485. https://doi.org/10.1016/j.jcp.2007.01.037

Skliris N, Marsh R, Mecking J, Zika JD (2020) Changing water cycle and freshwater transports in the Atlantic Ocean in observations and CMIP5 models. Clim Dyn 54:4971–4989. https://doi.org/10.1007/s00382-020-05261-y

Sprintall J, Tomczak M (1992) Evidence of the barrier layer in the surface layer of the tropics. J Geophys Res Oceans 97(C5):7305–7316. https://doi.org/10.1029/92JC00407

Tchilibou M, Delcroix T, Alory G, Arnault S, Reverdin G (2015) Variations of the tropical Atlantic and Pacific SSS minimum zones and their relations to the ITCZ and SPCZ rain bands (1979–2009). J Geophys Res Oceans 120(7):5090–5100. https://doi.org/10.1002/2015JC010836

Tian B, Dong X (2020) The double-ITCZ bias in CMIP3, CMIP5, and CMIP6 models based on annual mean precipitation. Geophys Res Lett 47(8):e2020GL087232. https://doi.org/10.1029/2020GL087232

Toniazzo T, Woolnough S (2014) Development of warm SST errors in the southern tropical Atlantic in CMIP5 decadal hindcasts. Clim Dyn 43(11):2889–2913. https://doi.org/10.1007/s00382-013-1691-2

Valcke S (2013) The OASIS3 coupler: a European climate modelling community software. Geosci Model Dev 6(2):373. https://doi.org/10.5194/gmd-6-373-2013

Vialard J, Delecluse P (1998) An OGCM study for the TOGA decade. part I: Role of salinity in the physics of the Western Pacific fresh pool. J Phys Oceanogr 28(6):1071–1088. https://doi.org/10.1175/1520-0485(1998)028<1071:AOSFTT>2.0.CO;2

Vimont DJ, Kossin JP (2007) The Atlantic Meridional Mode and hurricane activity. Geophys Res Lett. https://doi.org/10.1029/2007GL029683

Wang C, Lee SK, Enfield DB (2008) Atlantic warm pool acting as a link between Atlantic Multidecadal Oscillation and Atlantic tropical cyclone activity. Geochem Geophys Geosyst. https://doi.org/10.1029/2007GC001809

Wang LC, Jin FF, Wu CR, Hsu HH (2017) Dynamics of upwelling annual cycle in the equatorial Atlantic Ocean. Geophys Res Lett 44(8):3737–3743. https://doi.org/10.1002/2017GL072588

Xie SP (2009) Ocean-atmosphere interaction and tropical climate. The Encyclopedia of Life Support Systems (EOLSS). Trop Meteorol 13

Xu Z, Chang P, Richter I, Tang G (2014) Diagnosing southeast tropical Atlantic SST and ocean circulation biases in the CMIP5 ensemble. Clim Dyn 43(11):3123–3145. https://doi.org/10.1007/s00382-014-2247-9

Yan Y, Li L, Wang C (2017) The effects of oceanic barrier layer on the upper ocean response to tropical cyclones. J Geophys Res Oceans 122(6):4829–4844. https://doi.org/10.1002/2017JC012694

Yu L, Jin X, Weller RA (2008) Multidecade global flux datasets from the objectively analyzed air-sea fluxes (OAFlux) project: Latent and sensible heat fluxes, ocean evaporation, and related surface meteorological variables. Woods Hole Oceanographic Institution, OAFlux Project Tech Rep OA-2008-01 74, http://oaflux.whoi.edu/

Zheng Y, Alapaty K, Herwehe JA, Del Genio AD, Niyogi D (2016) Improving high-resolution weather forecasts using the Weather Research and Forecasting (WRF) model with an updated Kain-Fritsch scheme. Mon Weather Rev 144(3):833–860. https://doi.org/10.1175/MWR-D-15-0005.1

Zika JD, Skliris N, Blaker AT, Marsh R, Nurser AG, Josey SA (2018) Improved estimates of water cycle change from ocean salinity: the key role of ocean warming. Environ Res Lett 13(7):074036. https://doi.org/10.1088/1748-9326/aace42

Bibliography

Adachi, S.A., Tomita, H., 2020. Methodology of the constraint condition in dynamical downscaling for regional climate evaluation: A review. Journal of Geophysical Research: Atmospheres 125. doi:10.1029/2019jd032166.

Allan, R., Barlow, M., Byrne, M.P., Cherchi, A., Douville, H., Fowler, H.J., Gan, T.Y., Pendergrass, A.G., Rosenfeld, D., Swann, A.L., et al., 2020. Advances in understanding large-scale responses of the water cycle to climate change. Annals of the New York Academy of Sciences doi:10.1111/nyas.14337.

Androulidakis, Y., Kourafalou, V., Halliwell, G., Le Hénaff, M., Kang, H., Mehari, M., Atlas, R., 2016. Hurricane interaction with the upper ocean in the Amazon-Orinoco plume region. Ocean Dynamics 66, 1559–1588. doi:10.1007/s10236-016-0997-0.

Arias, P.A., Bellouin, N., Coppola, E., Jones, R.G., Krinner, G., Marotzke, J., Naik, V., Palmer, M.D., Plattner, G.K., Rogelj, J., Rojas, M., Sillmann, J., Storelvmo, T., Thorne, P.W., Trewin, B., et al., 2021. Technical Summary. In: Climate Change 2021: The Physical Science Basis. Contribution of Working Group I to the Sixth Assessment Report of the Intergovernmental Panel on Climate Change. Cambridge University Press. In Press.

Awo, F.M., Alory, G., Da-Allada, C.Y., Delcroix, T., Jouanno, J., Kestenare, E., Baloïtcha, E., 2018. Sea surface salinity signature of the tropical Atlantic interannual climatic modes. Journal of Geophysical Research: Oceans 123, 7420–7437. doi:10.1029/2018jc013837.

Balaguru, K., Chang, P., Saravanan, R., Jang, C.J., 2012a. The barrier layer of the Atlantic warmpool: formation mechanism and influence on the mean climate. Tellus A: Dynamic Meteorology and Oceanography 64, 18162. doi:10.3402/tellusa.v64i0.18162.

Balaguru, K., Chang, P., Saravanan, R., Leung, L.R., Xu, Z., Li, M., Hsieh, J.S., 2012b. Ocean barrier layers' effect on tropical cyclone intensification. Proceedings of the National Academy of Sciences 109, 14343–14347. doi:10.1073/pnas.1201364109.

Balaguru, K., Foltz, G.R., Leung, L.R., Kaplan, J., Xu, W., Reul, N., Chapron, B., 2020. Pronounced impact of salinity on rapidly intensifying tropical cyclones. Bulletin of the American Meteorological Society 101, E1497–E1511. doi:10.1175/BAMS-D-19-0303.1.

Banzon, V., Smith, T.M., Chin, T.M., Liu, C., Hankins, W., 2016. A long-term record of blended satellite and in situ sea-surface temperature for climate monitoring, modeling and environmental studies. Earth System Science Data 8, 165–176. URL: https://www.earth-syst-sci-data.net/8/165/2016/, doi:10.5194/essd-8-165-2016.

Barichivich, J., Gloor, E., Peylin, P., Brienen, R.J., Schöngart, J., Espinoza, J.C., Pattnayak, K.C., 2018. Recent intensification of Amazon flooding extremes driven by strengthened Walker circulation. Science advances 4. doi:10.1126/sciadv.aat8785.

Behrenfeld, M.J., O'Malley, R.T., Siegel, D.A., McClain, C.R., Sarmiento, J.L., Feldman, G.C., Milligan, A.J., Falkowski, P.G., Letelier, R.M., Boss, E.S., 2006. Climate-driven trends in contemporary ocean productivity. Nature 444, 752–755. doi:10.1038/nature05317.

Berger, H., Treguier, A.M., Perenne, N., Talandier, C., 2014. Dynamical contribution to sea surface salinity variations in the eastern Gulf of Guinea based on numerical modelling. Climate dynamics 43, 3105–3122. doi:10.1007/s00382-014-2195-4.

Bessières, L., Leroux, S., Brankart, J.M., Molines, J.M., Moine, M.P., Bouttier, P.A., Penduff, T., Terray, L., Barnier, B., Sérazin, G., 2017. Development of a probabilistic ocean modelling system based on NEMO 3.5: application at eddying resolution. Geoscientific Model Development 10, 1091–1106. doi:10.5194/gmd-10-1091-2017.

Betts, A., Miller, M., 1986. A new convective adjustment scheme. Part II: Single column tests using gate wave, bomex, atex and arctic air-mass data sets. Quarterly Journal of the Royal Meteorological Society 112, 693–709. doi:10.1002/qj.49711247308.

Bindoff, N., Cheung, W.W., Kairo, J., Arstegui, J., Guinder, V., Hallberg, R., Hilmi, N., Jiao, N., Karim, M., Levin, L., et al., 2019. Changing ocean, marine ecosystems, and dependent communities. In: IPCC special report on the ocean and cryosphere in a changing climate.

Bjerknes, J., 1969. Atmospheric teleconnections from the equatorial Pacific. Monthly Weather Review 97, 163–172. doi:10.1175/1520-0493(1969)097<0163:ATFTEP>2.3.CO;2.

Boisier, J.P., Ciais, P., Ducharne, A., Guimberteau, M., 2015. Projected strengthening of Amazonian dry season by constrained climate model simulations. Nature Climate Change 5, 656–660. doi:10.1038/nclimate2658.

Bopp, L., Resplandy, L., Orr, J.C., Doney, S.C., Dunne, J.P., Gehlen, M., Halloran, P., Heinze, C., Ilyina, T., Séférian, R., Tjiputra, J., Vichi, M., 2013. Multiple stressors of ocean ecosystems in the 21st century: projections with CMIP5 models. Biogeosciences 10, 6225–6245. doi:10.5194/bg-10-6225-2013.

Bourles, B., Molinari, R.L., Johns, E., Wilson, W.D., Leaman, K.D., 1999. Upper layer currents in the western tropical North Atlantic (1989–1991). Journal of Geophysical Research: Oceans 104, 1361–1375. doi:10.1029/1998JC900025.

Boutin, J., Chao, Y., Asher, W.E., Delcroix, T., Drucker, R., Drushka, K., Kolodziejczyk, N., Lee, T., Reul, N., Reverdin, G., et al., 2016. Satellite and in situ salinity: Understanding near-surface stratification and subfootprint variability. Bulletin of the American Meteorological Society 97, 1391–1407. doi:10.1175/BAMS-D-15-00032.1.

Boutin, J., Vergely, J.L., Khvorostyanov, D., 2020. SMOS SSS L3 maps generated by CATDS CEC LOCEAN, debias v5.0 doi:10.17882/52804.

Boutin, J., Vergely, J.L., Marchand, S., d'Amico, F., Hasson, A., Kolodziejczyk, N., Reul, N., Reverdin, G., Vialard, J., 2018. New SMOS sea surface salinity with reduced systematic errors and improved variability. Remote Sensing of Environment 214, 115–134. doi:10.1016/j.rse.2018.05.022.

Boyce, D.G., Lewis, M.R., Worm, B., 2010. Global phytoplankton decline over the past century. Nature 466, 591–596. doi:10.1038/nature09268.

de Boyer Montégut, C., Madec, G., Fischer, A.S., Lazar, A., Iudicone, D., 2004. Mixed layer depth over the global ocean: An examination of profile data and a profile-based climatology. Journal of Geophysical Research: Oceans 109. doi:10.1029/2004JC002378.

de Boyer Montégut, C., Mignot, J., Lazar, A., Cravatte, S., 2007a. Control of salinity on the mixed layer depth in the world ocean: 1. General description. Journal of Geophysical Research: Oceans 112. doi:10.1029/2006JC003953.

de Boyer Montégut, C., Vialard, J., Shenoi, S.S.C., Shankar, D., Durand, F., Ethé, C., Madec, G., 2007b. Simulated seasonal and interannual variability of the mixed layer heat budget in the Northern Indian Ocean. Journal of Climate 20, 3249–3268. doi:10.1175/JCLI4148.1.

Brêda, J.P.L.F., de Paiva, R.C.D., Collischon, W., Bravo, J.M., Siqueira, V.A., Steinke, E.B., 2020. Climate change impacts on South American water balance from a continental-scale hydrological model driven by CMIP5 projections. Climatic Change 159, 503–522. doi:10.1007/s10584-020-02667-9.

Breugem, W.P., Chang, P., Jang, C., Mignot, J., Hazeleger, W., 2008. Barrier layers and tropical Atlantic SST biases in coupled GCMs. Tellus A: Dynamic Meteorology and Oceanography 60, 885–897. doi:10.1111/j.1600-0870.2008.00343.x.

Cabos, W., Sein, D.V., Durán-Quesada, A., Liguori, G., Koldunov, N.V., Martínez-López, B., Alvarez, F., Sieck, K., Limareva, N., Pinto, J.G., 2018. Dynamical downscaling of historical climate over CORDEX Central America domain with a regionally coupled atmosphere–ocean model. Climate Dynamics 52, 4305–4328. doi:10.1007/s00382-018-4381-2.

Camara, I., Kolodziejczyk, N., Mignot, J., Lazar, A., Gaye, A.T., 2015. On the seasonal variations of salinity of the tropical Atlantic mixed layer. Journal of Geophysical Research: Oceans 120, 4441–4462. doi:10.1002/2015JC010865.

Caniaux, G., Giordani, H., Redelsperger, J.L., Guichard, F., Key, E., Wade, M., 2011. Coupling between the Atlantic cold tongue and the West African monsoon in boreal spring and summer. Journal of Geophysical Research: Oceans 116. doi:10.1029/2010JC006570.

Capotondi, A., Alexander, M.A., Bond, N.A., Curchitser, E.N., Scott, J.D., 2012. Enhanced upper ocean stratification with climate change in the CMIP3 models. Journal of Geophysical Research: Oceans 117. doi:10.1029/2011JC007409.

Carton, J.A., 1991. Effect of seasonal surface freshwater flux on sea surface temperature in the tropical Atlantic Ocean. Journal of Geophysical Research: Oceans 96, 12593–12598. doi:10.1029/91JC01256.

Carton, J.A., Cao, X., Giese, B.S., Da Silva, A.M., 1996. Decadal and interannual sst variability in the tropical atlantic ocean. Journal of Physical Oceanography 26, 1165–1175. doi:10.1175/1520-0485(1996)026<1165:DAISVI>2.0.CO;2.

Carton, J.A., Zhou, Z., 1997. Annual cycle of sea surface temperature in the tropical Atlantic Ocean. Journal of Geophysical Research: Oceans 102, 27813–27824. doi:10.1029/97JC02197.

Chadwick, R., Boutle, I., Martin, G., 2013. Spatial patterns of precipitation change in CMIP5: Why the rich do not get richer in the tropics. Journal of Climate 26, 3803–3822. doi:10.1175/JCLI-D-12-00543.1.

Chadwick, R., Good, P., Martin, G., Rowell, D.P., 2015. Large rainfall changes consistently projected over substantial areas of tropical land. Nature Climate Change 6, 177–181. doi:10.1038/nclimate2805.

Chang, P., Ji, L., Li, H., 1997. A decadal climate variation in the tropical Atlantic Ocean from thermodynamic air-sea interactions. Nature 385, 516–518. doi:10.1038/385516a0.

Chiang, J.C., Vimont, D.J., 2004. Analogous Pacific and Atlantic meridional modes of tropical atmosphere–ocean variability. Journal of Climate 17, 4143–4158. doi:10.1175/JCLI4953.1.

Chou, M.D., 1992. A solar radiation model for use in climate studies. Journal of Atmospheric Sciences 49, 762–772. doi:10.1175/1520-0469(1992)049<0762:ASRMFU>2.0.CO;2.

Chou, M.D., Suarez, M.J., 1999. A solar radiation parameterization for atmospheric studies. volume 15. National Aeronautics and Space Administration, Goddard Space Flight Center.

Chou, M.D., Suarez, M.J., Liang, X.Z., Yan, M.M.H., Cote, C., 2001. A thermal infrared radiation parameterization for atmospheric studies. volume 19. National Aeronautics and Space Administration, Goddard Space Flight Center.

Christian, J.R., Murtugudde, R., 2003. Tropical Atlantic variability in a coupled physical–biogeochemical ocean model. Deep Sea Research Part II: Topical Studies in Oceanography 50, 2947 – 2969. doi:10.1016/j.dsr2.2003.07.005.

Coles, V.J., Brooks, M.T., Hopkins, J., Stukel, M.R., Yager, P.L., Hood, R.R., 2013. The pathways and properties of the Amazon river plume in the tropical North Atlantic Ocean. Journal of Geophysical Research: Oceans 118, 6894–6913. doi:10.1002/2013JC008981.

Cook, B., Zeng, N., Yoon, J.H., 2012. Will Amazonia dry out? magnitude and causes of change from IPCC climate model projections. Earth Interactions 16, 1–27. doi:10.1175/2011ei398.1.

Crespo, L.R., Keenlyside, N., Koseki, S., 2019. The role of sea surface temperature in the atmospheric seasonal cycle of the equatorial Atlantic. Climate Dynamics 52, 5927–5946. doi:10.1007/s00382-018-4489-4.

Cronin, M.F., McPhaden, M.J., 2002. Barrier layer formation during westerly wind bursts. Journal of Geophysical Research: Oceans 107, SRF 21–1–SRF 21–12. doi:10.1029/2001jc001171.

Da-Allada, C.Y., Alory, G., du Penhoat, Y., Kestenare, E., Durand, F., Hounkonnou, N.M., 2013. Seasonal mixed-layer salinity balance in the tropical Atlantic Ocean: Mean state and seasonal cycle. Journal of Geophysical Research: Oceans 118, 332–345. doi:10.1029/2012JC008357.

Da-Allada, C.Y., Du Penhoat, Y., Jouanno, J., Alory, G., Hounkonnou, N.M., 2014. Modeled mixed-layer salinity balance in the Gulf of Guinea: Seasonal and interannual variability. Ocean Dynamics 64, 1783–1802. doi:10.1007/s10236-014-0775-9.

Da-Allada, C.Y., Jouanno, J., Gaillard, F., Kolodziejczyk, N., Maes, C., Reul, N., Bourlès, B., 2017. Importance of the Equatorial Undercurrent on the sea surface salinity in the eastern equatorial Atlantic in boreal spring. Journal of Geophysical Research: Oceans 122, 521–538. doi:10.1002/2016JC012342.

Dai, A., Rasmussen, R.M., Ikeda, K., Liu, C., 2017a. A new approach to construct representative future forcing data for dynamic downscaling. Climate Dynamics 55, 315–323. doi:10.1007/s00382-017-3708-8.

Dai, A., Rasmussen, R.M., Liu, C., Ikeda, K., Prein, A.F., 2017b. A new mechanism for warm-season precipitation response to global warming based on convection-permitting simulations. Climate Dynamics 55, 343–368. doi:10.1007/s00382-017-3787-6.

Dai, A., Trenberth, K.E., 2002. Estimates of freshwater discharge from continents: Latitudinal and seasonal variations. Journal of hydrometeorology 3, 660–687. doi:10.1175/1525-7541(2002)003<0660:EOFDFC>2.0.CO;2.

Decharme, B., Delire, C., Minvielle, M., Colin, J., Vergnes, J.P., Alias, A., Saint-Martin, D., Séférian, R., Sénési, S., Voldoire, A., 2019. Recent changes in the ISBA-CTRIP land surface system for use in the CNRM-CM6 climate model and in global off-line hydrological applications. Journal of Advances in Modeling Earth Systems 11, 1207–1252. doi:10.1029/2018MS001545.

Dee, D.P., Uppala, S.M., Simmons, A., Berrisford, P., Poli, P., Kobayashi, S., Andrae, U., Balmaseda, M., Balsamo, G., Bauer, d.P., et al., 2011. The ERA-Interim reanalysis: Configuration and performance of the data assimilation system. Quarterly Journal of the royal meteorological society 137, 553–597. doi:10.1002/qj.828.

Denamiel, C., Budgell, W.P., Toumi, R., 2013. The Congo River plume: Impact of the forcing on the far-field and near-field dynamics. Journal of Geophysical Research: Oceans 118, 964–989. doi:10.1002/jgrc.20062.

Deppenmeier, A.L., Haarsma, R.J., LeSager, P., Hazeleger, W., 2020. The effect of vertical ocean mixing on the tropical Atlantic in a coupled global climate model. Climate Dynamics 54, 5089–5109. doi:10.1007/s00382-020-05270-x.

Deser, C., Terray, L., Phillips, A.S., 2016. Forced and internal components of winter air temperature trends over North America during the past 50 years: Mechanisms and implications. Journal of Climate 29, 2237–2258. doi:10.1175/jcli-d-15-0304.1.

Dossa, A., Da-Allada, C., Herbert, G., Bourlès, B., 2019. Seasonal cycle of the salinity barrier layer revealed in the northeastern Gulf of Guinea. African Journal of Marine Science 41, 163–175. doi:10.2989/1814232X.2019.1616612.

Drumond, A., Marengo, J., Ambrizzi, T., Nieto, R., Moreira, L., Gimeno, L., 2014. The role of the Amazon Basin moisture in the atmospheric branch of the hydrological cycle: a lagrangian analysis. Hydrology and Earth System Sciences 18, 2577–2598. doi:10.5194/hess-18-2577-2014.

Dufresne, J.L., Foujols, M.A., Denvil, S., Caubel, A., Marti, O., Aumont, O., Balkanski, Y., Bekki, S., Bellenger, H., Benshila, R., Bony, S., Bopp, L., Braconnot, P., Brockmann, P., Cadule, P., Cheruy, F., Codron, F., Cozic, A., Cugnet, D., de Noblet, N., Duvel, J.P., Ethé, C., Fairhead, L., Fichefet, T., Flavoni, S., Friedlingstein, P., Grandpeix, J.Y., Guez, L., Guilyardi, E., Hauglustaine, D., Hourdin, F., Idelkadi, A., Ghattas, J., Joussaume, S., Kageyama, M., Krinner, G., Labetoulle, S., Lahellec, A., Lefebvre, M.P., Lefevre, F., Levy, C., Li, Z.X., Lloyd, J., Lott, F., Madec, G., Mancip, M., Marchand, M., Masson, S., Meurdesoif, Y., Mignot, J., Musat, I., Parouty, S., Polcher, J., Rio, C., Schulz, M., Swingedouw, D., Szopa, S., Talandier, C., Terray, P., Viovy, N., Vuichard, N., 2013. Climate change projections using the IPSL-CM5 Earth System Model: from CMIP3 to CMIP5. Climate Dynamics 40, 2123–2165. doi:10.1007/s00382-012-1636-1.

Durack, P.J., 2015. Ocean salinity and the global water cycle. Oceanography 28, 20–31. doi:10.5670/oceanog.2015.03.

Durand, F., Shetye, S.R., Vialard, J., Shankar, D., Shenoi, S.S.C., Ethe, C., Madec, G., 2004. Impact of temperature inversions on SST evolution in the South-Eastern Arabian Sea during the pre-summer monsoon season. Geophysical Research Letters 31. doi:10.1029/2003GL018906.

Dussin, R., Barnier, B., Brodeau, L., Molines, J., 2016. The making of the Drakkar forcing set DFS5. DRAKKAR/MyOcean Rep , 01–04.

Dutheil, C., Bador, M., Lengaigne, M., Lefèvre, J., Jourdain, N.C., Vialard, J., Jullien, S., Peltier, A., Menkes, C., 2019. Impact of surface temperature biases on climate change projections of the South Pacific Convergence Zone. Climate Dynamics 53, 3197–3219. doi:10.1007/s00382-019-04692-6.

Espinoza, J.C., Guyot, J.L., Ronchail, J., Cochonneau, G., Filizola, N., Fraizy, P., Labat, D., de Oliveira, E., Ordoñez, J.J., Vauchel, P., 2009a. Contrasting regional discharge evolutions in the Amazon basin (1974–2004). Journal of Hydrology 375, 297–311. doi:10.1016/j.jhydrol.2009.03.004.

Espinoza, J.C., Ronchail, J., Guyot, J.L., Cochonneau, G., Naziano, F., Lavado, W., De Oliveira, E., Pombosa, R., Vauchel, P., 2009b. Spatio-temporal rainfall variability in the Amazon basin countries (Brazil, Peru, Bolivia, Colombia, and Ecuador). International Journal of Climatology: A Journal of the Royal Meteorological Society 29, 1574–1594. doi:10.1002/joc.1791.

Espinoza, J.C., Segura, H., Ronchail, J., Drapeau, G., Gutierrez-Cori, O., 2016. Evolution of wet-day and dry-day frequency in the western Amazon basin: Relationship with atmospheric circulation and impacts on vegetation. Water Resources Research 52, 8546–8560. doi:10.1002/2016WR019305.

Evans, J.L., Webster, C.C., 2014. A variable sea surface temperature threshold for tropical convection. Aust. Meteorol. Oceanogr. J 64, S1–S8. doi:10.22499/2.6401.007.

Ferry, N., Parent, L., Garric, G., Bricaud, C., Testut, C., Le Galloudec, O., Lellouche, J., Drevillon, M., Greiner, E., Barnier, B., et al., 2012. GLORYS2V1 global ocean reanalysis of the altimetric era (1992-2009) at mesoscale. Mercator Ocean-Quaterly Newsletter 44.

Ferry, N., Reverdin, G., 2004. Sea surface salinity interannual variability in the western tropical Atlantic: An ocean general circulation model study. Journal of Geophysical Research: Oceans 109. doi:10.1029/2003JC002122.

Ffield, A., 2005. North Brazil current rings viewed by TRMM Microwave Imager SST and the influence of the Amazon Plume. Deep Sea Research Part I: Oceanographic Research Papers 52, 137–160. doi:10.1016/j.dsr.2004.05.013.

Ffield, A., 2007. Amazon and orinoco river plumes and NBC rings: Bystanders or participants in hurricane events? Journal of Climate 20, 316–333. doi:10.1175/JCLI3985.1.

Fieux, M., 2010. L'océan planétaire. Les Presses de l'ENSTA. doi:10.1051/978-2-7598-2150-1.

Filizola, N., Latrubesse, E.M., Fraizy, P., Souza, R., Guimarães, V., Guyot, J.L., 2014. Was the 2009 flood the most hazardous or the largest ever recorded in the Amazon? Geomorphology 215, 99–105. doi:10.1016/j.geomorph.2013.05.028.

Foltz, G.R., Grodsky, S.A., Carton, J.A., McPhaden, M.J., 2004. Seasonal salt budget of the northwestern tropical Atlantic Ocean along 38°W. Journal of Geophysical Research: Oceans 109. doi:10.1029/2003JC002111.

Foltz, G.R., McPhaden, M.J., 2008. Seasonal mixed layer salinity balance of the tropical North Atlantic Ocean. Journal of Geophysical Research: Oceans 113. doi:10.1029/2007JC004178.

Foltz, G.R., McPhaden, M.J., 2009. Impact of barrier layer thickness on SST in the central tropical North Atlantic. Journal of Climate 22, 285–299. doi:10.1175/2008JCLI2308.1.

Foltz, G.R., McPhaden, M.J., Lumpkin, R., 2012. A strong Atlantic meridional mode event in 2009: The role of mixed layer dynamics. Journal of Climate 25, 363–380. doi:10.1175/JCLI-D-11-00150.1.

Foltz, G.R., Schmid, C., Lumpkin, R., 2015. Transport of surface freshwater from the equatorial to the subtropical North Atlantic Ocean. Journal of Physical Oceanography 45, 1086–1102. doi:10.1175/JPO-D-14-0189.1.

Fonseca, C.A., Goni, G.J., Johns, W.E., Campos, E.J., 2004. Investigation of the north Brazil current retroflection and north equatorial countercurrent variability. Geophysical Research Letters 31. doi:10.1029/2004GL020054.

Fournier, S., Vandemark, D., Gaultier, L., Lee, T., Jonsson, B., Gierach, M.M., 2017. Interannual variation in offshore advection of Amazon-Orinoco plume waters: Observations, forcing mechanisms, and impacts. Journal of Geophysical Research: Oceans 122, 8966–8982. doi:10.1002/2017JC013103.

Fox-Kemper, B., Ferrari, R., Hallberg, R., 2008. Parameterization of mixed layer eddies. part i: Theory and diagnosis. Journal of Physical Oceanography 38, 1145–1165. doi:10.1175/2007JPO3792.1.

Gaillard, F., Reynaud, T., Thierry, V., Kolodziejczyk, N., von Schuckmann, K., 2016. In situ–based reanalysis of the global ocean temperature and salinity with ISAS: Variability of the heat content and steric height. Journal of Climate 29, 1305–1323. doi:10.1175/JCLI-D-15-0028.1.

Gévaudan, M., Jouanno, J., Durand, F., Morvan, G., Renault, L., Samson, G., 2021. Influence of ocean salinity stratification on the tropical Atlantic Ocean surface. Climate Dynamics 57, 321–340. doi:10.1007/s00382-021-05713-z.

Giannini, A., Saravanan, R., Chang, P., 2004. The preconditioning role of tropical Atlantic variability in the development of the ENSO teleconnection: Implications for the prediction of Nordeste rainfall. Climate Dynamics 22, 839–855. doi:10.1007/s00382-004-0420-2.

Gidden, M.J., Riahi, K., Smith, S.J., Fujimori, S., Luderer, G., Kriegler, E., Vuuren, D.P.v., Berg, M.v.d., Feng, L., Klein, D., et al., 2019. Global emissions pathways under different socioeconomic scenarios for use in CMIP6: a dataset of harmonized emissions trajectories through the end of the century. Geoscientific Model Development 12, 1443–1475. doi:10.5194/gmd-12-1443-2019.

Giffard, P., Llovel, W., Jouanno, J., Morvan, G., Decharme, B., 2019. Contribution of the Amazon river discharge to regional sea level in the tropical Atlantic Ocean. Water 11, 2348. doi:10.3390/w11112348.

Gloor, M., Barichivich, J., Ziv, G., Brienen, R., Schöngart, J., Peylin, P., Cintra, B.B.L., Feldpausch, T., Phillips, O., Baker, J., 2015. Recent Amazon climate as background for possible ongoing and future changes of Amazon humid forests. Global Biogeochemical Cycles 29, 1384–1399. doi:10.1002/2014GB005080.

Gloor, M., Brienen, R.J., Galbraith, D., Feldpausch, T.R., Schöngart, J., Guyot, J.L., Espinoza, J.C., Lloyd, J., Phillips, O.L., 2013. Intensification of the Amazon hydrological cycle over the last two decades. Geophysical Research Letters 40, 1729–1733. doi:10.1002/grl.50377.

Godfrey, J.S., Lindstrom, E.J., 1989. The heat budget of the equatorial western Pacific surface mixed layer. Journal of Geophysical Research: Oceans 94, 8007–8017. doi:10.1029/JC094iC06p08007.

Gouveia, N., Gherardi, D., Aragão, L., 2019a. The role of the Amazon river plume on the intensification of the hydrological cycle. Geophysical Research Letters 46, 12221–12229. doi:10.1029/2019GL084302.

Gouveia, N.A., Gherardi, D.F.M., Wagner, F.H., Paes, E.T., Coles, V.J., Aragão, L.E.O.C., 2019b. The salinity structure of the Amazon river plume drives spatiotemporal variation of oceanic primary productivity. Journal of Geophysical Research: Biogeosciences 124, 147–165. doi:10.1029/2018jg004665.

Grodsky, S.A., Carton, J.A., Bingham, F.M., 2006. Low frequency variation of sea surface salinity in the tropical atlantic. Geophysical Research Letters 33. doi:10.1029/2006GL026426.

Grodsky, S.A., Johnson, B.K., Carton, J.A., Bryan, F.O., 2015. Interannual Caribbean salinity in satellite data and model simulations. Journal of Geophysical Research: Oceans 120, 1375–1387. doi:10.1002/2014JC010625.

Grodsky, S.A., Reul, N., Lagerloef, G., Reverdin, G., Carton, J.A., Chapron, B., Quilfen, Y., Kudryavtsev, V.N., Kao, H.Y., 2012. Haline hurricane wake in the Amazon/Orinoco plume: AQUARIUS/SACD and SMOS observations. Geophysical Research Letters 39. doi:10.1029/2012GL053335.

Grodsky, S.A., Reverdin, G., Carton, J.A., Coles, V.J., 2014. Year-to-year salinity changes in the Amazon plume: Contrasting 2011 and 2012 Aquarius/SACD and SMOS satellite data. Remote Sensing of Environment 140, 14–22. doi:10.1016/j.rse.2013.08.033.

Grodsky, S.A., Vandemark, D., Feng, H., 2018. Assessing coastal SMAP surface salinity accuracy and its application to monitoring Gulf of Maine circulation dynamics. Remote Sensing 10, 1232. doi:10.3390/rs10081232.

Guimberteau, M., Ciais, P., Ducharne, A., Boisier, J.P., Aguiar, A.P.D., Biemans, H., Deurwaerder, H.D., Galbraith, D., Kruijt, B., Langerwisch, F., Poveda, G., Rammig, A., Rodriguez, D.A., Tejada, G., Thonicke, K., Randow, C.V., Randow, R.C.S.V., Zhang, K., Verbeeck, H., 2017. Impacts of future deforestation and climate change on the hydrology of the Amazon Basin: a multi-model analysis with a new set of land-cover change scenarios. Hydrology and Earth System Sciences 21, 1455–1475. doi:10.5194/hess-21-1455-2017.

Hastenrath, S., Greischar, L., 1993. Circulation mechanisms related to northeast Brazil rainfall anomalies. Journal of Geophysical Research: Atmospheres 98, 5093–5102. doi:10.1029/92JD02646.

Hausfather, Z., Peters, G.P., 2020. Emissions – the 'business as usual' story is misleading. Nature 577, 618–620. doi:10.1038/d41586-020-00177-3.

Hellweger, F.L., Gordon, A.L., 2002. Tracing Amazon river water into the Caribbean Sea. Journal of Marine Research 60, 537–549. doi:10.1357/002224002762324202.

Hernandez, O., Jouanno, J., Durand, F., 2016. Do the Amazon and Orinoco freshwater plumes really matter for hurricane-induced ocean surface cooling? Journal of Geophysical Research: Oceans 121, 2119–2141. doi:10.1002/2015JC011021.

Hernandez, O., Jouanno, J., Echevin, V., Aumont, O., 2017. Modification of sea surface temperature by chlorophyll concentration in the Atlantic upwelling systems. Journal of Geophysical Research: Oceans 122, 5367–5389. doi:10.1002/2016JC012330.

Hlywiak, J., Nolan, D.S., 2019. The influence of oceanic barrier layers on tropical cyclone intensity as determined through idealized, coupled numerical simulations. Journal of Physical Oceanography 49, 1723–1745. doi:10.1175/JPO-D-18-0267.1.

Hong, S.Y., Lim, J.O.J., 2006. The WRF single-moment 6-class microphysics scheme (WSM6). Asia-Pacific Journal of Atmospheric Sciences 42, 129–151.

Hong, S.Y., Noh, Y., Dudhia, J., 2006. A new vertical diffusion package with an explicit treatment of entrainment processes. Monthly Weather Review 134, 2318–2341. doi:10.1175/MWR3199.1.

Hopkins, J., Lucas, M., Dufau, C., Sutton, M., Stum, J., Lauret, O., Channelliere, C., 2013. Detection and variability of the Congo River plume from satellite derived sea surface temperature, salinity, ocean colour and sea level. Remote Sensing of Environment 139, 365–385. doi:10.1016/j.rse.2013.08.015.

Hormann, V., Lumpkin, R., Foltz, G.R., 2012. Interannual North Equatorial Countercurrent variability and its relation to tropical Atlantic climate modes. Journal of Geophysical Research: Oceans 117. doi:10.1029/2011JC007697.

Hu, C., Montgomery, E.T., Schmitt, R.W., Muller-Karger, F.E., 2004. The dispersal of the Amazon and Orinoco River water in the tropical Atlantic and Caribbean sea: Observation from space and S-PALACE floats. Deep Sea Research Part II: Topical Studies in Oceanography 51, 1151–1171. doi:10.1016/j.dsr2.2004.04.001.

Hu, Z.Z., Huang, B., 2006. Physical processes associated with the tropical Atlantic SST meridional gradient. Journal of Climate 19, 5500–5518. doi:10.1175/JCLI3923.1.

Huang, B., Mehta, V.M., 2010. Influences of freshwater from major rivers on global ocean circulation and temperatures in the MIT ocean general circulation model. Advances in Atmospheric Sciences 27, 455–468. doi:10.1007/s00376-009-9022-6.

Huffman, G.J., Bolvin, D.T., Nelkin, E.J., Wolff, D.B., Adler, R.F., Gu, G., Hong, Y., Bowman, K.P., Stocker, E.F., 2007. The TRMM multisatellite precipitation analysis (TMPA): Quasi-global, multiyear, combined-sensor precipitation estimates at fine scales. Journal of Hydrometeorology 8, 38–55. doi:10.1175/JHM560.1.

Iacono, M.J., 2011. Application of improved radiation modeling to general circulation models doi:10.2172/1010861.

IPCC, 2013. Annex II: Climate System Scenario Tables. In: Climate Change 2013: The Physical Science Basis. Contribution of Working Group I to the Fifth Assessment Report of the Intergovernmental Panel on Climate Change. Cambridge University Press, Cambridge, United Kingdom and New York, NY, USA. book section AII. p. 1395–1446. doi:10.1017/CBO9781107415324.030.

Jahfer, S., Vinayachandran, P., Nanjundiah, R.S., 2017. Long-term impact of Amazon river runoff on northern hemispheric climate. Scientific reports 7, 1–9. doi:10.1038/s41598-017-10750-y.

Jahfer, S., Vinayachandran, P., Nanjundiah, R.S., 2020. The role of Amazon river runoff on the multidecadal variability of the Atlantic ITCZ. Environmental Research Letters 15, 054013. doi:10.1088/1748-9326/ab7c8a.

Janjić, Z.I., 1994. The step-mountain eta coordinate model: Further developments of the convection, viscous sublayer, and turbulence closure schemes. Monthly Weather Review 122, 927–945. doi:10.1175/1520-0493(1994)122<0927:TSMECM>2.0.CO;2.

Jiménez, P.A., Dudhia, J., González-Rouco, J.F., Navarro, J., Montávez, J.P., García-Bustamante, E., 2012. A revised scheme for the WRF surface layer formulation. Monthly Weather Review 140, 898–918. doi:10.1175/MWR-D-11-00056.1.

Johns, W.E., Lee, T., Beardsley, R., Candela, J., Limeburner, R., Castro, B., 1998. Annual cycle and variability of the North Brazil Current. Journal of Physical Oceanography 28, 103–128. doi:10.1175/1520-0485(1998)028<0103:ACAVOT>2.0.CO;2.

Johnson, N.C., Xie, S.P., 2010. Changes in the sea surface temperature threshold for tropical convection. Nature Geoscience 3, 842–845. doi:10.1038/NGEO1008.

Jouanno, J., Hernandez, O., Sanchez-Gomez, E., 2017. Equatorial Atlantic interannual variability and its relation to dynamic and thermodynamic processes. Earth System Dynamics 8, 1061. doi:10.5194/esd-8-1061-2017.

Jouanno, J., Marin, F., du Penhoat, Y., Molines, J.M., Sheinbaum, J., 2011. Seasonal modes of surface cooling in the Gulf of Guinea. Journal of Physical Oceanography 41, 1408–1416. doi:10.1175/jpo-d-11-031.1.

Jousse, A., Hall, A., Sun, F., Teixeira, J., 2016. Causes of WRF surface energy fluxes biases in a stratocumulus region. Climate Dynamics 46, 571–584. doi:10.1007/s00382-015-2599-9.

Jullien, S., Masson, S., Oerder, V., Samson, G., Colas, F., Renault, L., 2020. Impact of ocean–atmosphere current feedback on ocean mesoscale activity: Regional variations and sensitivity to model resolution. Journal of Climate 33, 2585–2602. doi:10.1175/jcli-d-19-0484.1.

Jury, M.R., 2019. Factors underlying changes in salinity around the southeastern Antilles. Journal of Marine Systems 199, 103208. doi:10.1016/j.jmarsys.2019.103208.

Kataoka, T., Kimoto, M., Watanabe, M., Tatebe, H., 2019. Wind–mixed layer–SST feedbacks in a tropical air–sea coupled system: Application to the Atlantic. Journal of Climate 32, 3865–3881. doi:10.1175/JCLI-D-18-0728.1.

Kato, S., Loeb, N.G., Rose, F.G., Doelling, D.R., Rutan, D.A., Caldwell, T.E., Yu, L., Weller, R.A., 2013. Surface irradiances consistent with CERES-derived top-of-atmosphere shortwave and longwave irradiances. Journal of Climate 26, 2719–2740. doi:10.1175/JCLI-D-12-00436.1.

Kawase, H., Yoshikane, T., Hara, M., Kimura, F., Yasunari, T., Ailikun, B., Ueda, H., Inoue, T., 2009. Intermodel variability of future changes in the Baiu rainband estimated

by the pseudo global warming downscaling method. Journal of Geophysical Research 114. doi:10.1029/2009jd011803.

Keenlyside, N.S., Latif, M., 2007. Understanding equatorial Atlantic interannual variability. Journal of Climate 20, 131–142. doi:10.1175/JCLI3992.1.

Kent, C., Chadwick, R., Rowell, D.P., 2015. Understanding uncertainties in future projections of seasonal tropical precipitation. Journal of Climate 28, 4390–4413. doi:10.1175/jcli-d-14-00613.1.

Killworth, P.D., 1983. Deep convection in the world ocean. Reviews of Geophysics 21, 1–26. doi:10.1029/RG021i001p00001.

Kolodziejczyk, N., Prigent-Mazella, A., Gaillard, F., 2017. ISAS-15 temperature and salinity gridded fields doi:10.17882/52367.

Krishnamohan, K., Vialard, J., Lengaigne, M., Masson, S., Samson, G., Pous, S., Neetu, S., Durand, F., Shenoi, S., Madec, G., 2019. Is there an effect of Bay of Bengal salinity on the northern Indian Ocean climatological rainfall? Deep Sea Research Part II: Topical Studies in Oceanography 166, 19 – 33. doi:10.1016/j.dsr2.2019.04.003.

Kumar, B.P., Cronin, M.F., Joseph, S., Ravichandran, M., Sureshkumar, N., 2017. Latent heat flux sensitivity to sea surface temperature: Regional perspectives. Journal of Climate 30, 129–143. doi:10.1175/JCLI-D-16-0285.1.

Kumar, B.P., Vialard, J., Lengaigne, M., Murty, V., Mcphaden, M.J., 2012. Tropflux: Air-sea fluxes for the global tropical oceans — description and evaluation. Climate Dynamics 38, 1521–1543. doi:10.1007/s00382-011-1115-0.

Kwiatkowski, L., Torres, O., Bopp, L., Aumont, O., Chamberlain, M., Christian, J.R., Dunne, J.P., Gehlen, M., Ilyina, T., John, J.G., Lenton, A., Li, H., Lovenduski, N.S., Orr, J.C., Palmieri, J., Santana-Falcón, Y., Schwinger, J., Séférian, R., Stock, C.A., Tagliabue, A., Takano, Y., Tjiputra, J., Toyama, K., Tsujino, H., Watanabe, M., Yamamoto, A., Yool, A., Ziehn, T., 2020. Twenty-first century ocean warming, acidification, deoxygenation, and upper-ocean nutrient and primary production decline from CMIP6 model projections. Biogeosciences 17, 3439–3470. doi:10.5194/bg-17-3439-2020.

Latif, M., Grötzner, A., 2000. The equatorial Atlantic oscillation and its response to ENSO. Climate Dynamics 16, 213–218. doi:10.1007/s003820050014.

Lauer, A., Zhang, C., Elison-Timm, O., Wang, Y., Hamilton, K., 2013. Downscaling of climate change in the hawaii region using CMIP5 results: On the choice of the forcing fields. Journal of Climate 26, 10006–10030. doi:10.1175/jcli-d-13-00126.1.

Lengaigne, M., Menkes, C., Aumont, O., Gorgues, T., Bopp, L., André, J.M., Madec, G., 2007. Influence of the oceanic biology on the tropical Pacific climate in a coupled general circulation model. Climate Dynamics 28, 503–516. doi:10.1007/s00382-006-0200-2.

Lengaigne, M., Neetu, S., Samson, G., Vialard, J., Krishnamohan, K.S., Masson, S., Jullien, S., Suresh, I., Menkes, C.E., 2018. Influence of air–sea coupling on Indian Ocean tropical cyclones. Climate Dynamics 52, 577–598. doi:10.1007/s00382-018-4152-0.

Lentz, S.J., 1995. The Amazon River plume during AMASSEDS: subtidal current variability and the importance of wind forcing. Journal of Geophysical Research: Oceans 100, 2377–2390. doi:10.1029/94JC00343.

Lewis, M.R., Carr, M.E., Feldman, G.C., Esaias, W., McClain, C., 1990. Influence of penetrating solar radiation on the heat budget of the equatorial Pacific Ocean. Nature 347, 543–545. doi:10.1038/347543a0.

Li, W., Fu, R., Dickinson, R.E., 2006. Rainfall and its seasonality over the Amazon in the 21st century as assessed by the coupled models for the IPCC AR4. Journal of Geophysical Research: Atmospheres 111. doi:10.1029/2005JD006355.

Lindzen, R.S., Nigam, S., 1987. On the role of sea surface temperature gradients in forcing low-level winds and convergence in the tropics. Journal of Atmospheric Sciences 44, 2418–2436. doi:10.1175/1520-0469(1987)044<2418:OTROSS>2.0.CO;2.

Liu, C., Ikeda, K., Rasmussen, R., Barlage, M., Newman, A.J., Prein, A.F., Chen, F., Chen, L., Clark, M., Dai, A., Dudhia, J., Eidhammer, T., Gochis, D., Gutmann, E., Kurkute, S., Li, Y., Thompson, G., Yates, D., 2016. Continental-scale convection-permitting modeling of the current and future climate of North America. Climate Dynamics 49, 71–95. doi:10.1007/s00382-016-3327-9.

Losada, T., Rodríguez-Fonseca, B., Janicot, S., Gervois, S., Chauvin, F., Ruti, P., 2010. A multi-model approach to the Atlantic Equatorial mode: impact on the West African monsoon. Climate Dynamics 35, 29–43. doi:10.1007/s00382-009-0625-5.

Lübbecke, J.F., McPhaden, M.J., 2017. Symmetry of the atlantic niño mode. Geophysical Research Letters 44, 965–973. doi:10.1002/2016GL071829.

Lübbecke, J.F., Rodríguez-Fonseca, B., Richter, I., Martín-Rey, M., Losada, T., Polo, I., Keenlyside, N.S., 2018. Equatorial Atlantic variability — Modes, mechanisms, and global teleconnections. WIREs Climate Change 9, e527. doi:10.1002/wcc.527.

Lukas, R., Lindstrom, E., 1991. The mixed layer of the western equatorial Pacific Ocean. Journal of Geophysical Research: Oceans 96, 3343–3357. doi:10.1029/90JC01951.

Ma, J., Chadwick, R., Seo, K.H., Dong, C., Huang, G., Foltz, G.R., Jiang, J.H., 2018. Responses of the tropical atmospheric circulation to climate change and connection to the hydrological cycle. Annual Review of Earth and Planetary Sciences 46, 549–580. doi:10.1146/annurev-earth-082517-010102.

Madec, G., the NEMO team, 2016. NEMO ocean engine. Note du Pôle de modélisation, Institut Pierre-Simon Laplace (IPSL), France 27, 1288–1619.

Maes, C., O'Kane, T.J., 2014. Seasonal variations of the upper ocean salinity stratification in the tropics. Journal of Geophysical Research: Oceans 119, 1706–1722. doi:10.1002/2013JC009366.

Mahajan, S., Saravanan, R., Chang, P., 2010. Free and forced variability of the tropical Atlantic ocean: Role of the wind–evaporation–sea surface temperature feedback. Journal of Climate 23, 5958–5977. doi:10.1175/2010JCLI3304.1.

Mamalakis, A., Randerson, J.T., Yu, J.Y., Pritchard, M.S., Magnusdottir, G., Smyth, P., Levine, P.A., Yu, S., Foufoula-Georgiou, E., 2021. Zonally contrasting shifts of the tropical rain belt in response to climate change. Nature Climate Change 11, 143–151. doi:10.1038/s41558-020-00963-x.

Marengo, J.A., Borma, L.S., Rodríguez, D.A., Pinho, P., Soares, W.R., Alves, L.M., 2013. Recent extremes of drought and flooding in Amazonia: vulnerabilities and human adaptation doi:10.4236/ajcc.2013.22009.

Marengo, J.A., Espinoza, J.C., 2016. Extreme seasonal droughts and floods in Amazonia: causes, trends and impacts. International Journal of Climatology 36, 1033–1050. doi:10.1002/joc.4420.

Maritorena, S., d'Andon, O.H.F., Mangin, A., Siegel, D.A., 2010. Merged satellite ocean color data products using a bio-optical model: Characteristics, benefits and issues. Remote Sensing of Environment 114, 1791–1804. doi:10.1016/j.rse.2010.04.002.

Masson, S., Delecluse, P., 2001. Influence of the Amazon river runoff on the tropical Atlantic. Physics and Chemistry of the Earth, Part B: Hydrology, Oceans and Atmosphere 26, 137 – 142. doi:10.1016/S1464-1909(00)00230-6.

Masson, S., Luo, J.J., Madec, G., Vialard, J., Durand, F., Gualdi, S., Guilyardi, E., Behera, S., Delecluse, P., Navarra, A., Yamagata, T., 2005. Impact of barrier layer on winter-spring variability of the southeastern Arabian Sea. Geophysical Research Letters 32. doi:10.1029/2004GL021980.

Materia, S., Gualdi, S., Navarra, A., Terray, L., 2012. The effect of Congo River freshwater discharge on Eastern Equatorial Atlantic climate variability. Climate Dynamics 39, 2109–2125. doi:10.1007/s00382-012-1514-x.

McClain, C.R., Cleave, M.L., Feldman, G.C., Gregg, W.W., Hooker, S.B., Kuring, N., 1998. Science quality SeaWiFS data for global biosphere research. Sea Technology 39, 10–16.

McPhaden, M.J., Busalacchi, A.J., Anderson, D.L., 2010. A toga retrospective. Oceanography 23, 86–103. doi:10.5670/oceanog.2010.26.

McSweeney, C.F., Jones, R.G., 2013. No consensus on consensus: the challenge of finding a universal approach to measuring and mapping ensemble consistency in GCM projections. Climatic Change 119, 617–629. doi:10.1007/s10584-013-0781-9.

Menkes, C.E.R., Vialard, J.G., Kennan, S.C., Boulanger, J.P., Madec, G.V., 2006. A modeling study of the impact of tropical instability waves on the heat budget of the Eastern Equatorial Pacific. Journal of Physical Oceanography 36, 847–865. doi:10.1175/JPO2904.1.

Meynadier, R., de Coëtlogon, G., Leduc-Leballeur, M., Eymard, L., Janicot, S., 2016. Seasonal influence of the sea surface temperature on the low atmospheric circulation and precipitation in the eastern equatorial Atlantic. Climate Dynamics 47, 1127–1142. doi:10.1007/s00382-015-2892-7.

Meynadier, R., de Coëtlogon, G., Bastin, S., Eymard, L., Janicot, S., 2015. Sensitivity testing of WRF parameterizations on air–sea interaction and its impact on water cycle in the Gulf of Guinea. Quarterly Journal of the Royal Meteorological Society 141, 1804–1820. doi:10.1002/qj.2483.

Mignot, J., de Boyer Montégut, C., Lazar, A., Cravatte, S., 2007. Control of salinity on the mixed layer depth in the world ocean: 2. Tropical areas. Journal of Geophysical Research: Oceans 112. doi:10.1029/2006JC003954.

Mignot, J., de Boyer Montégut, C., Tomczak, M., 2009. On the porosity of barrier layers. Ocean Science 5, 379–387. doi:10.5194/os-5-379-2009.

Mignot, J., Lazar, A., Lacarra, M., 2012. On the formation of barrier layers and associated vertical temperature inversions: A focus on the northwestern tropical Atlantic. Journal of Geophysical Research: Oceans 117. doi:10.1029/2011JC007435.

Mignot, J., Mejia, C., Sorror, C., Sylla, A., Crépon, M., Thiria, S., 2020. Towards an objective assessment of climate multi-model ensembles – a case study: the Senegalo-Mauritanian upwelling region. Geoscientific Model Development 13, 2723–2742. doi:10.5194/gmd-13-2723-2020.

Miller, J.R., 1976. The salinity effect in a mixed layer ocean model. Journal of Physical Oceanography 6, 29–35. doi:10.1175/1520-0485(1976)006<0029:TSEIAM>2.0.CO;2.

Mlawer, E.J., Taubman, S.J., Brown, P.D., Iacono, M.J., Clough, S.A., 1997. Radiative transfer for inhomogeneous atmospheres: RRTM, a validated correlated-k model for the longwave. Journal of Geophysical Research: Atmospheres 102, 16663–16682. doi:10.1029/97JD00237.

Molleri, G.S., Novo, E.M.d.M., Kampel, M., 2010. Space-time variability of the Amazon River plume based on satellite ocean color. Continental Shelf Research 30, 342–352. doi:10.1016/j.csr.2009.11.015.

Morel, A., 1988. Optical modeling of the upper ocean in relation to its biogenous matter content (case I waters). Journal of geophysical research: oceans 93, 10749–10768. doi:10.1029/JC093iC09p10749.

Morel, A., Berthon, J.F., 1989. Surface pigments, algal biomass profiles, and potential production of the euphotic layer: Relationships reinvestigated in view of remote-sensing applications. Limnology and oceanography 34, 1545–1562. doi:10.4319/lo.1989.34.8.1545.

Müller-Karger, F., McClain, C., Fisher, T., Esaias, W., Varela, R., 1989. Pigment distribution in the Caribbean sea: Observations from space. Progress in Oceanography 23, 23–64. doi:10.1016/0079-6611(89)90024-4.

Müller-Karger, F.E., McClain, C.R., Richardson, P.L., 1988. The dispersal of the Amazon's water. Nature 333, 56–59. doi:10.1038/333056a0.

Myers, T.A., Mechoso, C.R., DeFlorio, M.J., 2018. Importance of positive cloud feedback for tropical Atlantic interhemispheric climate variability. Climate Dynamics 51, 1707–1717. doi:10.1007/s00382-017-3978-1.

Nagura, M., Terao, T., Hashizume, M., 2015. The role of temperature inversions in the generation of seasonal and interannual SST variability in the far northern bay of Bengal. Journal of Climate 28, 3671–3693. doi:10.1175/JCLI-D-14-00553.1.

Newinger, C., Toumi, R., 2015. Potential impact of the colored Amazon and Orinoco plume on tropical cyclone intensity. Journal of Geophysical Research: Oceans 120, 1296–1317. doi:10.1002/2014JC010533.

Nikiema, O., Devenon, J.L., Baklouti, M., 2007. Numerical modeling of the Amazon River plume. Continental Shelf Research 27, 873–899. doi:10.1016/j.csr.2006.12.004.

Niu, G.Y., Yang, Z.L., Mitchell, K.E., Chen, F., Ek, M.B., Barlage, M., Kumar, A., Manning, K., Niyogi, D., Rosero, E., et al., 2011. The community Noah land surface model with multiparameterization options (Noah-MP): 1. Model description and evaluation with local-scale measurements. Journal of Geophysical Research: Atmospheres 116. doi:10.1029/2010JD015139.

Nobre, P., Shukla, J., 1996. Variations of sea surface temperature, wind stress, and rainfall over the tropical Atlantic and South America. Journal of Climate 9, 2464–2479. doi:10.1175/1520-0442(1996)009<2464:VOSSTW>2.0.CO;2.

Olivier, L., Reverdin, G., Hasson, A., Boutin, J., 2020. Tropical Instability Waves in the Atlantic Ocean: Investigating the relative role of sea surface salinity and temperature from 2010 to 2018. Journal of Geophysical Research: Oceans 125. doi:10.1029/2020jc016641.

Pailler, K., Bourlès, B., Gouriou, Y., 1999. The barrier layer in the western tropical Atlantic Ocean. Geophysical Research Letters 26, 2069–2072. doi:10.1029/1999GL900492.

Peter, A.C., Le Hénaff, M., du Penhoat, Y., Menkes, C.E., Marin, F., Vialard, J., Caniaux, G., Lazar, A., 2006. A model study of the seasonal mixed layer heat budget in the equatorial Atlantic. Journal of Geophysical Research: Oceans 111. doi:10.1029/2005JC003157.

Pleim, J.E., 2006. A simple, efficient solution of flux–profile relationships in the atmospheric surface layer. Journal of applied meteorology and climatology 45, 341–347. doi:10.1175/JAM2339.1.

Pleim, J.E., 2007. A combined local and nonlocal closure model for the atmospheric boundary layer. part I: Model description and testing. Journal of Applied Meteorology and Climatology 46, 1383–1395. doi:10.1175/JAM2539.1.

Polo, I., Rodríguez-Fonseca, B., Losada, T., García-Serrano, J., 2008. Tropical Atlantic variability modes (1979–2002). Part I: Time-evolving SST modes related to West African rainfall. Journal of Climate 21, 6457–6475. doi:10.1175/2008JCLI2607.1.

Polovina, J.J., Howell, E.A., Abecassis, M., 2008. Ocean's least productive waters are expanding. Geophysical Research Letters 35. doi:10.1029/2007gl031745.

Radenac, M.H., Jouanno, J., Tchamabi, C.C., Awo, M., Bourles, B., Arnault, S., Aumont, O., 2020. Physical drivers of the nitrate seasonal variability in the Atlantic cold tongue. doi:10.5194/bg-17-529-2020.

Rasmussen, R., Liu, C., Ikeda, K., Gochis, D., Yates, D., Chen, F., Tewari, M., Barlage, M., Dudhia, J., Yu, W., Miller, K., Arsenault, K., Grubišić, V., Thompson, G., Gutmann, E., 2011. High-resolution coupled climate runoff simulations of seasonal snowfall over Colorado: A process study of current and warmer climate. Journal of Climate 24, 3015–3048. doi:10.1175/2010jcli3985.1.

Reeves Eyre, J.J., Zeng, X., 2021. The Amazon water cycle: Perspectives from water budget closure and ocean salinity. Journal of Climate 34, 1439–1451. doi:10.1175/JCLI-D-20-0309.1.

Reffray, G., Bourdalle-Badie, R., Calone, C., 2015. Modelling turbulent vertical mixing sensitivity using a 1-D version of NEMO. Geoscientific Model Development 8. doi:10.5194/gmd-8-69-2015.

Renault, L., Masson, S., Oerder, V., Jullien, S., Colas, F., 2019. Disentangling the mesoscale ocean-atmosphere interactions. Journal of Geophysical Research: Oceans 124, 2164–2178. doi:https://doi.org/10.1029/2018JC014628.

Renault, L., Molemaker, M.J., McWilliams, J.C., Shchepetkin, A.F., Lemarié, F., Chelton, D., Illig, S., Hall, A., 2016. Modulation of wind work by oceanic current interaction with the atmosphere. Journal of Physical Oceanography 46, 1685–1704. doi:10.1175/JPO-D-15-0232.1.

Reul, N., Fournier, S., Boutin, J., Hernandez, O., Maes, C., Chapron, B., Alory, G., Quilfen, Y., Tenerelli, J., Morisset, S., et al., 2014. Sea surface salinity observations from space with the SMOS satellite: A new means to monitor the marine branch of the water cycle. Surveys in Geophysics 35, 681–722. doi:10.1007/s10712-013-9244-0.

Reverdin, G., Olivier, L., Foltz, G.R., Speich, S., Karstensen, J., Horstmann, J., Zhang, D., Laxenaire, R., Carton, X., Branger, H., Carrasco, R., Boutin, J., 2021. Formation and evolution of a freshwater plume in the northwestern tropical Atlantic in february 2020. Journal of Geophysical Research: Oceans 126. doi:10.1029/2020jc016981.

Richter, I., Tokinaga, H., 2020. An overview of the performance of CMIP6 models in the tropical Atlantic: mean state, variability, and remote impacts. Climate Dynamics 55, 2579–2601. doi:10.1007/s00382-020-05409-w.

Richter, I., Xie, S.P., 2008. On the origin of equatorial Atlantic biases in coupled general circulation models. Climate Dynamics 31, 587–598. doi:10.1007/s00382-008-0364-z.

Richter, I., Xie, S.P., Behera, S.K., Doi, T., Masumoto, Y., 2014. Equatorial Atlantic variability and its relation to mean state biases in CMIP5. Climate Dynamics 42, 171–188. doi:10.1007/s00382-012-1624-5.

Richter, I., Xie, S.P., Wittenberg, A.T., Masumoto, Y., 2012. Tropical Atlantic biases and their relation to surface wind stress and terrestrial precipitation. Climate Dynamics 38, 985–1001. doi:10.1007/s00382-011-1038-9.

Risien, C.M., Chelton, D.B., 2008. A global climatology of surface wind and wind stress fields from eight years of QuikSCAT scatterometer data. Journal of Physical Oceanography 38, 2379–2413. doi:10.1175/2008JPO3881.1.

Roberts, M.J., Camp, J., Seddon, J., Vidale, P.L., Hodges, K., Vannière, B., Mecking, J., Haarsma, R., Bellucci, A., Scoccimarro, E., Caron, L.P., Chauvin, F., Terray, L., Valcke, S., Moine, M.P., Putrasahan, D., Roberts, C.D., Senan, R., Zarzycki, C., Ullrich, P., Yamada, Y., Mizuta, R., Kodama, C., Fu, D., Zhang, Q., Danabasoglu, G., Rosenbloom, N., Wang, H., Wu, L., 2020. Projected future changes in tropical cyclones using the CMIP6 HighResMIP multimodel ensemble. Geophysical Research Letters 47. doi:10.1029/2020gl088662.

Rodríguez-Fonseca, B., Mohino, E., Mechoso, C.R., Caminade, C., Biasutti, M., Gaetani, M., Garcia-Serrano, J., Vizy, E.K., Cook, K., Xue, Y., et al., 2015. Variability and predictability of West African droughts: A review on the role of sea surface temperature anomalies. Journal of Climate 28, 4034–4060. doi:10.1175/JCLI-D-14-00130.1.

Ronchail, J., Labat, D., Callède, J., Cochonneau, G., Guyot, J.L., Filizola, N., de Oliveira, E., 2005. Discharge variability within the Amazon basin, in: Regional Hydrological Impacts of Climatic Change-Hydroclimatological Variability (Proceedings of symposium S6 held during the Seventh IAHS Scientific Assembly at Foz do Iguaçu, Brazil).

Ropelewski, C.F., Halpert, M.S., 1987. Global and regional scale precipitation patterns associated with the El Niño/Southern Oscillation. Monthly Weather Review 115, 1606–1626. doi:10.1175/1520-0493(1987)115<1606:GARSPP>2.0.CO;2.

Ruault, V., Jouanno, J., Durand, F., Chanut, J., Benshila, R., 2020. Role of the tide on the structure of the Amazon plume: a numerical modeling approach. Journal of Geophysical Research: Oceans 125. doi:10.1029/2019JC015495.

Rudzin, J.E., Shay, L.K., Johns, W.E., 2018. The influence of the barrier layer on SST response during tropical cyclone wind forcing using idealized experiments. Journal of Physical Oceanography 48, 1471–1478. doi:10.1175/JPO-D-17-0279.1.

Rugg, A., Foltz, G.R., Perez, R.C., 2016. Role of mixed layer dynamics in tropical North Atlantic interannual sea surface temperature variability. Journal of Climate 29, 8083–8101. doi:10.1175/JCLI-D-15-0867.1.

Ruiz-Barradas, A., Carton, J.A., Nigam, S., 2000. Structure of interannual-to-decadal climate variability in the tropical Atlantic sector. Journal of Climate 13, 3285–3297. doi:10.1175/1520-0442(2000)013<3285:SOITDC>2.0.CO;2.

Sabin, T.P., Babu, C.A., Joseph, P.V., 2013. SST–convection relation over tropical oceans. International Journal of Climatology 33, 1424–1435. doi:10.1002/joc.3522.

Saha, A., Serra, N., Stammer, D., 2021. Growth and decay of northwestern tropical atlantic barrier layers. Journal of Geophysical Research: Oceans 126, e2020JC016956.

Salisbury, J., Vandemark, D., Campbell, J., Hunt, C., Wisser, D., Reul, N., Chapron, B., 2011. Spatial and temporal coherence between Amazon River discharge, salinity, and light absorption by colored organic carbon in western tropical Atlantic surface waters. Journal of Geophysical Research: Oceans 116. doi:10.1029/2011JC006989.

Sallée, J.B., Pellichero, V., Akhoudas, C., Pauthenet, E., Vignes, L., Schmidtko, S., Garabato, A.N., Sutherland, P., Kuusela, M., 2021. Summertime increases in upper-ocean stratification and mixed-layer depth. Nature 591, 592–598. doi:10.1038/s41586-021-03303-x.

Samson, G., Masson, S., Durand, F., Terray, P., Berthet, S., Jullien, S., 2017. Roles of land surface albedo and horizontal resolution on the Indian summer monsoon biases in a coupled ocean-atmosphere tropical-channel model. Climate Dynamics 48, 1571–1594. doi:10.1007/s00382-016-3161-0.

Samson, G., Masson, S., Lengaigne, M., Keerthi, M.G., Vialard, J., Pous, S., Madec, G., Jourdain, N.C., Jullien, S., Menkès, C., et al., 2014. The NOW regional coupled model: Application to the tropical Indian Ocean climate and tropical cyclone activity. Journal of Advances in Modeling Earth Systems 6, 700–722. doi:10.1002/2014MS000324.

Sato, K., Suga, T., Hanawa, K., 2006. Barrier layers in the subtropical gyres of the world's oceans. Geophysical Research Letters 33. doi:10.1029/2005GL025631.

Schaaf, C.B., Liu, J., Gao, F., Strahler, A.H., 2010. Aqua and Terra MODIS albedo and reflectance anisotropy products, in: Land Remote Sensing and Global Environmental Change. Springer, pp. 549–561. doi:10.1007/978-1-4419-6749-7_24.

Schade, L.R., Emanuel, K.A., 1999. The ocean's effect on the intensity of tropical cyclones: Results from a simple coupled atmosphere–ocean model. Journal of the Atmospheric Sciences 56, 642–651. doi:10.1175/1520-0469(1999)056<0642:TOSEOT>2.0.CO;2.

Schär, C., Frei, C., Lüthi, D., Davies, H.C., 1996. Surrogate climate-change scenarios for regional climate models. Geophysical Research Letters 23, 669–672. doi:10.1029/96GL00265.

Schneider, T., Bischoff, T., Haug, G.H., 2014. Migrations and dynamics of the intertropical convergence zone. Nature 513, 45–53. doi:10.1038/nature13636.

Seneviratne, S., Zhang, X., Adnan, M., Badi, W., Dereczynski, C., Di Luca, A., Ghosh, S., Iskandar, I., Kossin, J., Lewis, S., Otto, F., Pinto, I., Satoh, M., Vicente-Serrano, S., Wehner, M., Zhou, B., 2021. Weather and Climate Extreme Events in a Changing

Climate. In: Climate Change 2021: The Physical Science Basis. Contribution of Working Group I to the Sixth Assessment Report of the Intergovernmental Panel on Climate Change. Cambridge University Press. In Press.

Seo, H., Xie, S.P., 2011. Response and impact of equatorial ocean dynamics and tropical instability waves in the tropical Atlantic under global warming: A regional coupled downscaling study. Journal of Geophysical Research 116. doi:10.1029/2010jc006670.

Sérazin, G., Jaymond, A., Leroux, S., Penduff, T., Bessières, L., Llovel, W., Barnier, B., Molines, J.M., Terray, L., 2017. A global probabilistic study of the ocean heat content low-frequency variability: Atmospheric forcing versus oceanic chaos. Geophysical Research Letters 44, 5580–5589. doi:10.1002/2017gl073026.

Siongco, A.C., Hohenegger, C., Stevens, B., 2015. The Atlantic ITCZ bias in CMIP5 models. Climate Dynamics 45, 1169–1180. doi:10.1007/s00382-014-2366-3.

Siongco, A.C., Hohenegger, C., Stevens, B., 2017. Sensitivity of the summertime tropical Atlantic precipitation distribution to convective parameterization and model resolution in ECHAM6. Journal of Geophysical Research: Atmospheres 122, 2579–2594. doi:10.1002/2016jd026093.

Skamarock, W.C., Klemp, J.B., 2008. A time-split nonhydrostatic atmospheric model for weather research and forecasting applications. Journal of computational physics 227, 3465–3485. doi:10.1016/j.jcp.2007.01.037.

Skliris, N., Marsh, R., Mecking, J., Zika, J.D., 2020. Changing water cycle and freshwater transports in the Atlantic Ocean in observations and CMIP5 models. Climate Dynamics 54, 4971–4989. doi:10.1007/s00382-020-05261-y.

Skliris, N., Zika, J.D., Nurser, G., Josey, S.A., Marsh, R., 2016. Global water cycle amplifying at less than the Clausius-Clapeyron rate. Scientific reports 6, 1–9. doi:10.1038/srep38752.

Smith, W.O., Demaster, D.J., 1996. Phytoplankton biomass and productivity in the Amazon river plume: correlation with seasonal river discharge. Continental Shelf Research 16, 291–319. doi:10.1016/0278-4343(95)00007-n.

Sorribas, M.V., Paiva, R.C., Melack, J.M., Bravo, J.M., Jones, C., Carvalho, L., Beighley, E., Forsberg, B., Costa, M.H., 2016. Projections of climate change effects on discharge and inundation in the Amazon basin. Climatic change 136, 555–570. doi:10.1007/s10584-016-1640-2.

Sprintall, J., Tomczak, M., 1992. Evidence of the barrier layer in the surface layer of the tropics. Journal of Geophysical Research: Oceans 97, 7305–7316. doi:10.1029/92JC00407.

Stocker, T., Qin, D., Plattner, G.K., Alexander, L., Allen, S., Bindoff, N., Bréon, F.M., Church, J., Cubasch, U., Emori, S., Forster, P., Friedlingstein, P., Gillett, N., Gregory, J., Hartmann, D., Jansen, E., Kirtman, B., Knutti, R., Krishna Kumar, K., Lemke, P., Marotzke, J., Masson-Delmotte, V., Meehl, G., Mokhov, I., Piao, S., Ramaswamy, V., Randall, D., Rhein, M., Rojas, M., Sabine, C., Shindell, D., Talley, L., Vaughan, D., Xie,

S.P., 2013. Technical Summary. In: Climate Change 2013: The Physical Science Basis. Contribution of Working Group I to the Fifth Assessment Report of the Intergovernmental Panel on Climate Change. Cambridge University Press, Cambridge, United Kingdom and New York, NY, USA. book section TS. p. 33–115. doi:10.1017/CBO9781107415324.005.

Sylla, A., Mignot, J., Capet, X., Gaye, A.T., 2019. Weakening of the Senegalo–Mauritanian upwelling system under climate change. Climate Dynamics 53, 4447–4473. doi:10.1007/s00382-019-04797-y.

Tanguy, Y., Arnault, S., Lattes, P., 2010. Isothermal, mixed, and barrier layers in the subtropical and tropical Atlantic Ocean during the ARAMIS experiment. Deep Sea Research Part I: Oceanographic Research Papers 57, 501–517. doi:10.1016/j.dsr.2009.12.012.

Tanimoto, Y., Xie, S.P., 2002. Inter-hemispheric decadal variations in SST, surface wind, heat flux and cloud cover over the Atlantic Ocean. Journal of the Meteorological Society of Japan. Ser. II 80, 1199–1219. doi:10.2151/jmsj.80.1199.

Terada, M., Minobe, S., Deutsch, C., 2020. Mechanisms of future changes in equatorial upwelling: CMIP5 intermodel analysis. Journal of Climate 33, 497–510. doi:10.1175/jcli-d-19-0128.1.

Tian, B., Dong, X., 2020. The double-ITCZ bias in CMIP3, CMIP5, and CMIP6 models based on annual mean precipitation. Geophysical Research Letters 47, e2020GL087232. doi:10.1029/2020GL087232.

Toniazzo, T., Woolnough, S., 2014. Development of warm SST errors in the southern tropical Atlantic in CMIP5 decadal hindcasts. Climate Dynamics 43, 2889–2913. doi:10.1007/s00382-013-1691-2.

Towner, J., Cloke, H.L., Lavado, W., Santini, W., Bazo, J., Coughlan de Perez, E., Stephens, E.M., 2020. Attribution of Amazon floods to modes of climate variability: A review. Meteorological Applications 27, e1949. doi:10.1002/met.1949.

Valcke, S., 2013. The OASIS3 coupler: a European climate modelling community software. Geoscientific Model Development 6, 373. doi:10.5194/gmd-6-373-2013.

Vannière, B., Roberts, M., Vidale, P.L., Hodges, K., Demory, M.E., Caron, L.P., Scoccimarro, E., Terray, L., Senan, R., 2020. The moisture budget of tropical cyclones in HighResMIP models: Large-scale environmental balance and sensitivity to horizontal resolution. Journal of Climate 33, 8457–8474. doi:10.1175/jcli-d-19-0999.1.

Varona, H., Veleda, D., Silva, M., Cintra, M., Araujo, M., 2019. Amazon River plume influence on Western Tropical Atlantic dynamic variability. Dynamics of Atmospheres and Oceans 85, 1–15. doi:10.1016/j.dynatmoce.2018.10.002.

Vecchi, G.A., Soden, B.J., 2007. Global warming and the weakening of the tropical circulation. Journal of Climate 20, 4316–4340. doi:10.1175/jcli4258.1.

Vecchio, R.D., 2004. Influence of the Amazon river on the surface optical properties of the western tropical North Atlantic Ocean. Journal of Geophysical Research 109. doi:10.1029/2004jc002503.

Vera, C., Silvestri, G., Liebmann, B., González, P., 2006. Climate change scenarios for seasonal precipitation in South America from IPCC-AR4 models. Geophysical Research Letters 33. doi:10.1029/2006gl025759.

Vialard, J., Delecluse, P., 1998. An OGCM study for the TOGA decade. part I: Role of salinity in the physics of the Western Pacific fresh pool. Journal of Physical Oceanography 28, 1071–1088. doi:10.1175/1520-0485(1998)028<1071:AOSFTT>2.0.CO;2.

Vimont, D.J., Kossin, J.P., 2007. The Atlantic Meridional Mode and hurricane activity. Geophysical Research Letters 34. doi:10.1029/2007GL029683.

Vincent, E.M., Lengaigne, M., Madec, G., Vialard, J., Samson, G., Jourdain, N.C., Menkès, C.E., Jullien, S., 2012. Processes setting the characteristics of sea surface cooling induced by tropical cyclones. Journal of Geophysical Research: Oceans 117. doi:10.1029/2011JC007396.

Wang, C., Enfield, D.B., 2001. The tropical Western Hemisphere warm pool. Geophysical research letters 28, 1635–1638. doi:10.1029/2000GL011763.

Wang, C., Lee, S.K., Enfield, D.B., 2008. Atlantic warm pool acting as a link between Atlantic Multidecadal Oscillation and Atlantic tropical cyclone activity. Geochemistry, Geophysics, Geosystems 9. doi:10.1029/2007GC001809.

Wang, L.C., Jin, F.F., Wu, C.R., Hsu, H.H., 2017. Dynamics of upwelling annual cycle in the equatorial Atlantic Ocean. Geophysical Research Letters 44, 3737–3743. doi:10.1002/2017GL072588.

Warren, B.A., 1983. Why is no deep water formed in the North Pacific? Journal of Marine Research 41, 327–347. doi:10.1357/002224083788520207.

Weingartner, T.J., Weisberg, R.H., 1991. On the annual cycle of equatorial upwelling in the central atlantic ocean. Journal of Physical Oceanography 21, 68–82. doi:10.1175/1520-0485(1991)021<0068:OTACOE>2.0.CO;2.

van Westen, R.M., Dijkstra, H.A., van der Boog, C.G., Katsman, C.A., James, R.K., Bouma, T.J., Kleptsova, O., Klees, R., Riva, R.E.M., Slobbe, D.C., Zijlema, M., Pietrzak, J.D., 2020. Ocean model resolution dependence of Caribbean sea-level projections. Scientific Reports 10. doi:10.1038/s41598-020-71563-0.

White, R., Toumi, R., 2014. River flow and ocean temperatures: The Congo River. Journal of Geophysical Research: Oceans 119, 2501–2517. doi:10.1002/2014JC009836.

Wyrtki, K., 1975. El niño—the dynamic response of the equatorial pacific ocean to atmospheric forcing. Journal of Physical Oceanography 5, 572–584. doi:10.1175/1520-0485(1975)005<0572:ENTDRO>2.0.CO;2.

Xie, S.P., 1999. A dynamic ocean–atmosphere model of the tropical Atlantic decadal variability. Journal of Climate 12, 64–70. doi:10.1175/1520-0442(1999)012<0064:ADOAMO>2.0.CO;2.

Xie, S.P., 2009. Ocean-atmosphere interaction and tropical climate. The Encyclopedia of Life Support Systems (EOLSS), Tropical Meteorology 13.

Xie, S.P., Carton, J.A., 2004. Tropical Atlantic variability: Patterns, mechanisms, and impacts. Earth's Climate: The Ocean-Atmosphere Interaction, Geophys. Monogr 147, 121–142.

Xie, S.P., Philander, S.G.H., 1994. A coupled ocean-atmosphere model of relevance to the ITCZ in the eastern Pacific. Tellus A 46, 340–350. doi:10.3402/tellusa.v46i4.15484.

Xu, Z., Chang, P., Richter, I., Tang, G., 2014. Diagnosing southeast tropical Atlantic SST and ocean circulation biases in the CMIP5 ensemble. Climate Dynamics 43, 3123–3145. doi:10.1007/s00382-014-2247-9.

Xu, Z., Han, Y., Yang, Z., 2018. Dynamical downscaling of regional climate: A review of methods and limitations. Science China Earth Sciences 62, 365–375. doi:10.1007/s11430-018-9261-5.

Yan, Y., Li, L., Wang, C., 2017. The effects of oceanic barrier layer on the upper ocean response to tropical cyclones. Journal of Geophysical Research: Oceans 122, 4829–4844. doi:10.1002/2017JC012694.

Yoon, J.H., Zeng, N., 2010. An Atlantic influence on Amazon rainfall. Climate Dynamics 34, 249–264. doi:10.1007/s00382-009-0551-6.

Yu, L., Jin, X., Weller, R.A., 2008. Multidecade global flux datasets from the objectively analyzed air-sea fluxes (OAFlux) project: Latent and sensible heat fluxes, ocean evaporation, and related surface meteorological variables. Woods Hole Oceanographic Institution, OAFlux Project Tech. Rep. OA-2008-01. 74. URL: `http://oaflux.whoi.edu/`.

Zalesak, S.T., 1979. Fully multidimensional flux-corrected transport algorithms for fluids. Journal of computational physics 31, 335–362. doi:10.1016/0021-9991(79)90051-2.

Zebiak, S.E., 1993. Air–sea interaction in the equatorial Atlantic region. Journal of Climate 6, 1567–1586. doi:10.1175/1520-0442(1993)006<1567:AIITEA>2.0.CO;2.

Zeng, N., Yoon, J.H., Marengo, J.A., Subramaniam, A., Nobre, C.A., Mariotti, A., Neelin, J.D., 2008. Causes and impacts of the 2005 Amazon drought. Environmental Research Letters 3, 014002. doi:10.1088/1748-9326/3/1/014002.

Zheng, Y., Alapaty, K., Herwehe, J.A., Del Genio, A.D., Niyogi, D., 2016. Improving high-resolution weather forecasts using the Weather Research and Forecasting (WRF) model with an updated Kain–Fritsch scheme. Monthly Weather Review 144, 833–860. doi:10.1175/MWR-D-15-0005.1.

Influence de la salinité sur la dynamique couplée océan-atmosphère de l'océan Atlantique tropical

Résumé — L'océan Atlantique reçoit des apports d'eau douce provenant des précipitations et des grands fleuves tropicaux (e.g. Amazone) qui contribuent très fortement à la stratification des couches de surface de l'océan. L'objectif de cette thèse est d'étudier l'influence de cette stratification induite par la salinité sur le climat de l'océan Atlantique tropical. Des simulations couplées océan-atmosphère montrent que la présence d'une forte stratification en sel réduit considérablement les apports d'eau froide par mélange vertical à la base de la couche mélangée. Cet effet est cependant atténué par une rétroaction négative de l'atmosphère, via une modulation du flux de chaleur latent et de la couverture nuageuse. Des projections indiquent que dans un climat futur, l'influence de la stratification sur le mélange vertical et sur l'atmosphère serait renforcée du fait de l'intensification de la stratification en température.

Mots-clés : Stratification en sel, interactions air-mer, Amazone, ZCIT, barrière de sel, convection atmosphérique, NEMO-OASIS-WRF

Influence of salinity on the coupled ocean-atmosphere dynamics of the tropical Atlantic Ocean

Abstract — The Atlantic Ocean receives freshwater inflow from precipitation and large tropical rivers (e.g. Amazon) that strongly contribute to the stratification of the ocean surface layers. The objective of this thesis is to study the influence of this salinity-induced stratification on the climate of the tropical Atlantic Ocean. Coupled ocean-atmosphere simulations show that the presence of a strong salt stratification significantly reduces the cold water inflow by vertical mixing at the base of the mixed layer. However, this effect is mitigated by a negative feedback from the atmosphere, via modulation of the latent heat flux and cloud cover. Projections indicate that in a future climate, the influence of stratification on vertical mixing and on the atmosphere would be increased due to enhanced temperature stratification.

Keywords: Salinity stratification, air-sea interactions, Amazon, ITCZ, barrier layers, atmospheric convection, NEMO-OASIS-WRF